# Design and Development of a Novel Hybrid Concentrating Photovoltaic Thermal System with Parabolic Trough Collector

**THESIS**

Submitted in partial fulfilment of the requirements for the degree of

**DOCTOR OF PHILOSOPHY**

by

**NIKHIL GAKKHAR**
**2010PH060431P**

Under the supervision of

**Dr. MANOJ KUMAR SONI**


BITS Pilani
Pilani | Dubai | Goa | Hyderabad

**BIRLA INSTITUTE OF TECHNOLOGY & SCIENCE**
**PILANI – 333031 (RAJASTHAN) INDIA**
**2019**

# Design and Development of a Novel Hybrid Concentrating Photovoltaic Thermal System with Parabolic Trough Collector

**THESIS**

Submitted in partial fulfilment of the requirements for the degree of

**DOCTOR OF PHILOSOPHY**

by

**NIKHIL GAKKHAR**
**2010PH060431P**

Under the supervision of

**Dr. MANOJ KUMAR SONI**


BITS Pilani
Pilani | Dubai | Goa | Hyderabad

**BIRLA INSTITUTE OF TECHNOLOGY & SCIENCE**

**PILANI – 333031 (RAJASTHAN) INDIA**

**2019**

*Dedicated to*

*my father*

*Late (Dr.) Anil Gakkhar*

*&*

*my family*

Birla Institute of Technology & Science, Pilani
Pilani Campus

# CERTIFICATE

This is to certify that the thesis titled "**Design and Development of a Novel Hybrid Concentrating Photovoltaic Thermal System with Parabolic Trough Collector**" submitted by **Nikhil Gakkhar** ID No **2010PH060431P** for award of Ph.D. of the Institute embodies original work done by him under my supervision.

Signature (Supervisor):_____

**Dr. MANOJ KUMAR SONI**

Associate Professor, Department of Mechanical Engineering,

BITS Pilani, Pilani campus

Date: _____

# ACKNOWLEDGMENTS

Undertaking this PhD has been a truly life-changing experience for me and it would not have been possible to do without the support and guidance that I have received from many people. First and foremost, I pray and thanks to almighty God for showering his divine blessings and giving me an inner strength and patience during this journey.

I pay obeisance unto the lotus feet of my supervisor, **Professor Manoj Kumar Soni** for his valuable guidance, excellent direction, everlasting encouragement and inspiration given to me without whom the present work would not have been possible. I feel indebted to him for not only teaching me each and every aspect of the art of doing research but also other important aspects of life. Without his trust and constant support, the successful achievement of this work would have remained a dream.

I am grateful to **Prof. Souvik Bhattacharyya,** Vice-Chancellor and **Prof. A. K. Sarkar,** Director, BITS Pilani, Pilani Campus for giving me the opportunity to pursue my research work at the Institute. I owe my sincere thanks to **Prof. Srinivas Krishnaswamy**, Dean, Academic – Graduate Studies & Research (AGSR) and **Prof. Jitendra Panwar**, Associate Dean, AGSR for their official support and encouragement.

I am highly indebted to my Doctoral Advisory Committee (DAC) members **Dr. Kuldip Singh Sangwan,** Professor, Department of Mechanical Engineering, Pilani Campus and **Dr. Pratik N Sheth,** Associate Professor, Department of Chemical Engineering, Pilani Campus for their insightful comments and encouragement. I would also like to acknowledge **Dr. Sharad Srivastava**, Convener, Departmental Research Committee, Associate Professor, Mechanical Engineering Department, Pilani Campus who has provided valuable comments during the departmental seminars.

I would like to express my gratitude and thanks to **Prof. K. S. Sangwan**, Faculty-in-charge, Central workshop, **Prof. Dipendu Bhunia,** Unit Chief, Estate Management and **Dr. Anshuman**, Ex Unit Chief, Estate Management who provided support for fabrication and installation of the experimental set-up. I thank **Prof. M. S. Dasgupta**, (Head of Department) and entire faculty and staff of Department of Mechanical Engineering, BITS-Pilani, Pilani Campus for their kind moral support and assistance.

My gratitude knows no bounds for **Dr. Sanjeev Jakhar** for his unstinting guidance, many valuable suggestions and kind help at various stages of the work. I cherish all the moments spent with my friends and highly talented research scholars, **Dr. Arun Nihal Singh, Dr.**

**Pankaj Munjal, Mr. Rahul Dandautiya, Mrs. Shweta Munjal, Ms. Sakshi Chabbra, Dr. Nilesh Purohit, Dr. Rajesh Kumar, Dr. Manpreet Singh, Mrs Paridhi Puri, Dr. Vikrant Bhakar, Mr. Narpat Ram Sangwa** and **Mr Himanshu Chawla**. I have learned a lot from each and everyone. I thank them for always there for me and making my time memorable in BITS Pilani. I wish them a very bright future.

I would also like thank to Post graduate students, Mr. Aravindha and Ms. Nisha Tamar, who has worked with me during my PhD journey. I also thank the non-teaching staff **Mr. Ramu Saini, Mr. Bhim Singh, Mr. Parvat Singh, Mr. Dhanna Ram Saini** and **Mr. Banwari Lal Saini** for their valuable help at each stage of the experimental work. My sincere thank to all those persons whom I miss to acknowledge, who had directly or indirectly helped me to accomplish this task.

I also would like to thank my colleagues from the office and the Ministry, **Mr Rohit Thakwani, Mr Anubhav Uppal, Mrs Priya, Dr. Anil K Sarma** and **Dr. Sachin Kumar**, for their constant support and suggestions.

Last but not the least, I would like to thank my family; to my father, **Late (Dr) Anil Gakkhar** and my mother, **Mrs Kanchan Gakkhar**. I also thank my uncle **Prof. (Dr) Anup K Gakkhar** and aunt **Mrs Poonam Gakkhar**. I am deeply indebted to all the pains taken by them to make my dream come true. Thank you for giving me the confidence and courage to make the choices I have made. I would also thank my parents-in-law and brother-in-law **Mr Saurabh Bhateja**. My sincere thank to loving brother and sisters, **Mrs Nikita Bhateja, Ms. Nishtha** and **Mr Nipun Gakkhar**. Their constant love and care empowered me to accomplish my thesis and also ignited me to take more challenges in my life. My special thanks and love goes to little **Riddhansh** and **Chikki** for being the light of my eyes and the joy of my heart. My words fail to express my gratitude and appreciation to my wife **Mrs. Minashu Gakkhar** for all that she silently endured during the difficult times and way she always supported me and stood by my side with unending patience during the period of this work.

Nikhil Gakkhar
July 2019

# ABSTRACT

Solar energy, which is available in abundance, can be used to generate electricity in two different ways, i.e. one using photovoltaic (PV) systems and other by using thermal energy in concentrating solar power (CSP) systems. PV systems are a commercially proven technology, but the efficiency of commercially available PV cells is up to 20%. Rest of the incident solar energy is lost in the form of heat. This waste heat can be utilized for different low-grade thermal applications. One of such technology is photovoltaic/thermal system which consists of PV panel attached to a heat recovery system in which coolant absorbs the excess heat. The extracted thermal energy can be utilized for different applications like distillation.

The state of Rajasthan is semi-arid region with water scarcity issue. However, the state possesses huge potential for solar energy utilization. In the present research work, an initial investigation has been carried out to identify the water availability and the potential for solar energy based distillations systems. The electrical solar power potential of each district was calculated by estimating the suitable wasteland area, solar radiation, and technical parameters of concerned technologies. From the pre-feasibility study, it is estimated that the Rajasthan has power generation potential of 1077.44 GW, 811.36 GW and 728.99 GW for mono-crystalline silicon, poly-crystalline silicon and thin film technologies respectively. Using concentrating technology, the power generation potential is 883.31 GW, 569.50 GW and 383.56 GW for linear Fresnel receiver, parabolic trough collector and central tower receiver respectively. Following the electric potential, an attempt has been done to identify the water availability for each district based on available resources. When the electric potential is coupled with water availability scenario, the highest potential for PV based distillation unit is found out to be for Pali district followed by Udaipur district. It is also seen that Jaipur district holds the top position for maximum availability of water supply to have concentrating technology based distillation plant.

After identifying the solar based distillation potential, a standalone novel hybrid concentrating photovoltaic thermal (HCPVT) system is proposed. Such system includes a PV module mounted on absorber of parabolic trough collector (PTC). The designed system allowed water through the absorber tube and within the annulus of absorber tube and glass cover of PTC receiver. This is to provide cooling of PV panel from both sides to improve its performance. During the process, water gets heated up and thus the system provides both

electrical outputs as well as hot water. Such systems can be a standalone system for combined heat and power applications and could be useful in remote areas.

The modeling and simulation of three different designs of absorber tube i.e. circular, semi-circular (D-shape) and triangular were carried out using simulation tools. The design of receiver was modeled and simulated using MATLAB following which the HCPVT system coupled with distillation unit was optimized using Aspen HYSYS. Using theoretical results, an experimental set up of PTC along with two novel designed receivers were fabricated. The experimental setup was installed on site and tested for D-shape absorber, at varying operating conditions. From the investigation, it was observed that the theoretical values of HCPVT outlet temperature, PV panel temperature and thermal efficiency obtained from the simulation are in good agreement with the results obtained from the experimental study. It was found out that the maximum overall efficiency could be achieved with inner tube flow rate of 0.1 kg/s and annulus flow rate of 0.008kg/s. The experimental and simulation results show that the maximum overall efficiency of 69.19% could be achieved at the combined flow rate of 0.108 kg/s.

Further, to identify the grey areas for improvement, the second law of thermodynamic analysis has been carried out for the novel proposed HCPVT system. The exergetic efficiency, exergy losses and exergy destruction were evaluated with varying annulus flow rate and varying inner tube flow rate. For the calculation of exergetic efficiency, three different approaches are taken: Case I, without exergy losses; Case II, considering exergy losses and exergy destruction; Case III, only exergy destruction. From the analysis, it was observed that the second law efficiency in Case III, was higher than the other two and it ranged from 38.28% to 44.78%, 31.51% to 38.02% and 26.16% to 31.75% for annulus mass flow rate of 0.008 kg/s, 0.017 kg/s and 0.025 kg/s respectively with constant inner flow rate of 0.075 kg/s.

The proposed standalone system could be used for low-grade thermal applications like distillation. Simulation results show that such system would provide a continuous output of 0.2328 kg/hr of distilled water, for each unit intake under the conditions of Pilani. The output could be increased by increasing the receiver length. However, there is a trade-off required in the length of absorber tube and length of PV panel. The current research is an attempt to develop a standalone solar based distillation system. Large scale setup of such distillation units could be utilized for the continuous supply of fresh water in the state of Rajasthan.

# TABLE OF CONTENTS

# LIST OF TABLES

# LIST OF FIGURES

# NOMENCLATURE

| | | |
|---|---|---|
| A/Ap/Aa | aperture area | $m^2$ |
| Cp | specific heat | kJ/kg.K |
| CR | concentration ratio | |
| D | Diameter | m |
| E | internal energy | kJ |
| Ex | Exergy | kJ |
| $\dot{Ex}$ | exergy rate | W |
| FF | fill factor | |
| FR | flow factor/heat removal factor | |
| Gz | Graetz number | |
| h | convective heat transfer coefficient | $W/m^2K$ |
| H | Enthalpy | kJ/kg |
| I | Current | A |
| Ir | Irradiance | $W/m^2$ |
| $\dot{Ir}$ | Irreversibility | kJ |
| J | Radiosity | |
| K | incident angle modifier | |
| k | thermal conductivity | W/m.K |
| L | Length | m |
| $\dot{m}$ | mass flow rate | kg/s |
| M | molar mass | |
| n | Number | |
| N | penalty factor | |
| η | Efficiency | % |
| Nu | Nusselt number | |

| | | |
|---|---|---|
| p | Pressure | kPa or bar |
| P | Power | W |
| ppm | parts per million | |
| Pr | Prandlt number | |
| Q | instantaneous heat transfer | W |
| $\dot{q}'$ | heat transfer per unit length | W/m |
| R | gas constant | |
| $Ra$ | Rayleigh number | |
| Re | Reynolds number | |
| S | Entropy | kJ/K |
| s | specific entropy | kJ/kg.K |
| Sgen | entropy generation | |
| t | Time | sec |
| T | temperature | °C |
| U | heat transfer coefficient | $W/m^2K$ |
| $U_{aw}$ | overall heat transfer coefficient from absorber to water flow | $W/m^2K$ |
| $U_{ct}$ | conductive heat transfer coefficient from solar cell to flowing water through tedlar | $W/m^2K$ |
| $U_{g,ted}$ | overall heat transfer coefficient from glass to tedlar through solar cell | $W/m^2K$ |
| V | Voltage | V |
| W | width of PV cell | m |
| x | mole fraction | |

**Subscripts**

| | |
|---|---|
| a | ambient condition |
| abs | absorber |

| | |
|---|---|
| act | actual |
| ap | aperture |
| b | back surface |
| br | brine |
| c | cell |
| ch | chemical |
| cl | cold |
| col | collector |
| conc | concentration |
| cond | conductive heat transfer |
| conv | convective heat transfer |
| dest | destruction |
| el | electrical |
| Ex | exergy |
| f | front surface |
| fl | fluid |
| g | glass |
| h | hot |
| i | inlet/input |
| irr | solar radiation |
| l | length |
| loss | losses |
| m | mass flow rate |
| max | maximum |
| mi | mirror |
| min | minimum |

| | |
|---|---|
| mod | Module |
| o | outlet/output |
| oc | open current |
| opt | optimum |
| P | pressure |
| ph | physical |
| PV-water | heat transfer between PV and water |
| r | receiver |
| rad | radiative heat transfer |
| rev | reversible |
| S | Sun |
| sc | short circuit |
| sea | salt concentration |
| sr | surface |
| st | steam |
| stag | stagnation point |
| Sun-PV | heat transfer between sun and PV |
| sw | seawater |
| t | tube |
| ted | tedlar |
| th | thermal |
| tot | total |
| u | useful |
| v | vapor |
| w | water |
| wd | Width |

| | | |
|---|---|---|
| z | height, axial length | |
| 0 | dead state/sink | |
| 1 | bulk surface of inner fluid | |
| 2 | inner surface of semi-circular tube | |
| 3 | outer surface of semi-circular tube | |
| 4 | inner surface of glass | |
| 5 | outer surface of glass | |
| 6 | surrounding/ambient conditions | |
| 7 | Sky | |
| 8 | bulk surface of annulus fluid on flat side | |
| 9 | bulk surface of annulus fluid on curved side | |

**Greek letters**

| | | |
|---|---|---|
| $\alpha$ | Absorptivity | |
| $\alpha_{56}$ | thermal diffusivity at temperature $t_{56}$ | $m^2/s$ |
| $\beta$ | volumetric coefficeint for thermal expansion | 1/K |
| $\gamma$ | packing factor | |
| $\delta$ | sun cone angle | |
| $\varepsilon$ | Emissivity | |
| $\eta$ | Efficiency | |
| $\mu$ | refractive index of the fluid | |
| $\nu$ | kinematic viscosity of air | $m^2/s$ |
| $\rho$ | Reflectivity | |
| $\rho o$ | density | $kg/m^3$ |
| $\sigma$ | Stefan-Boltzmann constant ($5.67 \times 10^{-7}$) | $W/m^2K^4$ |
| $\tau$ | Transmissivity | |

# LIST OF ABBREVIATIONS

| | |
|---|---|
| BIS | Bureau of Indian Standards |
| CFD | Computational fluid dynamics |
| CPV | Concentrated photovoltaic |
| CPVT | Concentrated photovoltaic-thermal |
| CR | Concentration ratio |
| CSP | Concentrating solar power |
| CTR | Central tower receiver systems |
| DNI | Direct normal irradiance |
| DWW | Domestic wastewater |
| ED | Electro dialysis |
| FPC | Flat plate collector |
| GHI | Global horizontal irradiance |
| GW | Groundwater |
| HCPVT | Hybrid concentrating photovoltaic thermal |
| HTF | Heat transfer fluid |
| LFR | Linear Fresnel reflector |
| MD | Membrane distillation |
| MED | Multi-effect distillation |
| MEE | Multi-effect evaporator |
| MLD | Million liter per day |
| MSF | Multi-stage flash |
| PCM | Phase change material |
| PTC | Parabolic trough collector |
| PV | Photovoltaic |
| PVT | Photovoltaic-thermal |

| | |
|---|---|
| RO | Reverse osmosis |
| RW | Rainwater |
| STC | Standard test condition |
| SWR | Surface water resources |
| TDS | Total dissolved solids |

# CHAPTER 1

# INTRODUCTION

*A brief background of the origin of the problem statement, energy and water scenario, available technologies which combines water and energy, research objectives, the methodology adopted, scope and limitations of the research are presented in this chapter.*

## 1.1 Background

### 1.1.1 Energy scenario

Earlier the energy from Sun, fossil fuels, oil, etc. was used to meet necessities of life like the cooking of food, heating of space, etc. With the onset of industrialization, the concept of energy changed from necessities to comfort level including energy requirement for locomotive, heating, and cooling of space, running of machines, etc. This requirement of energy has increased over the decades and it can be evident from the fact that the world primary energy supply has been increased from 6,101 Mtoe in 1973 to 13,763 Mtoe in 2016 [1]. The electricity is the most prominent form of final energy being used in the modern world. The electricity demand has been increasing worldwide continuously at the rate of 3% per year primarily due to the expanding industrialization, multiplying population and day by day improvement in human comfort level. In order to fulfill the electricity demand, the worldwide electricity generation has also increased from 6,131 TWh in 1973 to 25,551 TWh in 2017 [2]. Despite increasing electricity generation, it is estimated that out of the total 7.6 billion world population, 1.2 billion people do not have access to electricity and about 2.7 billion people still rely on traditional fuels and energy sources, such as biomass, for most of their energy requirement [3]. India is the second most populated country having approximately 18% of the world's total population and consumes only 6% of the total energy. India's total installed capacity for electricity generation is 356.10 GW as on 31.03.2019, out

of which 226.28 GW is from fossil fuel based power plants [4]. So, almost 66% of India's electricity comes through fossil fuels only. Same holds for the world where fossil fuel sources contribute more than 65% of the world's electricity, while the rest of the total electricity generation is through renewable, nuclear and other sources [5]. The carbon emissions from these fossils fuels based power plants are harmful to the environment and society.

Renewable energy sources have gathered considerable attention of governments, utilities and researchers to provide a clean source of energy and to reduce emission and other environmental concerns associated with fossil fuel based power generation. During 2008, the total installation of renewable power generation capacity in the world was 1,057 GW which rose to 2,179 GW in 2017, due to the widespread promotion of renewable energy across the world by various agencies. According to the international renewable energy agency, with 80.18 GW (as on 31.03.2019), India ranks sixth in the world in the total installed renewable power generation capacity [6].

In the Indian context, it is envisaged to increase renewable-based electricity generation to 175 GW by 2022. This includes 100 GW from solar power, 60 GW from wind power, 10 GW from bio-power and 5 GW from small hydropower. As on March 2019, the total installed capacity of renewable energy sources includes 35.62 GW from wind power, 29.69 GW from solar power, 10.26 GW from bio-power and 4.59 GW from small hydropower [7].

### 1.1.2 Water scenario

Water is an essential aspect of the development of human civilization. It is one of the most abundant resources on earth, covering three-fourths of the planet's surface. About 97% of the earth's water is in the oceans, which is not potable. Remaining 3% (about 36 million $km^3$ of volume) is fresh water contained in the poles (in the form of ice), groundwater, lakes and rivers, which is used for human and animal needs. Nearly, 70% of the world's fresh

water is frozen in glaciers, permanent snow cover, ice and permafrost [8]. Around 30% of all freshwater is underground, most of it in deep, hard-to-reach aquifers. Lakes and rivers together contain just a little more than 0.25% of all fresh water. With the increase in population, the demand for fresh water is increasing which is causing depletion of freshwater resources. Rapid urbanization and industrialization also lead to shrinking of lakes and pollution of water resources. The non-availability of freshwater for human and animal consumption is significant issues. Lack of fresh water for necessities affects the development and quality of life especially in rural regions of the developing countries [9]. According to the world water council report, by the year 2050, per capita availability of freshwater supply of world would fall from current 6,600 cubic meters to 4,800 cubic meters [10]. In India the per capita freshwater availability has reduced down from 5,177 cubic meters in 1951 to about 1,545 cubic meters in 2011 and is expected to further come down to 1,341 cubic meters in 2025 and 1,140 cubic meters in 2050 [11]. In arid areas, potable water is very scarce and the establishment of human habitats in these areas strongly depends on drinking water resources. In these regions, specifically in rural areas, women still have to walk long distances and need to spend up to four hours per day to fetch fresh water [12].

According to the annual report on Ground Water Scenario in India Pre-monsoon 2017, by the Ministry of Water Resources, the state of Rajasthan faces a maximum depth of groundwater level among other states [13]. The lowest depth of water level recorded in the state of Rajasthan during pre-monsoon 2017 was 134.22 m below ground level in Bikaner district. The lower level of groundwater, along with the high concentration of total dissolved solids (TDS) makes it unfit for drinking. Thus, there is an urgent need to make the groundwater potable to meet the current demand. With recent developments in technology, there is a need to create a sustainable ecosystem to harness energy from renewable sources

and use it not only for power requirement but also for sustainable technology to provide fresh water.

### 1.1.3 Energy and water: Available technologies

As discussed earlier, most of the water available in the world is in the ocean which is not drinkable. So to make it suitable for human consumption, many conventional and non-conventional techniques have been used. The most commonly used technique for water purification is distillation/desalination. Distillation is generally used for purification of groundwater, while desalination is used for seawater to remove salts from it. In this thermal energy can also be used, where water is heated up using thermal energy (heat source). It is evaporated and condensed back to get water free from impurities. The heat source may be solar energy, or any other conventional fossil-fuels as well as renewable energy sources like biomass, biofuels, etc. Besides these, non-thermal distillation technologies like membrane distillation (MD), reverse osmosis (RO) and electrodialysis (ED) uses electrical power to convert raw water into fresh water. In such systems, the direct electricity is used either to drive high-pressure pumps or to ionize salts and TDS contained in the water. The type of water purification technology deployed depends upon the amount of TDS level in the water. The permissible limit of TDS in fresh water is about 500 ppm. In the case of brackish water, (TDS <10,000 ppm) the distillation technology could be used. For the high amount of TDS, up to 35,000 or more, desalination technology could be used. Distillation/desalination could be achieved either by direct use of electricity from conventional sources / solar photovoltaic (PV) systems or by use of thermal energy (solar/conventional). It depends on the number of factors like plant size, feed water salinity, remoteness of the location, availability of energy source, technical infrastructure, etc. [14]

The process of distillation could be achieved by the direct or indirect use of solar energy. In direct solar energy based distillation systems, the solar energy heats the raw water, evaporates it and the vapors are then collected within the system, leaving behind the impurities like salts, heavy metals and microbiological organisms within in the raw water. In case of indirect distillation systems, two subsystems are employed, one for solar energy collection and other for distillation. Heat transfer fluid (HTF) is used in such systems to transfer heat within the subsystem. In both direct and indirect collection systems, thermal storage is used for extended operations beyond sunshine hours. Another technique of indirect distillation is the use of PV system, in which solar energy is directly converted into electricity which is then used for non-thermal distillation technologies. The classification of various processes for solar assisted water purification techniques is shown in Fig. 1.1.

Among direct distillation systems, solar stills are the simplest structures which use direct solar energy to purify water. It could be active or passive and can easily be coupled with flat plate collectors (FPC) or solar concentrators [15–17]. Solar stills are investigated in the literature based on their designs, like simple solar still, single-slope single-basin solar still, tubular-type and hemispherical solar still etc.

Thermal energy based indirect solar distillation systems have two subsystems, one for solar energy collection and another for distillation. The collector subsystems are classified as non-concentrating, which operates on the low-temperature range (up to 100 °C) or concentrating collectors, which operates on medium to the high-temperature range (up to 3500 °C or more). Among all, FPC is commonly used non-concentrating collectors.

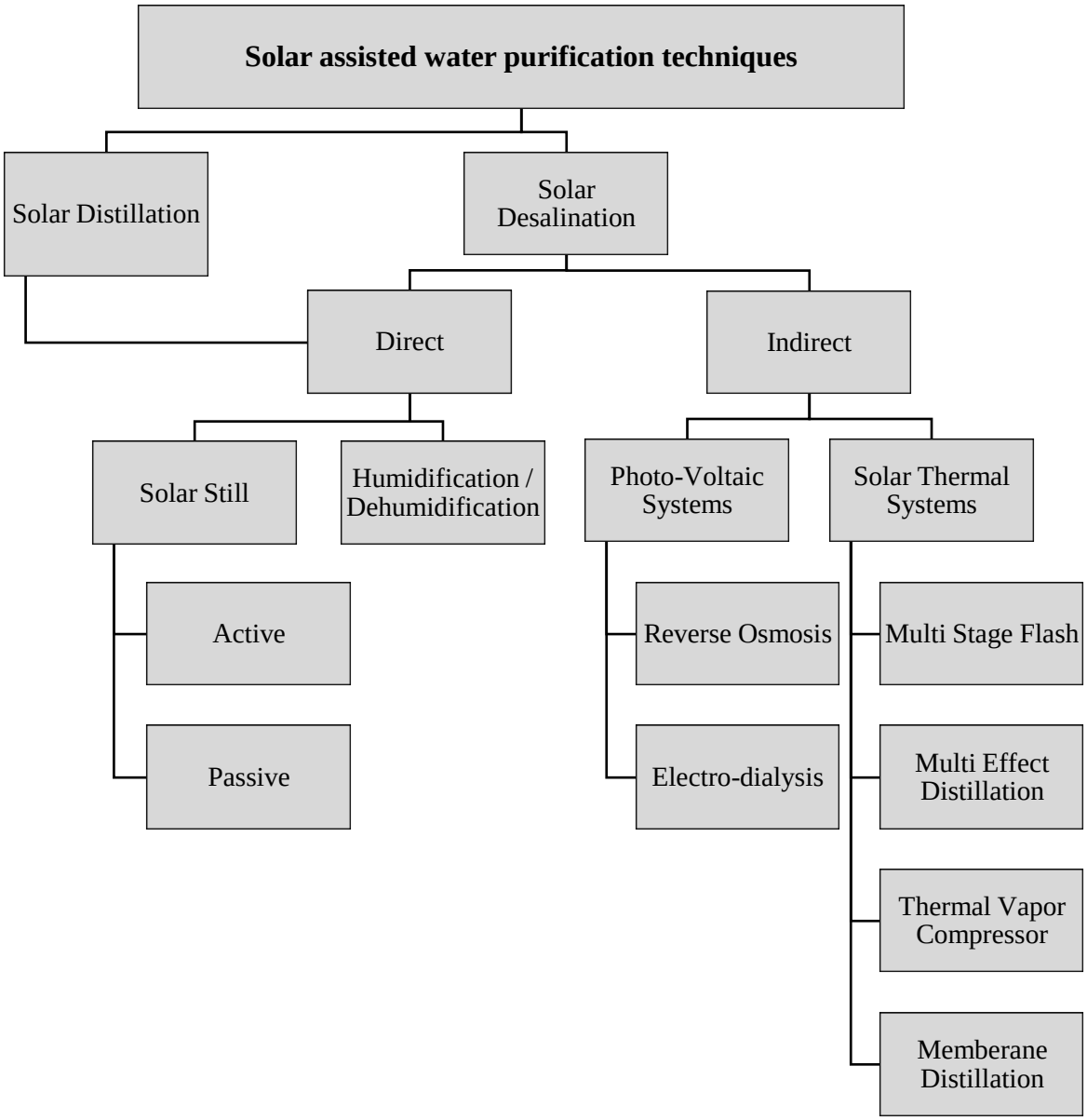


**Fig. 1.1 Solar assisted water purification techniques**

Concentrating collectors are categorized according to their focus geometry either as line-focus concentrators like parabolic trough collector (PTC) and linear Fresnel reflector (LFR) or as point-focus concentrators like central tower receiver systems (CTR), parabolic dish and Scheffler collectors [18]. In the medium temperature range concentrated technologies like PTC, LFR, etc. the temperature goes up to 400 °C which can be used for heating purposes, power generation and distillation etc. Among these, PTC has proven to be the most mature and low cost concentrating solar technology available today [19]. Literature

reveals that PTC is being used in desalination systems specifically in European and Middle East conditions.

The distillation subsystems of indirect solar distillation systems are further classified into four types:

- Multi-stage flash distillation (MSF)
- Multi-effect distillation (MED)
- Thermal vapor compression (TVC)
- Humidification dehumidification cycle (HDH)

MSF is the most commonly used distillation technology in which, water is heated in a solar thermal system and then flashed in different chambers by varying saturation pressure. In MED technology, water evaporates on the outside of heated tubes based on its saturation pressure and then passes to the next effects for additional vapor production [20]. In case of TVC, the distillation is obtained by using solar energy as a heat source for vapor compressor while in HDH, the air is heated through solar energy which then humidified by saline water injection. The humid air passes through a cooler for dehumidification to obtain distilled water [21].

The other category of indirect collection distillation system is the solar PV system which uses an array of silicon solar cells, to convert direct sunlight into electricity. This electricity could be directly utilized to drive types of equipment or to store energy in the form of batteries. Based on the requirement, the electricity could be used fresh water production using RO, MD, ED, etc.

## 1.2 Problem Statement

India, being a tropical country, is blessed with plenty of sunshine. The highest annual global radiation falls on the northwestern part of the country, majorly in the state of Rajasthan. The state is an arid and semi-arid region with water scarcity issues, as the quality

of groundwater is not as per the BIS standards and need to be treated to make it drinkable. Since the state also possesses huge potential for solar energy, there is a need for solar thermal technologies, which directly uses the energy of the Sun to distill groundwater and make it potable. Existing technologies like a solar still are less efficient in terms of output. On a large scale basis, solar concentrating technologies may provide higher system efficiency and output. These technologies also have an advantage over flat plate systems, as a smaller area is required due to concentration optics. The existing desalination plants across the world also use PTC technology for thermal energy requirement. In PTC solar energy is concentrated with the help of parabolic reflectors at the focal line. A receiver tube is placed at this focal line which carries the HTF through it. The radiation from the reflecting surface concentrates on this tube and heats up the HTF, which may be oil or water, flowing inside the tube. Generally, the receiver tube is circular in shape having absorber tube in between and has vacuum within outer glass tube and absorber tube. The efficiency of the system depends upon the concentration ratio (CR), flow rate of HTF and power required to pump HTF through the absorber tube. With the increase in PTC input, pumping power also increases. In remote locations where the power supply is intermittent, continuous running of the pump could be a considerable challenge. The standalone solar pumps, which are operated through PV, can be used in such cases, but it increases the capital cost.

In order to overcome the existing issues, there is a need of development of a standalone system which would provide combined heat and power. The electrical power could be obtained by using PV panel under high concentration. However, with high concentration panel temperature increases which result in decrease in efficiency of the system. To improve the performance of this system and to maximize the electrical output, cooling of PV panel is necessary. The HTF can be used to cool down the panel which carries away the excess heat. Such systems are known as photovoltaic-thermal (PVT) or

concentrated photovoltaic-thermal (CPVT) systems, when operated under non concentration or concentration respectively. The low-grade thermal energy, thus obtained, could be utilized for various heating applications like distillation. Such a standalone solar system could provide a sustainable solution for water purification especially in remote locations.

## 1.3 Objective of the Research

In the present research work, an analysis has been carried out to utilize solar energy for water distillation by proposing a design of novel hybrid concentrating photovoltaic thermal system (HCPVT) for combined heat and power. For the same, an initial investigation has been carried out to identify the quality of groundwater in the state and the potential for solar energy based distillations systems. After identifying its potential, the design of standalone HCPVT system is proposed. The low-grade thermal energy obtained from this system could be utilized for the distillation of groundwater. The specific objectives of the research are:

- To investigate the water availability potential and feasibility of solar energy based distillation units in Rajasthan.
- To study the existing systems of water distillation and concentrating solar parabolic trough collectors.
- To simulate and develop the model of the proposed system using suitable simulation tools.
- To develop the experimental setup of a novel HCPVT system for combined heat and power and to carry out the experimental investigations under varying operating conditions.
- To carry out the parametric study of the validated simulated model.

## 1.4 Methodology Adopted

A new concept of standalone HCPVT system is introduced for combined heat and power. The experimental design was developed using suitable tools like Aspen HYSYS, MATLAB, etc. The setup was fabricated and tested to validate the design. The following methodology under different phases has been used to achieve the objectives of the study:

**Phase I:** In the first phase, an extensive literature survey in areas of groundwater quality, PTC, the potential of solar energy, water distillation system, etc. was carried out. The research gaps in the literature were identified.

**Phase II:** In the second phase modeling and simulation of the proposed HCPVT system using simulation tools were carried out. The system design was optimized using Aspen HYSYS while simulation and analysis were carried out using MATLAB.

**Phase III:** Using simulated results, an experimental set up of PTC along with the novel HCPVT receiver was fabricated during this phase. The experimental setup was installed on site and tested out at varying operating conditions.

**Phase IV:** During this period, the validation of simulation was carried out using the results of experimentation. This includes the parametric variation of the validated simulated model. The exergy analysis of the system was also carried out to find out second law efficiency of the system.

**Phase V:** In this last phase, suitable conclusions and recommendations were drawn with documentation for journal articles and patent application.

## 1.5 Scope and Limitations

The scope of work includes the design and development of a novel HCPVT experimental setup system for combined heat and power. Such a system includes a PV panel upon which, the concentrated solar radiation falls with the help of PTC. The designed system included water within the annulus of PTC so as to provide cooling of PV panel to improve its efficiency. In the process, water gets heated up and thus the system provides both electrical outputs as well as hot water. Such systems can be a standalone system for combined heat and power and could be useful in remote areas. The limitation of such proposed HCPVT system is the higher convective losses in case of larger length of the receiver tube. The further development possibilities for the extension of the work are proposed in the future scope of the project.

## 1.6 Organization of the Thesis

Keeping the broad research objectives in mind, the thesis consists of seven chapters. Fig. 1.2 illustrates the thesis structure

**Chapter 1** discusses the background of energy, water, and status of renewable energy in India. The need for the novel standalone system is discussed followed by research objectives, the methodology adopted for research, scope and limitations and organization of the thesis.

**Chapter 2** investigates the potential of solar energy based distillation systems in the state of Rajasthan. This was achieved by identifying solar power generation potential and water availability potential in the state.

**Chapter 3** reviews the prior research work on solar energy based distillation, PTC and distillation technologies. Following the detailed review, the identified research gaps are discussed.

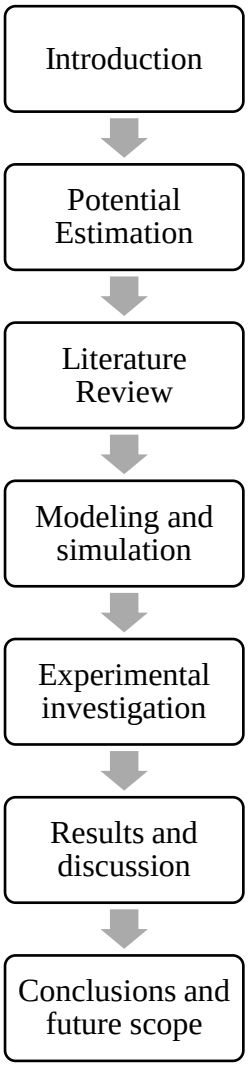


**Fig. 1.2 Thesis structure diagram**

**Chapter 4** discusses the modeling and simulation of a novel HCPVT system. The design was made using Aspen HYSYS while simulation and analysis based on the first law of thermodynamics, were carried out using MATLAB. The second law of thermodynamic analysis model using experimental results is also discussed.

**Chapter 5** describes the experimental setup, experimental procedures and measuring instruments used in detail. The field testing was conducted on novel HCPVT system by varying mass flow rate in different arrangements.

**Chapter 6** discusses the results obtained from the simulation which were validated against the data generated from the experimental testing of a novel HCPVT system. Based on the results, an optimized simulated system has been proposed using the first and second law of thermodynamics.

**Chapter 7** concludes the thesis by providing a summary of results, recommendations and future scope of the work.

**CHAPTER 2**

# PRE FEASIBILITY STUDY OF SOLAR ENERGY AND WATER POTENTIAL IN RAJASTHAN, INDIA

*This chapter discusses the pre-feasibility of solar based distillation units in the state of Rajasthan. For the same, the water availability and solar power potential in the state are identified using various available parameters. The district wise potential is mapped for graphical representation.*

## 2 Introduction

India, being a tropical country, is blessed with plenty of sunshine. The average daily solar radiation varies between 4 to 7 kWh/$m^2$ for different parts of the country. The western part of the country includes the state of Rajasthan, a major part of which is an arid and semi-arid region with high TDS level in groundwater. The state also receives the very high solar radiation throughout the year which provides tremendous potential for power generation from the Sun. This solar potential could also be harnessed for water purification technologies in this region. Such feasibility of having a solar distillation unit in the state of Rajasthan is discussed here.

The state of Rajasthan lies in the northwestern part of India and has the geographical area of 342,239 $km^2$, which stretches from 23.06° N to 30.19° N and 69.48° E to 78.25° E. It is India's largest state, occupies 10.4% of the geographical area of the country and has vast climatic diversity. It consists of semi-arid, and arid to humid and moderate climatic regions [22] and receives 6 - 7 kWh/$m^2$/day of peak solar radiation for more than 325 days a year [23]. The western part of the state is the desert area which receives scanty rainfall and is blessed with very high solar insolation [24]. The state has 33 districts which can be divided into seven different regions, i.e. north (Ganganagar, Hanumangarh, Bikaner, Churu), west

(Jaisalmer, Jodhpur, Barmer, Jalore, Sirohi, Pali), south (Udaipur, Chittorgarh, Rajsamand, Banswara, Dungarpur, Pratapgarh), center (Nagaur, Ajmer, Tonk, Bhilwara), north-east (Jhunjhunu, Sikar, Jaipur, Alwar, Dausa), south-east (Bundi, Kota, Baran, Jhalawar) and east (Bharatpur, Karauli, Dhaulpur, Sawaimadhopur). The district wise map of the Rajasthan is shown in Fig. 2.1 [25].

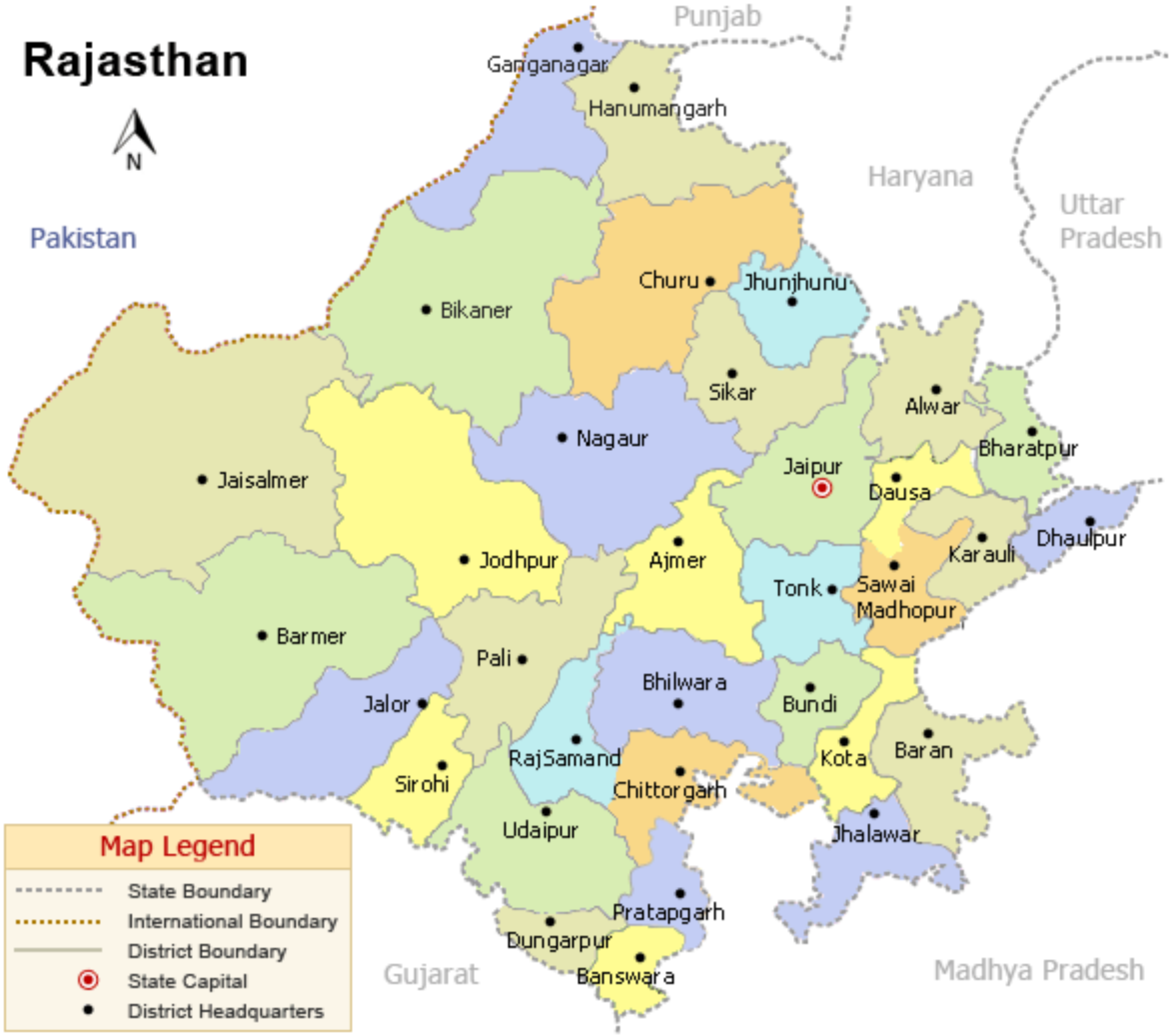


**Fig. 2.1 Map of Rajasthan [25]**

Rajasthan is the driest state in the country and is water scarce, having per capita water availability below 40 liters per day [26]. The water requirement for drinking, domestic activities, agriculture, etc. are increasing with the growth of population and higher living standards [10]. With existing high population growth rate, the per capita water availability is declining to alarmingly low levels, indicating the need for different techniques for water

treatment and making it potable [27]. Since the Rajasthan state has good solar insolation throughout the year, solar energy based technology for water distillation can prove to be a suitable technique in the state. The solar energy either using PV or concentrating solar power (CSP) can easily be coupled with distillation technology to obtain distilled water. The same can be achieved by using solar based distillation plants where the Sun provides the primary energy for the plant while input can be from raw feed water from various available resources.

## 2.1 Resource Availability in Rajasthan for Solar Distillation

The working of solar energy based distillation plant depends on the number of factors like plant size, feed water salinity, remoteness of the location, availability of electricity, technical infrastructure etc. Besides the technical parameters, the external factors like the availability of ample sunshine, land and water availability also play an important role in the establishment of a distillation plant. The external parameters which may be suitable for solar distillation plants in the state of Rajasthan are as discussed below.

### 2.1.1 Water availability from various sources

Water which can be brackish or saline in nature and available through different water resources like rivers, lakes, wells, etc., can play an important role in the estimation of distillation potential in the state. The distillation of such raw feeds can be achieved by either PV connected with RO system or CSP connected with MSF system. In both cases, the input water feed is a crucial and essential factor. Different water resources which can provide input raw feed for this purpose may be categorized as per the followings.

#### *2.1.1.1 Surface water resources*

The surface water resources (SWR) of the state depict the number of rivers, canals, lakes, water tributaries, dams etc. There are 15 defined river basins in the state and among those, only Chambal and Mahi rivers are perennial, located in the eastern and southern part of

the state, respectively. The water availability in these, however, mainly depends on the annual monsoon. Besides two major perennial rivers, the state has one major canal (Indira Gandhi canal) and India's largest salt lake (Sambhar lake). The state also has around 27 small tributaries, 15 lakes, 7 dams, and 3 river canals. The major source of water availability in the state is Chambal and Luni river. Brief information about the surface water resources of Rajasthan is summarized in Table 2.1.

**Table 2.1 Surface water resources of Rajasthan [28]**

| **Rivers and tributaries** | **Districts involved** | **Lakes** | **Districts involved** |
|---|---|---|---|
| Ahar | Udaipur | Ana Sagar Lake | Ajmer |
| Arvari | Alwar | Balsamand Lake | Jodhpur |
| Banas | Rajsamand, Sawaimadhopur, Tonk | Dhebar Lake | Udaipur |
| Bandi | Pali | Fateh Sagar Lake | Udaipur |
| Banganga | Bharatpur, Dausa, Jaipur | Foy Sagar Lake | Ajmer |
| Berach | Udaipur, Chittorgarh, Bhilwara | Kaylana Lake | Jodhpur |
| Chambal | Dhaulpur, Kota, Chittorgarh | Nakki Lake | Sirohi |
| Dai | Ajmer, Tonk | Pachpadra Lake | Barmer |
| Dheel | Jaipur, Tonk, Sawaimadhopur | Pichola Lake | Udaipur |
| Gambhir | Karauli, Dhaulpur | Pushkar Lake | Ajmer |
| Ghaggar-Hakra | Hanumangarh | Rajsamand Lake | Rajsamand |
| Gomati | Udaipur | Ramgarh Lake | Jaipur |
| Guhiya | Pali | Sambhar Salt Lake | Nagaur, Jaipur |
| Jawai | Udaipur, Jalore, Pali | Talwara Lake | Hanumangarh |
| Kali Sindh | Sawaimadhopur | Udaisagar Lake | Udaipur |
| Kalisil | Sawaimadhopur | **Dams** | **Districts involved** |
| Kothari | Rajsamand, Bhilwara | Bisalpur | Tonk |
| Luni | Ajmer, Barmer, Jalore, Jodhpur, Nagaur, Pali, Sirohi | Jakham | Pratapgarh |
| Mahi | Banswara, Dungarpur | Jawahar Sagar | Kota |
| Mej | Bhilwara, Kota, Bundi, Tonk | Jawai | Pali |
| Menali | Bhilwara | Kota Barrage | Kota |
| Mithari | Pali | Rana Pratap Sagar | Chittorgarh |
| Morel | Jaipur, Sawaimadhopur | Ummed Sagar | Jodhpur |
| Parbati | Dhaulpur, Sawaimadhopur | **Canal** | **Districts involved** |
| Sabarmati | Udaipur, Sirohi, Pali, Dungarpur | Agra Canal | Bharatpur |
| Sukali | Pali | Anupgarh canal | Ganganagar, Bikaner |
| Sukri | Pali, Jalore, Barmer | Ganges Canal (Rajasthan) | Hanumangarh, Ganganagar |
| West Banas | Sirohi | Indira Gandhi Canal | Barmer, Bikaner, Churu, Hanumangarh, Jaisalmer, Jodhpur, Ganganagar |

### *2.1.1.2 Rainfall*

There is a large variation in the rainfall pattern in Rajasthan due to its topography. The average annual rainfall which is expected over a state is calculated in term of 'mm of rainfall', which is equivalent to one-liter water received per square meter of area. Indian meteorological department which updates and forecast the monsoon activity in the country, divided the state into two parts i.e. eastern Rajasthan and western Rajasthan. The geographical existence of oldest mountain ranges i.e. Aravali hills isolates the two major water basins which cause the tropical climatic conditions of the state. The area west of Aravali mainly forms part of the Great Thar Desert and is an arid region having extreme temperatures, high wind velocities, and very low humidity. Some areas in the western part like Jaisalmer and Barmer districts receive rainfall as low as 200 mm per year. This area has an average rainfall of 318.7 mm and does not drain in any river as whatever rainfall occurs it percolates in the ground. The eastern part of the state is comparatively humid and rainfall ranges between 400 to 1000 mm with an average of 688.7 mm. In the south, some areas of the state like Mount Abu receive 1638 mm of rainfall per year. The annual rainfall, with an average of 570 mm for the state, operates majorly during monsoon season delivers the water supply to many rivers and dams of the state. As per the water resource department, Government of Rajasthan, rainwater harvesting projects helped the state to provide rainwater (RW) supply for a longer duration [29]. The annual average rainfall has a strong influence on groundwater quality as higher rainfall results in higher recharge, which in turn has a dilution effect on groundwater. The normal value of rainfall for each district as well as net groundwater availability, expressed in million cubic meters (mcm) is presented in Table 2.2 and is taken as the potential source of water availability for the solar projects [30].

**Table 2.2 Water availability through various resources in Rajasthan [31,32]**

| District | District average annual rainfall (mm) | Groundwater resource | Domestic wastewater generation (MLD) | | | |
|---|---|---|---|---|---|---|
| | | net ground water availability (mcm) | Actual domestic wastewater generation (MLD) | Projection | | |
| | | | | 2020 | 2040 | 2060 |
| Ajmer | 429.6 | 322.06 | 93.47 | 134.38 | 163.99 | 186.24 |
| Alwar | 555.3 | 731.69 | 22.88 | 91.44 | 147.51 | 182.33 |
| Banswara | 831.8 | 230.66 | 7.03 | 13.24 | 14.18 | 17.86 |
| Baran | 792.2 | 471.63 | 6.14 | 35.33 | 52.14 | 63.61 |
| Barmer | 243.4 | 247.29 | 15.15 | 20.58 | 23.76 | 30.64 |
| Bharatpur | 557.6 | 449.36 | 16.18 | 60.62 | 74.76 | 87.28 |
| Bhilwara | 580.9 | 419.55 | 21.65 | 62.62 | 87.63 | 103.06 |
| Bikaner | 228.7 | 240.01 | 69.17 | 111.8 | 145.53 | 170.19 |
| Bundi | 655.9 | 362.95 | 7.44 | 27.16 | 34.32 | 40.02 |
| Chittorgarh | 709.7 | 318.60 | 14.25 | 33.86 | 41.97 | 48.79 |
| Churu | 313.7 | 133.95 | 31.08 | 69.26 | 82.72 | 94.25 |
| Dausa | 612.1 | 259.30 | 3.78 | 28.1 | 42.5 | 53.04 |
| Dhaulpur | 650.0 | 237.53 | 14.17 | 34.35 | 49.23 | 59.57 |
| Dungarpur | 637.8 | 128.12 | - | 11.07 | 13.13 | 13.59 |
| Ganganagar | 201.4 | 367.19 | 27.25 | 62.27 | 74.5 | 85.00 |
| Hanumangarh | 252.5 | 203.84 | 23.91 | 41.18 | 47.87 | 54.79 |
| Jaipur | 524.6 | 645.52 | 397.31 | 522.85 | 736.99 | 871.54 |
| Jaisalmer | 158.4 | 61.59 | 4.87 | 10.08 | 10.61 | 12.21 |
| Jalore | 394.2 | 422.00 | 3.02 | 19.73 | 27.24 | 34.78 |
| Jhalawar | 855.1 | 412.23 | 6.96 | 28.82 | 41.05 | 50.74 |
| Jhunjhunu | 410.0 | 240.00 | 12.86 | 58.04 | 74.48 | 86.49 |
| Jodhpur | 274.5 | 387.13 | 167.30 | 184.02 | 249.93 | 295.23 |
| Karauli | 637.4 | 336.97 | 9.73 | 27.33 | 35.33 | 42.28 |
| Kota | 746.3 | 513.3 | 189.92 | 180.49 | 259.00 | 306.89 |
| Nagaur | 348.5 | 524.26 | 20.86 | 83.51 | 114.37 | 137.16 |
| Pali | 446.7 | 296.30 | 20.04 | 53.61 | 64.64 | 74.39 |
| Pratapgarh* | 845.8 | - | - | - | - | - |
| Rajsamand | 506.0 | 106.86 | 4.45 | 23.96 | 34.89 | 42.10 |
| Sawai madhopur | 664.0 | 360.42 | 11.33 | 32.94 | 42.98 | 50.61 |
| Sikar | 402.5 | 291.11 | 31.29 | 82.96 | 114.04 | 134.71 |
| Sirohi | 868.6 | 274.85 | 2.87 | 27.31 | 39.32 | 47.39 |
| Tonk | 566.0 | 438.94 | 11.60 | 39.34 | 50.61 | 60.47 |
| Udaipur | 591.3 | 252.91 | 62.35 | 81.16 | 107.38 | 127.45 |

* Pratapgarh is a recently formed district and its data is not available.

#### *2.1.1.3 Domestic wastewater*

With an increase in population and urbanization, the wastewater rejection has also increased. The latest policies by the state government give environmental & ecological guidelines for water quality and pollution. It includes proper treatment of sewage and toxic effluent from the industries before discharging it into natural streams or to groundwater recharge. After proper treatment, the domestic wastewater can be used as a raw feed source for distillation. Domestic wastewater (DWW) for various cities is presented in Table 2.2. The projection for DWW for various cities is also reported here [31,32].

#### *2.1.1.4 Groundwater availability*

The water below the earth stored in aquifers and its depth varies from place to place. Groundwater (GW) potential available at different levels depends on recharge draft, pre-monsoon level and post-monsoon levels. In many parts of Rajasthan, the groundwater is brackish with high fluoride content [33]. With an increase or decrease in depth and with the external factors like pollution, rainfall and natural calamities, the contamination level of groundwater changes. The depth of water level which varies from place to place marks the area as safe, semi-critical, critical or overexploited for the groundwater resource utilization. The Government of India has identified such areas by analyzing replenishable groundwater resource over a period of two decades [34]. In India, the Ministry of Water Resources [33] conducted various studies on groundwater availability and its contamination. One of its reports states that in Rajasthan, the groundwater level has reached the overexploited condition. Further reports by the central and state government, on the water level and water content in the region, show that the amount of TDS are quite high as compared to the BIS standards for water quality [35].

A research work related to fluoride content in Rajasthan was performed by Jain and Singh [36] in which authors pointed out that most of the groundwater quality in the state does

not comply with WHO standards. They also discussed that in some of the districts, the local consume the water with fluoride level-up to 6 mg/l. Another study by Suthar *et al.* [37] reported a high level of fluoride contamination in state groundwater. During their research, the average fluoride concentration in drinking water of northern Rajasthan was recorded above its permissible limits of 0.5–1.0 mg/l to 2.82 mg/l. They reported that due to the higher fluoride level in drinking water, several cases of dental and skeletal fluorosis have appeared at an alarming rate in this region. Yadav *et al.* [38] determined the fluoride concentration in groundwater for the town in Tonk district, Rajasthan. They observed substantial dental fluorosis and skeletal fluorosis for more than 60% of the population in the area. They stressed the need for developmental strategies for safe drinking water supplies in the region. Research work on the water level in Shekhawati region by Sharma *et al*. [39] showed that the water fluoride content has exceeded its permissible limit. Similar research on water quality for Pilani region by Mitharwal *et al.* [40] reported that fluoride content and nitrate content makes groundwater unfit for drinking. In order to make the groundwater drinkable, there is a need to treat the same. A couple of research work also shows the use of statistical tools in understanding the fluctuation and dependency on various factors which effects the quality of groundwater [41,42].

### 2.1.2 Solar energy availability

The northwestern part of the state is blessed with an abundance of sunshine. The availability of such a large area can be utilized for solar related projects which include PV as well as CSP. With over more than 325 sunny days, the region receives the annual radiation in the form of global horizontal irradiance (GHI) and direct normal irradiance (DNI) from 1600 to 2200 kWh/$m^2$/yr. The threshold value of the annual DNI for power generation has been discussed by some researchers which range from 1800 kWh/$m^2$/yr [43,44] to 2000 kWh/$m^2$/yr [18]. The same range has been taken in the study for estimation of solar potential.

**Table 2.3 Rajasthan state with district features [7, 45, 46]**

| Location | Latitude (N) | Longitude (E) | DNI ($kWh/m^2$/ day) | GHI ($kWh/m^2$/ day) | Geographical area ($km^2$) | Wasteland ($km^2$) | % of wasteland area to the geographical area |
|---|---|---|---|---|---|---|---|
| Ajmer | 26.45 | 74.64 | 5.73 | 5.14 | 8,481 | 2158.22 | 25.45 |
| Alwar | 27.34 | 76.38 | 5.25 | 4.91 | 8,380 | 969.20 | 11.57 |
| Banswara | 23.55 | 74.45 | 5.70 | 5.17 | 5,037 | 1105.09 | 21.94 |
| Baran | 25.1 | 76.55 | 5.45 | 5.03 | 6,955 | 1899.26 | 27.31 |
| Barmer | 25.75 | 71.41 | 5.71 | 5.15 | 28,387 | 5019.12 | 17.68 |
| Bharatpur | 27.25 | 77.50 | 5.34 | 4.89 | 5,092 | 555.51 | 10.91 |
| Bhilwara | 25.35 | 74.66 | 5.72 | 5.11 | 10,455 | 3108.42 | 29.73 |
| Bikaner | 28.01 | 73.36 | 5.57 | 4.94 | 27,244 | 8450.91 | 31.02 |
| Bundi | 25.45 | 75.68 | 5.55 | 5.07 | 5,550 | 1412.80 | 25.46 |
| Chittorgarh | 24.90 | 74.70 | 5.82 | 5.15 | 7,822 | 2212.84 | 28.29 |
| Churu | 28.31 | 75.01 | 5.30 | 4.91 | 16,830 | 589.25 | 3.50 |
| Dausa | 26.90 | 76.36 | 5.43 | 4.97 | 3,432 | 351.93 | 10.25 |
| Dhaulpur | 26.77 | 77.88 | 5.24 | 4.95 | 3,008 | 861.64 | 28.64 |
| Dungarpur | 23.83 | 73.83 | 5.70 | 5.25 | 3,770 | 1351.54 | 35.85 |
| Ganganagar | 29.92 | 73.88 | 5.52 | 4.89 | 10,978 | 1271.27 | 11.58 |
| Hanumangarh | 29.58 | 74.35 | 5.42 | 4.89 | 9,656 | 329.30 | 3.41 |
| Jaipur | 26.91 | 73.36 | 5.56 | 5.20 | 11,143 | 1813.66 | 16.28 |
| Jaisalmer | 26.91 | 70.95 | 5.75 | 5.17 | 38,401 | 25059.53 | 65.26 |
| Jalore | 25.36 | 72.96 | 5.81 | 5.24 | 10,640 | 1438.64 | 13.52 |
| Jhalawar | 24.60 | 76.15 | 5.54 | 5.08 | 6,219 | 1649.81 | 26.53 |
| Jhunjhunu | 28.10 | 75.33 | 5.35 | 4.91 | 5,928 | 675.54 | 11.40 |
| Jodhpur | 26.30 | 73.06 | 5.73 | 5.23 | 22,850 | 5094.87 | 22.30 |
| Karauli | 26.50 | 77.06 | 5.34 | 4.95 | 5,524 | 1579.89 | 28.60 |
| Kota | 25.16 | 75.86 | 5.54 | 5.07 | 5,481 | 1074.38 | 19.60 |
| Nagaur | 27.20 | 73.66 | 5.72 | 5.20 | 17,718 | 1710.60 | 9.65 |
| Pali | 25.76 | 73.88 | 5.81 | 5.19 | 12,387 | 2549.39 | 20.58 |
| Pratapgarh | 24.03 | 74.78 | 5.61 | 5.15 | 4,117 | - | - |
| Rajsamand | 25.07 | 73.88 | 5.84 | 5.19 | 4,768 | 1858.98 | 38.99 |
| Sawai Madhopur | 25.96 | 76.05 | 5.50 | 5.03 | 5,003 | 809.10 | 16.17 |
| Sikar | 27.60 | 75.25 | 5.59 | 5.03 | 7,732 | 929.31 | 12.02 |
| Sirohi | 24.88 | 72.86 | 5.84 | 5.15 | 5,136 | 1701.17 | 33.12 |
| Tonk | 26.18 | 75.83 | 5.46 | 5.04 | 7,194 | 786.63 | 10.93 |
| Udaipur | 24.58 | 73.68 | 5.69 | 5.15 | 11,724 | 4550.91 | 38.82 |

For the analysis, the data of average DNI is taken by considering the average value of NASA and MNRE data at a given location [7,46]. The value of GHI is taken from NASA by taking the average of the last twenty year annual data [46]. The obtained GHI and DNI for the corresponding location with latitude and longitude are shown in Table 2.3. The areas having GHI greater than 1800 kWh/m$^2$/yr have been taken as the threshold for PV power based RO system while areas having DNI more than 2000 kWh/m$^2$/yr have been taken for CSP based MSF. The uncertainties in values of GHI and DNI have been considered by taking the values 10% lower than data obtained for estimation.

The graphical representation of GHI and DNI for the state is shown in Fig. 2.2. The graphical representation is made using the GIS tool ArcGIS (v10.2). It shows that the southwestern part of the state enjoys GHI and DNI more than 5.23 kWh/m$^2$/day and 5.74 kWh/m$^2$/day respectively.

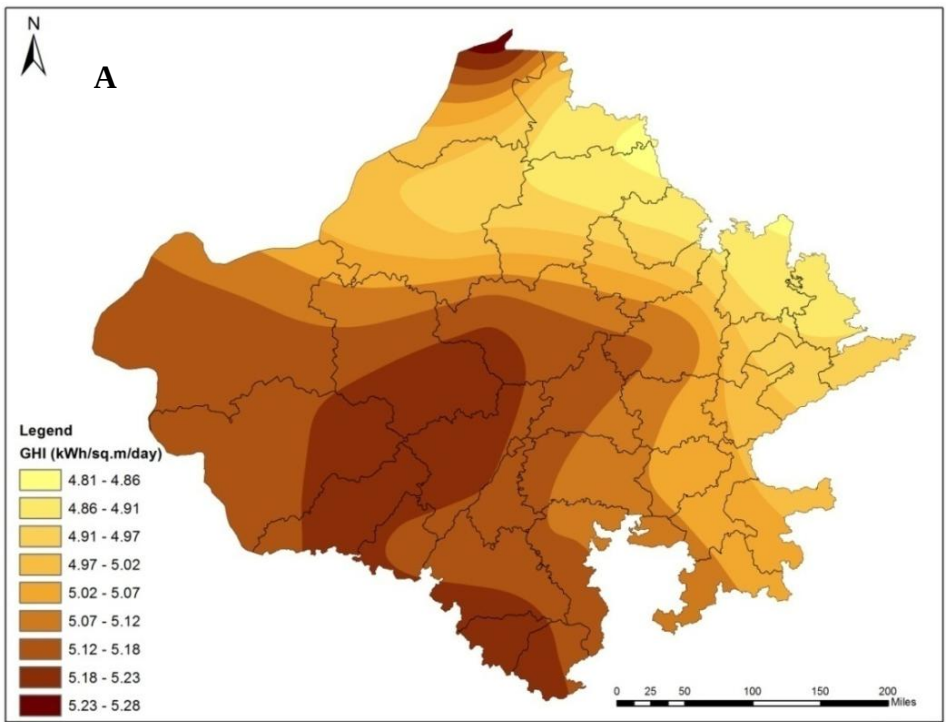


(a)

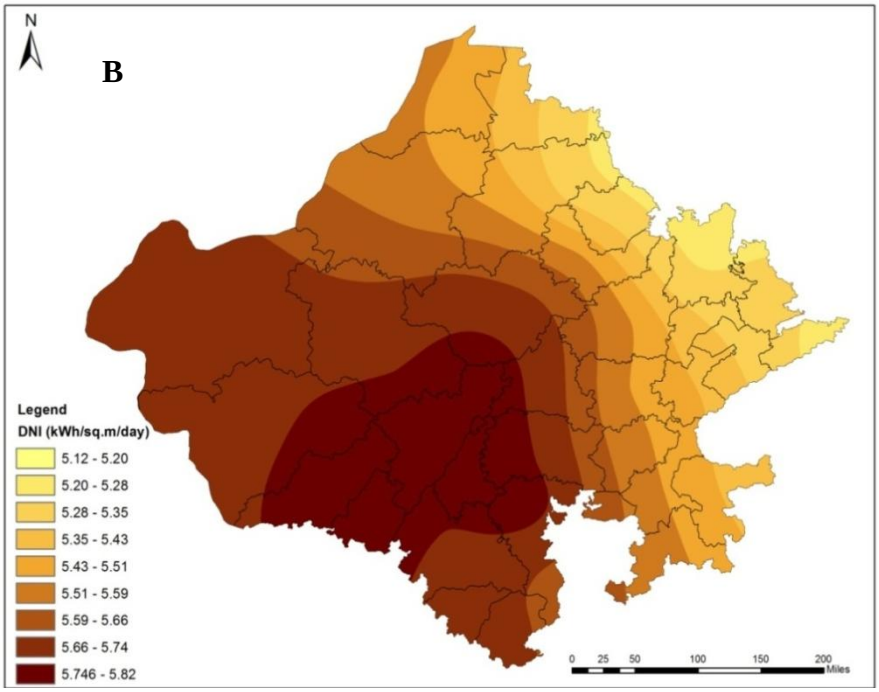


(b)

**Fig. 2.2 (a) GHI estimation of the Rajasthan state using current dataset (b) DNI estimation of the Rajasthan state using current dataset**

### 2.1.3 Land availability in Rajasthan

The land in Rajasthan consists of mixed terrain with a majority of underutilized flat wasteland. In the report of the department of land resources (DoLR), Government of Rajasthan [45], close to one-fourth of the state area is a wasteland. The available geographical and wasteland area of each district are shown in Table 2.3. From the table, it is observed that Jaisalmer district has major share of wasteland (65.25%) followed by Rajsamand district (39.64%). Thus the wasteland which is available in solar rich area can hold a huge potential for solar energy system installations. As per the DoLR, the wasteland in the state is categorized into 21 different types. Out of those categories, only 6 types of wasteland can be taken as solar suitable area according to the literature [47,48]. For the assessment of solar potential, a suitable wasteland for each district which is having solar radiation more than the threshold values are taken into consideration. The potentially solar suitable wasteland areas taken, as per their categories, are shown in Table 2.4. Since the solar

suitable areas also include tribal area, endangered species area, restricted area etc. thus, on the conservative side, only 30% of the solar suitable area is taken for geographical potential assessment [48]. Estimation for the suitable area is done by programming the threshold selection criteria in MATLAB (v2012a) and MS Office (2007). The wasteland area of each district, which as per the selection criteria seems suitable for solar power generation, is represented in Table 2.6. In terms of geographical potential, as per the said criteria, it is observed that maximum solar suitable area lies in Jaisalmer (43.88%) followed by Rajsamand (30.95%). Hanumangarh district has a minimum solar suitable area of 3.08% among all.

**Table 2.4 Selection of suitable wasteland area for PV and CSP projects. (Wasteland identification from DoLR) [45]**

| Sr. No. (DoLR category no) | Type of Wasteland | Suitability area for solar project ($km^2$) |
|---|---|---|
| 1. (1) | Gullied and/ or ravenous land (Medium) | 1087.52 |
| 2. (3) | Land with Dense Scrub | 21086.05 |
| 3. (4) | Land with Open Scrub | 15359.37 |
| 4. (13) | Degraded pastures/grazing land | 3438.40 |
| 5. (17) | Sands-Desertic | 3397.75 |
| 6. (19) | Sands semi-stabilized to stabilized dome 15–40 m | 14250.55 |
| | **Total suitable wasteland area of the state** | **58619.64** |

## 2.2 Estimation of Solar Potential and Water Availability

From the assessment of the available resources in the state, as discussed above, it is observed that solar energy can be effectively utilized to generate power in the state. For the same, the installation of solar power generation systems may be carried out on the identified wasteland, as per the selection criteria. It is also seen that there is an availability of water from various sources like rainwater, groundwater etc. By taking the raw feed from the available water resources, and with the selection criteria, it may be used in distillation units. These distillation units can easily be coupled with solar power generation systems.

The approach involved, to identify potential for solar PV and CSP combined with water distillation, is shown schematically in Fig. 2.3. This includes:

- Selection of data for solar irradiance, wasteland availability and water availability for the given location as per the threshold criteria.
- Estimating the potential for electricity generation, either by PV or CSP technologies that can be utilized for water distillation purpose.
- Selections of distillation technology, which can be coupled with solar based plant and provide fresh water from an input feed of raw water from different available sources.
- Mapping the potential of the state using GIS tool.

### 2.2.1 Solar PV potential

The suitable geographical wasteland area ($A_i$) which is obtained in $km^2$ is used for estimation of PV potential for electricity generation. Further within PV, the estimation has been carried out for the feasibility of using monocrystalline Silicon (m-Si), polycrystalline silicon (p-Si) and Thin Film (TF) technologies having power generation efficiency of 12.6%, 10.45% and 9% respectively. The technical potential ($E_i$) for each technology is calculated by using Eq. (2.1) which is given as [49,50].

$$E_i = A_i \times GHI \times h \times \eta_c \times p_r \quad (2.1)$$

In Eq. (2.1) for the grid cell *i*, the geographical area $A_i$ is a suitable area for PV installation, GHI is the solar insolation in $kWh/m^2/day$, $h$ is the number of sunshine hour in a year and is taken from 2700 to 3300 hr/yr depending upon the area, $\eta_c$ is the PV panel efficiency and $p_r$ is the performance ratio of the plant.

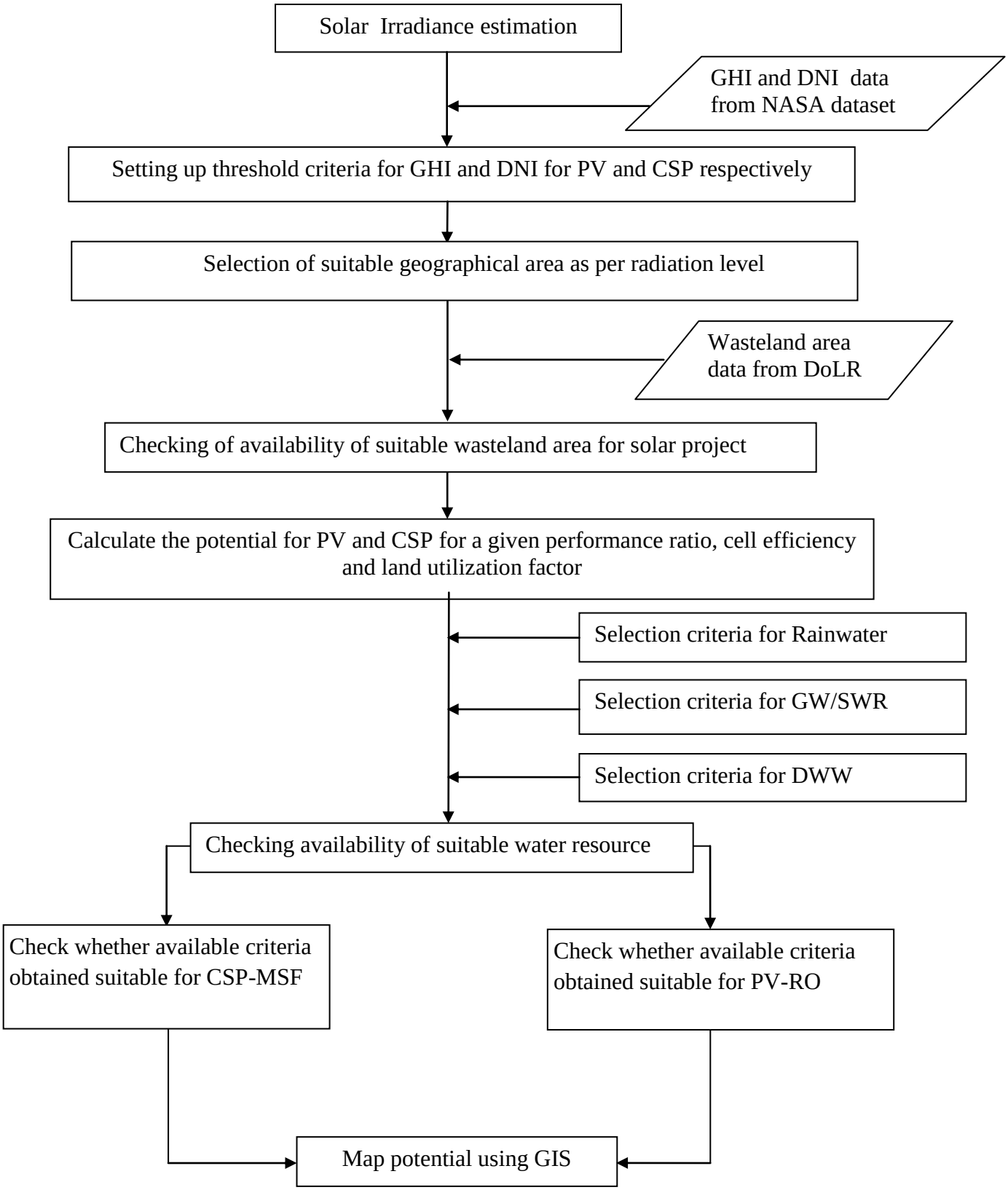


**Fig. 2.3 Schematic representation of the adopted methodology**

The sunshine hours of state are estimated by dividing state into seven zones by combining districts as north (2900 hr/yr), west (3300 hr/yr), south (3100 hr/yr), center (3000 hr/yr), northeast (2700 hr/yr) and southeast (2800 hr/yr). The cell efficiency depends upon the type of PV panel used as well as module temperature. The literature discusses cell efficiency in the range of 9-16%. The performance ratio ($p_r$), which is the ratio of actual performance of the cell to the performance of cell under standard conditions of 1000 W/m$^2$ solar insolation, 25 °C ambient temperature and air mass of 1.5. It is the worldwide accepted standard for measuring the performance of the plant to identify the relationship between actual and theoretical possible energy output of the plant. Generally, it is taken from 0.66 to 0.85 [51]. For the current study using three different types of solar cells i.e. m-Si, p-Si and TF, the potential estimation has been carried out for each scenario using efficiency and performance ratio as discussed in the literature.

### 2.2.2 Solar CSP potential

In case of CSP, the potential has been carried out for LFR, PTC and CTR technologies. The potential using these technologies also depends upon various factors like type of technology used, geographical area, land usage factor, land use efficiency, etc [18]. The range of land use factor and land use efficiency (Le) are discussed in Table 2.5 [52]. For the analysis, CSP plants with different technology are studied for the potential estimation for MSF. The land use efficiency for LFR, PTC and CTR technology are taken as per Table 2.5. The power generation technical potential ($E_i$) for each technology of CSP is then calculated using Eq. (2.2).

$$E_i = A_i \times DNI \times h \times Le \tag{2.2}$$

**Table 2.5 CSP type and their features [50,52]**

| Collector & power cycle technology | Solar-electric aperture related efficiency | Land use factor | Land use efficiency (Le) (%) |
|---|---|---|---|
| Parabolic trough steam cycle | 11-16 | 25-40 | 3.5-5.6 |
| Central receiver steam cycle | 12-16 | 20-25 | 2.5-4.0 |
| Linear Fresnel steam cycle | 8-12 | 60-80 | 4.8-9.6 |

Here DNI is beam radiation in kWh/m$^2$/day. The values of $A_i$ and $h$ are taken same as in Eq. (2.1). 'Solar-electric aperture related efficiency' is the ratio of average land use efficiency with land use factor. It represents the amount of radiation falling on the CSP receiver which can be converted into grid supplied electricity. Land use factor is the ratio of area cover by CSP collector system to the available land area. The estimated electric potential for each of the technologies in PV and CSP is calculated and is shown in Table 2.6. It is assumed that the electrical energy thus obtained is fully utilized in the distillation plants.

### 2.2.3 Water potential estimation for distillation

The water availability from various SWR like lakes, canals, dams and river in the state can provide sufficient water for distillation. However, while consuming water from these resources, the balance needs to be maintained to avoid any scarcity of water for other applications. In the current assessment for water availability for solar distillation units, a fraction of water, which ranges from 0 - 5 MLD is taken from available water resources. This may change with external factors like an increase in demand for river water, canal, water stored in dams etc.

**Table 2.6 Power generation potential estimation across the districts**

| Location | Wasteland suitable for solar ($km^2$) | % of solar suitable wasteland to geographical area | Potential of PV for various technologies (GW) | | | Potential for CSP for various technologies (GW) | | |
|---|---|---|---|---|---|---|---|---|
| | | | m-Si | p-Si | TF | LFR | PTC | CTR |
| Ajmer | 1770.50 | 20.88 | 31.54 | 23.75 | 21.34 | 26.02 | 16.78 | 11.30 |
| Alwar | 592.38 | 7.07 | 9.07 | 6.83 | 6.14 | 7.18 | 4.63 | 3.12 |
| Banswara | 367.94 | 7.30 | 6.81 | 5.13 | 4.61 | 5.56 | 3.58 | 2.41 |
| Baran | 625.18 | 8.99 | 10.17 | 7.66 | 6.88 | 8.16 | 5.26 | 3.54 |
| Barmer | 3043.13 | 10.72 | 59.75 | 44.99 | 40.43 | 49.03 | 31.61 | 21.29 |
| Bharatpur | 415.32 | 8.16 | 6.10 | 4.59 | 4.13 | 4.93 | 3.18 | 2.14 |
| Bhilwara | 2545.72 | 24.35 | 45.09 | 33.95 | 30.50 | 37.35 | 24.08 | 16.22 |
| Bikaner | 7307.81 | 26.82 | 120.95 | 91.08 | 81.83 | 100.93 | 65.07 | 43.82 |
| Bundi | 445.80 | 8.03 | 7.31 | 5.51 | 4.95 | 5.92 | 3.82 | 2.57 |
| Chittorgarh | 1209.11 | 15.46 | 22.30 | 16.79 | 15.09 | 18.65 | 12.03 | 8.10 |
| Churu | 570.70 | 3.39 | 9.39 | 7.07 | 6.35 | 7.50 | 4.84 | 3.26 |
| Dausa | 276.31 | 8.05 | 4.28 | 3.23 | 2.90 | 3.46 | 2.23 | 1.50 |
| Dhaulpur | 514.55 | 17.11 | 7.65 | 5.76 | 5.18 | 5.99 | 3.86 | 2.60 |
| Dungarpur | 976.60 | 25.90 | 18.36 | 13.83 | 12.42 | 14.75 | 9.51 | 6.41 |
| Ganganagar | 1253.81 | 11.42 | 22.26 | 16.77 | 15.06 | 17.16 | 11.06 | 7.45 |
| Hanumangarh | 297.81 | 3.08 | 4.88 | 3.67 | 3.30 | 4.00 | 2.58 | 1.74 |
| Jaipur | 1281.50 | 11.50 | 20.79 | 15.65 | 14.06 | 16.45 | 10.60 | 7.14 |
| Jaisalmer | 16850.29 | 43.88 | 332.12 | 250.10 | 224.71 | 273.37 | 176.25 | 118.70 |
| Jalore | 1041.12 | 9.78 | 20.80 | 15.66 | 14.07 | 17.07 | 11.00 | 7.41 |
| Jhalawar | 1101.45 | 17.71 | 18.10 | 13.63 | 12.25 | 14.61 | 9.42 | 6.34 |
| Jhunjhunu | 445.20 | 7.51 | 6.82 | 5.13 | 4.61 | 5.50 | 3.55 | 2.39 |
| Jodhpur | 4306.93 | 18.85 | 85.87 | 64.67 | 58.10 | 69.63 | 44.89 | 30.23 |
| Karauli | 439.69 | 7.96 | 6.54 | 4.92 | 4.42 | 5.22 | 3.37 | 2.27 |
| Kota | 516.24 | 9.42 | 8.47 | 6.38 | 5.73 | 6.85 | 4.41 | 2.97 |
| Nagaur | 1395.36 | 7.88 | 25.15 | 18.94 | 17.01 | 20.47 | 13.20 | 8.89 |
| Pali | 1967.75 | 15.89 | 38.93 | 29.32 | 26.34 | 32.26 | 20.80 | 14.01 |
| Rajsamand | 1475.65 | 30.95 | 27.43 | 20.65 | 18.56 | 22.84 | 14.73 | 9.92 |
| Sawaimadhopur | 439.56 | 8.79 | 6.64 | 5.00 | 4.49 | 5.37 | 3.46 | 2.33 |
| Sikar | 600.46 | 7.77 | 9.42 | 7.09 | 6.37 | 7.75 | 5.00 | 3.36 |
| Sirohi | 1057.71 | 20.59 | 20.77 | 15.64 | 14.05 | 17.43 | 11.24 | 7.57 |
| Tonk | 662.52 | 9.21 | 11.57 | 8.71 | 7.83 | 9.28 | 5.98 | 4.03 |
| Udaipur | 2825.55 | 24.10 | 52.11 | 39.24 | 35.26 | 42.61 | 27.47 | 18.50 |
| **Total** | **58619.65** | **--** | **1077.44** | **811.36** | **728.99** | **883.31** | **569.50** | **383.54** |

Another water source besides SWR is taken from rainwater harvesting and groundwater utilization. The rainwater harvesting technique is widely used to conserve water and use it for various applications. Literature shows that rainfall harvesting potential depends upon the amount of rainfall received and catchment area [39]. With proper planning and policies for the rainwater harvesting, the huge area of the state can provide tremendous potential for conserving water and meet daily needs [53,54]. For the study, it is taken that both rainwater and groundwater can provide an average of 2 MLD of water in the state. Similarly, based on the availability of DWW, it is assumed that after proper treatment, 70% of the DWW could be used as a raw source for distillation plants.

The study discusses the use of SWR which can be used as raw feed for solar based distillation plants. For the RO based plants, only the raw feed available from rainwater harvesting and river, canal etc is taken. On the other hand, for MSF, the treated water available from DWW and groundwater is considered. This assumption would help to reduce the extra energy consumption for RO and MSF plants, as treated DWW may require higher energy in RO units than MSF plants. Similarly, groundwater can easily be treated and make potable using MSF technology instead of RO systems. The river water and rainwater, which has low TDS, can easily be treated in RO systems by consuming less energy.

## 2.3 Choice of Distillation Technology

It is discussed in the previous section that solar energy assisted water purification technology solely depends on TDS level in the water. Thus, it can be termed as distillation or desalination based on the amount of TDS and type of technology used. In both cases, it is dependent upon energy requirement, availability of raw water, the capacity of plant etc. For instance, as per the literature [55], MSF process would require 35 $kWh/m^3$ of energy (equivalent electricity) to give fresh water having less than 10 ppm of TDS. However, to

make it potable suitable minerals need to be added. RO process consumes 0.4 - 7 kWh/$m^3$ of electrical energy to produce fresh water having less than 500 ppm of TDS, which is suitable for drinking purpose [55]. Thus to adopt suitable technology distillation, such parameters should be taken care of.

In the current study, two technologies i.e. MSF and RO are considered for analysis. These technologies can easily be coupled with solar thermal and PV respectively. The raw water feed for both the technologies is taken from the district water availability resource. For simplicity, it is assumed that the district headquarters will represent the entire district with respect to the water supply. As shown in Table 2.2, the water supply for such plant could be RW, GW, partially treated DWW or SWR. The estimation of potential for all the districts of the state has been carried out except Pratapgarh as it is a newly formed district and its data is not available. Water availability is calculated by estimating the number of rivers, canals, lakes and dams in the district which may provide water as raw feed. The water from the RW & SWR are taken as raw feed for the RO purpose as it is assumed that such water content has moderate TDS and are suitable for such systems. Sambhar Lake, being an exception, which lies on the border of Jaipur and Ajmer, is taken as feed for MSF system in Jaipur district as its water is saline in nature. Thus, besides salt production, MSF here would provide fresh water which may be utilized for drinking purpose after mineralization. For the rest of the MSF case, the raw feed of GW and treated DWW is taken for consideration. The availability might increase if RW and river water is taken as feed, but they are more suitable for RO systems because of low TDS content. For assessment of distillation potential at the district level, the raw water feed for both the technologies is taken from the available resource of that district.

### 2.3.1 PV assisted RO plants

The RO plant operates on the electrical energy for distilling water with the help of membranes. On average, a typical low concentration RO plant utilizes 5 kWh/$m^3$ of electrical energy and produces 6 million liters per day (MLD), as shown in Table 2.7 [56]. For higher concentration (TDS >10000) the energy varies from 7 - 10 kWh/$m^3$ [57]. The average electrical consumption of 7 kWh/$m^3$ is taken for the analysis, with a plant capacity of 6 MLD. During the analysis, it is assumed that the power generation from the PV will be utilized for the RO plant. Thus the regions having potential energy generation less than threshold energy requirement of RO plants are eliminated. For a plant of capacity 6 MLD, with electrical consumption of 7 kWh/$m^3$, the power requirement will be 42 MWh/day. The areas having threshold radiation more than 1800 kW/$m^2$/day and may generate the daily electrical power of 1.75 MW are chosen. The water availability for RO plant using raw feed water from RW harvesting and SWR is shown in Table 2.8. The availability of water resource determined the feasibility of RO plants.

**Table 2.7 Technical features of a typical distillation technology [56]**

| **Distillation technology** | **MSF** | **RO** |
|---|---|---|
| Typical average capacity (MLD) | 25 | 6 |
| Maximum average capacity (MLD) | 50 | 10 |
| Thermal energy consumption (kWh/$m^3$) | 80 | - |
| Electric energy consumption (kWh/$m^3$) | 4 | 5 |
| Total equivalent electric energy consumption (kWh/$m^3$) | 15 | 5 |

**Table 2.8 Power generation potential for different PV technologies along with water availability potential for RO**

| Location | GHI ($kWh/m^2/day$) | Potential of PV (GWh/yr) | | | Water availability potential for RO (MLD) |
|---|---|---|---|---|---|
| | | m-Si | p-Si | TF | |
| Ajmer | 5.14 | 31.54 | 23.75 | 21.34 | 10.14 |
| Alwar* | 4.91 | 9.07 | 6.83 | 6.14 | 6.47 |
| Banswara | 5.17 | 6.81 | 5.13 | 4.61 | 6.19 |
| Baran | 5.03 | 10.17 | 7.66 | 6.88 | 4.96 |
| Barmer | 5.15 | 59.75 | 44.99 | 40.43 | 13.64 |
| Bharatpur* | 4.89 | 6.10 | 4.59 | 4.13 | 6.97 |
| Bhilwara | 5.11 | 45.09 | 33.95 | 30.50 | 14.63 |
| Bikaner | 4.94 | 120.95 | 91.08 | 81.83 | 9.72 |
| Bundi | 5.07 | 7.31 | 5.51 | 4.95 | 5.60 |
| Chittorgarh | 5.15 | 22.30 | 16.79 | 15.09 | 14.97 |
| Churu* | 4.91 | 9.39 | 7.07 | 6.35 | 6.83 |
| Dausa | 4.97 | 4.28 | 3.23 | 2.90 | 4.20 |
| Dhaulpur | 4.95 | 7.65 | 5.76 | 5.18 | 8.73 |
| Dungarpur | 5.25 | 18.36 | 13.83 | 12.42 | 6.80 |
| Ganganagar | 5.30 | 22.26 | 16.77 | 15.06 | 8.14 |
| Hanumangarh* | 4.89 | 4.88 | 3.67 | 3.30 | 9.57 |
| Jaipur | 5.20 | 20.79 | 15.65 | 14.06 | 15.83 |
| Jaisalmer | 5.17 | 332.12 | 250.10 | 224.71 | 4.78 |
| Jalore | 5.24 | 20.80 | 15.66 | 14.07 | 10.37 |
| Jhalawar | 5.08 | 18.10 | 13.63 | 12.25 | 4.79 |
| Jhunjhunu* | 4.91 | 6.82 | 5.13 | 4.61 | 2.19 |
| Jodhpur | 5.23 | 85.87 | 64.67 | 58.10 | 17.23 |
| Karauli | 4.95 | 6.54 | 4.92 | 4.42 | 5.49 |
| Kota | 5.07 | 8.47 | 6.38 | 5.73 | 18.99 |
| Nagaur | 5.20 | 25.15 | 18.94 | 17.01 | 8.91 |
| Pali | 5.19 | 38.93 | 29.32 | 26.34 | 27.93 |
| Rajsamand | 5.15 | 27.43 | 20.65 | 18.56 | 7.63 |
| Sawaimadhopur | 5.19 | 6.64 | 5.00 | 4.49 | 16.84 |
| Sikar | 5.03 | 9.42 | 7.09 | 6.37 | 1.81 |
| Sirohi | 5.03 | 20.77 | 15.64 | 14.05 | 14.78 |
| Tonk | 5.15 | 11.57 | 8.71 | 7.83 | 16.96 |
| Udaipur | 5.04 | 52.11 | 39.24 | 35.26 | 20.49 |
| **Total** | **-** | **1077.44** | **811.36** | **728.99** | **332.58** |

* The area receives less radiation than the threshold criteria of GHI.

From Table 2.8, it is observed that PV power generation potential is the highest in the western part of the state. This is due to the fact that this region receives enormous solar insolation throughout the year. The maximum PV potential, irrespective of the technology used, is obtained in Jaisalmer district followed by Bikaner and Jodhpur. Hanumangarh districts have the minimum power potential in all three technologies. The total potential of entire state using m-Si, p-Si and TF technology is 1077.44 GW, 811.36 GW and 728.99 GW respectively. In terms of water availability for RO, Pali district has the maximum availability of raw feed water of 27.93 MLD from SWR and RW thus, suitable for such systems. Sikar district (1.81 MLD) has the minimum availability of water supply, even below the threshold requirement of RO plant due to the absence of any SWR in the district. The power potential and water availability potential for the state for m-Si, p-Si and TF technologies are mapped graphically using GIS in Fig. 2.4.

It is clear from Fig. 2.4 (a) that Hanumangarh district, though have sufficient water availability for RO plant of capacity 6 MLD or more, lacks sufficient power generation potential using m-Si, as per the criteria used in the current research. The availability of water from Ganga canal in Bikaner and from river Luni in Jodhpur makes these districts suitable location for m-Si based RO plants. Jaisalmer, although having the highest power potential in the state, lacks adequate water supply for RO system based on defined criteria. Dausa district is the only one lacking sufficient water as well as power potential as per the defined criteria. From Fig. 2.4 (b), it is observed that Hanumangarh, Bharatpur and Sawaimadhopur district although hold the sufficient water potential for RO system but lacks power potential using p-Si as solar radiation in these districts are below the threshold criteria of the current study. Fig. 2.4 (c), which depicts the potential of TF technology reveals that seven districts lack sufficient power generation capability and three districts lack water availability potential for RO plant of capacity 6 MLD.

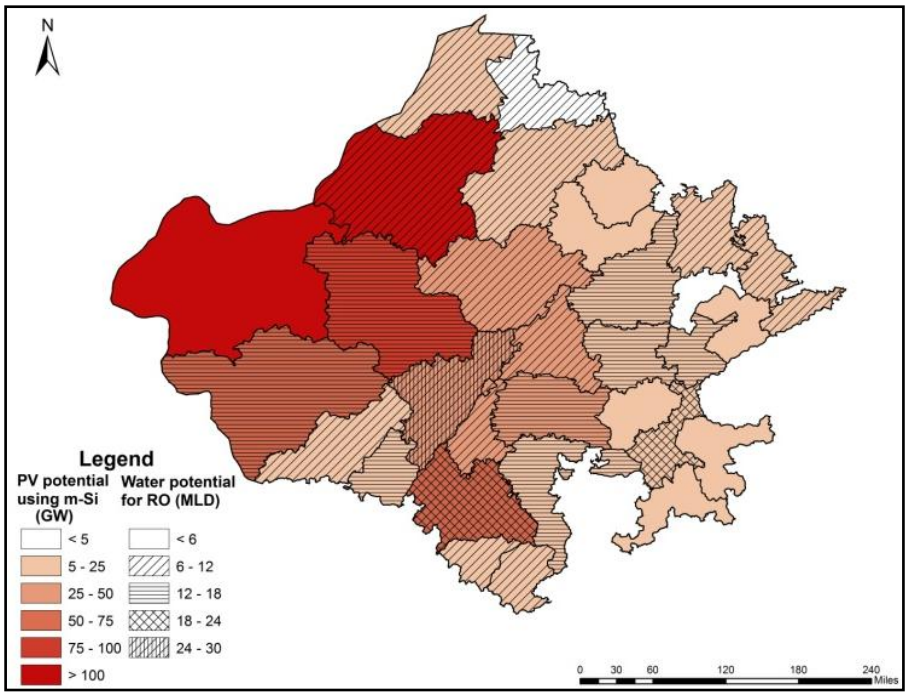
N
Legend
PV potential using m-Si (GW)
< 5
5 - 25
25 - 50
50 - 75
75 - 100
> 100
Water potential for RO (MLD)
< 6
6 - 12
12 - 18
18 - 24
24 - 30
0 30 60 120 180 240
Miles

(a)

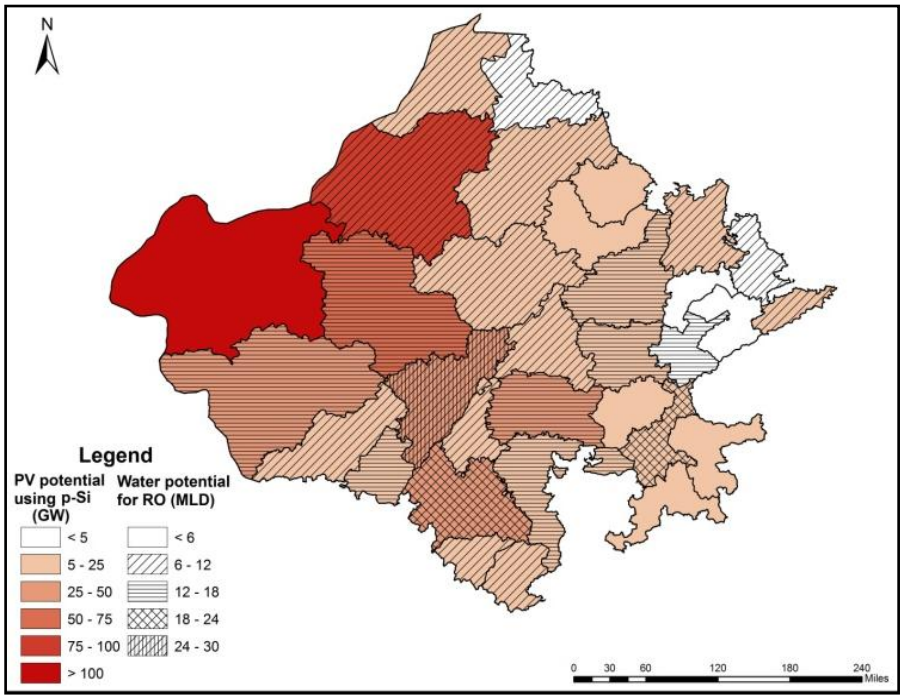
N
Legend
PV potential using p-Si (GW)
< 5
5 - 25
25 - 50
50 - 75
75 - 100
> 100
Water potential for RO (MLD)
< 6
6 - 12
12 - 18
18 - 24
24 - 30
0 30 60 120 180 240
Miles

(b)

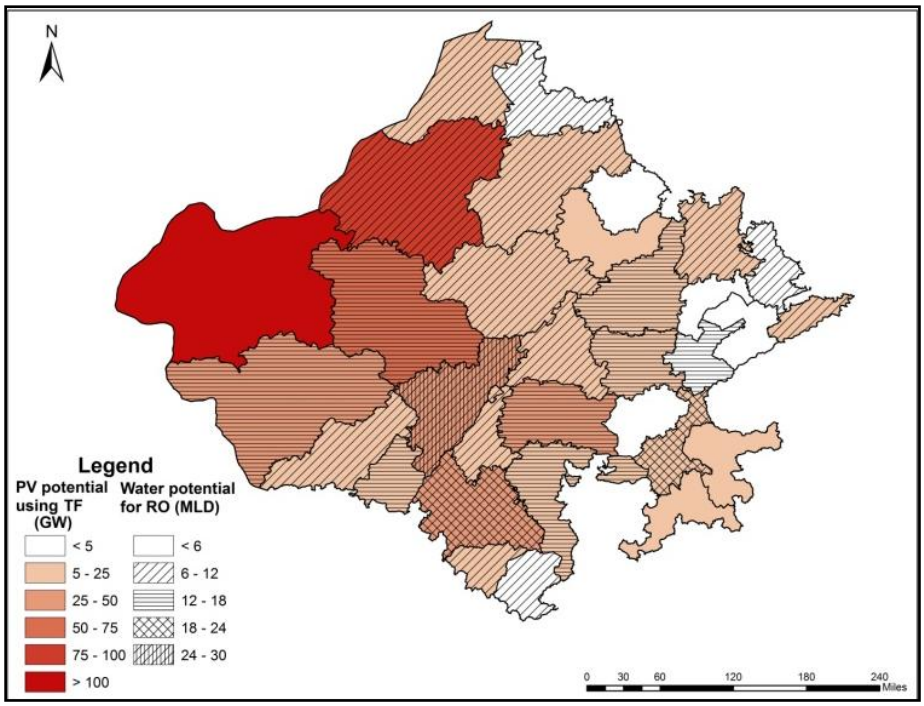


(c)

**Fig. 2.4 Available water potential for RO operated plant in Rajasthan using power from (a) monocrystalline silicon cell (m-Si) (b) polycrystalline silicon cell (p-Si) (c) thin film silicon cell (TF)**

### 2.3.2 CSP assisted MSF plants

Similar to the approach of RO plant selection, the MSF plants are selected for the average capacity of 25 MLD with power consumption of 35 kWh/$m^3$. The average energy consumption of MSF would be around 278.6 kJ/kg of water distillate [58]. For CSP based MSF plants, DNI greater than 2000 kWh/$m^2$/yr is considered. This gives the daily threshold requirement of 875 MWh equivalent electrical energy. Thus the districts having more than threshold solar radiation and can generate the electrical power of 15.6 MW with available water feed of more than 25 MLD are chosen. The raw water supply for MSF is taken as GW and treated DWW. The combined value represents the potential for water availability for MSF plants. Similarly, the power potential using different CSP technologies are estimated using Eq. (2.2) and is shown in Table 2.9 along with water availability potential for MSF plant. It is observed that similar to PV, the power generation scenario is highest in Jaisalmer

followed by Bikaner and Jodhpur for all CSP technologies. The minimum potential for power generation lies in Dausa district for each technology. This may be due to lack of sufficient DNI and solar suitable wasteland in the district. The total potential for CSP it is calculated as 883.31 GW, 569.50 GW and 383.54 GW for LFR, PTC and CTR respectively. The potential raw water availability estimation for MSF reveals that Jaipur has the maximum water availability (280.02 MLD), followed by Kota (133.46 MLD) and Jodhpur (117.50 MLD). These districts have a higher potential due to the fact that being urban cities, they can provide a large quantity of treated DWW for MSF operation. The location of India's largest Salt Lake in Jaipur district also plays an important role in increasing the water potential of the district. The minimum water availability potential is observed in district Sirohi (2.28 MLD) followed by Jalore (2.54 MLD) and Dausa (2.91 MLD).

The graphical representation of estimated potential for CSP coupled with MSF is shown in Fig. 2.5. It is observed that the lack of adequate water availability in district Jaisalmer makes it unsuitable for LFR based MSF technology. Only six districts have the feasibility of having MSF plant of this capacity under the current set of conditions. The situation changes when PTC technology is used instead of LFR for power generation. As shown in Table 2.9, the water potential for MSF remains same as that of LFR, but many districts would not be able to produce even 5 GW for MSF technology under the current set of assumptions. It is visible from Fig. 2.5 (b) that Kota district, which holds sufficient water availability, lacks power generation to sustain MSF plant. Thus, it is not advisable to setup PTC based MSF plant in such region under the current set of assumptions. A similar case of deficient power generation potential for Kota is also observed when CTR technology is used for MSF, which is mapped in Fig. 2.5 (c).

**Table 2.9 Power generation potential for different CSP technologies along with water availability potential for MSF**

| Location | DNI ($kWh/m^2/day$) | Potential for CSP (GW) | | | Water availability potential for MSF (MLD) |
|---|---|---|---|---|---|
| | | LFR | PTC | CTR | |
| Ajmer | 5.73 | 26.02 | 16.78 | 11.30 | 65.75 |
| Alwar* | 5.25 | 7.18 | 4.63 | 3.12 | 16.75 |
| Banswara# | 5.70 | 5.56 | 3.58 | 2.41 | 5.15 |
| Baran* | 5.45 | 8.16 | 5.26 | 3.54 | 4.77 |
| Barmer | 5.71 | 49.03 | 31.61 | 21.29 | 10.85 |
| Bharatpur* | 5.34 | 4.93 | 3.18 | 2.14 | 11.78 |
| Bhilwara | 5.72 | 37.35 | 24.08 | 16.22 | 15.57 |
| Bikaner | 5.57 | 100.93 | 65.07 | 43.82 | 48.66 |
| Bundi | 5.55 | 5.92 | 3.82 | 2.57 | 5.57 |
| Chittorgarh | 5.82 | 18.65 | 12.03 | 8.10 | 10.29 |
| Churu* | 5.30 | 7.50 | 4.84 | 3.26 | 21.89 |
| Dausa* | 5.43 | 3.46 | 2.23 | 1.50 | 2.91 |
| Dhaulpur* | 5.24 | 5.99 | 3.86 | 2.60 | 10.16 |
| Dungarpur# | 5.70 | 14.75 | 9.51 | 6.41 | - |
| Ganganagar | 5.52 | 17.16 | 11.06 | 7.45 | 19.44 |
| Hanumangarh* | 5.42 | 4.00 | 2.58 | 1.74 | 16.94 |
| Jaipur | 5.56 | 16.45 | 10.60 | 7.14 | 280.02 |
| Jaisalmer | 5.75 | 273.37 | 176.25 | 118.70 | 3.47 |
| Jalore | 5.81 | 17.07 | 11.00 | 7.41 | 2.54 |
| Jhalawar | 5.54 | 14.61 | 9.42 | 6.34 | 5.28 |
| Jhunjhunu* | 5.35 | 5.50 | 3.55 | 2.39 | 9.24 |
| Jodhpur | 5.73 | 69.63 | 44.89 | 30.23 | 117.50 |
| Karauli* | 5.34 | 5.22 | 3.37 | 2.27 | 7.15 |
| Kota | 5.54 | 6.85 | 4.41 | 2.97 | 133.46 |
| Nagaur | 5.72 | 20.47 | 13.20 | 8.89 | 15.13 |
| Pali | 5.81 | 32.26 | 20.80 | 14.01 | 14.32 |
| Rajsamand | 5.84 | 22.84 | 14.73 | 9.92 | 3.22 |
| Sawaimadhopur | 5.50 | 5.37 | 3.46 | 2.33 | 8.29 |
| Sikar | 5.59 | 7.75 | 5.00 | 3.36 | 22.19 |
| Sirohi | 5.84 | 17.43 | 11.24 | 7.57 | 2.28 |
| Tonk* | 5.46 | 9.28 | 5.98 | 4.03 | 8.56 |
| Udaipur | 5.69 | 42.61 | 27.47 | 18.50 | 43.90 |
| **Total** | **-** | **883.31** | **569.50** | **383.54** | **943.04** |

* The area receives less radiation than the threshold criteria of DNI.

# The districts have more than 50% of endangered tribal population.

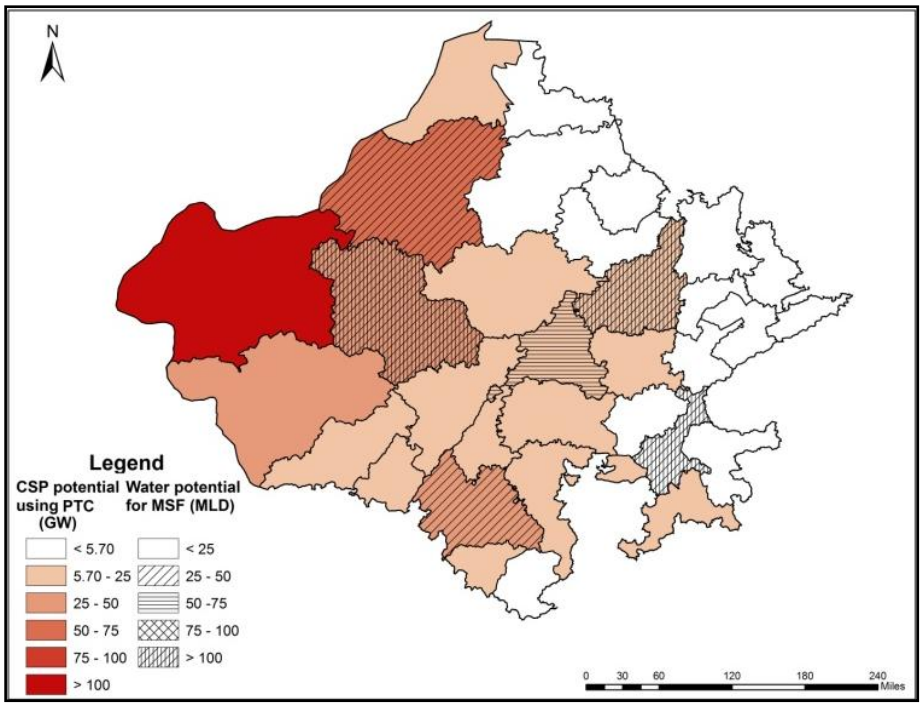
N
Legend
CSP potential using PTC (GW)
< 5.70
5.70 - 25
25 - 50
50 - 75
75 - 100
> 100
Water potential for MSF (MLD)
< 25
25 - 50
50 -75
75 - 100
> 100
0 30 60 120 180 240
Miles

(a)

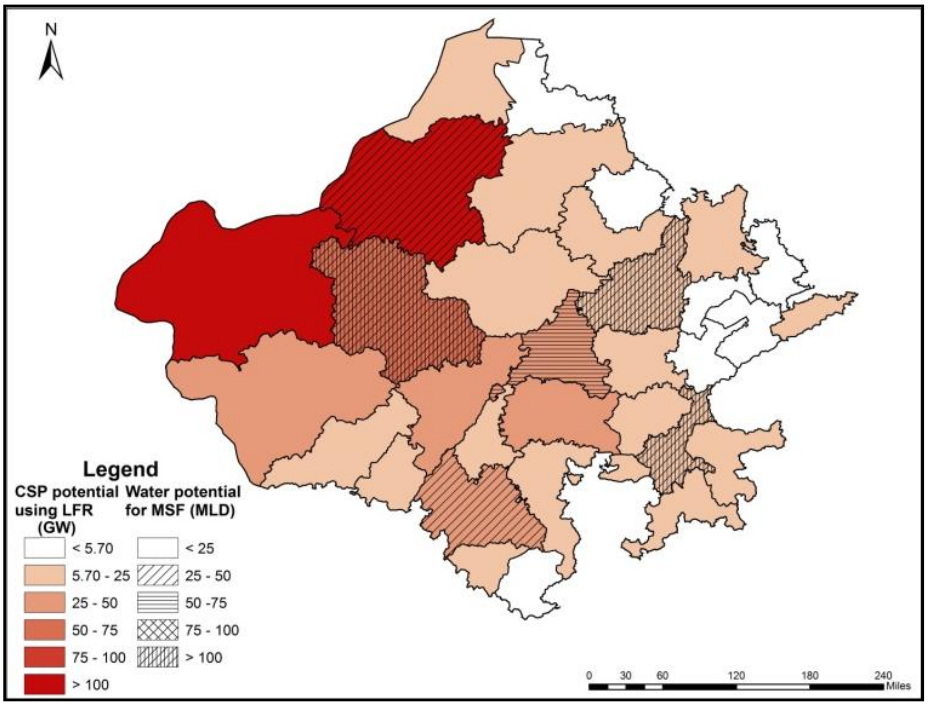
N
Legend
CSP potential using LFR (GW)
< 5.70
5.70 - 25
25 - 50
50 - 75
75 - 100
> 100
Water potential for MSF (MLD)
< 25
25 - 50
50 -75
75 - 100
> 100
0 30 60 120 180 240
Miles

(b)

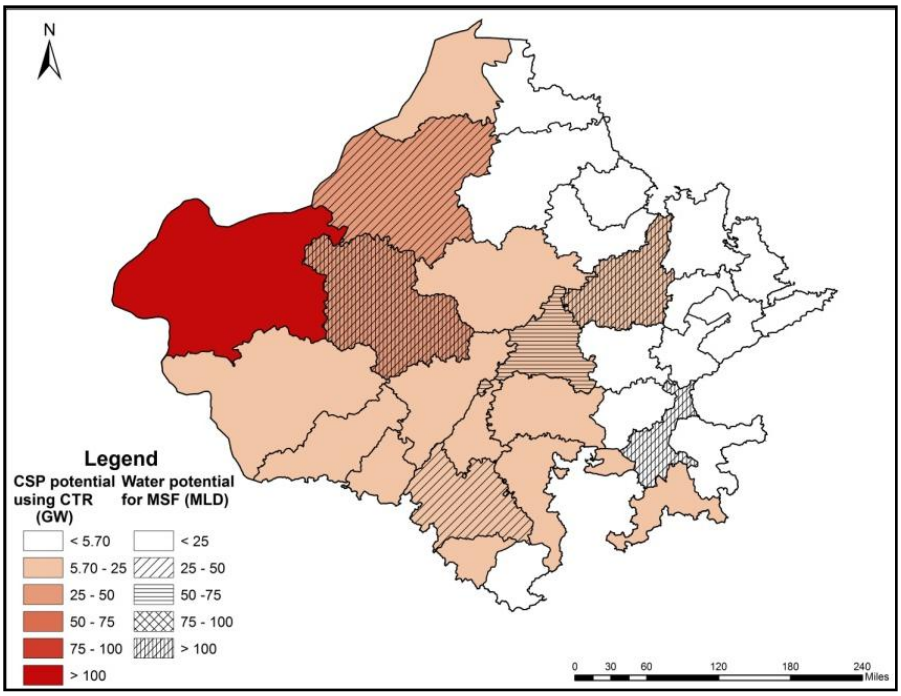


(c)

**Fig. 2.5 Available water potential for MSF operated plant using power from (a) linear Fresnel concentrator (LFR) (b) parabolic trough collector (PTC) (c) central tower receiver (CTR) in Rajasthan**

## 2.4 Concluding Remarks

An attempt has been done to carry out the pre-feasibility analysis for distillation using solar energy in the state of Rajasthan, India. The electrical solar power potential of each district is calculated by estimating the suitable wasteland area, annual GHI and DNI, and technical parameters of concerned technologies. It is observed that the western part of the state, *viz*, Jaisalmer, Bikaner and Jodhpur, has the highest PV and CSP power generation potential using any of the respective technologies. This region has the potential of 50% power generation for the entire state using respective PV and CSP technologies. The potential estimated for using m-Si, p-Si and TF technology for power generation is 1077.44 GW, 811.36 GW and 728.99 GW respectively. The Rajasthan has the power generation potential of 883.31 GW, 569.50 GW and 383.56 GW using LFR, PTC and CTR technology respectively.

The water availability in the state depends on available resources which primarily includes Indira Gandhi canal, Ganga canal, Luni and Chambal river, state annual monsoon and groundwater availability. An attempt has been done to identify the water availability of each district based on their parameters as discussed above. When combining the electrical potential with water availability scenario, Jaipur district holds the top position for maximum availability of water supply to have MSF solar plants using any of CSP technology because of the presence of Sambhar Lake in the district. For RO, Pali district, followed by Udaipur district has the highest water availability potential. It is observed that Dausa district is the only one which lacks adequate water supply to have RO plant with m-Si technology having capacity more than 6 MLD. Hanumangarh district has the minimum wasteland for solar power and thus lacks sufficient power generation potential although it has sufficient water availability for RO plants. The estimated potential for power generation and corresponding feasibility of having PV based RO or CSP based MSF plants are mapped using GIS tool.

# CHAPTER 3

# LITERATURE REVIEW

*This chapter presents a technical review of the prior research work carried out in the following areas:*

- *Water distillation technologies*
- *PTC technology*
- *PVT and CPVT technologies*
- *Second law of thermodynamics analysis of such technologies*

*The main purpose of this review is to identify the work carried out in Indian scenario as most of such works are related to European or US conditions and to identify research gaps in the area of solar based water distillation technologies.*

## 3.1 Review Work on PTC

Solar thermal energy can be directly utilized by using PTC, which is a commercially proven technology for power generation and most of the literature relates it. The first practical experience with PTC goes back to 1870's but the actual research work on utilizing solar energy with PTC began only after the 'Energy Crisis' in 1970s [59]. Parabolic trough technology has proven to be the most mature and low cost solar thermal technology available today [19]. The key work by Winston [60], Duffie and Beckman [61], Drew [62] and other researchers [63]–[65] laid the foundation of application of concentrated solar energy for heating purpose. Various studies have been performed throughout the world to discuss the utilization of solar energy using concentrating technology [47,66]. Most of which are related to power generation technologies. In the current scope of work, the review has been done on PTC for industrial applications, modeling, and simulations etc. Earlier work on PTC for simulation was carried out by Price [19] where the author developed a tool for optimum

design for cost and power generation. By developing a computer model, the author identified minimum cost of energy for a plant design. The work was further extended by Forristall [67] where he carried out the one dimensional and two dimensional analysis of absorber tube of PTC. The analytical results were validated with the experimental results from the literature.

The heat transfer analysis of PTC was also carried out by Padilla *et al*. [68], where they presented a model by using conduction, convection and radiative mode of heat transfer and validated it with the experimental results. The numerical simulation for three dimensional (3D) heat transfer characteristics for receiver tube was carried out by Cheng *et al.* [69], where they used Monte-Carlo ray tracing method with FLUENT software. The simulation results used Syltherm 800 liquid oil and LS2 (Luz System) collector parameters from the literature. They carried out the validation of three different models by taking (a) only conductive heat transfer, (b) convective heat transfer in the inner absorber and the conduction in the tube wall, and (c) all three types of heat transfer. Their simulated results were in agreement with experimental results with error up to 2%.

Xiao *et al.* [70] presented a novel design of a V-cavity absorber with rectangular fins in the PTC system. They carried out theoretical analysis by discussing optical performance, energy balance, and 3D numerical modeling of the system. The simulations were validated with an experimental setup which proved reasonable agreement between the two. Their results showed the proper utilization of sunlight due to triangle shape cavity. They carried out the simulations for different mass flow rates, solar insolation and cavity length to obtain optimum value of outlet temperature and efficiency. Further, they reported enhanced heat transfer and lesser heat losses due to rectangular fins.

A prototype model for industrial process heat was developed by Coccia *et al.* [71] where they manufactured of low-cost PTC using fiberglass and extruded polystyrene. Their system was designed at rim angle of 90° with a concentration ratio of 9.25 and worked in range of 70 °C to 250 °C. Using ASHRAE standard 93-2010, they tested out the setup using demineralized water for temperature up to 85 °C. Their results showed that the equation obtained for thermal efficiency was comparable to that available in the literature.

For the application of PTC under different climatic conditions, the work done by Al-Zahrani [72] deals with the performance of PTC in Yanbu (Saudi Arabia). The author carried out the experimental investigation and observed instantaneous efficiency as 62%, average thermal efficiency as 38.3% and overall efficiency as 38.9%. The work for Jordanian climate was carried out by Badran and Eck [73], where they discussed the use of PTC based power plant for electricity production at two different sites. In an article by Scrivani *et al.* [74], the authors reported a concept of utilizing PTC for water purification, remediation and waste treatment for clean water production. They discussed solar distillation, atmospheric condensation, and waste processing for solar power plant in Mojave Desert, California, USA.

## 3.2 Review Work on Distillation Technologies

The distillation technology (or desalination, when used for seawater) has been explored widely in the literature. The basic driving energy source for distillation is either electrical or thermal energy. The distillation technologies operated with thermal energy are discussed here.

### 3.2.1 Distillation using solar stills

Solar stills are one of the simplest type of distillation (or desalination) equipment which uses the greenhouse effect to evaporate saline water. Solar stills are the first to be used on large-scale distilled water production. Based on the design and structure, many researchers investigated the performance of solar stills for their output and cost. Tiwari and Sinha [16] carried out the analysis of an active regenerative solar still on the basis of energy balances for its different components. Analytical expressions were derived for water and glass temperatures, daily yield and thermal efficiency as a function of climatic as well as design parameters. They observed that in passive regenerative solar still, thermal efficiency increased with an increase in flow rate and had better performance than that of active regenerative solar stills.

Prasad and Tiwari [75] reported the effect of climate and design parameters on double effect active solar distillation unit. They derived an analytical expression for hourly yield for a typical day in Delhi using steady state conditions. The results of their model were compared with single effect, active solar distillation unit. They observed significant improvement in the performance in upper basin for lesser flow rates. Further extending work on solar distillation, Tripathi and Tiwari [76] conducted outdoor experiments to study the effect of water depth on internal heat and mass transfer for active solar distillation system. For their study, experiments were conducted for 24 hours during winter months for different water depths in the basin (0.05, 0.1 and 0.15 m) for passive as well as active solar distillation system. They studied the effect of different water depths in the basin on the heat and mass transfer coefficients and observed that more yield was obtained during the off sunshine hours as compared to daytime for higher water depths in solar still due to thermal storage effect. Later, Tiwari *et al.* [77] studied the performance of an active solar distillation system and evaluated theoretical yield from the active solar stills integrated with flat plate collector, concentrating

collector, evacuated tube collector with and without heat pipe. In their research, hourly yield, hourly exergy efficiency, and hourly overall thermal efficiency of active solar stills were evaluated for 0.05 m water depth for a typical day in the month of December for the climatic conditions of Delhi. They concluded that active solar still integrated with evacuated tube collector with heat pipe has the maximum yield of 4.24 kg/$m^2$/day.

Kumar and Bai [78] performed an experiment on a basin type solar still (0.5 $m^2$) with improved condensation technique. A performance study was carried out with different samples such as tap water, seawater and dairy industry effluent. They observed that the condensation occurred due to the temperature difference not only on the glass surface but also on the four sidewalls, which can be cooled by water circulation through tubes attached on the wall surface for efficiency enhancement. They reported that the maximum daily production of the solar still was about 1.4 l/$m^2$/day, and its efficiency was about 30%. Arjunan *et al.* [79] carried out experimental study in an attempt to store the excess solar radiation energy by putting the blue stones in the hearth of the still and keeping the glass cover tilt at 10°, paralleled with a conventional still and observed an increase in the productivity of the modified solar still by 5% when using blue metal stones as a storage medium and that the internal and external heat transfers influence the productivity of the solar still. They also observed that the maximum amount of heat loss occurring in the solar still was the combined effect of radiation and convection heat transfer from glass to ambient.

Tiwari and Tiwari [80] had performed an experiment for performance analysis and thermal modeling of single slope passive solar still for different inclination of condensing covers mainly 15°, 30° and 45°. Each experiment has been carried over for 24 h for the Delhi climatic conditions. It was observed that the 15° inclination of condensing cover gave maximum annual yield and distillation efficiency. Dwivedi and Tiwari [81] had done energy and exergy analyses of single and double slope passive solar stills on the basis of annual

experimental data for water depth of 0.01 m, 0.02 m and 0.03 m. Tiwari *et. al* [82] studied thermal analysis of solar distillation to optimize the inclination of the glass cover for maximum yield. Further, the effect of inclination on the internal heat and mass transfer relation, the water and the glass cover temperature had also been carried out by them. They observed that the yield increases with increase of inclination in winter and vice-versa in summer and there was a significant reduction in evaporative heat transfer coefficient with increase of inclination in summer and winter.

Tleimat and Howe [83] carried out the research on solar stills and found that the solar distillation plant using solar still with daily capacity of about 200 liters was more economical than the higher capacity plants. Sinha *et al*. [84] carried out a techno-economic analysis of an active solar still and compared it with a solar water heater while considering the design life of 14 years. They concluded that annual operational cost of solar still is less as compared to solar water heater due to low investment.

A detailed review work on solar still coupled with active solar distillation system was done by Sampathkumar *et al.* [15]. They stated that the concentrator assisted regenerative solar still had much higher thermal efficiency than that of flat plate collector assisted regenerative still at all water depths and they inferred that there was less thermal loss in the concentrator compared to the flat plate collector panel. They finally gave a conclusion that the direct stream generation parabolic trough is a promising technology for solar assisted seawater desalination.

Experimental work on solar still with phase change material (PCM) for thermal storage, to obtain the continuous supply of water was carried out by Tabrizi *et al.* [85], El-Sebaii [86] and Dashtban [87]. Mahkanov and Akhatov [88] performed an experimental investigation on multistage flat plate solar thermal desalination system and reported that the

productivity of their system was twice than that of the conventional solar distillers. Singh *et al.* [89] found an analytical expression for water temperature of a solar still with FPC and PTC through natural circulation mode. Zeinab and Ashraf [90] conducted an experimental and theoretical study of a solar still desalination system coupled with PTC and simple heat exchanger. They reported that, the temperature first increases and then decreases with respect to the variation in solar radiation. Experimental work on solar stills to achieve a continuous supply of fresh water from raw feed was also carried out by Radhwan [91] and Voropoulos [92]. Al-harahsheh *et al.* [93] performed the investigation on a solar still having PCM for water desalination and achieved the highest daily productivity of 4300 ml/day.$m^2$ of which 40% was produced after sunset. Table 3.1 shows the summary of research work on solar still based distillation, for the Indian scenario.

### 3.2.2 Distillation using concentrating solar energy

Besides solar still, research work related to solar desalination has also been done by using concentrating technologies, all over the world. The work on water desalination using concentrating solar was also started after 1970s, when few researchers proposed the use of PTC for desalination on commercial basis [94, 95]. In a research article by Kalogirou [14], various PTC based desalination methods were discussed in context to their primary energy consumption, seawater treatment requirement and equipment cost. The PTC was selected due to its ability to function at high temperatures with high efficiency. Kalogirou [96] further tested the PTC according to ASHRAE standards, with the design parameter based on his research work [97].

**Table 3.1 Research on solar still based distillation in Indian scenario**

| Author, Year | Types of solar still | Specifications | Experimental Results | Remarks | Reference |
|---|---|---|---|---|---|
| Tiwari and Garg, 1985 | Preheated water active solar still | Solar area: 1 m x1 m, Insulation thickness: 0.05 m | Yield increases on increasing the inlet temperature of water | Can be used in utilization of waste heat | [98] |
| Kumar and S. Sinha, 1996 | Regenerative solar collector with parabolic concentrator | Insulation thickness: 0.004 m, Flow rate: 0.05 kg/s, Wind speed: 5 m/s | The overall efficiency of regenerative parabolic concentrator is higher than that of flat plate | Regenerative increases the yield | [99] |
| Kumar and Tiwari, 1996 | Active double effect solar still | Area: 1 $m^2$, Still angle: 15°, Collector Angle: 45°, Flow rate: 40 ml/s | Average around 7.5 l/day of distilled water was obtained per day | It is difficult to maintain uniform flow rate at the glass cover | [100] |
| Prasad and Tiwari, 1996 | Double effect still coupled with parabolic concentrator | Solar still area: 1 $m^2$, Parabolic collector area: 1 $m^2$, Flow rate:0.0027 kg/s | Since there is waste of heat from upper basin total yield per hour decreases | Maintaining glass cover temperature is crucial factor | [75] |
| Tiwari *et al.*, 2007 | Solar still coupled with evacuated tube collector | Solar Area: 1 $m^2$, mass of water in the basin: 50 kg, Flow rate: 0.035 kg/s | Overall thermal efficiency is 17.22% higher than flat plate collector | Produce hot and distilled water simultaneously | [77] |
| Kumar and Tiwari 2009 | Active Solar still couples with PVT system | Single still solar still | Higher capacity than passive solar still | Investment is high | [101] |
| Velmurugan *et al.*, 2009 | Solar still coupled with solar pond | Area: 1 m x 1 m, Still angle: 10° Dimension of solar pond: 0.9 x 0.3 x 0.3 $m^3$ | Maximum productivity of 80% is achieved during this. | Best option for industrial applications | [102] |

Garcia-Rodriguez did extensive work on renewable energy based desalination technologies, particularly in solar. One of his works includes the review of desalination technologies by use of various renewable energy system [103]. He presented the review of pilot desalination plants and perspectives of its development. He suggested the reasons why the use of renewable energies in desalination were suitable for remote areas and pointed out that the desalination systems driven by renewable energies were scarce and they tend to have a limited capacity. An article by Garcia-Rodriguez and Gomez-Camacho [104] discussed the experimental investigation of PTC based MED plant for seawater desalination. Kalogirou [105] also presented an extensive review on desalination technologies using renewable energy systems. Though both direct and indirect collection systems were included for his review work, but only industrially-tested desalination systems were included in his study. He suggested that the selection of the appropriate renewable energy system for desalination technology depends on a number of factors like plant size, feed water salinity, remoteness, availability of grid electricity, technical infrastructure and potential of the local renewable energy resources.

Chaouchi, *et. al* [106] designed and built a small solar desalination unit equipped with a parabolic dish. They found out that imperfections in paraboloid geometry and tracking could cause the relative error of 42% for the distillate flow rate. Alanis-Noyola *et al.* [55] have presented the pre-feasibility analysis of renewable energy based desalination plant for Greece, which used solar and wind energy as an energy source. Touati *et al.* [107] provided a feasibility study for hybrid PV-Fuel cell based desalination plant. Other researchers like Trieb [108, 109] and Fernández-García [110] also carried out work on desalination coupled with concentrating solar.

In Indian scenario, work related to concentrating technology specifically for distillation is limited. Although, some work related to solar hybrid system for desalination

was discussed in literature. One of the studies on cogeneration by Sahoo *et al.* [111] discussed the polygeneration based solar-biomass hybrid system for cooling as well as desalination. They discussed multi effect dehumidification water desalination system where water capacity was 3 $m^3$/day. The temperature of hot water was taken as 75 °C with volume flow rate of 4.8 $m^3$/h and sea water inlet temperature of 18 °C with flow rate of 6 $m^3$/h. They achieved 420 l/h of fresh water at heat source of 85 °C to 90 °C. The summary of prominent work done in the field of desalination using solar energy is shown in Table 3.2. It is important to mention here that a very little research has been found related to concentrated solar based desalination for Indian context.

### 3.2.3 Desalination using reverse osmosis

The first country to use desalination on a large scale for municipal drinking water production was in the Middle East. In 1960s the first industrial desalination plant opened in Kuwait [112]. Many other countries have begun to utilize desalination for drinking water production, but no other region of the world has implemented desalination on as large a scale as of the Middle East [113]. Membrane processes such as RO are currently widely used desalination technique in world. The RO system depends on the properties of semi-permeable membranes, which, when used to separate water from a salt solution, allow freshwater to pass into the brine compartment under the influence of osmotic pressure. For pressure above osmotic pressure, the fresh water is forced through the membrane leaving behind high concentration of impurities in saline water, which is rejected and flushed away. Theoretically, the only energy requirement is to pump the feedwater at a pressure above osmotic pressure. Many researchers discussed the desalination process with RO for drinking water production [114, 115].

**Table 3.2 Summary of prominent research on solar desalination across the world**

| Author, Year | Technology used | Capacity | Desalination Technology | Remarks | Reference |
|---|---|---|---|---|---|
| Chaouchi *et. al*, 2007 | Parabolic dish | - | Concentrating Plate | Developed a theoretical model to calculate the absorber average temperature as well as the distillate flow rate as a function of solar irradiation | [106] |
| Scrivani *et al.*, 2007 | PTC | - | Through collector, extraction from air | Author explored the potential of parabolic collector for water distillation. Discuss clean water production by processes such as solar distillation , atmospheric condensation & water processing | [74] |
| Sinha and Tiwari, 1992 | Cylindrical parabolic concentrator | - | Active, Double Slope Solar Still | Expression For Thermal Efficiency & Analysis of Concentrated Assisted solar still in terms of concentrator & Solar still parameters | [116] |
| Van der Bruggen and Vandecasteele, 2002 | Mixed | - | | Overview of recent improvements in seawater desalination using RO , MSF, MED & ED. | [117] |
| Leblanc *et al*., 2005 | Solar gradient potential, MSF | 0.33 $m^3$ of fresh water | salinity-gradient solar pond with MSF | Discussed the production of potable water from seawater or brackish water by using a salinity gradient potential pond | [118] |
| Nafey *et al.*, 2007 | Flat plate solar collector | 1.04 to 1.45 $kg/m^2/day$ | Vertical flash unit attached to a preheater | A mathematical model was developed to calculate the productivity of the system under different operating conditions. | [119] |
| Kalogirou, 1998 | PTC | - | | Various desalination methods were analyzed. Compared various distillation plants based on PTC. Design presented didn't use thermal storage. | [14] |
| Blanco *et al*, 2013 | PTC | 3.5 $m^3/day$ | PTC Coupled with MED, MSF, RO | Studied thermodynamic characterization and an economic evaluation of different configurations for coupling parabolic through & desalination facilities | [120] |
| Zhani, 2013 | Solar energy | - | Humidification & Dehumidification | Theoretical and experimental study of a new generation of water desalination unit by solar energy using the humidification and dehumidification (HD)principle | [121] |
| Li *et. al*, 2013 | Solar energy | - | | Reviewed the current solar desalination research activities followed by discussion of solar assisted desalination processes. | [122] |
| Riffat and Mayere, 2013 | V-trough solar concentrator | Efficiency 38 % | CSP (Multiple) | Compared with the common parabolic trough solar concentrators, the new concentrator has two parabolic troughs which form a V-shape with the focal line at the bottom of the troughs | [123] |
| Trieb and Müller-Steinhagen, 2008 | Concentrating Technologies | - | | Presented a case study of feasibility of Concentrating solar power for seawater desalination in MENA (Middle East and North Africa) region. | [108] |

In India, two major RO based desalination plants are located in Chennai, Tamil Nadu. With the plant area of 60 acre, Minjur plant, is the first largest desalination plant in India. It was established in 2010 with a capacity of 100 MLD. Following its success, second desalination plant, Nemmeli plant, become operational in 2013. It has the capacity to treat 100 million litres of seawater a day.

Despite commercially adopted technology, the household RO units for distillation cause up to 80 per cent of the water rejection, based on the local TDS level. The commercial disadvantage of RO is its high maintenance expenses, high sensitivity of membranes to fouling, removal of essential minerals and huge wastage of water [124]. The problem of RO waste can be dealt with the use of solar based thermal technologies for desalination.

## 3.3 Review Work on Photovoltaic and Concentrated Photovoltaic Technologies

The maximum conversion efficiency achieved in PV cells is around 15-20%. Rest of the energy is lost in the form of heat [125]. Nowadays, the systems are designed to utilize the excess waste heat into a useful form. One such technology is PVT system which consists of PV module attached to a heat recovery arrangement. It can be a non-concentrating, in which cooling can be carried out by fixing heat sinks or channels at the back surface, or a concentrating, which operates on higher concentration with cooling mechanism on back side which carries away the excess heat. Both the system converts solar radiation into thermal and electrical energy. In case of concentrated photovoltaic (CPV) cells in PVT system, the PV cells are cooled down as the coolant absorbs the excess heat from the back side of PV panel and gets heated up from which thermal energy can be extracted and utilized for different applications [126]. In case of CPV systems, using PTC, much higher efficiency is reported as smaller area of cell is required due to concentration optics. The application of CPV using various techniques has been discussed in the literature. Muller *et al.* [127] reported the

methodology for determining cell temperatures in CPV systems. The performance of CPV cells under high concentrating was also reported by Bunthof *et al.* [128, 129] and Reis *et al.* [130]. However, in such systems, the cell temperature increases with higher concentration ratio (CR). This increase in temperature leads to reduction in the cell efficiency and too high of a cell temperature may damage the cell's integrity. If the temperature exceeds a certain limit its life-span would reduce rapidly [131]. Literature discusses the degradation of cells under high temperature and emphasis on cooling requirement for CPV systems to maintain the temperature within the limit. A simple cooling system design may also help to reduce maintenance costs. While a variety of approaches have been used to the keep the cells cool, most of them are based upon removal of heat from the back of the cell (opposite surface of the incident flux exposed surface) [132]. The both side cooling of flat CPV cell was discussed by Zhu *et al.* [133, 134] while liquid immersion cooling of CPV cells was discussed by Han *et al.* [135], Xiang *et al.* [136].

For CPVT systems, a detailed historical review of their configurations and cooling system was carried out by Jakhar *et al.* [137]. They reported that new cooling designs like earth water heat exchanger could provide economical solutions for cooling of CPVT system specifically for arid and semi-arid regions of India. The cooling of CPVT systems is also discussed by few researchers at different CRs and concentrating technologies. Coventry [138] investigated the performance of a CPVT collector where the rows of cells were cooled by liquid flowing through an internally finned aluminum pipe with optical concentration of 37 Suns. The author reported electrical and thermal efficiencies of 11% and 58% respectively, with overall efficiency of the system as 69%. Chaabane *et al.* [139] carried out 3D CFD analysis of water cooled CPVT system and observed increased thermal and electrical efficiencies of the system with increase in number of water cooling pipes behind CPV cells. They reported that the panel temperature could be reduced by 17 °C when two water

rectangular shaped cooling system was used, which leads to increase in thermal efficiency by 28.3% and electrical efficiency by 0.92% in compared to normal CPV system.

A research work done by Darwish and Boehm [140] discussed the concept of cooling of CPV in high concentrations by analyzing its optical and thermal performances. The system utilized the high concentration to generate power from flat CPV cell as well as obtaining hot water as its by-product. However, the research work was in the preliminary stage for development of CPVT and discussed in terms of cell efficiency. Their research shows that there is a need of a novel receiver system especially for PTC which can not only provides hot water but also caters the need of power by generating electricity from the same system.

## 3.4 Review of Second Law of Thermodynamics for Solar Based Distillation Units

The second law of thermodynamics provides insight on useful amount of work which can be derived from a system. Exergy analysis quantifies the collection and useful consumption of exergy and pinpoints the unrecoverable losses, leading the way to improve the system. Although a number of studies have been done to find out the energetic performance analysis of different solar components, a few studies have found on the second law analysis of the same [141]. An extensive review of second law analysis and assessment of renewable energy sources was performed by Hepbasli [142]. Literature also shows the review work carried on research related to exergy analysis of solar energy applications [143], heat exchangers [144] and solar distillation system [145, 146]. The detailed sub-component wise review is given below.

### 3.4.1 Review of studies related to exergy analysis for PTC

The energy falling on the collector depends on various parameters like aperture area, reflectivity, ambient temperature etc. while for the absorber it depends on CR which already depends on aperture area), mass flow rate, temperature of fluid operating etc. By changing these parameters the energy and exergy analysis can be performed to find out the optimum conditions. Bejan *et al.* [147] provided a second law analysis of collector system with exergy flow analysis. Using Gouy-Stodola Theorem, they derived the optimum collector temperature ($\theta_{opt}$) in dimensionless form (as a function of $T/T_o$) for minimum irreversibility

$$\theta_{opt} = \left(\theta_{stag}\right)^{1/2} = \left(1 + \frac{Ir}{U_c T_a}\right)^{1/2} \tag{3.1}$$

where $Ir$ is the rate of solar radiation, $\theta_{stag}$ is the dimensionless temperature at stagnation point. This gives the optimum collector efficiency for minimum irreversibility as

$$\eta_{opt} = \frac{\left(\theta_{stag}\right)^{\frac{1}{2}}}{\left(\theta_{stag}\right)^{\frac{1}{2}} + 1} < 1 \tag{3.2}$$

The second law analysis using mass flow rate was taken by Padilla *et al.* [148] where they presented an exergy analysis of PTC by taking mass flow rate and inlet temperature as the key parameters. The exergy loss equation, occurring in the collector, was obtained using Petela expression as

$$\dot{E}x_{loss} = (1 - \eta_o) Ir A_{abs} \psi + \sum_j \dot{Q}_{j,loss} \left(1 - \frac{T_a}{T_{coll,j}}\right) \tag{3.3}$$

Here $\eta_o$ is the optical efficiency of the collector and $\psi$ is Petela expression given as

$$\psi = 1 - \frac{4}{3}\left(\frac{T_a}{T_s}\right) + \frac{1}{3}\left(\frac{T_a}{T_s}\right)^4 \tag{3.4}$$

Within the absorber the exergy destruction would occur because of the friction of viscous fluid and heat transfer due to temperature difference [149].

$$\dot{E}x_{dest} = \left( T_a \dot{m} \sum_j \frac{\Delta p_j}{\rho o_j} \frac{\ln\left(\frac{T_{o,j}}{T_{i,j}}\right)}{T_{o,j} - T_{i,j}} \right) + \left( \eta_o Ir A \psi - \sum_j \eta_0 Ir' \Delta z A \left(1 - \frac{T_a}{T_{abs,j}}\right) \right) + \left( T_a \dot{m} \left[ \int_{T_i}^{T_o} Cp(T) \frac{dT}{T} - \sum_j \frac{1}{T_{abs,j}} \int_{T_{i,j}}^{T_{o,j}} Cp(T)\, dT \right] \right) \quad (3.5)$$

In this expression $Ir'$ was taken as the irradiance falling per unit length along the absorber. From the analysis the author concluded that the maximum exergy losses were due to the optical losses while maximum exergy destruction is due to the heat transfer between the sun and the absorber. Further they concluded that HTF inlet temperature affects the exergy leakage due to thermal losses. Also vacuum in annulus affects the performance of the absorber tube as its absence increases the thermal losses and reduces the exergy efficiency. The absorber tube losses were further discussed by Zhai *et al.* [150] in which they took a case study of hybrid heating, cooling and power generation system using PTC, for western China. For the receiver, they used triangular shaped cavity which according to them has best optical performance and minimizes convective heat losses. For the cavity receiver, the authors used the Eq. (3.6) for the energy efficiency of the collector

$$\eta_c = \eta_o - c_1 \frac{\left(\frac{T_i + T_o}{2} - T_a\right)}{Ir} \quad (3.6)$$

In the above expression, $\eta_o$ and $c_1$ were taken as 0.70 and 0.41 (W/m$^2$.K) respectively. The authors obtained the exergy received from the solar radiation by modifying 'Petela Expression' by introducing dilution factor $f$ $(1.3 \times 10^{-5})$, which they defined as the measure of mixing ratio of radiation from two sources i.e., the radiance of the Sun and the radiance of the surroundings [151].

$$\dot{E}x_s = \left[1 - \frac{4}{3}\frac{T_a}{T_s}(1 - 0.28 \ln f)\right] \dot{Q}_s \quad (3.7)$$

Useful exergy delivered by solar collector is given in terms of steam mass flow ($\dot{m}_{st}$) rate as:

$$\dot{Ex}_c = \dot{m}_{st}\{(h_i - h_o) - T_a(s_i - s_o)\} \quad (3.8)$$

Their result analysis showed that the second law efficiency of the collector was within 28.4% to 33.7%, thus making on an average of 70.4% exergy loss in collector receiver circuit, due to the transform of high quality energy to low quality thermal energy.

Hernández-Román *et al.* [152] performed the exergetic and thermo-economic analysis of solar air heating system where the energy source was PTC. For the energy balance, they assumed open system with negligible change in kinetic and potential energy. They calculated first law efficiency of their system using correlation given by Duffie and Beckman [153]. They carried out the exergy analysis using conventional equations. For the parametric optimization, they took four parameters i.e. length, flow-rate, diameter and aperture area. They observed that exergetic efficiency increases by increase in length or aperture area, but decreases by increase in flow-rate or diameter. Thus, by keeping the trade-off between these parameters and cost, they suggested the optimum length as 3 m to 5 m, flow rate as 0.03 kg/s, diameter between 10 mm to 30 mm and aperture area as 3 $m^2$. They reported maximum energetic and exergetic efficiency of 28% and 3.2% respectively, over the duration of one year.

Literature also discusses the exergy analysis of PTC, along with other components, when used for power generation or industrial applications. In one of the study, Singh *et al.* [154] discussed the in-depth exergy analysis of conceptual solar based power plant in Delhi, India. The mass flow rate of thermal fluid was taken as 0.02134 kg/s with 42 numbers of collectors in series, making an average CR of the system as 11.62. Their exergy analysis showed the second law efficiency of collector as 29.03%, for receiver as 68.38% and for collector receiver circuit as 19.85%,

Montes *et al.* [155] presented the exergy analysis of PTC based power plant for three different working fluid i.e. Therminol VP-1, solar salts and water. For the study they correlated the change in absorber tube diameter and collector loop length with exergy analysis. They reported that for solar salts, the heat transfer fluid temperature ranged from 290 °C to 566 °C with inlet loop pressure of 8.5 bars and the mass flow per loop of 4.4 kg/s. For Therminol, operating ranges were 250 °C to 395 °C, 32 bar and 4.4 kg/s. For water, they reported it was 229.2 °C to 550 °C, 97 bar and 1.3 kg/s respectively. They observed maximum energy efficiency of water/steam, solar salt and Therminol VP-1 as 68.4%, 64.1% and 68.1% respectively. In second law efficiency, they found that the solar salts had higher exergetic efficiency (38.2%) followed by Therminol VP-1 (35.5%) and water/steam (34.4%).

Gupta and Kaushik [156] presented the exergy analysis to optimize parameters for solar thermal power plant. Using a conceptual 5 MW plant design, investigations were carried out to optimize the inlet conditions. They found out the large amount exergy loss occur in solar collector field, comprising of PTCs. For the exergy analysis of collector system, they ignored kinetic and potential energy change and assumed steady-state conditions. They considered total energy input by collector as

$$Q_u = \eta_0 Q_i = \eta_o (Ir.r_b.A_a.n_{coll}.n_{row}) \tag{3.9}$$

Where $r_b$ was tilt factor for incident beam radiation and depends upon beam angle and zenith angle. For exergy equation, they took $T_s$ as 5600 K as apparent black body temperature of the Sun. The exergy gain for flowing water in absorber was given by its empirical formula given in Eq. (3.9). They calculated the exergy of heat absorbed by receiver at mean receiver temperature ($T_r$) which varies from 523 K to 723 K. They reported that the maximum energy loss occurred in the condenser followed by the collector receiver circuit, while the maximum exergy loss occurs in the solar collector field. Their results showed maximum exergy loss of 55.08% in collector and 13.90% in receiver, making total loss of 68.98% in collector receiver

field. The maximum irreversibility they found in collector field was 22717.46 kW. They also calculated the second law efficiency of collector as 44.91% while for receiver it was 69.05%. The combined second law efficiency of collector field was just 31.02%.

Baghernejad and Yaghoubi [157] presented the exergy analysis of an integrated solar combined cycle system (ISCCS) using equations from Bejan [158]. In their research, they used the functional exergy efficiency approach. During the analysis, they got the overall second law efficiency as 27% respectively. They observed that the collector receiver system was least efficient component in the whole system and suggested more efforts are required to increase the exergy efficiency of it, where material and physical constraints play an important role. This work was further explored by the author [159, 160] where exergo-economic principles and genetic algorithms were used to optimize the plant. For the same, the authors developed a code using MATLAB software and validated the results with mathematical optimization approach discussed by Silveira and Tuna [161]. The simulated results confirmed the increase in exergy efficiency of ISCCS system from 43.79% to 46.8% while the exergy destruction cost reduced by 14.82%.

Sharaf *et al.* [162] presented the exergy and thermo-economic analysis of solar MED desalination system where they compared it with and without power generation scenario. For the PTC collector efficiency they used the equation as [163]

$$\eta_c = \eta_o + a(T_c - T_a) + \mathrm{b}\frac{(T_{coll} - T_a)}{Ir} + c\left(\frac{T_{coll} - T_a}{Ir}\right)^2 \tag{3.10}$$

With an operating temperature between 170 °C to 450 °C. Here $\eta_o$, *a*, *b* and *c*are the coefficients with values as 0.75, $-4.5 \times 10^{-6}$ ($°C^{-1}$), $-0.039$ ($W/(m^2.°C)$) and $-3 \times 10^{-4}$ ($W^2/(m^4.°C^2)$) respectively. Irreversibility in the collector was obtained by using following correlation [164]

$$\dot{Ir} = A_c . Ir . \psi + \dot{m}_{coll} [h_i - h_o - T_a (s_i - s_o)] \quad (3.11)$$

From the literature review, it was observed that the method of exergy analysis for system optimization had been done widely by finding out the key parameters [165]. The exergy analysis of overall system where PTC worked as subsystem was discussed by Elsafi [166]. Table 3.3 summaries the comparison made for exergy analysis by various investigators for PTC based solar power plant. In such cases, usually, exergy analysis of collector receiver circuit was taken as overall subsystem performance, instead of individual components.

### 3.4.2 Review of studies related to exergy analysis for distillation technology

Seawater desalination on large scale basis was commercialized after 1957 when first flashing unit was established in Kuwait. Since then, many plants have been established for desalination using various techniques. A detailed history and understanding of seawater desalination process have been discussed by El-Dessouky and Ettouney [167]. In case of second law analysis, one of the earlier work in exergy for MSF has been done by Al-Sulaiman and Ismail [168] where they compared the performance of three MSF plants in Saudi Arabia and performed the second law analysis.

**Table 3.3 Investigation carried out on exergy analysis by researchers on solar thermal based power plant**

| Authors | Location of integrated power plant | Maximum exergy loss (component) ($Ex_{dest}$) | Exergy Efficiency of Solar field (%) | | | Heat Exchanger efficiency (%) | Reference |
|---|---|---|---|---|---|---|---|
| | | | Collector | Receiver | CRC | | |
| Kaushik *et al.*, 2000 | New Delhi, India | 217.05 kW (collector receiver circuit) | 29.03 | 68.38 | 19.85 | 96.42[a] | [169] |
| Baghernejad and Yaghoubi, 2009 | Yazd, Iran | 260.89 MW (Combustor) | | | 27.00 | 77.00 | [157] |
| Zhai *et al.*, 2009 | Western China | 183.0 kW[b] (Collector) | | | 28.40[c] | | [150] |
| Baghernejad and Yaghoubi, 2010 | Yazd, Iran | 260.89 MW (Combustor) | 41.10 | 66.50 | 27.30 | 77.00 | [159] |
| Gupta and Kaushik, 2010 | Almeria, Spain | 22717.46 kW (Collector field) | 44.91 | 69.05 | 31.02 | | [156] |
| Reddy *et al.*, 2012 | New Delhi and Jodhpur, India | 124474.4 kW (collector receiver circuit) | 56.20 | 69.56 | 39.09 | 84.85[d] | [170] |
| Reddy *et al.*, 2012 | New Delhi and Jodhpur, India | 124474.4 kW (collector receiver circuit) | 56.20 | 69.56 | 39.09 | 86.12[e] | [170] |

[a] Boiler Heat Exchanger
[b] The values are given for summer conditions. In winter conditions, the losses were 174.1 kW
[c] The efficiency calculated for summer conditions. During winter the efficiency increases to 33.7%.
[d] Boiler is taken as Heat exchanger where steam directly fed to turbines at 90 bar, 643 K
[e] The inlet turbine conditions are changed to 105 bar, 643 K

Exergy balance along with cost optimization for MD has been done by Khayet [171] while Spiegler and El-Sayed [172] compared and derive the exergy balance equations for RO, ED and MSF to get exergy generation in these processes. Gomri [173] performed an experimental analysis of seawater desalination using flat plate collectors and single effect absorber system. The schematic diagram of setup used by the author is shown in Fig. 3.1. The vessel separator in desalination unit was assumed to be adiabatic system. He took latent heat of vaporization of seawater as 2414.4 kJ/kg. For first law analysis, the ratio of useful energy in the absorber to incident radiation along with pump work was used.

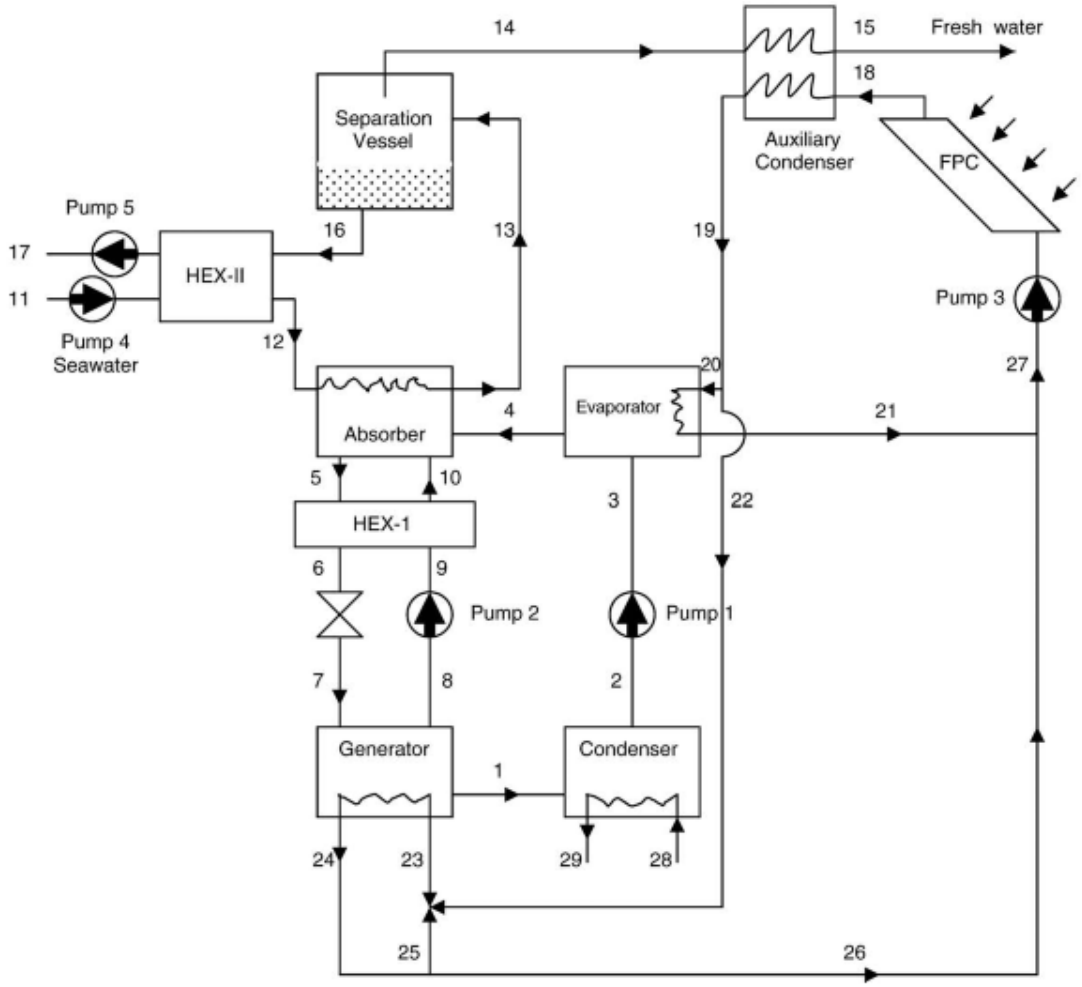


**Fig. 3.1 Schematic diagram of experimental setup by Gomri [173]**

$$\eta_{th} = \frac{Q_u}{IrA_{coll}\, n_{coll} + P_{pump}} \tag{3.12}$$

For the exergy analysis, sum of exergy loss in each component was taken by him as total exergy loss in the system. The exergy efficiency was calculated as per the Eq. (3.13)

$$\eta_{Ex} = \frac{Q_u \left(1 - \frac{T_a}{T_{abs}}\right)}{IrA_{coll}\, n_{coll} \left(1 - \frac{T_a}{T_{abs}}\right) + P_{pump}} \tag{3.13}$$

From the experimental calculations, the author concluded that the energy efficiency of water production desalination unit was higher than any other components. Also, daily exergetic efficiency of absorber unit was found to be higher than distillation unit, which was higher than FPC. The author also observed maximum exergy destruction in solar collectors (absorber).

Nematollahi *et al.* [174] carried out the experimental and theoretical first and second law analysis for solar desalination system. Their setup consists of solar FPC and humidification tower. The exergy analysis for the humidification was performed on mole basis. For gas liquid mixture the exergy efficiency was defined as [175]

$$\eta_{Ex} = \frac{\left(Ex_{gas} + Ex_w\right)_o}{\left(Ex_{gas} + Ex_w\right)_i} \tag{3.14}$$

For Eq. (3.14) they considered dead state with $T_0$ as 30.1 °C, $p_0$ as 1 atm with absolute humidity of 0.003 kg/kg. Based on the operating conditions exergy destruction was calculated by them for packed bed system, inlet streams, air and distilled water. They observed improvement in overall exergy efficiency with decrease in inlet air temperature whereas inverse trends in exergy efficiency were observed with increase in air tower height. Exergy destruction was calculated for packed bed system with air flow rate of 0.036 kg/s and water

flow rate of 0.114 kg/s. It gave the error of 13.78 % when validated with their experimental observations.

Uche *et al.* [176] performed the exergo-economic analysis of integrated power plant with desalination unit, where brine is re-circulated. For the sake of simplicity, they assumed the MSF plant as a single plant component with seawater flow having zero exergy. For the model, they took the fuel to product ratio as per the exergy balance. For the analysis, six different cases were taken by them, where one of the cases is taken as pure distillation unit, without any power generation scenario. The maximum fresh water output was taken by them as 2.418 $m^3$/hr. They considered two more cases where some amount of live steam was throttled to a second MSF unit. Their exergy analysis showed minimum exergy destruction (67,482.6 kW) occurring in the case of pure distillation than cogenerations cases (117,924.4 kW and 106,596.9 kW), with exergetic efficiency of 9.3%. They further concluded that low exergy value of freshwater contributes to a high exergy cost.

A comparative case study of four desalination plants (Jeddah, Al-Jubail, Al Khobar and Al-Khafji) of Saudi Arabia was presented by Hamed *et al.* [177]. For the same, they used MSF process simulation program reported by El-Sayed [178]. During the exergy analysis, they used specific exergy losses as the ratio of total exergy losses to the total distillate produce and the exergy efficiency as the ratio of useful chemical exergy output to the thermo-mechanical exergy input. From the exergy analysis, they concluded that (i) exergy efficiency of the distillers ranged between 4.3% to 6.7% because of relatively low number of stages (ii) the highest exergy destruction flux occurred in brine heater because of high influence of steam temperature (iii) overall exergy losses could be reduced by increasing the number of stages.

For European conditions, García-Rodríguez and Gómez-Camacho [179] presented exergy-economic analysis of solar based desalination plant SOL-14 at Plataforma Solar de Almeria, Spain. They considered solar field consists of single axis PTC with Santotherm 55 as HTF. The schematic diagram of both MSF and MED plant is shown in Fig. 3.2. In their research, they used MSF unit of 100 $m^3$/h capacity, having 24 stages, two heat rejection stages, maximum brine temperature as 101 °C and MSF performance ratio as 10. The exergetic efficiency of solar field was observed by them as 19.4% while for MSF it was 10.0 %. They concluded that the cost of the exergy consumption of the desalination plant strongly influences the fresh water costs.

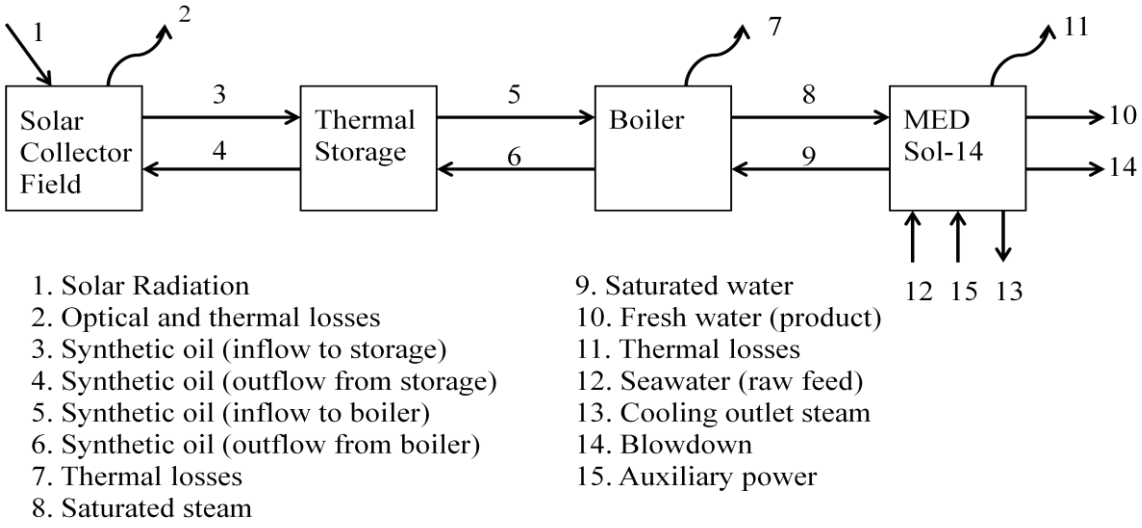


**Fig. 3.2 Schematic diagram of solar MED system (SOL-14) at PSA, Spain [179, 180]**

The exergy analysis of SOL-14, has further expanded by García-Rodríguez and Gómez-Camacho [180] where they used 14 cell MED distillation unit with capacity of 3 $m^3$/h unit. In the modified system, which they term as Phase 2, they replaced Phase 1 vacuum system with double effect absorption heat pump (DEAHP) and observed improvement in the exergetic efficiency of both solar field and MED. In Phase 1, they reported that the exergetic efficiency of solar field and MED unit as 17.4% and 14.3% respectively. In Phase 2, with the help of DEAHP the exergetic efficiency goes up to 24.0% and 25.7% for respective cases, as observed by them. This also increased the global system efficiency from 1.4% to 4.7%. They

concluded that the increase in overall exergetic efficiency was due to increase in operating temperature of the solar field.

Exergetic analysis of solar based MD system was performed by Banat and Jwaied [164] where they used the methodology reported in Kahraman and Cengel [181]. For the experimentation, they used two systems i.e. compact system, where condenser and evaporated is directly connected to solar collector and large system, where heat exchanger was used between MD and collector. They assumed adiabatic heat exchanger and neglected the exergy destruction in pipes. From the analysis, they found exergetic efficiency of 0.3% for the compact system and 0.5% for the large system. They concluded that the maximum irreversibility occurred in the order of 98.81% and 55.14% of input exergy for compact and large units respectively.

Nafey *et al.* [182] developed a visual design and simulation package to estimate the exergy and thermo-economic analysis of MSF plant. They discussed thermodynamic modeling of the plant and provided the exergy relation of MSF input as

$$\dot{Ex}_{loss} = \dot{E}x_{heating\ steam} + \dot{E}x_{sw} + \dot{E}x_{pump} - \dot{E}x_{condenser} \quad (3.15)$$

The exergy destruction for the system is the summation of exergy destruction at each unit.

$$\dot{E}x_{dest} = \dot{E}x_{dest,\ splitter} + \dot{E}x_{dest,\ distillate\ tray} + \dot{E}x_{dest,\ heat\ exchanger} \quad (3.16)$$

For the analysis, they used the operating conditions for Aoun Mousa MSF desalination plant [183]. With exergy input of 10.7 MW, their design package calculated 0.2 MW of exergy in the distilled stream. During the plant operation they observed the exergy destruction of 6.46 MW and the exergetic efficiency of 1.87%. Further, they considered exergy cost analysis of the plant. They concluded the unit product cost of the MSF desalination plant as 2.63 \$/m$^3$. The exergy analysis was also performed by them on partial

load conditions, as shown in Table 3.4. They reported that the maximum exergy output of distilled water was obtained during full load conditions.

**Table 3.4 Exergy analysis at different partial load conditions [182]**

| **Load conditions** | **100 %** | **90%** | **70%** | **63%** | **50%** |
|---|---|---|---|---|---|
| $Ex_i$ (MW) | 10.70 | 10.90 | 10.00 | 9.00 | 8.30 |
| $Ex_{loss}$ (MW) | 4.00 | 4.72 | 4.65 | 4.69 | 4.74 |
| $Ex_{dest}$ (MW) | 6.46 | 5.95 | 5.34 | 4.23 | 3.44 |
| $Ex_o$ (MW) | 0.20 | 0.19 | 0.16 | 0.12 | 0.10 |
| $\eta_{II}$ (%) | 1.87 | 1.75 | 1.58 | 1.33 | 1.21 |

A detailed review of solar assisted desalination process was discussed by Li *et al.* [122] were they reviewed various solar thermal desalination systems and found that AQUASOL project, which was 14-effect MED system with 500 $m^2$ collector field and thermal storage of 24 $m^3$ capacity, had lowest experimental specific energy cost. They also discussed the assessment of various desalinating plants on exergy basis. Extending this work, in [184] they discussed exergy relations for non-solar desalination system which includes, RO as well as mechanical vapor compression (MVC) systems and used the following relation to estimate the exergy destruction.

$$Ex_{dest} = T_a S_{gen} = \frac{T_0 H_{fg}}{18} \frac{\Delta T}{\bar{T}^2} \tag{3.17}$$

Where $\bar{T}$ was mean of vaporization and condensation temperatures. They estimated the exergy destruction in MED, MVC and MSF which is shown in Table 3.5.

**Table 3.5 Exergetic assessment of various desalination systems by Li *et al.* [184]**

| | $T$ (°C) | $\bar{T}$ (°C) | $Ex_{dest}$ (kJ/kg) |
|---|---|---|---|
| MED | 1.50 | 50.75 | 9.94 |
| MVC | 1.50 | 60.75 | 10.16 |
| MSF | 3.00 | 71.50 | 17.52 |

Using low grade heat source, Al-Kharabsheh [185] discussed exergy destruction and exergetic efficiency for condenser. The author's experimental results showed that exergy

destruction increased with time. The author proposed that this irreversibility could be minimized if the latent heat of condensation of the produced vapor was utilized in a multistage evaporator. It was concluded that the temperature of heat source played a key role in the performance of the system.

The exergy analysis of an existing MEE plant with capacity of 1500 $m^3$/day, was done by Nafey [186], where the author discussed the influence of number of effects on the system performance. The author found out that with increase in number of effects from one to six, the system exergetic efficiency also increases from 3.84% to 8.4%. By performing thermo-economic analysis the author observed that unit product cost obtained for two evaporators were almost same as three evaporators, but evaporator being highest exergy destruction source, increases the exergy destruction in later case.

The literature also revealed various exergy based analysis of combined systems with power plant, like Gas turbine combined desalination system [187], organic Rankine cycle with MED distillation [188], Combined RO, Nanofiltration and ED plants [189] etc.

### 3.4.3 Review of exergy studies on PV/CPVT

Literature shows considerable amount of work done on the first and second law of analysis on PVT systems. Rajoria *et al.* [190] carried out the thermal and exergy analysis of PVT system for different configurations. For the same, they developed one-dimensional heat transfer model and simulated the same for different cities of India. They discussed two different designs of integrated columns for cooling fluid and reported that two integrated column design has better efficiency than other design. Qu *et al.* [191] performed the experimental investigation on PVT system integrated with a heat pump based water heating system. During the experimentation, they reported decrease in PV cell temperature up to 45 °C with the use of water cooling and obtained cell efficiency of 10.3%. Evola and Marletta

[192] presented a simulation based exergy analysis of water cooled PVT system. They reported that exergy generated within the system could be maximized by optimizing inlet water temperature which should fall within the range of the solar thermal system. Tripathi and Tiwari [193] conducted an exergetic analysis of PVT coupled with compound parabolic collectors and reported the exergy output of 15.45 kWh for their design. Kalorigou *et al.* [194] presented a review of exergy analysis of solar collectors, solar thermal system and their processes.

In case of second law analysis for CPVT, Calise *et al.* [195] presented a finite volume model of CPVT system using triangular receiver mounted on PTC to get high concentration. They reported high exergy losses due to higher radiative and convective losses occurring in the system. Chaabane *et al.* [196] performed numerical simulations to optimize the cooling of CPVT system. Using different designs, they optimize to achieve lowest cell temperature and maximum efficiency. They reported that using two pipe design for water cooling, the cell temperature reduced by 17 °C which leads to an increase in thermal and electrical efficiency of 28.3% and 0.92% respectively. The performance analysis of high concentration GaAs cell based CPVT system was carried out by Abdelhamid *et al.* [197, 198]. They reported the maximum thermal and electrical efficiency of 37% and 8% respectively. Candilli [199] carried out the exergy analysis of novel CPV system. The author developed a thermodynamic model, validated it experimentally and reported energy and exergy efficiency of the system as 7.3% and 1.16% respectively. Exergy analysis of novel CPVT system was carried out by Gurel [200] in which author uses paraffin wax to absorb excess heat of PV modules. In their study, the author reported the average PV cell temperature as 30 °C with 14.67% electrical efficiency.

## 3.5 Research Gaps Identified

From the above literature reviews following research gaps are identified:

1. Most of the research work on PTC is related to power generation scenario. A couple of research work is also available for hybrid PTC systems. In Indian context, the major research work on PTC is still in a preliminary stage. This provides a potential for the research work in the field of hybrid PTC.

2. Existing studies of PTC based desalination systems are based on European, Middle East or US conditions. In Indian scenario, most of the researches in solar distillation (or desalination) are done on solar stills. It has been observed that a few amounts of work has been carried out on desalination using PTC. The second law analysis for PTC based distillation units is also rarely available for Indian scenario.

3. No attempt has been made to integrate CPV with other energy conversion systems to increase the combined efficiency for Indian scenario.

4. Liquid immersion cooling of CPV using PTC technology is not available in the literature. Such a hybrid system could be used for combined heat and power. The thermal energy from such a hybrid system could be utilized for low-grade thermal applications like distillation.

# CHAPTER 4

# MODELING AND SIMULATION OF NOVEL HYBRID RECEIVER

*This chapter discusses the design of novel hybrid receiver using simulation tools. For the modeling, the three designs are proposed. The first design (circular) is developed in MATLAB and validated with COMSOL. The other two designs (semi-circular and triangular shape) are also developed in MATLAB in similar way and compared. At the end of this chapter, simulation is also carried out to propose a distillation unit coupled with proposed hybrid system, for fresh water production.*

## 4. Design and Development of Hybrid Receiver

From the literature review, having established the need of hybrid system which would provide low grade thermal and electrical energy, a novel receiver of PTC termed as hybrid concentrating photovoltaic thermal (HCPVT) receiver is proposed. This chapter presents modeling and simulation of such HCPVT receiver, for the climatic conditions of Pilani, Rajasthan. The main component of the hybrid system is receiver part which operates under high concentration of PTC and provides combined heat and power. The hybrid receiver has two components, one is absorber tube and another is customized PV module. In the present work, three different designs of absorber tube, i.e. circular, semi-circular (D-shape) and triangular, of HCPVT receiver are proposed. The conventional receiver of PTC has vacuum in between glass and absorber tube. The presence of vacuum reduces the thermal losses to the environment. However, to obtain the electrical output along with the high temperature fluid, the design of receiver needs to be modified. Modifications are done on the outer surface of absorber tube where a PV panel is mounted to provide electrical output. The modified receiver will provide heat as well as electrical output. In order to reduce the temperature of PV panel owing to high concentration, the water is used as cooling medium. The water,

which acts as a HTF, is allowed to flow through the absorber tube as well as annulus between absorber and glass tube. The proposed receiver consists of non-evacuated glass tube, absorber tube and PV module (flexible/customized) mounted on absorber tube with the help of epoxy.

The analytical model of three different HCPVT receivers was made using MATLAB (v2012a), which includes one dimensional analysis. The purpose of the model is to understand the nature of heat transfer occurring within the absorber system. For the same, a detailed thermodynamic model has been developed by applying energy balance using the first law of thermodynamics. The analysis has been carried out by simulating the model at various operating conditions. A theoretical model was developed for circular absorber using data available from the literature. Further, for validation, simulation of proposed design was carried out using COMSOL (v5.1). The results of cross-sectional view obtained from COMSOL were compared with the analytical results obtained from MATLAB. After validation of the model for circular absorber, the other two designs of absorber tube, i.e. D-shape and triangular shape, are also analyzed. Using the proposed D-shape novel HCPVT receiver, analysis for distillation system was also carried out in Aspen HYSYS (v8.4) to obtain optimum mass flow rate through the receiver. The schematic indicating components modeling is shown in Fig. 4.1.

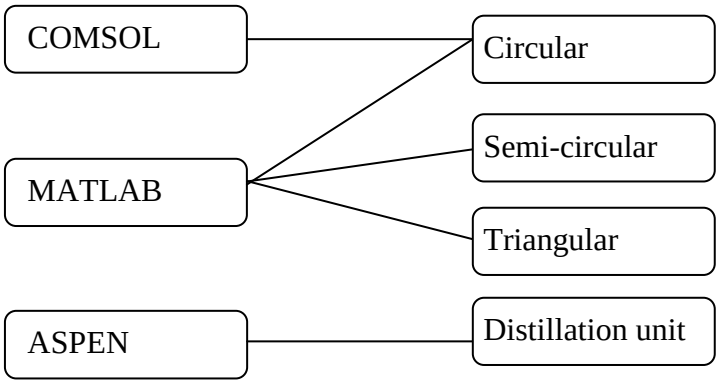


**Fig. 4.1 Schematic indicating component wise modeling in simulation tools**

## 4.1 Thermodynamic Model for Circular Absorber Tube

The circular absorber tube receiver was designed by considering flexible multi-junction PV panel mounted on the outer surface of absorber tube facing the concentration. The thermal model for proposed novel circular absorber tube is developed by applying energy balance. For the same, the following assumptions are taken:

- Proposed receiver is at steady state condition.
- The heat flux is circumferentially uniform across the absorber tube.
- Thermal properties of the fluid and surrounding air are uniform.
- The flexible PV panel has negligible thickness and has same thermal conductivity as that of absorber tube.
- The epoxy thickness is considered to be negligible.

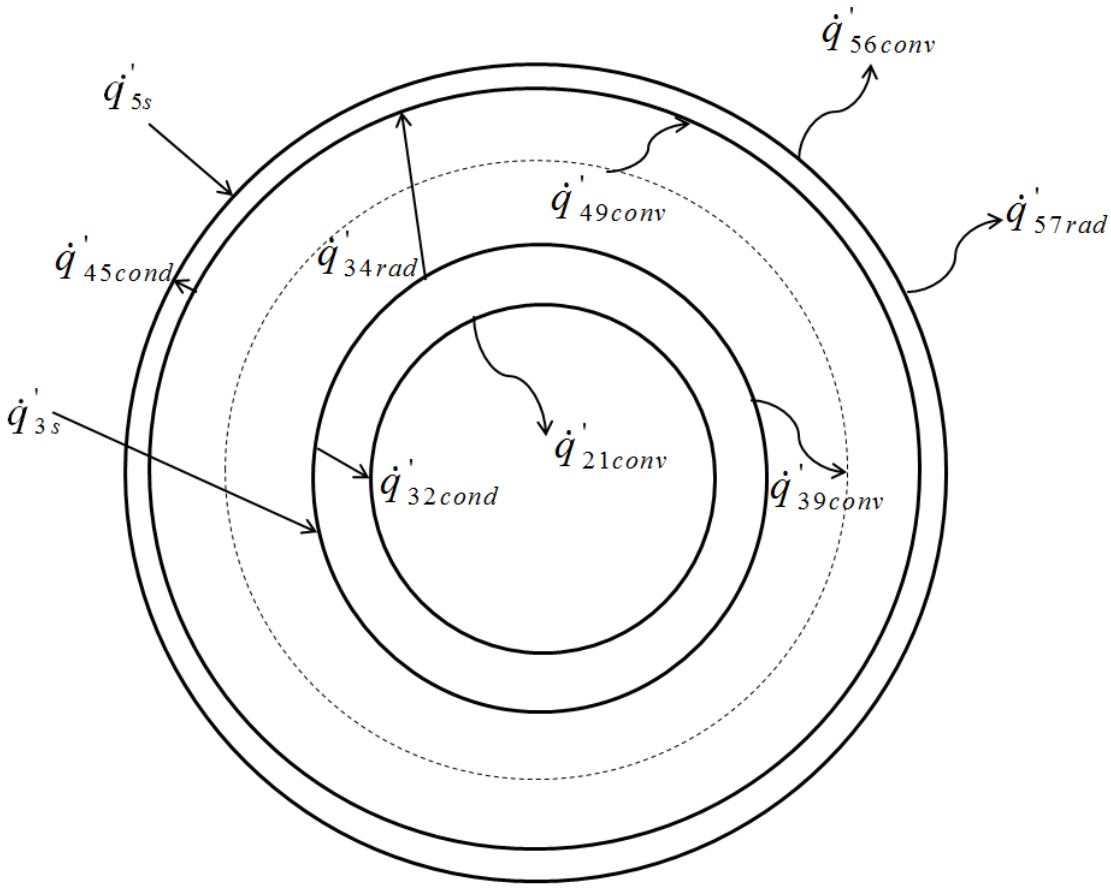


**Fig. 4.2 Energy balance of circular absorber tube**

The energy balance is performed on receiver which consists of glass tube and absorber pipe, as shown in Fig. 4.2. The flexible PV panel is mounted on irradiance side of absorber tube so that it receives maximum solar radiation. The HTF fluid flows inside the absorber tube as well as through the annulus.

### 4.1.1 Analytical model in MATLAB

The one dimensional energy balance is done similar to given in the literature [201, 202]. The energy model is modified by balancing the incoming solar radiation and optical losses. In this novel receiver, uniform circumferential heat flux is assumed and is taken from Forristall [67]. All the temperatures and thermodynamic properties are also assumed to be uniform across the circumference. Six surfaces are identified for the heat transfer analysis across the receiver. The mode and direction of energy transfer across the surfaces are shown in Table 4.1.

**Table 4.1 Heat transfer with the surfaces in circular absorber tube**

| **Heat Flux (W/m)*** | **Heat transfer mode** | **Heat transfer from** | **Heat transfer to** |
|---|---|---|---|
| $\dot{q}'_{5s}$ | Solar irradiation absorption | Incident solar radiation | Outer glass cover surface |
| $\dot{q}'_{45cond}$ | Conduction | Inner glass surface | Outer glass surface |
| $\dot{q}'_{56conv}$ | Convection | Outer glass surface | Ambient conditions |
| $\dot{q}'_{57rad}$ | Radiation | Outer glass surface | Sky |
| $\dot{q}'_{49conv}$ | Convection | Annulus fluid bulk surface | Inner glass surface |
| $\dot{q}'_{34rad}$ | Radiation | Outer absorber tube surface | Inner glass surface |
| $\dot{q}'_{39\ conv}$ | Convection | Outer absorber tube surface | Annulus fluid bulk surface |
| $\dot{q}'_{3s}$ | Solar irradiation absorption | Incident solar radiation | Outer absorber tube surface |
| $\dot{q}'_{32cond}$ | Conduction | Outer absorber tube surface | Inner absorber tube surface |
| $\dot{q}'_{bc}$ | Conduction | Outer absorber tube surface | Support bracket |
| $\dot{q}'_{21conv}$ | Convection | Inner absorber tube surface | Inner fluid |
| $\dot{q}'_{heatloss}$ | Convection and Radiation | Entire receiver | Ambient and sky |

*per unit aperture length

The incoming solar radiation falls on surface 5 ($\dot{q}'_{5s}$), which is glass envelope outer surface, as well as on surface 3 ($\dot{q}'_{3s}$) which is outer surface of absorber tube. Across the glass tube, the absorbed energy is transferred through conduction ($\dot{q}'_{45cond}$) and by convection ($\dot{q}'_{49conv}$) from surface 4. The surface 4 which is inner surface of glass tube allows heat transfer though convection from HTF (which is flowing within the annulus and taken as bulk surface 9). It also absorbs the long wavelength radiation emitted by surface 3. The surface 3 transfers the heat through convection ($\dot{q}'_{39conv}$) and conduction ($\dot{q}'_{32cond}$) to the HTF and inner surface of tube respectively. From surface 2, the inner of absorber tube, the heat transfer occurs by convection ($\dot{q}'_{21conv}$) to the inner fluid. The heat transfer through convection ($\dot{q}'_{56conv}$) and radiation ($\dot{q}'_{57rad}$) to the surrounding are the external losses from the outer surface 5 and are considered by taking ambient and sky conditions with subscript 6 and 7 respectively.

Using Fig. 4.2, the energy balances are applied on incoming and outgoing heat transfer on each surface and is represented in Eq. (4.1) to (4.5) [203].

$$\dot{q}'_{5s} + \dot{q}'_{45cond} = \dot{q}'_{56conv} + \dot{q}'_{57rad} \tag{4.1}$$

$$\dot{q}'_{49conv} = \dot{q}'_{45cond} + \dot{q}'_{34rad} \tag{4.2}$$

$$\dot{q}'_{39\,conv} = \dot{q}'_{49conv} \tag{4.3}$$

$$\dot{q}'_{3s} = \dot{q}'_{39\,conv} + \dot{q}'_{32cond} + \dot{q}'_{34rad} + \dot{q}'_{bc} \tag{4.4}$$

$$\dot{q}'_{32cond} = \dot{q}'_{21conv} \tag{4.5}$$

This is to mention here that solar absorptance on surface 5 ($\dot{q}'_{5s}$) and on surface 3 ($\dot{q}'_{3s}$) are taken as heat flux term. As discussed by Forristall [67], this assumption simplifies and makes the conduction equation linear across the glass and absorber tube. Though this

assumption introduces minimal error, for small absorbtance coefficient of the glass, this error can be neglected.

In Eq. (4.2) and (4.4) $\dot{q}'_{34rad}$ is the radiation emitted by the absorber tube. It is long wavelength radiations and got absorbed between the HTF fluid present in between the annulus. The heat transfer for each component is discussed in the further sections.

#### *4.1.1.1 Incident solar irradiation*

The incident solar radiation falling on the outer surface of the glass is treated as heat flux to simplify the thermal analysis. Also, the incident irradiation is taken as uniform over the entire circumferential surface. The variation in incident angle which causes optical losses by the incident rays which are not normal to the surface is given by Incident Angle Modifier (*K*) as

$$K = \cos\theta + 0.000884\theta - 0.00005369\theta^2 \tag{4.6}$$

Thus, *K* includes cosine losses at the concentrator aperture. The optical efficiency of the glass is given by radiation absorbed by the glass envelop by the incident normal irradiation. Forristall [67] also defines the solar absorption in glass as

$$\dot{q}'_{5s} = \dot{q}'_{irr}\eta_g\alpha_g \tag{4.7}$$

where $\eta_g = \epsilon_t\rho_{mi}K$, in which $\epsilon_t$ is the estimates of effective optical efficiency as given by Price [19] as $\epsilon_t = \epsilon_1.\epsilon_2.\epsilon_3.\epsilon_4.\epsilon_5.\epsilon_6$ and is shown in Table 4.2.

Where, $\dot{q}'_{irr}$ is the solar radiation falling on the receiver per unit length (W/m), $\eta_g$ is the effective optical efficiency of the glass, $\rho_{cl}$ is the clean mirror reflectance and $\alpha_g$ is the absorptance of the glass.

**Table 4.2 Technical specifications taken for the MATLAB model [19]**

| | | |
|---|---|---|
| $\epsilon_1$ | Receiver shadowing by shielding, support etc. | 0.974 |
| $\epsilon_2$ | Tracking error | 0.994 |
| $\epsilon_3$ | Geometry error (mirror alignment) | 0.98 |
| $\rho_{mi}$ | Mirror reflectance | 0.935 |
| $\epsilon_4$ | Dirt of mirror | Reflectivity/$\rho_{cl}$ |
| $\epsilon_5$ | Dirt on receiver and collector | $(1+\epsilon_4)/2$ |
| $\epsilon_6$ | Unaccounted | 0.96 |

The incident solar radiation on the absorber tube after passing through the glass envelops and HTF can also be treated as heat flux. The equation of solar absorption becomes

$$\dot{q}'_{3s} = \dot{q}'_{irr}\eta_t\alpha_t \tag{4.8}$$

while $\eta_t = \eta_g\tau_g\tau_f$, in which $\tau_g$ is the transitivity of glass envelope, $\tau_f$ is the transitivity of HTF and $\alpha_t$ is the absorptance of absorber tube.

### *4.1.1.2 Conductive heat transfer*

The conduction heat transfer takes place on three surfaces in the given model. One is within the glass and the other is within the absorber tube. The third case is actually heat losses in the form of conduction from the support brackets. The conduction heat transfer within the glass and tube are governed by Eq. (4.9) and (4.10), respectively

$$\dot{q}'_{45cond} = \frac{2\pi k_g(T_4 - T_5)}{\ln\left(\frac{D_4}{D_3}\right)} \tag{4.9}$$

$$\dot{q}'_{32cond} = \frac{2\pi k_t(T_2 - T_3)}{\ln\left(\frac{D_2}{D_1}\right)} \tag{4.10}$$

where $k_g$ and $k_t$ are thermal conductivity of glass envelope and absorber tube respectively. $D_1$ and $D_3$ are the inner diameter of absorber tube and glass envelope respectively, while $D_2$ and $D_4$ are outer diameter of absorber tube and glass envelope respectively. $T$ is the temperature corresponds to the respective surface. The value of thermal conductivity of glass envelope and absorber tube are assumed to be uniform throughout the surface and is taken from the Bergman *et al.* [204].

The conduction from the support bracket depends on the contact area between absorber tube and bracket. To estimate the heat losses from bracket, it is treated as an infinite fin with base temperature 10 degree less than the $T_3$ [67]. For the simplification the perimeter of the support bracket is taken as 0.2032 m having area of 1.613 x $10^{-4}$ $m^2$. The thermal conductivity of bracket is assumed to be 50 W/m.K. The convective heat transfer coefficient depends on wind or no-wind case. From the literature [19], it is taken within the range of 2 $W/m^2$.K to 25 $W/m^2$.K (for no-wind) and 25 $W/m^2$.K to 250 $W/m^2$.K (for wind). The conduction equation for such system is given as:

$$\dot{q}_{bc}^{'} = \frac{\sqrt{h_b P_b k_b A_b}(T_b - T_6)}{L_r} \tag{4.11}$$

In Eq. (4.11), $h_b$ is the convection coefficient of the bracket, $P_b$ is perimeter of the bracket, $k_b$ is the thermal conductivity of bracket, $A_b$ is the cross-sectional area of bracket, $T_b$ is the base temperature of bracket, $T_6$ is ambient temperature and $L_r$ is the length of receiver.

#### *4.1.1.3 Convective heat transfer*

The convection occurs at four surfaces in this model. From surface 5, the convection ($\dot{q}_{56conv}^{'}$) occurs from outer glass surface to the ambient conditions. The temperature difference is assumed to be linear here. The convection term is given by

$$\dot{q}'_{56conv} = h_{56} D_4 \pi (T_5 - T_6) \tag{4.12}$$

with

$$h_{56} = Nu_{56} \frac{k_g}{D_4} \tag{4.13}$$

where $h_{56}$ is the convective heat transfer coefficient from surface 5 to ambient and $Nu_{56}$ is the Nusselt number.

The value of Nusselt number for the Eq. (4.13) can be obtained by assuming cross-sectional flow over the long cylinder. The flow velocity over the cylinder governs the Reynolds number and thus Nusselt number. To assess the convection coefficient, wind and no-wind cases are used. For the no-wind case, the convection from the glass surface to the surrounding will only by natural convection. To estimate the natural convection, the correlation given by Churchill and Chu was used as [205]

$$Nu_{56} = \left\{ 0.60 + 0.387 \frac{Ra_{56}^{\frac{1}{6}}}{\left[1 + \left(\frac{0.559}{Pr_{56}}\right)^{\frac{9}{16}}\right]^{\frac{8}{27}}} \right\}^2 \tag{4.14}$$

$$Ra_{56} = \frac{g\beta(T_5 - T_6)D_4^3}{\alpha_{56}\nu_{56}} \tag{4.15}$$

$$\beta = \frac{1}{T_{56}} \tag{4.16}$$

$$Pr_{56} = \frac{\nu_{56}}{\alpha_{56}} \tag{4.17}$$

where $Ra_{56}$ is Rayleigh number for glass outer cover at $D_5$, $\alpha_{56}$ is thermal diffusivity at temperature $T_{56}$, $\beta$ is volumetric coefficient for thermal expansion, $Pr_{56}$ is Prandtl number

at temperature $T_{56}$, $\nu_{56}$ is kinematic viscosity of air at $T_{56}$ and $T_{56}$ is the film temperature and is average of $T_5$ and $T_6$.

The Eq. (4.14) is valid for $10^5$< Ra < $10^{12}$. In case of wind, the convection will be forced and the correlation for Nusselt number can be obtained by using Churchill and Bernstein equation. This correlation is valid for all ranges of Reynolds number with $Re_D Pr >$ 0.2 [204].

$$Nu = 0.3 + \frac{0.62 Re^{\frac{1}{2}} Pr^{\frac{1}{3}}}{\left[1 + \frac{0.4}{Pr_{56}^{\frac{2}{3}}}\right]^{\frac{1}{4}}} \left[1 + \left(\frac{Re_{56}}{282000}\right)^{\frac{5}{8}}\right]^{\frac{4}{5}} \tag{4.18}$$

This correlation assumes long horizontal cylinder with isothermal conditions. The fluid (air) properties are taken as ambient conditions, while $Pr_{56}$ is evaluated at the film temperature on surface 5.

The convection within the absorber tube can be estimated by taking the fluid flow inside the tube. The correlations as suggested by Petukhov are [153]

$$\dot{q}'_{21conv} = h_{21} D_1 \pi (T_2 - T_1) \tag{4.19}$$

$$Nu = \frac{\left(\frac{f}{8}\right) RePr}{1.07 + 12.7\sqrt{\frac{f}{8}}\left(Pr^{\frac{2}{3}} - 1\right)} \left(\frac{Pr_{56}}{Pr_5}\right)^n \tag{4.20}$$

where n = 0.11 (for heating)

$$f = (0.79 \ln Re - 1.64)^{-2} \tag{4.21}$$

The other two convections occur between the annulus, from the outer surface of the absorber tube to the HTF ($\dot{q}'_{39\,conv}$) and from the inner surface of the glass cover to the HTF ($\dot{q}'_{49conv}$). The convective heat transfer for surface 3 and surface 4 can be calculated by using

Petukhov correlation, Eq. (4.19). Gnielinski [206] modified the correlation, Eq. (4.20), by adding the effect of characteristics length during the convection.

$$Nu = \frac{\left(\frac{f}{8}\right) RePr}{1 + 12.7\sqrt{\frac{f}{8}}\left(Pr^{\frac{2}{3}} - 1\right)} . \left[1 + \left(\frac{d}{L}\right)^{\frac{2}{3}}\right] \tag{4.22}$$

where

$$f = (1.8 \log Re \ - 1.5)^{-2} \tag{4.23}$$

In this correlation, for $\dot{q}'_{39\,conv}$ (convection between surface 3, $T_3$, and bulk mean temperature of water, $T_9$) and for $\dot{q}'_{49conv}$ (convection between surface 4, $T_4$, and bulk mean temperature of water, $T_9$), the hydraulic diameter ($d_h$) is taken as characteristics length for the estimation of Reynolds Number. It is given by

$$d_h = D_3 - D_2 \tag{4.24}$$

#### *4.1.1.4 Radiation heat transfer*

The radiation occurs from glass surface to the sky ($\dot{q}'_{57rad}$) and from the absorber tube to the glass ($\dot{q}'_{34rad}$). The later one occurs due to high temperature of the absorber tube and is of long wavelength. It will get absorbed within the HTF and thus increases the temperature of the HTF. The radiation term for $\dot{q}'_{57rad}$ is given by Stefan-Boltzmann law and is given by

$$\dot{q}'_{57rad} = \sigma \epsilon_g \pi D_4 (T_5^4 - T_7^4) \tag{4.25}$$

where $\sigma$ is the Stefan-Boltzmann constant (5.67 x $10^{-7}$ W/m$^2$K$^4$), $\epsilon_g$ is the emissivity of the glass envelope and $T_7$ is the Sky temperature.

The absorber tube radiation can be treated as the radiation between two concentric cylinders with participating media in between. Here, for the simplicity the scattering and

attenuation effects have been neglected between the fluid molecules. The radiation equation for this case is given as [207]

$$\dot{q}'_{34rad} = \frac{\mu^2 \sigma (T_3^4 - T_4^4)}{\frac{1}{\Psi} + \frac{1}{\epsilon_t} - 1 + \frac{\left(\frac{D_2}{D_3}\right)}{\left(\frac{1}{\epsilon_g}\right)-1}} \tag{4.26}$$

where $\mu$ is the refractive index of the HTF, $\epsilon_t$ is the emissivity of the absorber tube at temperature $T_3$. $\Psi$ is a non-dimensional radiative heat flux in terms of surface radiosities and is given by

$$\Psi = \frac{q_h}{J_1 - J_2} \tag{4.27}$$

In Eq. (4.27), $q_h$ is the heat loss from the non scattering isothermal absorber tube, at any instance, while $J_1$ and $J_2$ are the radiosity for the inner and outer surface respectively.

This $\Psi$ depends upon the ratio of two cylinders diameter ($D_2/D_3$) and is taken from Modest [207]. Further this term can be neglected if we assumed all the long wave radiation got absorbed within the next fluid layer to the absorber tube. The radiation between the fluid layer and from fluid layer to the glass can be estimated by using generic equations for long infinite concentric cylinder with participating media [204].

$$\dot{q}'_{34rad} = \frac{\sigma \pi D_2 (T_n^4 - T_{n-1}^4)}{\frac{1}{\epsilon_t} + \frac{1-\epsilon_g}{\epsilon_g}\left(\frac{D_2}{D_3}\right)} \tag{4.28}$$

where $T_n$ and $T_{n-1}$ are the intermediate fluid temperature at *n* and *n-1* layer respectively.

#### *4.1.1.5 Heat Losses*

The heat losses in the receiver include the convection and radiation heat loss from the outer glass envelope to the environment and the conduction losses from the support bracket. It is given as:

$$\dot{q}'_{heatloss} = \dot{q}'_{57rad} + \dot{q}'_{56conv} + \dot{q}'_{bc} \quad (4.29)$$

The Eq. (4.1) to (4.29) is solved using MATLAB using the following algorithm, as shown in Fig. 4.3. The solutions obtained from the MATLAB simulations are then compared with the results obtained from the COMSOL simulation.

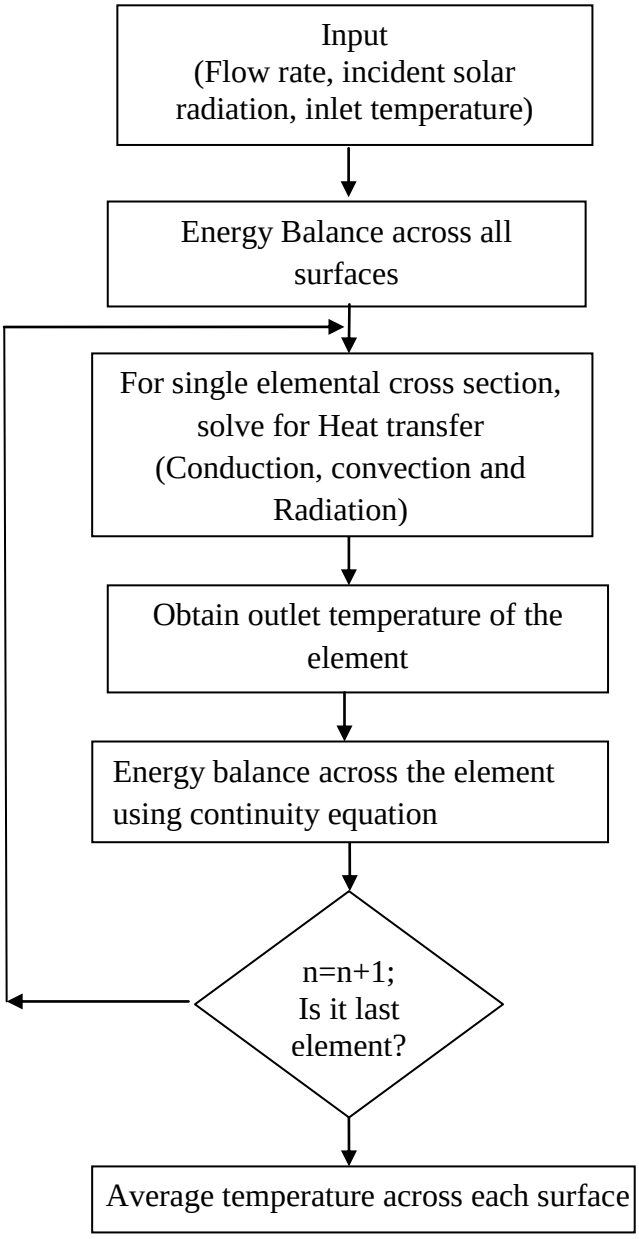


**Fig. 4.3 Schematic representation of solution algorithm for modeling in MATLAB**

### 4.1.2 Simulation model in COMSOL

The validation of proposed model is done by simulating the system using COMSOL (v5.1). For the simplified solution, the 3D model of the receiver is taken as 2D symmetrical model and thermal analysis is done by selecting heat transfer multiphysics. The length of receiver tube is taken as 1.2 m with glass tube outer diameter of 125 mm and inner diameter of 110 mm. The absorber tube outer diameter is considered as 70 mm and inner diameter as 65.6 mm. The thickness of PV cell is taken as 0.5 mm. Since back side of PV panel is attached to the absorber tube, the surface 2, which is in contact with fluid, is taken as the back cell temperature. For multiphysics, simple heat transfer in solid along with laminar flow model is used. The meshing is taken with normal approach with the curvature factor of 0.3, as per the simulation tool. The two physics are coupled with temperature coupling. The parameters taken for the simulations are shown in Table 4.3. The simulated model of receiver tube is shown in Fig. 4.4 in which the temperature variation along the length is presented.

**Table 4.3 Circular receiver tube specification used in the model**

| Parameters | Value |
|---|---|
| Receiver tube length | 1.2 m |
| Absorber internal diameter | 0.0656 m |
| Emissivity of glass | 0.82 |
| Absorber tube external diameter | 0.07 m |
| Absorber tube (copper) thermal conductivity | 401 W/m.K |
| Glass cover internal diameter | 0.110 m |
| Emissivity of absorber tube | 0.4 |
| Optical efficiency of glass envelop | 0.8 |
| Absorptance of glass envelope | 0.04 |
| Thermal conductivity of glass | 1.04 W/m.K |
| Thermal conductivity of air | 0.026 W/m.K |
| Thermal conductivity of fluid | 0.1357 W/m.K |
| Density of air | 1.2 $kg/m^3$ |
| Density of fluid | 1060 $kg/m^3$ |
| Dimensionless radiative heat transfer coefficient | 0.96 |

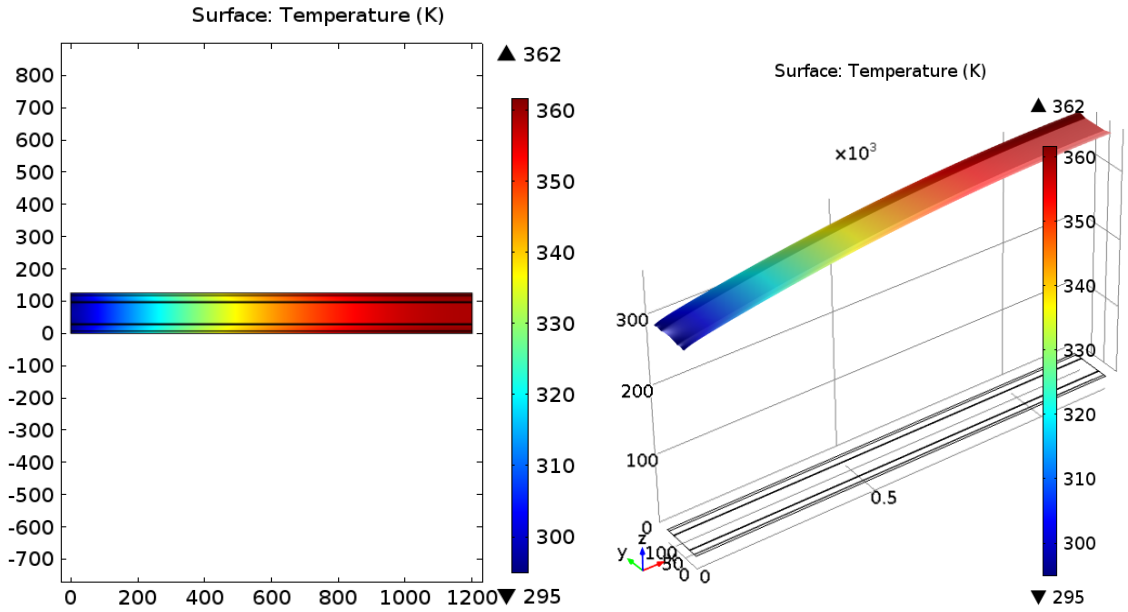


**Fig. 4.4 Temperature plot of receiver tube along the length (mm)**

### 4.1.3 Results and discussion

The COMSOL simulation of proposed system having flexible PV module mounted on the absorber tube with HTF on both sides of the panels is simulated using parameters mentioned in Table 4.3. The temperature variation across the six different surfaces along the length is shown in Fig. 4.5. It is observed that the temperature at the outer glass surface (surface 5) increases gradually as compared to inner most fluid (surface 1). The temperature at surface 2 and 3 are almost identical with the fact that it is the inner and outer surface of the absorber tube having smaller thickness. Similar trend is observed in inner and outer surface of glass tube. The inlet temperature of annulus (which is assumed to be 295 K) converges to around 360 K, at the exit. The temperature results obtained are then compared with the results obtained through analytical model using MATLAB. The results for fixed outer glass envelope cross section is compared with the values obtained from COMSOL and are shown in Fig. 4.6.

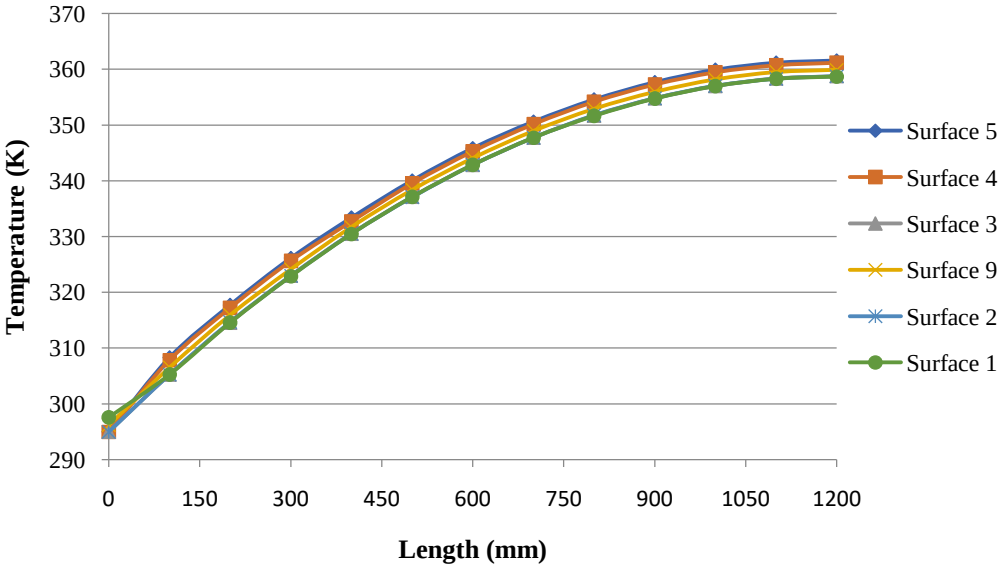


**Fig. 4.5 Temperature variation over various surface obtained using COMSOL**

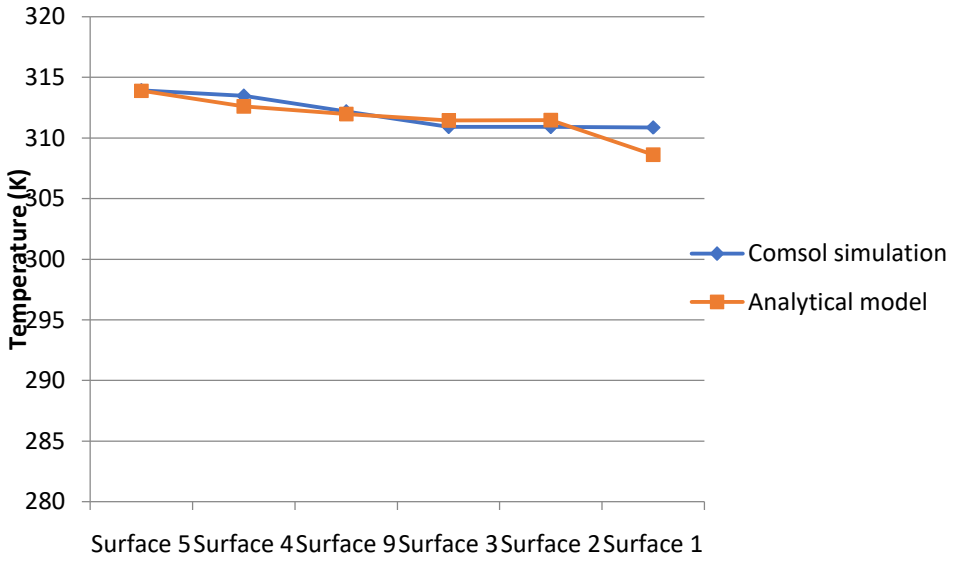


**Fig. 4.6 Modeling on COMSOL compared with analytical model for same outer glass envelope temperature**

The maximum temperature obtained at the end of the receiver was 361 K in case of COMSOL simulation, while it was obtained as 355 K in case of analytical model. This validation shows that the proposed model is within the range with a slight variation (error of ±1.7%). The error arose due to the assumptions which are taken during the analytical model. The COMSOL model is also varied with the condition when no water flows through the annulus, by making it similar to stagnant air tube conditions. The simulations in the

COMSOL reveal the maximum panel temperature that could be achieved in case of no fluid within the annulus. The plot obtained in such case is shown in Fig. 4.7. The graphical representation shows that without fluid flow, the maximum temperature obtained as 407 K which is 46 degrees higher than the fluid flow case. Thus without fluid flow, or cooling from one side, the absorber tube temperature would be much higher. This higher temperature of outer surface of absorber tube will lead to higher PV panel temperature. This leads to degradation of the cell and reduces its electrical efficiency. Thus, there is need to cool down the cell under high concentration to maintain cell integrity. With both sides cooling not only the operating efficiency of PV cells will increase but also the heat gained by the fluids in the annulus as well as in the absorber tube will enhance the overall utility of the system.

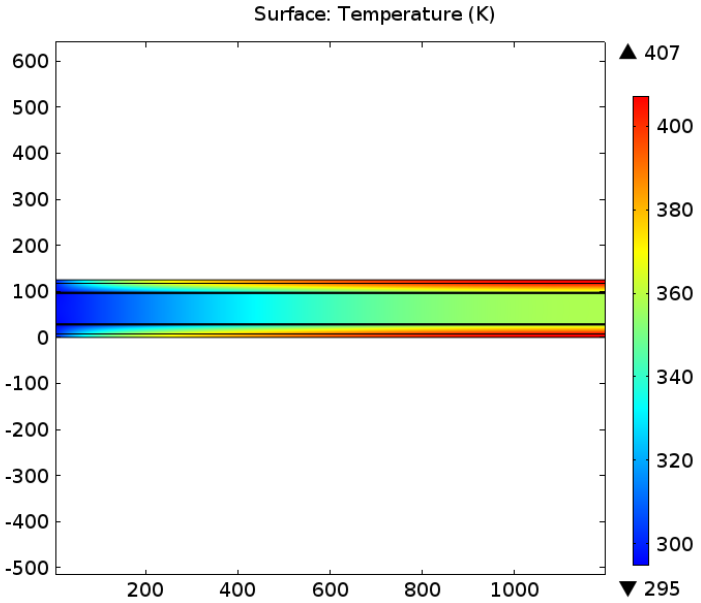


**Fig. 4.7 COMSOL plot for no fluid flow case within the annulus**

## 4.2 Analytical Model of Novel Semi-circular HCPVT Receiver

This section presents numerical modeling of proposed HCPVT receiver for the climatic conditions of Pilani, Rajasthan. The model was designed using MATLAB (v2012a), which includes one dimensional model of novel HCPVT receiver system. The first law analysis of the proposed receiver was carried out by considering assumptions similar to the one taken for circular absorber tube, as discussed in Sec. 4.1.

The first law analysis of the proposed novel absorber receiver is carried out using equations given in the literature [19, 68]. Using the same methodology of circular absorber tube, as discussed in Sec. 4.1.1, the energy balance is carried out on incoming solar radiation and optical losses to the surroundings. In the model, six surfaces and two bulk surfaces are identified for the heat transfer analysis across the receiver. The incoming solar radiation ($\dot{q}'_{5s}$ , $\dot{q}'_{3s}$), conduction ($\dot{q}'_{45cond}$ , $\dot{q}'_{32cond}$), convection ($\dot{q}'_{49conv}$ , $\dot{q}'_{39conv}$ , $\dot{q}'_{21conv}$ , $\dot{q}'_{56conv}$) and radiation ($\dot{q}'_{34rad}$ , $\dot{q}'_{57rad}$) are taken same as discussed in Sec. 4.1.1. The concentrated radiation falls on the front surface of PV cell ($\dot{q}'_{f}$) passing through the glass and fluid in the annulus. The flat part of the tube transfers heat mainly through convection to bulk surface 8 (annulus between front of PV cell and inner glass surface) and surface 4. The energy balance equations of the system, as shown in Fig. 4.8, are represented from Eq. (4.30) to (4.34).

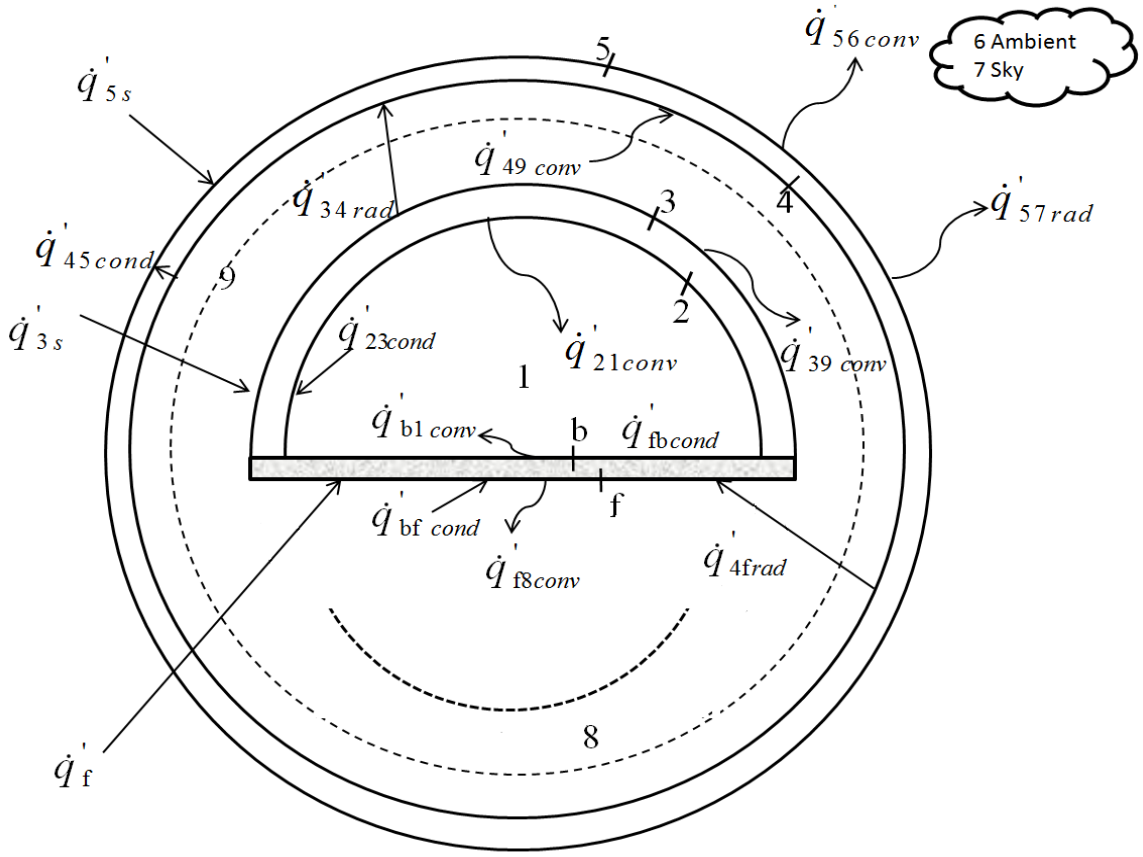


**Fig. 4.8 One dimensional steady state energy balance of D-shape absorber tube**

$$\dot{q}'_{21conv} + \dot{q}'_{b1conv} = \dot{q}'_{23cond} \quad (4.30)$$

$$\dot{q}'_{3s} + \dot{q}'_{f} + \dot{q}'_{fbcond} = \dot{q}'_{39\,conv} + \dot{q}'_{23cond} + \dot{q}'_{34rad} + \dot{q}'_{f8conv} + \dot{q}'_{4f\,rad} \quad (4.31)$$

$$\dot{q}'_{49conv} + \dot{q}'_{4f\,rad} + \dot{q}'_{48conv} = \dot{q}'_{45cond} + \dot{q}'_{34rad} \quad (4.32)$$

$$\dot{q}'_{5s} + \dot{q}'_{45cond} = \dot{q}'_{56conv} + \dot{q}'_{57rad} \quad (4.33)$$

$$\dot{q}'_{39\,conv} + \dot{q}'_{48\,conv} = \dot{q}'_{49conv} \quad (4.34)$$

In Eq. (4.31) and (4.32), and $\dot{q}'_{4f\,rad}$ is the radiation emitted by the semi-circular surface and PV panel mounted on the absorber tube. It is long wavelength radiations and got absorbed between the HTF present in between the annulus.

### 4.2.1 Heat transfer analysis across D-shape absorber tube

The incident solar radiation ($\dot{q}'_{5s}$) falling on the outer surface of the glass of the D-shape receiver would be same as Eq. (4.7) as discussed in Sec. 4.1.1.1. Similarly, the solar radiation falling on the absorber tube ($\dot{q}'_{3s}$), after passing through the glass envelop would be same as Eq. (4.8). The radiation falling on the PV cell surface *f*, is the concentrated radiation and is given as

$$\dot{q}'_{f} = CR.\dot{q}'_{5s} \quad (4.35)$$

The rest of the receiver part consists of glass tube, absorber tube and cooling water. Within them, the heat transfer would occur by all three modes, i.e., conduction, convection and radiation.

#### *4.2.1.1 Conduction heat transfer*

In the proposed D-shape receiver, the conductive heat transfer occurs within glass, absorber tube and PV panel. The correlation for conduction within the glass ($\dot{q}'_{45cond}$) and

tube ($\dot{q}'_{23cond}$) would be same as Eq. (4.9) and Eq. (4.10) respectively, as discussed in Sec. 4.1.1.2. It is assumed that the thermal conductivity of glass envelope and absorber tube is uniform throughout the surface and are taken from the literature [204]. The conductive heat transfer within the PV cell ($\dot{q}'_{fb\ cond}$) is taken from Jakhar *et al.* [208].

#### *4.2.1.2 Convection heat transfer*

In the current model, the convective heat transfer occurs at five different surfaces. As discussed in Sec. 4.1.1.3, the convection across outer glass surface ($\dot{q}'_{56conv}$) is given in Eq. (4.12). The convection within the semi-circular absorber tube can be evaluated by taking the correlations for Nusselt number given by Manglik and Bergles [209].

$$\dot{q}'_{21conv} = h_{21} D_h \pi (T_2 - T_1) \tag{4.36}$$

In this relation, Nusselt Number and hydraulic diameter ($D_h$) is given by [208]

$$Nu = 5.626[1 + 0.0533(Gz)^{0.914}]^{0.476} \tag{4.37}$$

$$D_h = \frac{\pi D}{\pi + 2} \tag{4.38}$$

The convective heat transfer $\dot{q}'_{39\ conv}$, $\dot{q}'_{49conv}$ and $\dot{q}'_{48conv}$ can be calculated by using modified Petukhov correlation as discussed in Eq. (4.22). The convection from the PV cell front surface '*f*' to the bulk surface 8 ($\dot{q}'_{f8conv}$) as well as from the back surface '*b*' to bulk surface 1 ($\dot{q}'_{b1conv}$) can be calculated using the following Nusselt number

$$Nu_{f8} = 0.678\, Re^{0.5}\, Pr^{0.3} \tag{4.39}$$

#### *4.2.1.3 Radiation heat transfer*

The radiation heat transfer from the D-shape receiver is similar to radiation heat transfer from circular absorber tube, except radiation from the flat surface. The radiation

($\dot{q}'_{57rad}$ and $\dot{q}'_{34rad}$) would be same as Eq. (4.25) and Eq. (4.26) respectively, as discussed in Sec. 4.1.1.4. Similarly radiation from surface 4 to cell front surface ($\dot{q}'_{4frad}$) can be evaluated through Eq. (4.26) by considering the radiosity between flat surface to curved surface.

### 4.2.2 Heat transfer across PV panel in D-shape absorber tube

In case of D-shape receiver, the PV panel thickness is considered for heat transfer and first law analysis. For the same, one dimensional steady state heat transfer is assumed across the absorber tube with negligible heat capacity. It is also assumed that heat transfer to support structure is negligible. The epoxy thickness within the absorber tube and PV panel is considered to be negligible and have same thermal conductivity as that of the absorber tube. Within the PV module, temperature gradient and Ohmic losses are neglected.

Using the first law analysis of PV system, the electrical and thermal efficiencies of the hybrid receiver are evaluated. The energy balance for the PV module would become [210]

$$\tau_{g,c}\alpha_c\gamma_c IrWdx + \tau_g(1-\gamma_c)\alpha_{ted} IrWdx = \left[U_{c,fl}\left(T_c - T_{fl}\right) + U_{ct}(T_c - T_{ba})\right]Wdx + \eta_{c,el}\gamma_c\tau_g IrWdx \quad (4.40)$$

Where $T_c, T_{ba}, T_{fl}, W, Ir$, $\eta_{c,el}$ and $\gamma_c$ are PV panel temperature, back surface temperature of absorber, fluid temperature over panel, width of absorber, incident solar radiation, electrical efficiency of solar cell and packing factor of solar cell respectively.

By solving the Eq. (4.40), the equation for the mean solar cell temperature obtained as:

$$\overline{T_c} = \frac{\tau_g[\alpha_c\gamma_c + (1-\gamma_c)\alpha_{ted} - \eta_{c,el}\gamma_c]Ir + U_{c,fl}T_{fl} + U_{ct}\overline{T}_{bf}}{U_{c,fl} + U_{ct}} \quad (4.41)$$

The average absorber temperature $\overline{T}_{bf}$ is dependent upon average fluid temperature $\overline{T}_W$ within the inner tube and the radiation falling on this as given below [210]

$$\overline{T}_{ba} = \frac{N(\alpha\tau)_{eff} Ir + U_{g,ted} T_{fl} + U_{aw} \overline{T}_W}{U_{g,ted} + U_{aw}} \tag{4.42}$$

Here, N is the penalty factor due to presence of cell material, glass and ethylene vinyl acetate film. The overall heat transfer coefficient from glass to tedlar is calculated as [211]

$$U_{gt} = \frac{U_{c,fl} \times U_{ct}}{U_{c,fl} + U_{ct}} \tag{4.43}$$

After obtaining $\overline{T}_{ba}$ from Eq. (4.42) the expression for an average solar cell temperature $\overline{T_c}$ can be evaluated from Eq. (4.41). The maximum power output from a PV panel is evaluated which is given as

$$P_{max} = V_{max} . I_{max} \tag{4.44}$$

Where $V_{max}$ and $I_{max}$ are voltage and current at maximum power point respectively.

The efficiency $(\eta_c)$ of the PV panel, which is dependent on STC conditions can be calculated using expressions from Evans [212] and Schott [213]

$$\eta_c = \eta_o [1 - \beta_0 (T_c - T_{STC})] \tag{4.45}$$

While the PV panel efficiency depends upon the reflectivity, transmittance of the glass surface and cell efficiency. It is given as [214]

$$\eta_{mod} = \rho_c \tau_g \eta_c \tag{4.46}$$

The instantaneous electrical efficiency of HCPVT receiver is calculated as [215]

$$\eta_{el} = \frac{FF\ I_{sc} V_{oc}}{A_c Ir} \tag{4.47}$$

The instantaneous thermal efficiency of the HCPVT receiver is [214]

$$\eta_{th} = \frac{Q_{th}}{A_a . Ir} = \frac{m_w cp_w \ (T_{w,o} - T_{w,i})}{A_a . Ir} \tag{4.48}$$

The overall efficiency of the system is summation of the thermal and electrical efficiency and given as

$$\eta_{tot} = \eta_{th} + \eta_{el} \tag{4.49}$$

The design parameters of D-shape, which are taken for the analytical model are given in Table 4.4.

**Table 4.4 Design parameters of D-shape HCPVT receiver**

| **Parameters** | **Value** |
|---|---|
| Width of PV cell | 0.072 mm |
| Thermal conductivity of the insulating material | 0.041 W/m.K |
| Thermal conductivity of the absorber tube (copper) | 401 W/m.K |
| Thermal conductivity of glass | 1.04 |
| Thermal conductivity of the solar cell | 0.036 W/m.K |
| Absorptivity of solar cell ($\alpha_c$) | 0.90 |
| Transmissivity of solar cell ($\tau_c$) | 0.90 |
| Transmissivity of glass ($\tau_g$) | 0.96 |
| Absorptivity of tedlar ($\alpha_{ted}$) | 0.75 |
| Emissivity of glass ($\varepsilon_g$) | 0.82 |
| Emissivity of copper absorber tube ($\varepsilon_t$) | 0.4 |
| Reflectivity of mirror ($\rho_{mi}$) | 0.935 |
| Reflectivity of cell ($\rho_c$) | 0.83 |

## 4.3 Analytical Model of Novel Triangular HCPVT Receiver

Similar to the analytical approach of circular and semi-circular HCPVT receiver, a novel design comprising triangular shape HCPVT receiver is also proposed. The model was also developed and designed using MATLAB for the climatic conditions of Pilani. Using one dimensional technique, the first law analysis of the novel triangular shaped novel is carries

out. In the current model, the PTC (collector part) would remain same as that of semi-circular HCPVT system. Similarly, the heat transfer between the PV panel and absorber tube would be same. Hence, the same equation as discussed in Sec. 4.2.2 would be applicable here. In the current section, only heat transfer analysis of triangular absorber tube is presented by considering assumptions similar to the one taken for circular and semi-circular absorber tube, as discussed in Sec. 4.1 and Sec. 4.2 respectively.

The first law analysis of the proposed novel absorber receiver is carried out using equations given in the literature [70]. Using the same methodology of circular absorber tube, as discussed in Sec. 4.1.1, the energy balance is carried out on incoming solar radiation and optical losses to the surroundings. In the model, six surfaces and one bulk surface are identified for the heat transfer analysis across the receiver. The incoming solar radiation ($\dot{q}'_{5s}$, $\dot{q}'_{3s}$), conduction ($\dot{q}'_{45cond}$ , $\dot{q}'_{32cond}$), convection ($\dot{q}'_{49conv}$ , $\dot{q}'_{39conv}$ , $\dot{q}'_{21conv}$ , $\dot{q}'_{56conv}$) and radiation ($\dot{q}'_{34rad}$ , $\dot{q}'_{57rad}$) are taken same as discussed in Sec. 4.1.1. The concentrated radiation ($\dot{q}'_{f}$) is taken same as discussed in Sec. 4.2.1. The triangular sides (*f*) transfer heat ($\dot{q}'_{f9\,conv}$) to the bulk surface 9 (annulus between front of PV cell and inner glass surface) and to the inner surface (*b*). The energy balance equations of the system, as shown in Fig. 4.9, are represented from Eq. (4.50) to (4.54).

$$\dot{q}'_{21conv} + 2\dot{q}'_{b1conv} = \dot{q}'_{23cond} \tag{4.50}$$

$$\dot{q}'_{3s} + 2\dot{q}'_{f} + \dot{q}'_{fbcond} = \dot{q}'_{39\,conv} + \dot{q}'_{23cond} + \dot{q}'_{34rad} + 2\dot{q}'_{f9conv} + 2\dot{q}'_{4f\,rad} \tag{4.51}$$

$$\dot{q}'_{49conv} + 2\dot{q}'_{4f\,rad} = \dot{q}'_{45cond} + \dot{q}'_{34rad} \tag{4.52}$$

$$\dot{q}'_{5s} + \dot{q}'_{45cond} = \dot{q}'_{56conv} + \dot{q}'_{57rad} \tag{4.53}$$

$$\dot{q}'_{39\,conv} + 2\dot{q}'_{f9\,conv} = \dot{q}'_{49conv} \tag{4.54}$$

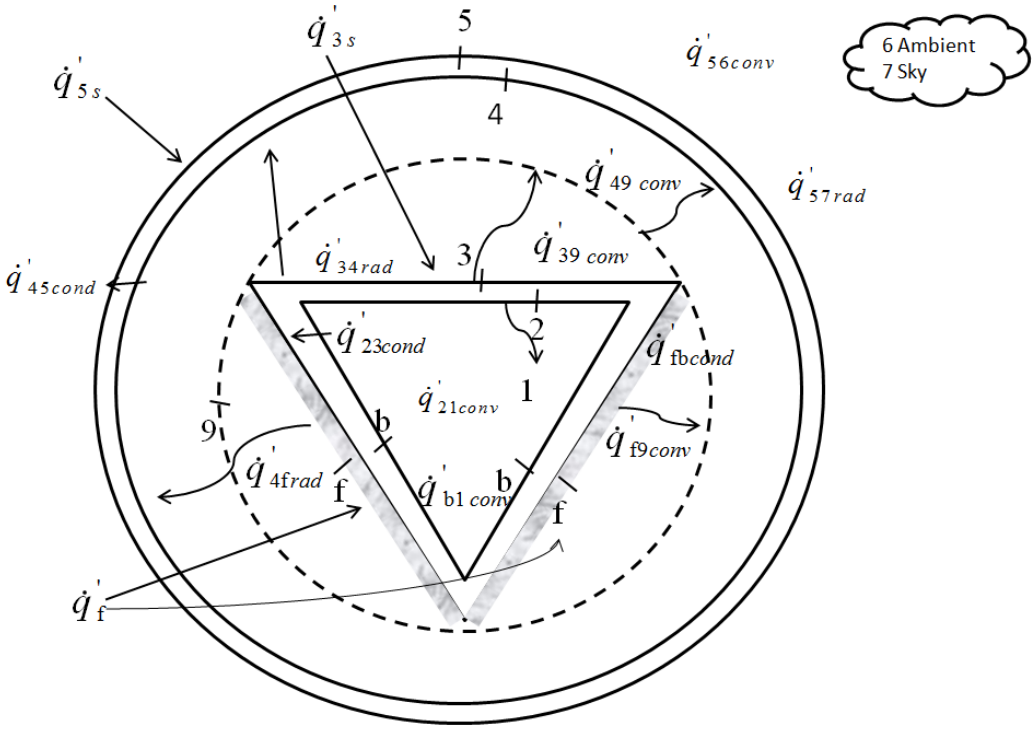


**Fig. 4.9. One dimensional steady state energy balance of triangular absorber**

In Eq. (4.51) and (4.52), $\dot{q}'_{34rad}$ and $\dot{q}'_{4frad}$ are the radiation emitted by the triangular side surfaces and PV panel respectively. It is long wavelength radiations and got absorbed between the HTF present in between the annulus.

### 4.3.1 Heat transfer analysis across triangular shape absorber tube

The incident solar radiation ($\dot{q}'_{5s}$) falling on the outer surface of the glass of the triangular shape receiver would be same as Eq. (4.7) as discussed in Sec. 4.1.1.1. Similarly, the solar radiation falling on the triangular absorber ($\dot{q}'_{3s}$), after passing through the glass envelop would be same as Eq. (4.8). The radiation falling on the PV cell surface would be same as Eq. (4.35). The rest of the receiver part consists of glass tube, triangular absorber and cooling water. Within them, the heat transfer would occur by all three modes which as discussed as:

#### *4.3.1.1 Conduction heat transfer*

In the proposed triangular shape receiver, the conductive heat transfer occurs within glass, absorber tube and PV cell, similar to D-shape receiver. The correlation for conduction within the glass ($\dot{q}'_{45cond}$) and tube ($\dot{q}'_{23cond}$) would be same as Eq. (4.9) and Eq. (4.10) respectively, as discussed in Sec. 4.1.1.2. It is assumed that the thermal conductivity of glass envelope and absorber is uniform throughout the surface and are taken from the literature [204]. The conductive heat transfer within the PV cell ($\dot{q}'_{fb\ cond}$) is taken from Jakhar *et al.* [208] and is discussed in Sec. 4.2.2.

#### *4.3.1.2 Convection heat transfer*

In the current model, the convective heat transfer occurs at five different surfaces, as shown in Fig. 4.9 As discussed in Sec. 4.1.1.3, the convection across outer glass surface ($\dot{q}'_{56conv}$) is given in Eq. (4.12). The convection within the triangular absorber tube can be evaluated by taking the correlations for Nusselt number as [209].

$$\dot{q}'_{21conv} = h_{21} A_a (T_2 - T_1) \tag{4.55}$$

In this relation, $A_a$, inner area of the triangular absorber and $h_{21}$ is given as

$$h = 0.59 \frac{\lambda_a (Gr.Pr)^{0.25}}{d_o} \tag{4.56}$$

Here, $\lambda_a$ is the thermal conductivity of fluid under the characteristic temperature, which is average of back surface of cell temperature and water temperature.

$$Gz = \frac{g\alpha \Delta T d_o^3}{\nu^2} \tag{4.57}$$

In Eq. (4.57), $\alpha$ is thermal diffusivity, $\nu$ is kinematic viscosity and $d_o$ is the depth of the triangular absorber. The convective heat transfer $\dot{q}'_{39\ conv}$ and $\dot{q}'_{49conv}$ can be calculated by using modified Petukhov correlation by adding the effect of characteristics length during the convection [70]

$$Nu = 3.669 + \frac{0.169\left(Re.Pr.\frac{D_h}{L}\right)^{0.25}}{1 + 0.191\left(Re.Pr.\frac{D_h}{L}\right)^{\frac{7}{12}}}\left(\frac{\mu_f}{\mu_w}\right)^{0.1} \quad (4.58)$$

The convection from the PV cell front surface '$f$' to the bulk surface 9 ($\dot{q}'_{f9conv}$) as well as from the back surface '$b$' to bulk surface 1 ($\dot{q}'_{b1conv}$) can be calculated similar to convection of D-shape absorber, using Eq. (4.39).

#### *4.3.1.3 Radiation heat transfer*

The radiation heat transfer from the triangular shape absorber tube is similar to radiation heat transfer from circular and semi-circular absorber tube, except radiation from the triangular surfaces. The radiation $\dot{q}'_{57rad}$ and $\dot{q}'_{34rad}$ would be same as Eq. (4.25) and Eq. (4.26) respectively, as discussed in Sec. 4.1.1.4. Similarly radiation from surface 4 to cell front surface ($\dot{q}'_{4f\,rad}$) can be evaluated through Eq. (4.26) by considering the radiosity between triangular surface to curved surface.

### 4.3.2 Comparison of results of D-shape and triangular receiver

The results obtained from the simulation of D-shape and triangular receiver obtained in MATLAB are compared and it was found out that temperature range of PV panel and HCPVT outlet obtained in D-shape is more than that of triangular receiver. This may be due to the fact that in the design, the length of PV is taken as 1.5 m for D-shape absorber. To maintain the same dimensions of PV panel, the panel length of 0.75 m was taken for triangular shape absorber, as two PV panels were mounted on the adjacent sides. The HCPVT outlet temperature of D-shape absorber tube is slightly higher than triangular absorber tube due to it geometry. The temperature obtained by keeping inner flow rate of 0.075 kg/s and annulus flow rate of 0.008 kg/s is shown in Fig. 4.10. It is clearly seen that PV panel temperature is 3.3 degrees higher for D-shape absorber tube at peak radiation.

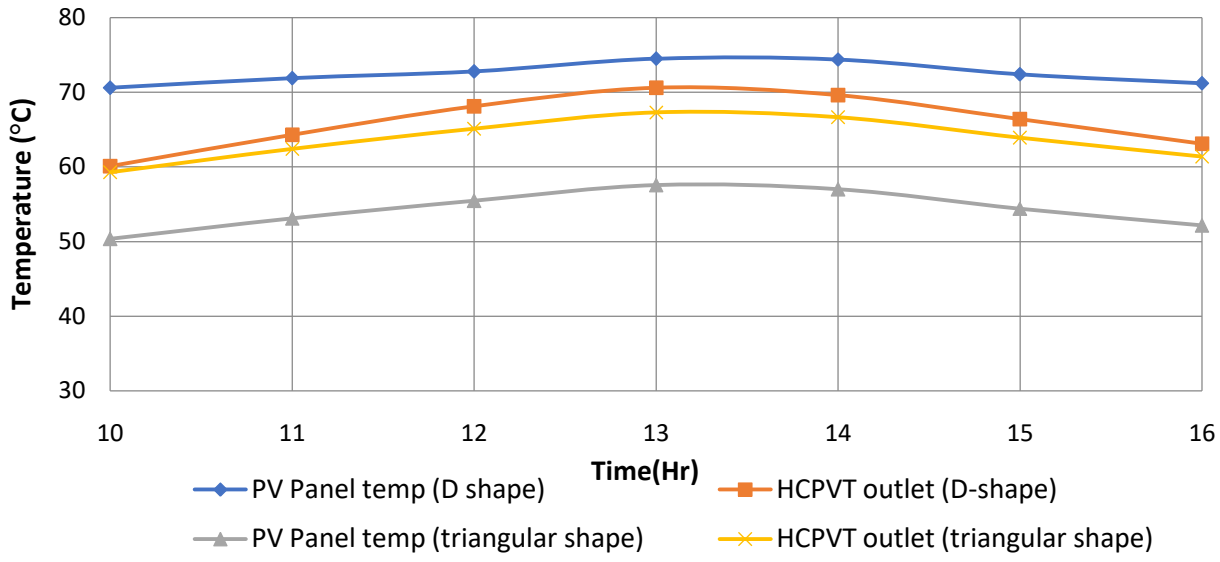


**Fig. 4.10 Comparison of simulation results for D-shape and triangular receiver**

## 4.4 Model of Distillation Unit in Aspen HYSYS

The heat transfer variation of two different designs of novels HCPVT is identified previously. It is expected that the designed HCPVT receiver would couple with PTC to provide low grade thermal energy which would be easily connected to distillation unit to produce fresh distillate from raw feed of groundwater. The HCPVT system would be standalone system which would provide sufficient power to operate pump and provide thermal energy for distillation unit. The temperature ranges obtained from the analysis of receiver in Sec. 4.2 are considered as input of distillation unit. For the analysis purpose, two designs of distillation units are taken and simulations are carried out on Aspen HYSYS (v8.4). It is a process simulation system tool is used to model the steady-state processes to estimate the operating conditions. For the current simulations, the Peng Robinson model is used in this simulation tool.

### 4.4.1 Analysis of direct fluid inlet into single flash chamber

A simple model which consists of single flash chamber connected to PTC with novel D-shape HCPVT receiver is taken. The proposed distillation unit would provide the distilled

water from the outlet stream of HCPVT receiver. Thus, it is estimated that the outlet temperature obtained from the HCPVT receiver, after mixing of inner tube and annulus flow, would be the inlet water temperature of single flash chamber distillation unit. The distillation system is designed and simulated by varying its operating parameters. For the process simulation of single stage flash unit, the following Aspen HYSYS components were taken:

- Flash chamber
- Pump
- Heat input (PTC)
- Heat exchanger

The pump, by consuming power, would supply raw water to the heat exchanger, where it gets preheated and then supplied to inlet of HCPVT. Under high concentration with the help of PTC, the raw feed-water would convert into vapors which then flashed into flash chamber. From the flash chamber, the high temperature vapor stream is sent to heat exchanger to pre-heat the inlet feed which leads to its condensation. The condensed distilled water is then collected from the outlet of distillation unit. The process diagram of the same is represented in Fig. 4.11. The parameters taken for the simulation are shown in Table 4.5.

**Table 4.5 Parameters taken during simulation of single stage distillation unit**

| **Parameters** | **Properties** |
|---|---|
| HCPVT outlet temperature | 110 °C |
| Flash chamber inlet pressure | 143.5 kPa |
| Mass flow rate of steam | 0.017-0.25 kg/s (1 LPM to 15 LPM) |
| Heat exchanger | Shell and tube |
| No of feed plates | 1-10 |
| Vapor fraction | 0-1 |
| Fluid density | 1000 kg/m$^3$ |
| Fluid thermal conductivity | 0.55 W/m.K |

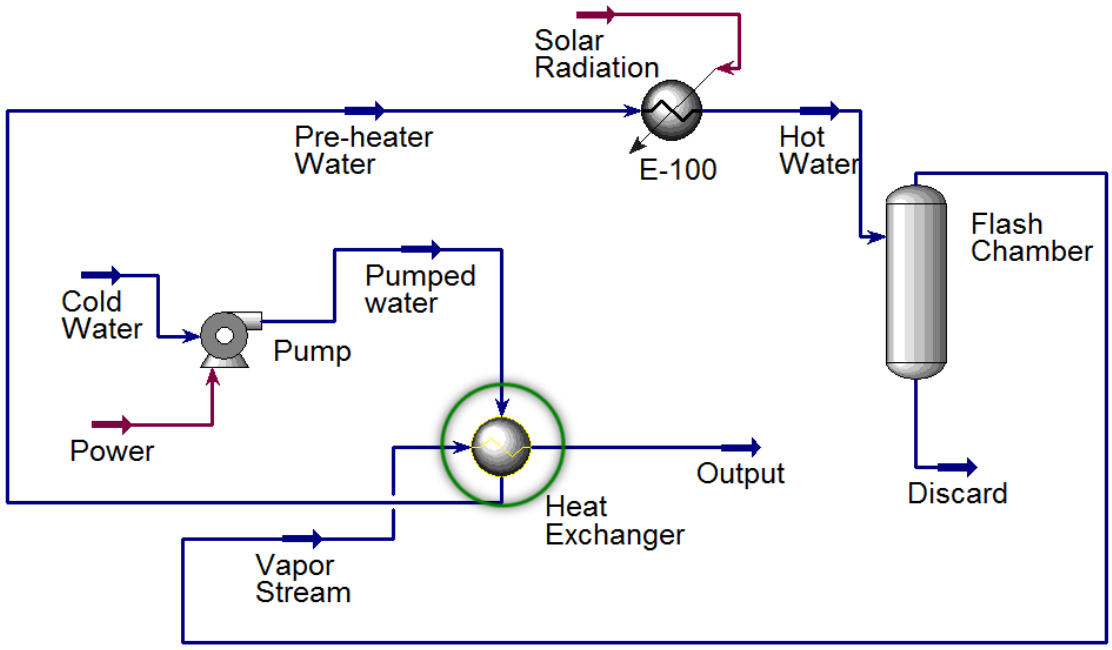


**Fig. 4.11 Schematic diagram of process of single stage distillation unit**

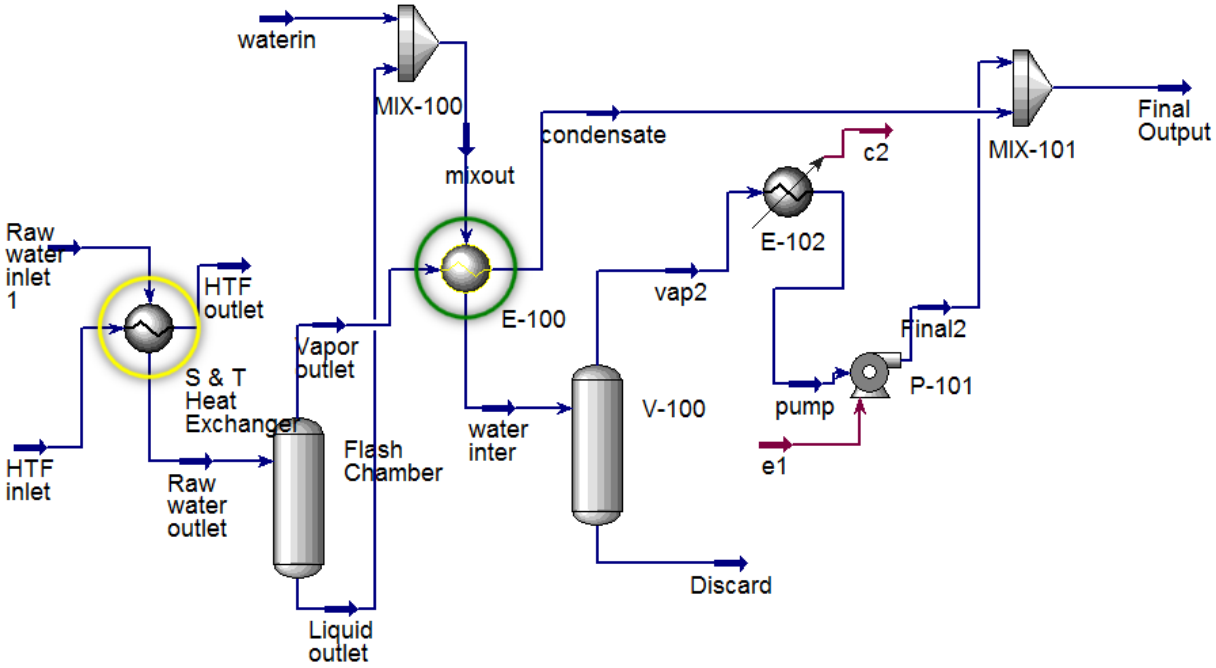


**Fig. 4.12 Schematic diagram of process of indirect distillation unit**

### 4.4.2 Analysis of indirect fluid heat transfer to multi flash chamber

Similar to the analysis of single stage flash unit, the analysis is also carried out for indirect heat transfer with multi flash chamber feed inputs. In this process, the discards of first flash chamber is mixed with another fresh stream, preheated with heat exchanger and send to second flash chamber. The vapor from the first flash chamber is condensed in the process and collected as output. The mixer is used to mix the fresh inlet feed with the discard of flash chamber. In the second flash chamber, the process is repeated to obtain the combined output. For the current analysis, the HTF fluid flow rate was taken as 500 kg/h while the input parameters for multi flash units are same as that of single unit. The process diagram of the multi stage unit is shown in Fig. 4.12.

### 4.4.3 Results and discussion

During the simulation, inlet temperature was assumed to be constant for all flow rates. From the simulation results of HCPVT, the maximum temperature achieved in MATLAB was about 110 °C. The simulations pertaining to distillate output was carried out by taking HCPVT outlet at 110 °C. In case of single stage flash chamber, it is found out that, if 2 LPM is feed through a duration of four hours (simulation time), all of the input would be distilled out at this flow rate and temperature. The distillate output increases with increase in flow rate initially but then decreases with increase in mass flow rate. This is because for higher mass flow rate, the time taken to heat up would be less, which leads to less steam formation and lower output. The mean output for different flow rate varies from 260 L to 410 L for inlet temperature of 110 °C. The graphical representation of the observed data is shown in Fig. 4.13. It is observed that for the single stage, at 110 °C, the maximum output could be achieved at mass flow rate of 0.12 kg/s (7 LPM).

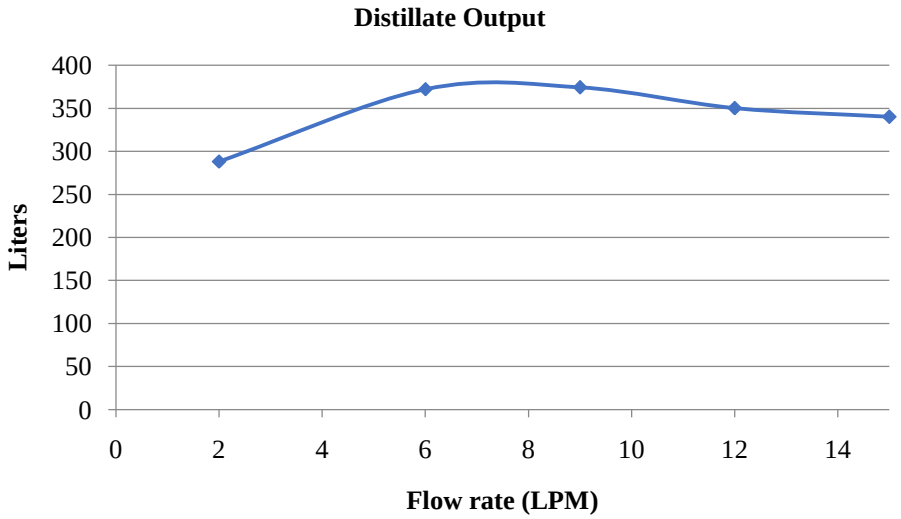


**Fig. 4.13 Distillate output variation at different flow rates**

In case of indirect distillation unit with multi effects, it is found out that with increase in number of stages and subsequent flashing of vapor, the output increases as more heat is provided at each stage. However, this would also increase the cost as the number of equipment increases. For the current study, the results of single stage distillation unit are taken for experimentation. Thus, through the novel HCPVT receiver, the mass flow rate varied in inner tube and annulus to achieve combined flow rate ranging from 5 to 7 LPM.

## 4.5 Exergy Model of Novel HCPVT System

The maximum amount of useful work which can be extracted from the system at a particular condition, with respect to the ambient conditions, is known as exergy or availability. It is useful in designing, optimizing and identifying the grey areas for improvement of the system. The performance of the HCPVT was evaluated by carrying out the first and second law of thermodynamic analysis using the experimental results. The equations used are taken which available from the literature. By considering control volume, the exergy balance of the system can be written as [216]

$$\sum \dot{E}\, x_{i,tot} = \sum \dot{E}\, x_{o,tot} + \sum \dot{E}\, x_{loss,tot} \tag{4.59}$$

### 4.5.1 Exergy input of HCPVT

The overall exergy input includes the inflow of exergy along with the HTF and the exergy from the Sun. It is given as [217]

$$\sum \dot{E}\, x_{i,tot} = \dot{E}x_i + \dot{E}x_{rad} \tag{4.60}$$

The exergy inflow due to HTF depends upon the physical conditions of fluid and ambient conditions. It is given as [218]

$$\dot{E}x_i = H_i - H_a - T_a(S_i - S_a) \tag{4.61}$$

The exergy from the Sun is calculated by taking Sun's temperature as 5777 K and using Petela expression ($\psi$) and is given by [194]

$$\dot{E}x_{rad} = Ir.A.\psi \tag{4.62}$$

### 4.5.2 Exergy output from HCPVT

The total exergy output from the system is given as sum of thermal and electrical exergy outflow and given as [217]

$$\sum \dot{E}\, x_{o,tot} = \dot{E}x_{th} + \dot{E}x_{el} \tag{4.63}$$

The thermal exergy outflow can be calculated as [219]

$$\dot{E}x_{th} = H_o - H_a - T_a(S_o - S_a) + Q_{th}\left(1 - \frac{T_a}{T_o}\right) \tag{4.64}$$

Whereas, the $Q_{th}$ is given as [210]

$$Q_{th} = \dot{m}C_p(T_o - T_i)\log\left(\frac{T_o}{T_i}\right) \tag{4.65}$$

The exergy electrical is the electrical output of PV cell, which is a high grade form of energy.

### 4.5.3 Exergy losses occurring in HCPVT

In Eq. (4.92) the overall losses are actually a combination of thermal and optical losses and exergy destruction occurring within the system and can be given as [220]

$$\sum \dot{E}\, x_{loss,tot} = \sum \dot{E}\, x_{loss,optical} + \sum \dot{E}\, x_{loss,th} + \sum \dot{E}\, x_{dest,tot} \tag{4.66}$$

The optical losses in the system can be calculated as [221]

$$\sum \dot{E}\, x_{loss,optical} = (1-\eta_o) Ir.A_a.\psi \tag{4.67}$$

Where $\eta_o$ is the optical efficiency of the glass and is given as product of transmissivity and absorptivity.

The thermal losses are given as [222]

$$\sum \dot{E}\, x_{loss,th} = Q_{th}\left(1-\frac{T_a}{T_c}\right) \tag{4.68}$$

Where

$$Q_{loss} = UA(T_c - T_a) \tag{4.69}$$

Exergy destruction occurs within the system in two ways, one due to pressure drop and other due to heat transfer from higher to lower temperature. Here, the heat transfer occurs from the Sun to absorber surface and from high temperature PV cell to water. Thus, the total exergy destruction would become

$$\sum \dot{E}\, x_{dest,tot} = \dot{E}x_{dest,P} + \dot{E}x_{dest,S-PV} + \dot{E}x_{dest,PV-w} \tag{4.70}$$

The exergy destruction due to pressure drop is given as

$$\dot{E}x_{dest,P} = \frac{T_a . m_f . \Delta P}{\rho . \overline{T_f}} \tag{4.71}$$

where

$$\overline{T_f} = \frac{T_o - T_i}{\ln \frac{T_o}{T_i}} \tag{4.72}$$

The exergy destruction due to heat transfer between Sun and PV is given as [210]

$$\dot{E}x_{dest,S-PV} = (\alpha\tau) Ir . A_a . \psi - (\alpha\tau) Ir . A_a \left(1 - \frac{T_a}{T_c}\right) \tag{4.73}$$

The exergy destruction due to heat transfer between PV and water is given as [223]

$$\dot{E}x_{dest,PV-w} = (\alpha\tau) Ir A_a \left(1 - \frac{T_a}{T_c}\right) - Q_{loss} \left(1 - \frac{T_a}{T_c}\right) - Q_{th} \left(1 - \frac{T_a}{T_o}\right) \tag{4.74}$$

### 4.5.4 Exergetic efficiency of HCPVT

The thermal and electrical exergy efficiency of the HCPVTS is calculated as [204]:

$$\eta_{Ex,th} = \frac{\dot{E}x_{th}}{\sum \dot{E}\, x_{i,tot}} \tag{4.75}$$

$$\eta_{Ex,el} = \frac{\dot{E}x_{el}}{\sum \dot{E}\, x_{i,tot}} \tag{4.76}$$

For the calculation of second law efficiency, the literature discusses different approaches. Accordingly, three different cases are taken.

***Case I:***

The exergetic efficiency of the system is calculated as a ratio of total exergy output to the total exergy input and is given as [220, 224–226]

$$\eta_{Ex} = \frac{\sum \dot{E}\, x_{o,tot}}{\sum \dot{E}\, x_{i,tot}} \tag{4.77}$$

***Case II:***

As per Yazdanpanahi *et al.* [223], the second law efficiency is calculated in terms of exergy losses and exergy destruction and is given as

$$\eta_{Ex} = 1 - \frac{\sum \dot{E}\, x_{loss,tot}}{\sum \dot{E}\, x_{i,tot}} \tag{4.78}$$

***Case III:***

As per the standard definition of second law efficiency it is calculated in terms of exergy destruction and is given as [222]

$$\eta_{Ex} = 1 - \frac{\sum \dot{E}\, x_{dest,tot}}{\sum \dot{E}\, x_{i,tot}} \tag{4.79}$$

# CHAPTER 5

# DESIGN AND FABRICATION OF A NOVEL HCPVT SYSTEM

*In the current chapter, the development of experimental setup of a novel HCPVT system and experimental procedure are discussed in detail. Two receivers got fabricated and testing was carried out only on D-shape receiver. The experiments were aimed to validate the results obtained from the simulations.*

## 5.1 Purpose and Description of the Experimental Setup

The novel HCPVT system consists of two parts; a reflective parabolic trough and a novel designed HCPVT receiver. The trough, which includes reflective anodized aluminum sheet, support structure and tracking mechanism, was fabricated entirely in the central workshop of the institute. The novel designed receivers got fabricated externally. Out of the two designed and fabricated receivers, the D-shape receiver was used for outdoor testing. The fabricated PTC coupled with D-shape receiver was installed, behind SR Bhavan hostel of the institute (28°21'58.2" N 75°35'07.9" E). The tests were conducted on the fabricated setup during May and June 2017, for local conditions of Pilani. It is hot semi-arid region having composite climate with high temperatures for the most part of the year. For the design and testing, the values of annual maximum temperature, annual minimum temperature and daily average solar radiation are taken as 46 °C, 2 °C and 400 W/m$^2$ respectively, from NASA's POWER Data Access Viewer [227].

The main purpose of developing the experimental test setup was to carry out the outdoor testing of the designed novel HCPVT system by varying operating parameters. The HCPVT receiver was designed to obtain thermal as well as electrical energy from the receiver. In previous chapter, the design and simulations were carried out for D-shape and triangular receivers. In both the receivers, absorber consists of customized PV module

mounted on the concentrated radiation facing surface. The receivers were designed in such a way that the HTF flows through the absorber tube as well as the annulus between absorber tube and glass cover. This arrangement of HTF flowing through the front and rear surface to PV module helps reducing its temperature. Based on the design and fabrication of novel HCPVT, a patent (Named: A Liquid-Cooled Hybrid Solar Energy Collector) was filed during March 2017, which got published in 28$^{th}$ September 2018 [228].

The experimental investigation on novel HCPVT receiver was carried out during clear days of May and June 2017. The experimental data like intensity of solar insolation, ambient air temperature, temperature at surface and rear of the PV module mounted on absorber tube, temperature and pressure at the inlet and outlet of HCPVT receiver, flow rate through absorber tube and annulus, short circuit current and open circuit voltage was recorded at an interval of one minute using data logger. The measured data were then averaged out on an hourly basis for analysis.

## 5.2 Design and Fabrication of Novel HCPVT System

In the current design, the absorber tube is modified into D-shape with a PV module mounted on the flat surface of the absorber tube. The design and fabrication of PTC and novel receiver are discussed in this section.

### 5.2.1 Fabrication of PTC

The design of PTC depends upon various parameters, which includes focal length, rim angle, length, etc. The length of the collector is independent parameter and can vary as per the requirement. The other parameters like focal length, rim angle, concentration ratio, etc. are dependent upon each other. To define these parameters, the calculations are made as per the geometrical design of parabolic trough, which is shown in Fig. 5.1.

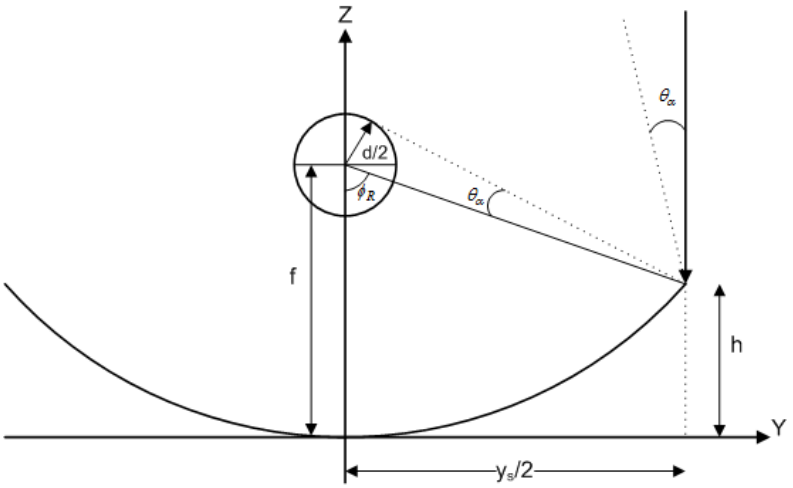


**Fig. 5.1 Geometrical design of parabolic trough**

As represented in Fig. 5.1, focal length of parabola is denoted by '$f$', and is dependent upon rim angle ($\phi_R$). The acceptance angle ($2\theta_\alpha$), which is the angular range over which all or almost all rays are accepted without moving all or part of the collector, is related to rim angle as

$$\sin\theta_\alpha = \frac{\sin\phi_R}{\pi C} \tag{5.1}$$

In Eq. (5.1), $C$ is the geometric CR and is the ratio of the area of aperture to the area of the receiver. Aperture area is the opening through which the solar radiation enters in the receiver.

$$\sin\theta_\alpha = \frac{d}{2f\left[1+\left(\frac{y_s}{2f}\right)^2\right]} \tag{5.2}$$

In Eq. (5.2), for diameter of the absorbing tube as $d$, the range over which the all incident rays are accepted is given as $y_s$.

The rim angle ($\phi_R$) is related to aperture and focal length '$f$' by

$$\tan\left(\frac{\phi_R}{2}\right) = \frac{2y_s}{4f} = \frac{y_s}{2f} \tag{5.3}$$

or

$$\tan \phi_R = \left( \frac{8\left(\frac{f}{y_s}\right)}{16\left(\frac{f}{y_s}\right)^2 - 1} \right) \quad (5.4)$$

Thus, by fixing the rim angle and the focal point, the parabola's aperture is automatically fixed. The length of the collector is totally dependent on the requirement. In the current design focal length was taken as 0.22 m and length as 2 m. This focus was chosen due to the constraint in the wooden dimension that was used in for making the base of parabolic trough. This constrain was also applicable to the selection of length. This constraint gives rim angle as 110°, height of the parabola as 0.43 m and aperture width as 1.15 m. With two parabolic sheets together, the aperture area was 3.6 $m^2$ and maximum geometrical CR as 15.

#### *5.2.1.1 Fabrication of wooden parabolic base*

For the fabrication of wooden parabolic base, a parabola was initially drawn on the plywood (thickness 19 mm), using the above dimensions and cut it out into the desired shaped using a jig-saw machine. The accuracy of curvature was maintained by filling it from edges to match the exact curve. Three curved base were made for supporting the aluminium parabolic trough sheet. The support of three curved bases behind the aluminium sheet provides the rigidity to the sheet which otherwise would not confer into parabolic shape due to bending by self weight. The fabrication of parabolic trough plywood base using jig-saw is shown in Fig. 5.2.

#### *5.2.1.2 Bending of Aluminium sheet*

The aluminium sheet, which is reflective and light in nature, was used as sheet for parabolic trough. For the same, two aluminium sheets were used in series which were cut and

bent by 90° at both sides. The bending of edges provides a shading effect and ensures least exposure of the base plywood to the direct Sun and rain.


**Fig. 5.2 The fabrication of parabolic trough plywood base using jig saw**

After bending edges at 90°, the rest of the sheets were rolled using the rollers. Multiple rolling was carried out to ensure the correct parabolic curvature, as per the desired dimensions. Soft hammering was also carried out to even out the sheet from all side. Fig. 5.3 shows the bending and rolling operations carried out on aluminium sheets to make parabolic curvature.

(a) (b)

**Fig. 5.3 (a) Bending of sheets at ends (b) Rolling of parabolic trough sheet**

### *5.2.1.3 Assembly of PTC*

The rolling machine used for the rolling of aluminum sheet has constraint of width. It could roll a sheet of maximum width of 3 feet (approx 90 cm), while the requirement was more than 5.5 feet (approx 170 cm). As a result two sheets were butt joined using rivets to achieve the required width. Before riveting, one sheet was screwed to the wooden base, in the end, following which the other sheet was screwed from one side onto the wood only at the center. The butt joint was made using rivets while maintaining the focal point. Finally, two arms were welded on each end of parabolic sheet to be attached to support structure. The arms also had adjustable screw mechanism to vary the height of receiver tube along its focal length. The final parabolic trough obtained after fixing aluminium sheets on wooden base in desired dimensions is shown in Fig. 5.4 and Fig. 5.5.

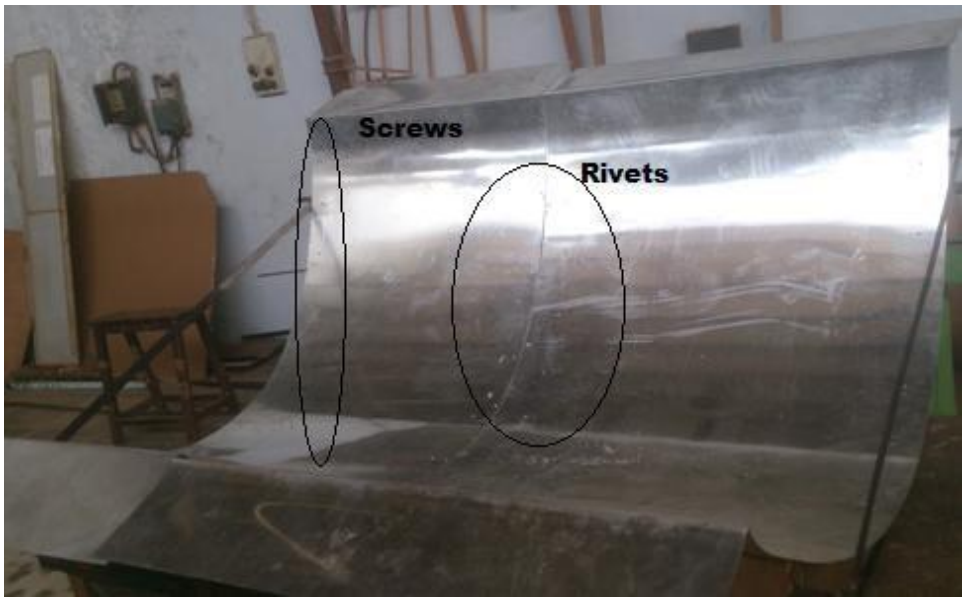


**Fig. 5.4 Assembly of parabolic trough on wooden base**

**Fig. 5.5 Final parabolic trough with arms for support and screw mechanism**

### 5.2.2 Fabrication of support structure with tracking mechanism

The PTC needs to be mounted on the support structure to enable the tracking system. In this design, the support system was fabricated by taking two GI pipes (outer diameter: 0.0254 m) having the height more than the aperture width of the parabola. The base of the rod was welded with square plate to make strong grip in the soil while grouting. It was grouted by digging a pit of volume 1 $ft^3$. The poles were grouted straight with the help of cement and the structure was allowed to dry for two days. One of the GI pipes had worm gear based tracking mechanism which manually tracked the parabolic trough from east to west. The mechanism was then welded on one of the arms of the parabolic trough. The support structure with tracking mechanism and final assembly is shown in Fig. 5.6.

### 5.2.3 Fabrication of novel D-shape receiver

The novel D-shape absorber was designed to accommodate PV cell to provide combined heat and power. As discussed earlier, it was proposed to mount flexible CPV panel on the circular absorber tube of the PTC. However due to the non availability of the flexible panel and fabrication constraint, the design was modified to accommodate customized long PV panel facing concentration area. Accordingly, two novel absorber tubes were designed. The copper was selected as a tube material because of its higher thermal conductivity. The

borosilicate glass tube was selected for the outer cover. The header to join glass with absorber tube which allowed annulus water flow was also fabricated externally based on the design given. For electric power generation, a customized PV module was procured from Shanghai, China. The physical specifications of the D-shape absorber tube are shown in Table 5.1. The fabrication procedure involving mounting of PV panel on flat surface of novel D-shape receiver is shown in Fig. 5.7.

(a) (b)

**Fig. 5.6 (a) Support mechanism with worm gear based tracking mechanism (b) Final assembled parabolic trough on support structure**

**Table 5.1 Physical specifications of the D-shape absorber tube and PV panel**

| **Absorber tube (dimensions in mm)** | | **PV panel (dimensions in mm)** | |
|---|---|---|---|
| Length of glass | 1500 | Type | Mono crystalline silicon PV panel |
| Glass OD (borosilicate) | 115 | Model | HTMO 18-16 |
| Glass thickness | 5 | Make | Shanghai Wintrans International Trade Co. Ltd) |
| Copper tube diameter | 75 | Length | 1500 |
| Copper tube thickness | 2 | Width | 72 |
| Length of copper tube | 2000 | Thickness | 4.2 |

(a) (b)

**Fig. 5.7 (a) Customized silicon PV panel (b) Mounting of PV panel on flat surface of novel D-shape receiver**

Fig. 5.7 (a) shows the customized PV module procured for the setup. Fig. 5.7 (b) shows the mounting of PV panel on flat surface of the tube. Before mounting with the PV, a layer of epoxy adhesive (make: Omega, OB-200) was applied on the flat surface of receiver tube. Three K-type thermocouples (CR-AL, Alpha engineering company, accuracy of ±2.71% and temperature range -150 ºC to 1350 ºC) were mounted at a distance of 400, 800 and 1200 mm from the inlet of absorber tube between the PV panel and the copper tube. Three additional K-type thermocouples were also mounted on the front surface of PV panel at the same distance. Thus a total of six thermocouples were used to measure the surface temperature of front and back side of the PV panel. All the thermocouple wires were brought out from the hole provided in the header which was then sealed with anti-leakage sealant to avoid any leakage and were connected to temperature scanning logger. The designed HCPVT receiver is shown in Fig. 5.8 (a), (b) & (c).

(a)

(b)

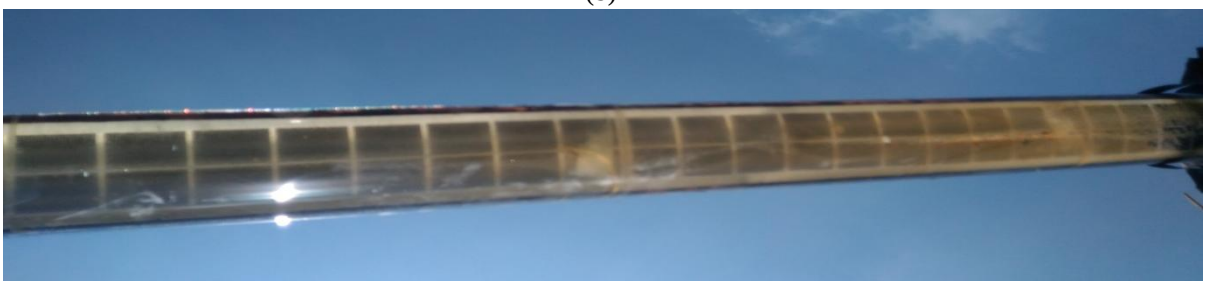

(c)

**Fig. 5.8 (a) Assembly with PV panel on concentrated face of HCPVT (b) back surface of HCPVT (c) HCPVT during experimentation**

### 5.2.4 Fabrication of novel triangular shape receiver

In D-shape absorber tube, the length of PV panel was 1500 mm. To maintain the same dimensions of PV panel, two panels of half the length (750 mm) were used for triangular shape absorber. The panels were mounted on adjacent sides of triangular absorber, facing the concentration. The customized PV panels were procured from Shanghai, China. The physical specifications of the absorber tube and PV panel are shown in Table. 5.2.

In the design of triangular absorber, the borosilicate glass tube was selected for the outer cover similar to D-shape absorber. The header to join glass with absorber tube, which allowed annulus water flow, was procured externally based on the design given. The fabrication procedure of the triangular absorber is shown in Fig. 5.9.

**Table 5.2 Physical specifications of the triangular shape absorber and PV panel**

| **Absorber tube (dimensions in mm)** | | **PV panel (dimensions in mm)** | |
|---|---|---|---|
| Length of glass | 1500 | Type | Mono crystalline silicon PV panel |
| Glass OD (borosilicate) | 115 | Make | Shanghai Wintrans International Trade Co. Ltd) |
| Glass thickness | 5 | Length | 750 |
| Triangular tube side length | 75 | Width | 72 |
| Triangular tube thickness | 2 | Thickness | 4.5 |
| Length of triangular tube | 2000 | | |

(a) (b)

**Fig. 5.9 (a) Triangular copper tube (b) PV panel to be mounted on tube**

Fig. 5.9 (a) shows the triangular absorber fabricated by bending of copper tube into equilateral triangle of desired length while Fig. 5.9 (b) shows the customized PV modules procured which was mounted on triangular absorber. PV panels are mounted using epoxy adhesive (make: Omega, OB-200). Three K-type thermocouples (make: Alpha Engineering Company, accuracy of ±2.71% and temperature range -150 ºC to 1350 ºC) were mounted in

between absorber tube and each PV panel at a distance of 250, 500 and 750 mm. Three additional K-type thermocouples were also mounted on the front surface of each PV panel at the same distance in similar way as that of D-shape absorber. Thus a total of twelve thermocouples were mounted to measure the surface temperature of front and back side of concentration facing PV modules.

All the thermocouple wires were brought out from the hole made in the header which was then sealed with anti-leakage sealant to avoid any leakage and were connected to temperature scanning logger. The developed triangular absorber is shown in Fig. 5.10. Earlier it was decided to procure the PTC externally for both the designed receivers. However, the external PTC procured was not as per the designed criteria. Further the vendor didn't turn up for the correction. Thus, in-house PTC was fabricated as discussed in the Sec. 5.2.1 and Sec. 5.2.2. On the fabricated PTC, only D-shape receiver was tested out in field.

**Fig. 5.10 Assembled triangular shape receiver**

## 5.3 On Site Experimental Setup of Novel HCPVT System

The experimental setup was assembled for outdoor testing. On the support structure, the PTC structure was mounted in the north-south direction and welded in the accurate alignment for east to west tracking. The high reflective anodized aluminum sheets having area of 16 $ft^2$ (1.48 $m^2$) mounted on the existing parabolic trough. By adjusting focal length with the help of screw mechanism, the novel HCPVT receiver with D-shape absorber was mounted on the same. The minor adjustments were carried out to achieve perfect alignment

of falling solar radiation. The thermocouples wires coming out of header hole were connected to temperature scanning logger for continuous reading during the test days.

The schematic diagram of the experimental setup is as shown in Fig. 5.11. With the current dimension of receiver and high reflective anodized aluminum sheets, the CR of the system comes out to be 6 Suns. In the setup, two tanks were used, one connected to the inlet and another to the outlet of HCPVT system. The inlet tank (100 L) was mounted at the height of 10 feet to provide sufficient head for water to circulate through HCPVT receiver. The water from the gravity potential flows into the receiver through two rotameters and flow control valves (ball valves).The first rotameter (make: JPM, range 0 – 0.33 kg/s, accuracy ±1.14%) fitted in between the higher tank outlet and HCPVT receiver. The second one (make: JPM, range 0 – 0.08 kg/s, accuracy ±1.14%) was fitted in between outlet of 'T joint' and inlet of annulus of novel HCPVT receiver.

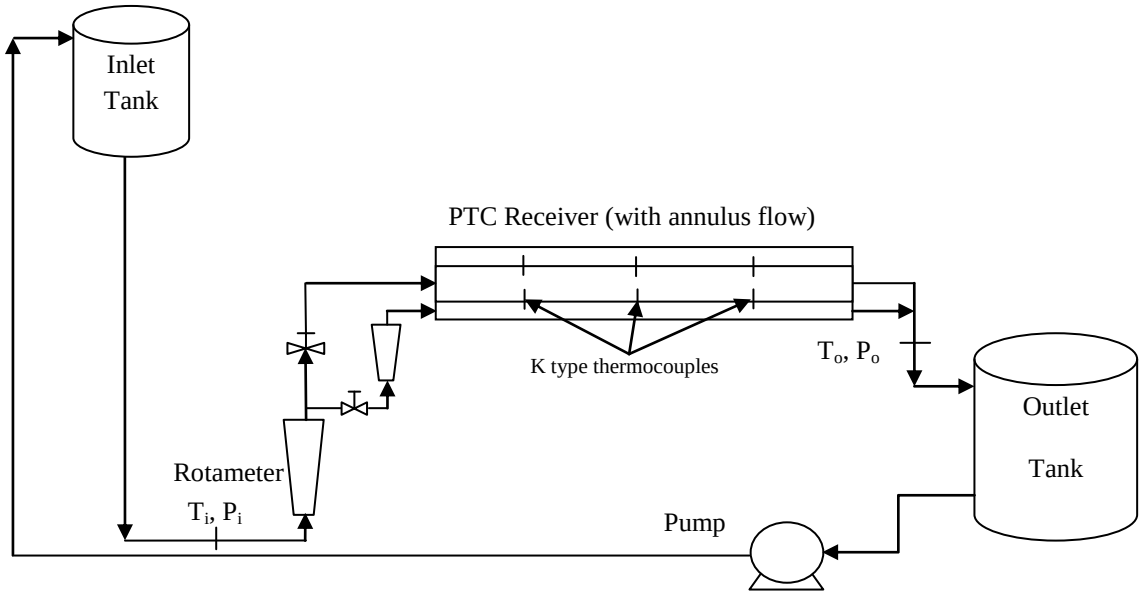


**Fig. 5.11 Schematic diagram of the experimental setup**

The mass flow rate was controlled by using two ball valves as shown in Fig. 5.11. Two RTDs (Pt-100, least count 0.1 °C) were installed at inlet and outlet of the HCPVT receiver to measure the respective temperatures. The water coming out from HCPVT receiver

was then collected into the outlet tank (350 L) which was placed at ground level. A monobloc pump (make: KD Industries, head = 15 m) was used for circulation of water from lower tank to higher tank, at the end of the day. All the pipes and junctions were properly insulated with glass wool to minimize the thermal losses. The onsite experimental setup is shown in Fig. 5.12.

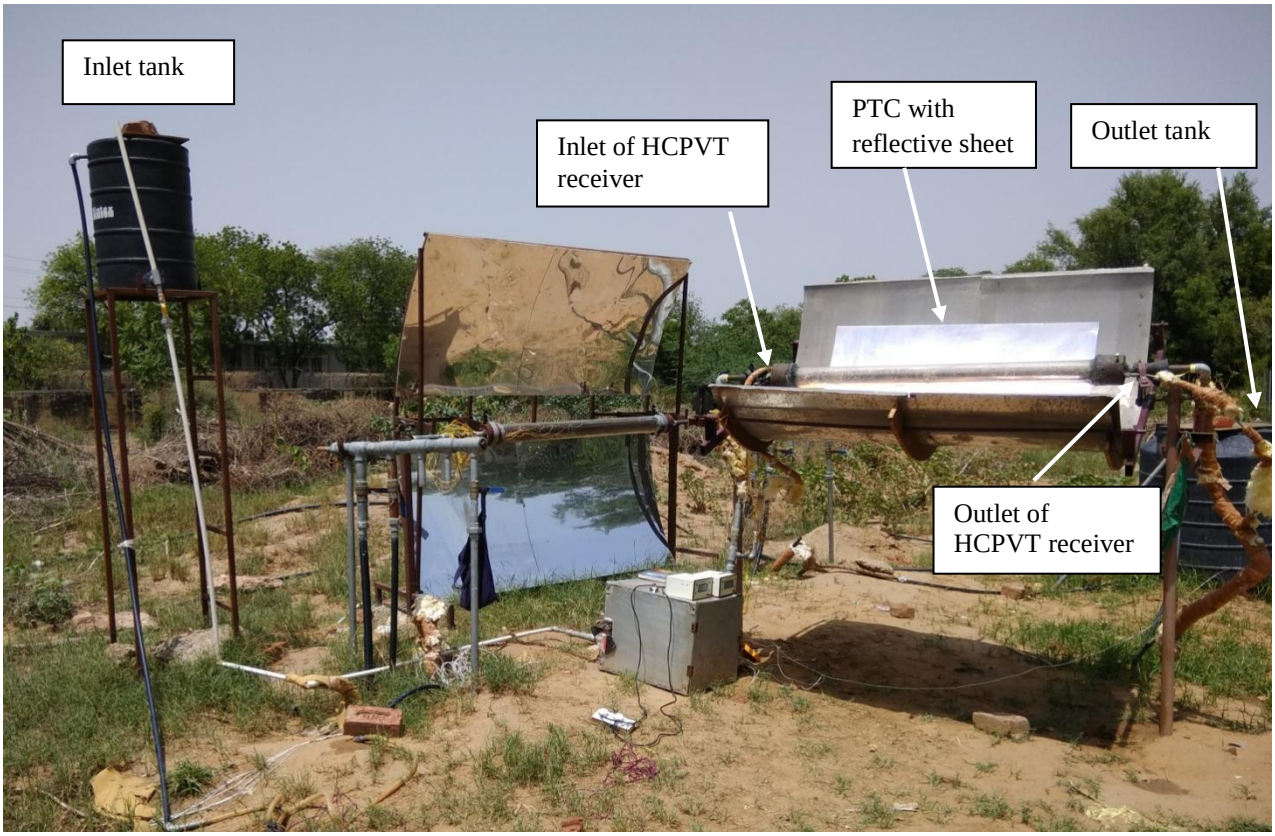


**Fig. 5.12 On-site experimental setup of HCPVT receiver coupled on PTC**

The global solar radiation was measured using pyranometer (make: Kipp and Zonen, accuracy ±1.3%, temperature dependence of sensitivity ±1%) at an interval of one minute using data logger (make: Campbell Scientific, model CR1000) and was averaged out for hourly basis for analysis purpose. The open circuit voltage and current of the PV panel were measured by digital multi-meter (make: RISH, accuracy of 0.1 A and 0.1 V). The six K-type thermocouples, $T_1$ to $T_6$, were used to measure the temperature variation across the front and rear of the PV panel as mentioned earlier. Another K-type thermocouple ($T_a$) was used for

ambient temperature measurement. For the experiment, three calibrated temperature scanning loggers (make: Countronics, model: CT716, accuracy ±1 °C for thermocouples and ±0.1 °C for Pt-100) were used to record the temperature. Two pressure gauges (make: KI instruments, accuracy ±2%) were mounted at inlet and outlet of the absorber tube.

## 5.4 Instruments Used in Experimentation

For HCPVT system, high quality, accurate and calibrated instruments were used for measuring the different parameters viz. ambient temperature, intensity of solar insolation, mass flow rate of water, pressure, current and voltage, etc. Description and specification of the instruments used for measuring the data are given below.

### 5.4.1 Pyranometer and weather station

For the measurement of solar radiation during the test days, a pyranometer with data logger was installed in the close vicinity of experimental setup. Data logging system was also a part of pyranometer which automatically saves all the values at a specific interval. The pyranometer didn't need any external power source. The temperature of ambient air was measured using thermocouple and compared with the dry bulb temperature installed at the institute's weather station. Technical specifications and other technical details of pyranometer and associated data logger are shown in Table 5.3.

**Table 5.3 Technical specifications of the Pyranometer and data logger**

| **Pyranometer** | | **Data Logger** | |
|---|---|---|---|
| Make | Kipp & Zonen | Make | Cambell Scientific |
| Model | CMP 11 | Model | CR1000 |
| Serial number | 140443 | Voltage | 9.6 – 16 V DC |
| Sensitivity | 9.39 μV/W/$m^2$ | Processor | 16 BIT CPU |
| Impedance | 30Ω | Clock accuracy | ±3 min/yr |
| Uncertainty of the WRR | ±0.3% | Clock resolution | 10 ms |

### 5.4.2 Thermocouples

To measure the front surface and rear surface temperature of PV panel, within the tube, K-type thermocouples were used. These thermocouples are reliable, have high accuracy and temperature range than other surface thermocouples. In K-type thermocouple, two element junctions, (Chrome and Alumel) are used which are joined together to measure the temperature of the surface. The used K-type thermocouples had an accuracy of ±2.71% and temperature range between -150 ºC to 1350 ºC. All the thermocouples were attached to temperature scanning loggers (thermocouple) for readings.

### 5.4.3 Resistance temperature detectors (RTD)

These are sensors used to measure temperature by correlating the resistance of the RTD element with temperature. Most RTD elements consist of a length of fine coiled wire wrapped around a ceramic or glass core. The RTD element is made from a pure material whose resistance at various temperatures has been documented. The material has a predictable change in resistance as the temperature changes; it is this predictable change that is used to determine temperature. Commonly RTD elements used are Nickel (Ni), Copper (Cu) or Platinum (Pt). Among various commercial available variants, Platinum RTD is most stable and reproducible temperature sensor having linear positive temperature coefficient from -200 to 800 °C with resistance variant as 100 ohm or 1000 ohm. In the current study, Pt-100 having least count of 0.1 ˚C was used as RTD. These RTDs were tested and calibrated as per DIN 43760 standards. The RTDs were placed at the inlet and outlet of the absorber tube to measure the respective temperatures. To ensure the proper working of the RTDs, during the installation, the resistance between the elements was checked with the help of digital multimeter. Both the RTDs were connected to temperature scanning loggers (RTD) for continuous readings.

### 5.4.4 Temperature scanning logger

Using RTD's resistance versus temperature characteristics, the logger measures the resistance and hence temperature at the surface. Similarly for thermocouples the logger measures the temperature at junction. During the experiment, three temperature scanner CT716 (make: Countronics) were used which has RTD/thermocouple socket. Two of them dedicatedly used for K type thermocouples which were attached to PV front and rear surface and the last was used for Pt-100 RTDs. The used scanning logger device was compact and highly accurate. All temperature scanners were properly calibrated by the manufacturer (Countronics) during the make. In this system, temperature data was directly saved in readable format (.csv) which can be easily retrieved using a USB pen drive. The technical specifications and other details of used temperature scanner logger are given in Table 5.4. The image of one of the temperature scanner logger used during the experimentation is shown in Fig. 5.13.

**Table 5.4 Technical specifications of temperature scanner logger**

| | |
|---|---|
| Make and Model | Countronics, CT716 |
| RTD and thermocouple sensor type | PT 100 2W/3W and J/K/R thermocouple |
| Range for RTD | -100 to 600 ºC |
| Range for thermocouple | 0 to 1250 ºC |
| Accuracy for RTD | ±0.1 ºC ±1 ºC least significant digit for RTD |
| Accuracy for thermocouple | ±1 ºC ±1 ºC least significant digit for thermocouple |
| Power Supply | 230V AC ± 15%, 50/60 Hz |
| Installation | The RTD sensor should be connected using proper cables to minimize errors due to cable resistance. |
| Front facia | 96 mm × 192 mm |


**Fig. 5.13 Temperature scanning logger**

### 5.4.5 Centrifugal pump

Centrifugal pump was used to re-circulate water from outlet tank to the inlet tank. Firstly, the outlet tank was filled by water which provided intake source for centrifugal pump. The pump lifts the water from outlet tank to inlet tank, which by gravity potential circulates water within the receiver tube during experimentation. Centrifugal pump used in the experimental study is as shown in Fig. 5.14. The specifications of the pump are as given in Table 5.5.


**Fig. 5.14 Centrifugal pump used in experiment**

**Table 5.5 Technical specifications of centrifugal pump**

| | |
|---|---|
| Make: | KD Industries, Monoblock Pump |
| Input: | 230 V AC/DC |
| Power: | 50 W |
| Head | 15 m |
| Maximum volume flow: | 240 LPH |

### 5.4.6 Rotameter

The mass flow rate of HTF was measured with the help of rotameter (make: JPM, range 0 – 0.33 kg/s, accuracy ±1.14%), which was variable area meter type. It measured flow rate by varying the cross-sectional area through which fluid flows. The rotameters used in experiment is shown in Fig. 5.15.

**Fig. 5.15 Rotameters used in experiment.**

### 5.4.7 Pressure gauge

Pressure gauge is used to measure the pressure and displays it in an integral unit. During the experimentation, two pressure gauges were used to determine the pressure at the inlet and outlet of the novel absorber tube. The pressure gauge used had range up to 7 kg/cm$^2$

with accuracy of ±2%. The pressure gauges used in the experimental setup are shown in Fig. 5.16.

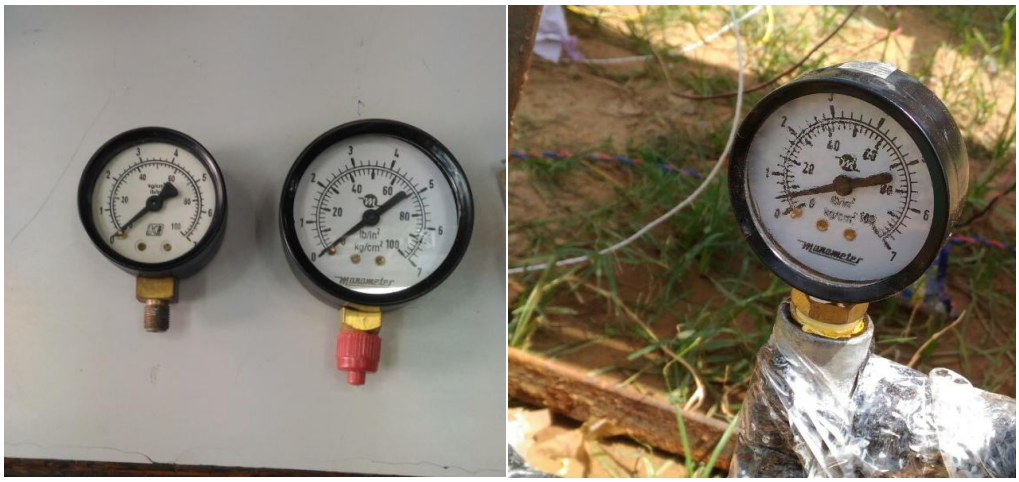

**Fig. 5.16 Pressure gauge used during the experiment**

### 5.4.8 Multimeter

A multimeter is a device which measures all three parameters of voltage, current and resistance respectively within the circuit. In the present experimental study, both short circuit current and open circuit voltage were measured with the help of digital multimeter. Due to smaller magnitude of the generated power, the resistance load was not provided. Fig. 5.17 shows the testing of PV panel using multimeter during pre-installation and Table 5.6 gives the technical details of the instrument used.

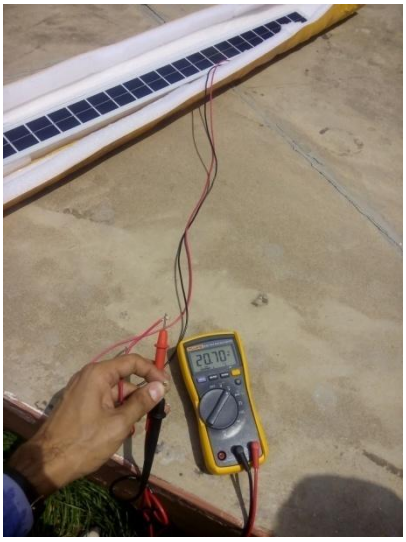

**Fig. 5.17 Testing of PV panel using multimeter during pre installation**

**Table 5.6 Technical specifications of multimeter used during the experiment**

| | |
|---|---|
| Make and Model | RISH max10 |
| Display | 3 ¾ digit |
| Counts | 3999 |
| DC Voltage range | 400 mV-1000 V |
| DC Voltage accuracy | ±0.5 |
| DC current range | 40 mA-10 A |
| DC current accuracy | ±0.8 |
| Power input | AAA (1.5 V×2) |
| Dimensions | 92x154x 25 mm |

## 5.5 Error and Uncertainty Analysis in Experiment

An uncertainty analysis was carried out on both electrical and thermal efficiencies from the energy balance view-points. The experimental uncertainties were calculated with the help of analysis of errors in the experimental through various instruments employed. During the measurement, the observed values on the instrument indicated the level of uncertainty in a measurement. In order to maintain high precision, the errors within the measurement need to be determined. The physical measurement of the instrument has two components: (a) A numerical value (in a specified system of units) giving the best estimate possible of the quantity measured and (b) the degree of uncertainty associated with this estimated value. Since different measuring instruments were used for the experimental measurement, the maximum error during the measurement can be calculated as the ratio of least count of the measuring instrument and minimum recorded value of the parameter. For the estimation of mathematical uncertainty within the calculations, the equation used is [229]:

$$\omega_R = \left[\left(\frac{\partial R}{\partial x_1}\omega_1\right)^2 + \left(\frac{\partial R}{\partial x_2}\omega_2\right)^2 + \cdots \left(\frac{\partial R}{\partial x_n}\omega_n\right)^2\right]^{1/2} \quad (5.5)$$

Where R is a function of 'n' independent linear parameters as $R = X(x_1, x_2, x_3 \ldots\ldots\ldots x_n)$. Thus, using Eq. (5.5) the uncertainty has been calculated for the thermal and electrical efficiency of the system.

Thermal efficiency of the HCPVT depends up on mass flow rate and inlet and outlet temperature of the fluid from HCPVT. So the Eq. (5.5) is solved for all dependent variables in case of thermal efficiency and found resultant equation as:

$$\frac{\omega_R}{Q} = \left[\frac{a^2}{q^2} + \frac{b^2}{(T_i - T_o)^2} - \frac{e^2}{(T_i - T_o)^2}\right]^{1/2} \tag{5.6}$$

Where $q = mc\,\Delta T$, while $T_i$ and $T_o$ are the inlet and outlet temperature of the HCPVT respectively. And *a, b, e* are the percentage errors in the measuring instruments. Electrical efficiency of the PV panel depends up on current, voltage and solar radiation. Thus, the equation used for all dependent variables in case of electrical efficiency is:

$$\frac{\omega_R}{\eta} = \left[\frac{a_1^2}{I^2} + \frac{b_1^2}{V^2} - \frac{e_1^2}{G^2}\right]^{1/2} \tag{5.7}$$

Where I, V and G are the current, voltage and solar radiation respectively. And $a_1$, $b_1$, $e_1$ are the percentage errors in the measuring instruments. The uncertainties related to the measuring instruments of the experimental setup are presented in Table 5.7.

**Table 5.7 Uncertainties of measured and calculated parameters in the experiment**

| Parameter | Unit | Maximum uncertainty (in experiments) |
|---|---|---|
| HCPVT inlet and outlet temperature | °C | ±0.6 |
| HCPVT inlet and outlet pressure | kPa | ±0.01 |
| Ambient temperature | °C | ±0.6 |
| PV panel temperature | °C | ±1.6 |
| Mass flow rate | kg/s | ±0.0008 |
| Solar radiation intensity | W/m$^2$ | ±6 |
| Open circuit voltage | V | ±0.2 |
| Short circuit current | A | ±0.1 |
| Electrical efficiency | % | ±0.25 |
| Thermal efficiency | % | ±2.11 |

## 5.6 Statistical Analysis

To quantify the degree of agreement between the simulation (theoretical) results ($X_i$) and the experimental results ($Y_i$), the root mean square percent deviation ($e$) has been evaluated by using the following expressions:

$$\text{Root mean square percent deviation } e = \sqrt{\frac{\sum(e_i)^2}{N}} \tag{5.8}$$

$$\text{where, } e_i = \left[\frac{X_i - Y_i}{X_i}\right] \times 100 \tag{5.9}$$

## 5.7 Experimental Methodology

Out of two designed and fabricated novel receiver tube, the experimentation and validation were carried out for D-shape receiver. The setup of novel D-shape absorber was tested without cooling for few hours. The experiments were conducted during clear sky days for 6 hours i.e. from 10 AM to 4 PM for three consecutive days (26-28 May, 9-11 June and 14-16 June) in the month of May and June 2017. The experiment setup started at 9 AM to achieve steady state condition and avoid any thermal shocks due to sudden temperature variation. By keeping the parallel flow arrangement, the mass flow rate was varied from 0.083 kg/s to 0.117 kg/s through HCPVT receiver. During 26-28 May, it was achieved by keeping mass flow rate through the inner tube as 0.075 kg/s and varying the annulus flow rate as 0.008 kg/s, 0.017 kg/s and 0.025 kg/s to get combined flow rate ranging from 0.083 kg/s to 0.10 kg/s. During 9-11 June, the mass flow rate through the inner tube was kept constant at 0.083 kg/s and during 14-16 June, the same was maintained at 0.092 kg/s, with varying annulus flow rate of 0.008 kg/s, 0.017 kg/s and 0.025 kg/s, so as to get that the combined flow rate ranges from 0.083 kg/s to 0.117 kg/s during these days. Measurement and recording of hourly data for the experimental setup were carried out using various instruments. The

parameters measured were intensity of solar insolation, ambient air temperature, temperature at surface and rear of the PV panel mounted on absorber tube, temperature at the inlet and outlet of HCPVT system, pressure at the inlet and outlet of HCPVT system, flow rate at both pipe inlets, short circuit current and open circuit voltage.

# CHAPTER 6

# RESULTS AND DISCUSSION

*In the current chapter, the performance analysis of the proposed HCPVT is carried out using different parameters. The results obtained by experimentation for six days (26-28 May and 14-16 June) are discussed in details. Further, the exergetic analysis based on experimental results obtained from HCPVT system was carried out using equations as discussed in Chapter 4. In the end, results are discussed out and a mechanism is proposed to utilize the available thermal energy for distillation purpose.*

## 6. Experimental Procedure Adopted

As discussed earlier, one-dimensional steady-state mathematical model of the proposed system was developed using MATLAB to simulate the performance of novel HCPVT system. The developed analytical model was validated with the experimental results. The real-time testing of the experimental setup was carried out for the conditions of Pilani, Rajasthan, for 6 hour duration on set of three consecutive days (26-28 May, 9-11 June and 14-16 June) in the month of May and June 2017. By keeping the parallel flow arrangement, the mass flow rate was varied from 0.083 kg/s to 0.117 kg/s through HCPVT receiver.

## 6.1 Performance analysis of HCPVT system with varying annulus flow rate

The performance of HCPVT was evaluated by varying annulus flow rate. On 26-28 May, the mass flow rate through the inner tube was kept at 0.075 kg/s and the annulus flow rate was varied as 0.008 kg/s, 0.017 kg/s and 0.025 kg/s to get combined flow rate ranging from 0.083 kg/s to 0.10 kg/s. On 9-11 June, the mass flow rate through the inner tube was kept constant at 0.083 kg/s and on 14-16 June, the same was maintained at 0.092 kg/s, with varying annulus flow rate of 0.008 kg/s, 0.017 kg/s and 0.025 kg/s, so as to get that the combined flow rate ranges from 0.083 kg/s to 0.117 kg/s during these days. Measurement and

recording of hourly data for the experimental setup were carried out using various instruments.

### 6.1.1 Results obtained by keeping the inner tube flow rate at 0.075 kg/s

During 26 – 28 May, 2017, the HCPVT system was analyzed by keeping mass flow rate through the inner tube as 0.075 kg/s and varying the annulus flow rate as 0.008 kg/s, 0.017 kg/s and 0.025 kg/s to get combined flow rate ranging from 0.083 kg/s 0.10 kg/s. By doing so, Reynolds's Number during the experiments varied in the range of 1000 to 5000. The obtained dataset for solar radiation and ambient temperature during the test days (26-28 May) is shown in Fig. 6.1.

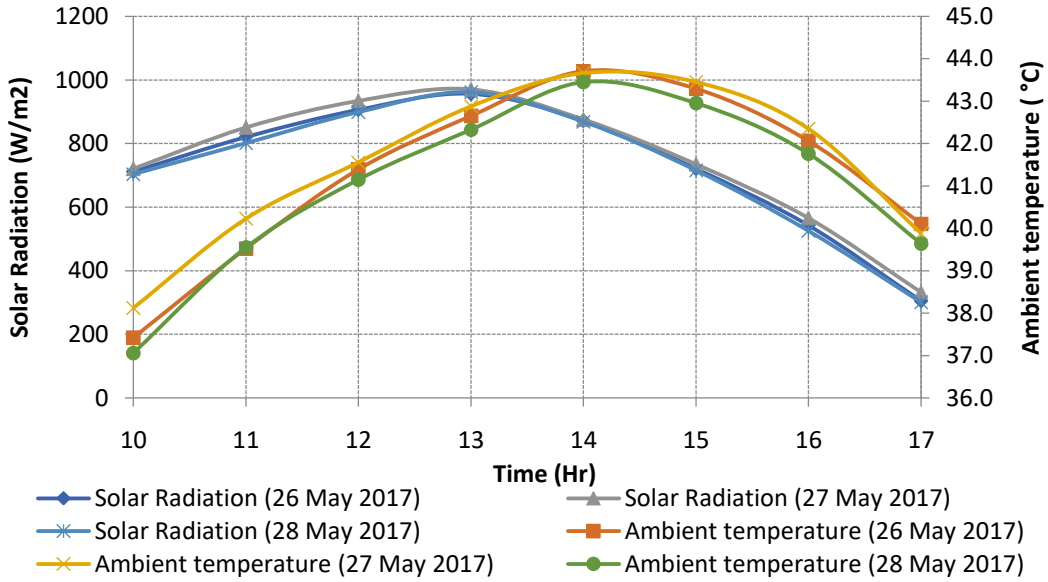


**Fig. 6.1 Variation of solar radiation and ambient temperature during test days (26-28 May, 2017)**

It is observed that during experiments, the solar radiation was ranged between 525.7 W/m$^2$ to 970.5 W/m$^2$ while the ambient temperature was ranging from 37.1 °C to 43.7 °C, so the maximum deviation observed for solar radiation and ambient temperature was ± 3.31% and ± 1.37% respectively. As it is observed within the close range, it can be inferred that, at any hour of operation, the outdoor testing conditions are almost similar during the experimentation and gives the relative performance of each day.

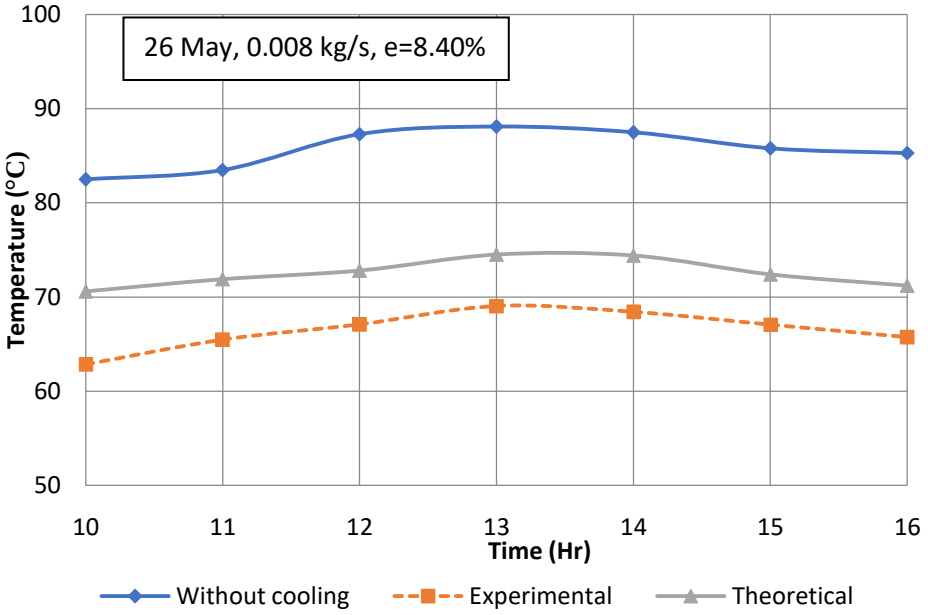
26 May, 0.008 kg/s, e=8.40%
100
90
80
70
60
50
Temperature (°C)
10
11
12
13
14
15
16
Time (Hr)
Without cooling
Experimental
Theoretical

(a)

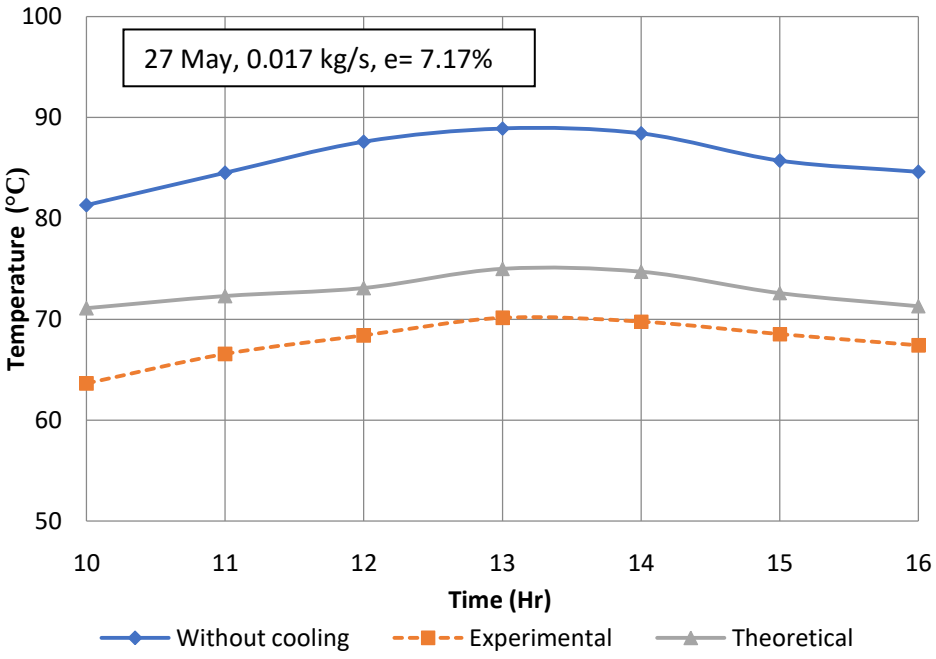
27 May, 0.017 kg/s, e= 7.17%
100
90
80
70
60
50
Temperature (°C)
10
11
12
13
14
15
16
Time (Hr)
Without cooling
Experimental
Theoretical

(b)

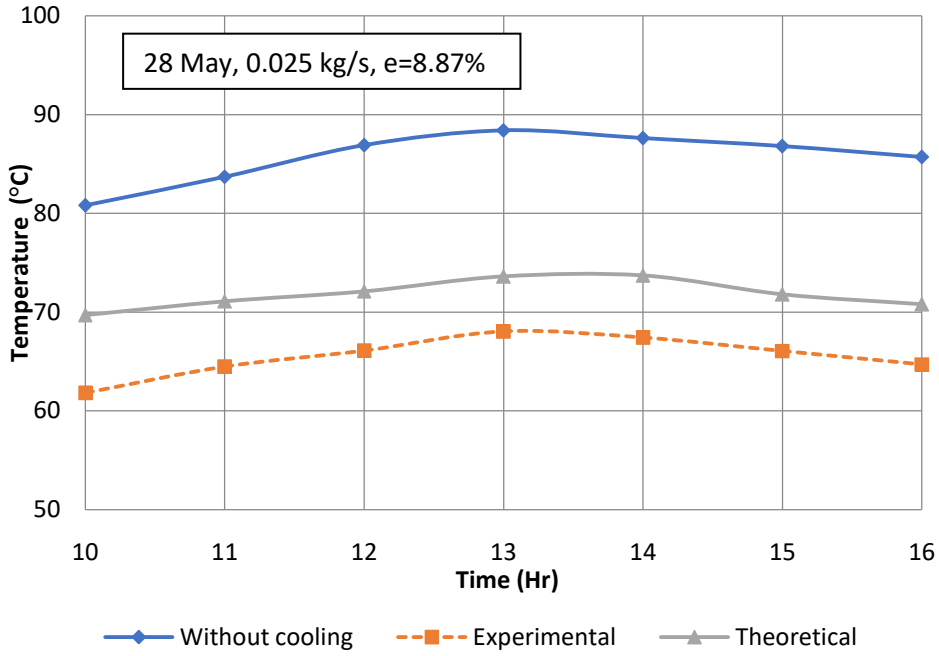


(c)

**Fig. 6.2 (a), (b) & (c) Simulated and experimental values of PV panel temperature in the HCPVT system during the test days (26-28 May, 2017)**

The hourly variation of PV panel temperature without cooling and with cooling with annulus liquid flow rates of 0.008 kg/s, 0.017 kg/s and 0.025 kg/s are shown in Fig. 6.2 (a), (b) & (c). From the experiments, it was observed that without the inner and annulus flow of water, the PV panel temperature ranged from 82.5 °C to 88.1 °C, 81.3 °C to 88.9 °C and 80.8 °C to 88.4 °C during 26, 27 and 28$^{th}$ May 2017 respectively. On the other hand, the PV panel temperature dropped with water cooling and ranged from 70.6 °C to 74.5 °C, 71.1 °C to 75.0 °C and 69.7 °C to 73.7 °C at constant inner flow rate of 0.075 kg/s with 0.008 kg/s, 0.017 kg/s and 0.025 kg/s annulus flow rates respectively. During the peak afternoon, the panel temperature rises due to the increase in solar radiation. Experimentally the PV panel temperature observed and ranged from 62.8 °C to 69.0 °C, 63.6 °C to 70.1 °C and 61.8 °C to 68.1 °C at respective flow rates. As mentioned in the previous section, the mean square percent deviation (e) is a suitable tool to identify the close agreement between theoretical simulations and experimental results. During the experimentation, the mean square percent deviation (e) varied from 7.17% to 8.87%.

The variation of HCPVT inlet and outlet temperature during the test days is represented graphically in Fig. 6.3 (a), (b) & (c). Experimental results obtained during the testing are validated with the theoretical results obtained by energy and mass balance. From the analysis, it was observed that the simulated HCPVT outlet temperature was on a higher side as compared to the experimental value. The maximum experimental HCPVT outlet temperature at fixed inner flow rate of 0.075 kg/s and 0.008 kg/s, 0.017 kg/s and 0.025 kg/s of annulus flow are 65.3 °C, 61.2 °C and 57.7 °C respectively. The HCPVT inlet temperature ranged between 35.8 °C to 37.9 °C for all the flow rates. This showed that maximum change in temperature of 28.7 °C was observed for annulus mass flow rate of 0.008 kg/s. The variation in HCPVT outlet temperature also depends upon the CR of PTC and solar radiation falling upon the collector. From the statistical point of view, the root mean square percent deviation comes out to be in the range of 5.87% to 6.80% which indicates that the experimental and theoretical results are in a good agreement, as shown in Fig. 6.3 (a), (b) & (c).

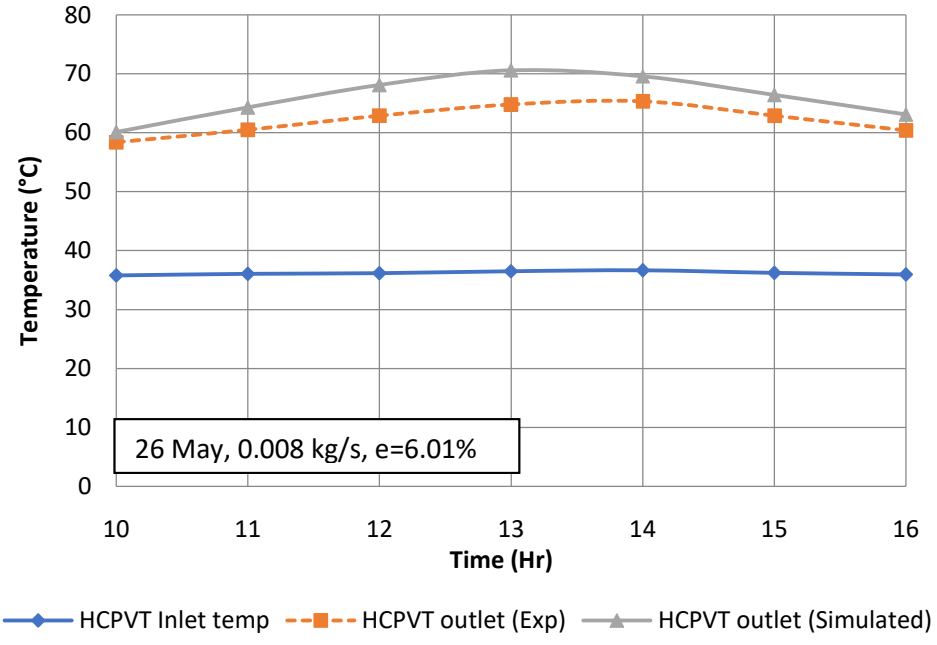


(a)

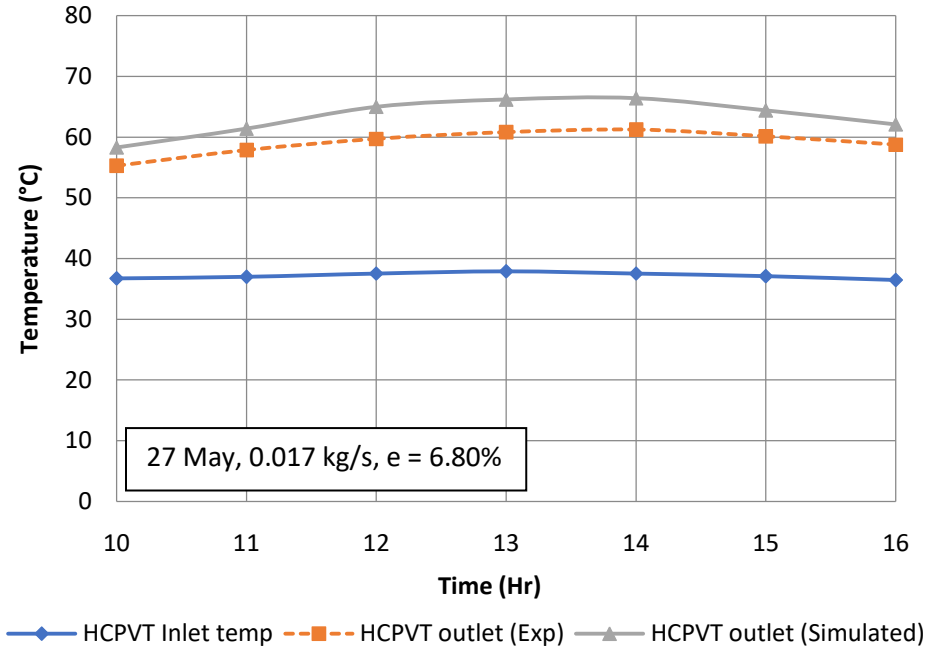


(b)

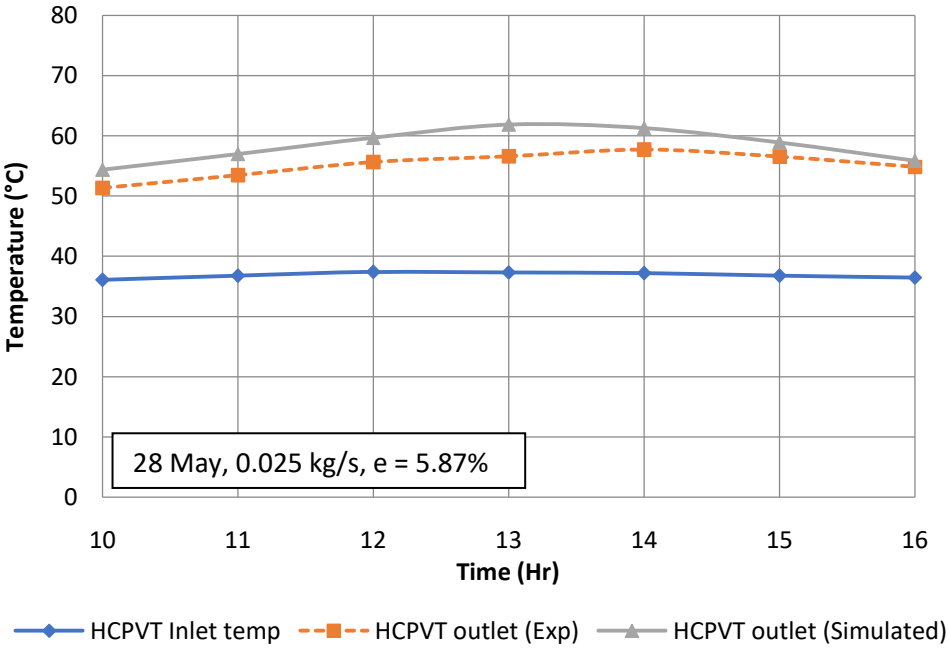


(c)

**Fig. 6.3 (a), (b) & (c) Simulated and experimental values of HCPVT inlet and outlet temperature during the test days (26-28 May, 2017)**

Fig. 6.4 (a), (b) and (c) indicates the graphical representation of electrical efficiency of HCPVT system obtained without cooling and with cooling for different mass flow rates of water. Two cases were taken for comparing the electrical efficiencies, first when the PV

panel in the HCPVT system was cooled by water flowing within the annulus and inner tube, and in second case it was without any cooling. In the case of no cooling of PV panel, the electrical efficiency was observed varying from 10.45% to 10.99% due to high temperature during experimentation. While with water cooling, the experimental electrical efficiency was observed varying from 11.77% to 12.18%, 11.69% to 12.13% and 11.84% to 12.25% for annulus flow rates of 0.008 kg/s, 0.017 kg/s and 0.025 kg/s respectively. From the same, it can be concluded that with cooling of PV panel, the electrical efficiency of system increased by 1.24% to 1.34%, 1.13% to 1.27% and 1.25% to 1.39% for annulus flow rate of 0.008 kg/s, 0.017 kg/s and 0.025 kg/s respectively as compared to no cooling. This may be due to the fact that, without cooling, the panel temperature increases and hence PV panel efficiency decreases. Through the day, with the change in ambient conditions and panel temperature changes and PV panel efficiency was observed on the higher side during morning and evening period as compared to peak sunshine hours.

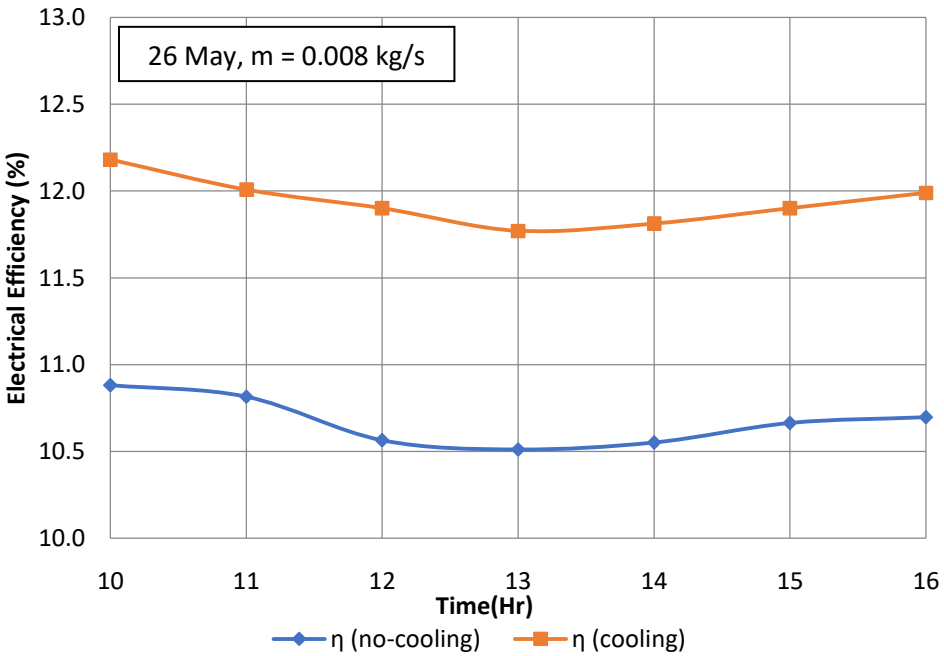


(a)

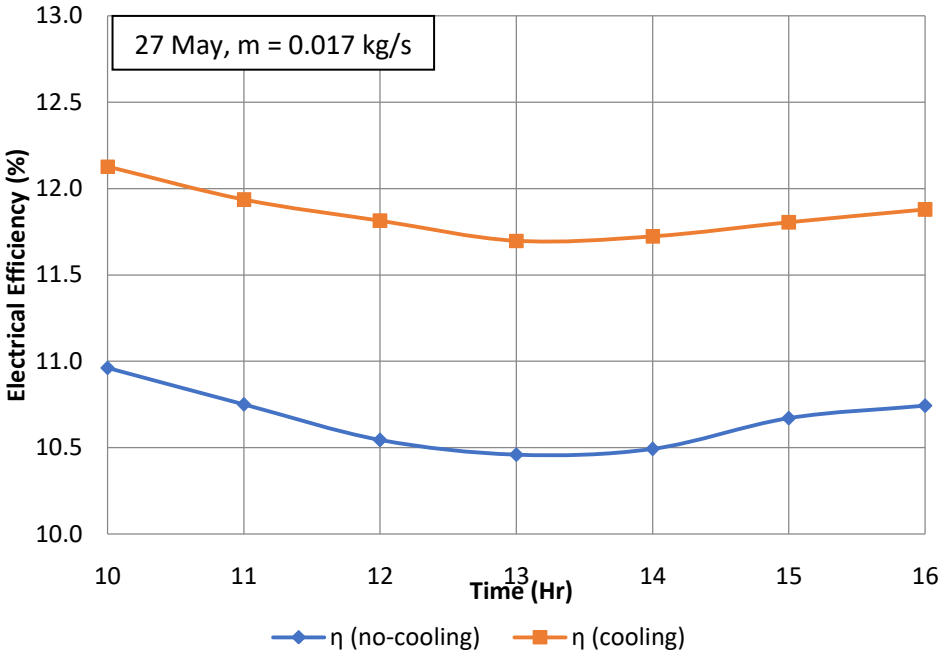


(b)

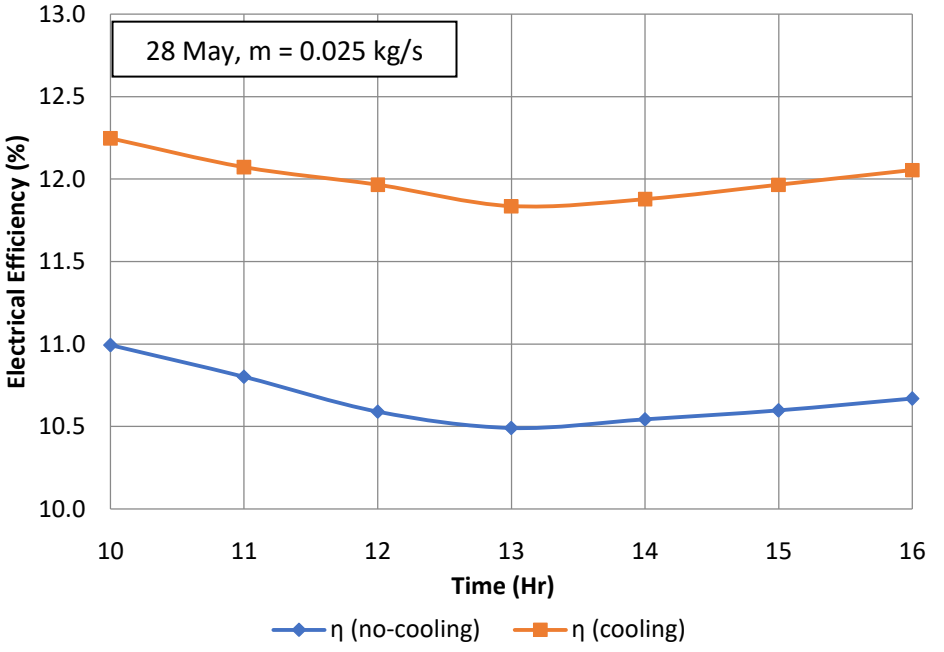


(c)

**Fig. 6.4 (a), (b) & (c) Electrical efficiency of HCPVT system with and without cooling during the test days (26-28 May, 2017)**

The experimental and simulated hourly variation of HCPVT system thermal efficiency is shown in Fig. 6.5 (a), (b) & (c) for different flow rates of cooling water. It reveals that the experimental thermal efficiency ranged from 44.35% to 60.72%, 40.01% to 59.84% and 37.67% to 58.76% for annulus flow rates of 0.008 kg/s, 0.017 kg/s and 0.025 kg/s respectively with constant inner flow rate of 0.075 kg/s. The root mean square percent deviation (e) obtained by validating with theoretical results were within the range from 9.74% to 12.96%, which show the good agreement between the two. The variation between the results may arise due to various factors including losses from pipe junctions, convection losses and insulation losses during the experiment.

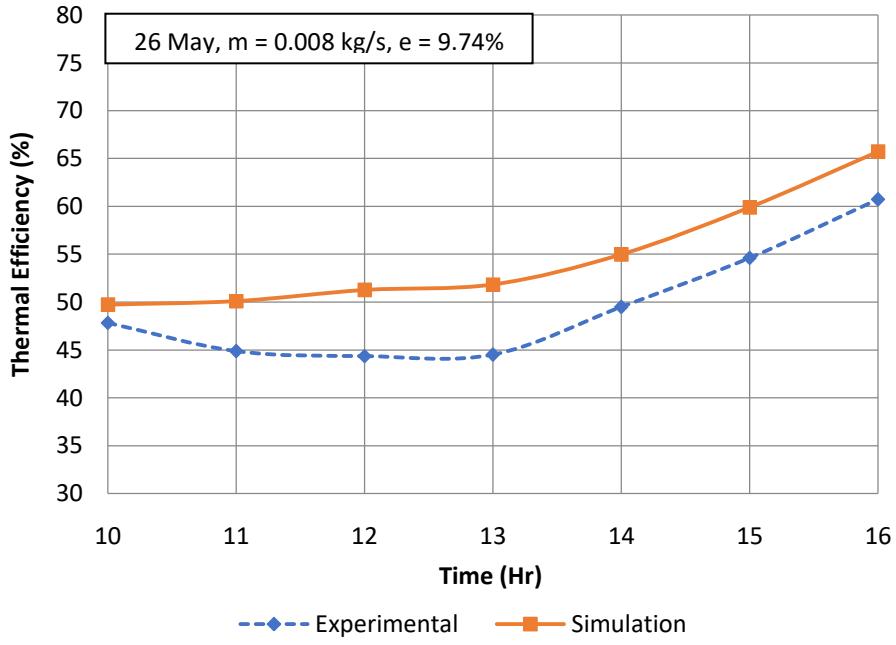


(a)

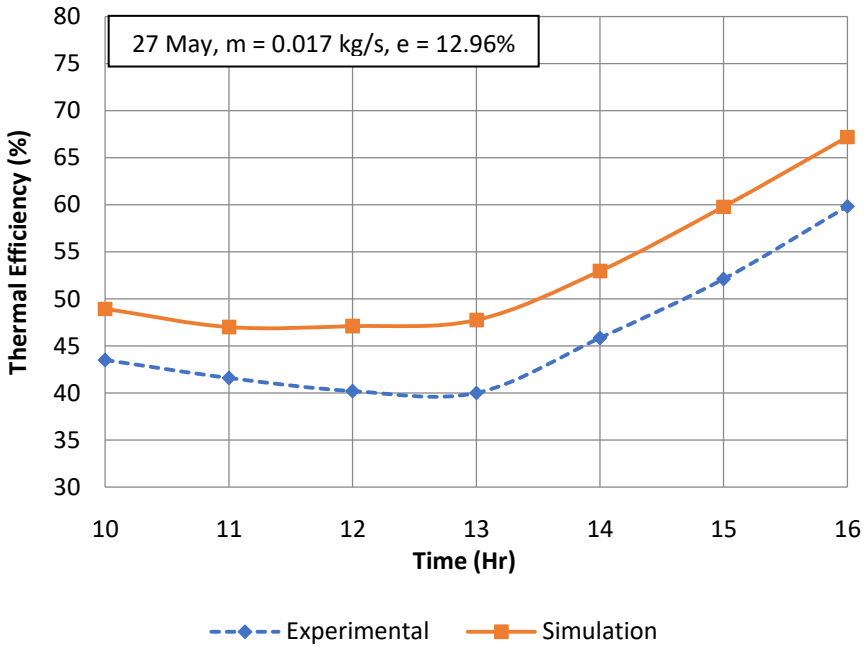


(b)

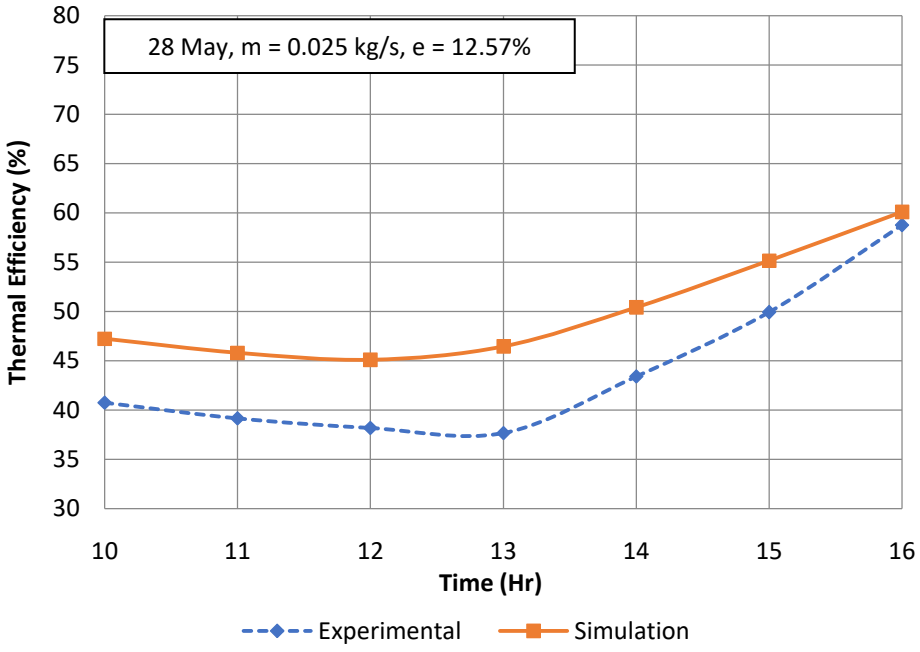


(c)

**Fig. 6.5 (a), (b) & (c) Simulated and experimental values of thermal efficiency of HCPVT during the test days (26-28 May, 2017)**

The overall efficiency of the system is calculated as per Eq. (4.49) and hourly variation of HCPVT system for all the test days is shown in Fig. 6.6. The mean overall efficiency of the system ($\eta_{tot}$) for the mass flow rate of 0.008 kg/s, 0.017 kg/s and 0.025 kg/s was observed as 61.42%, 58.01% and 55.99% respectively. It was seen that the overall efficiency decreases slightly during noon due to higher losses to the surroundings.

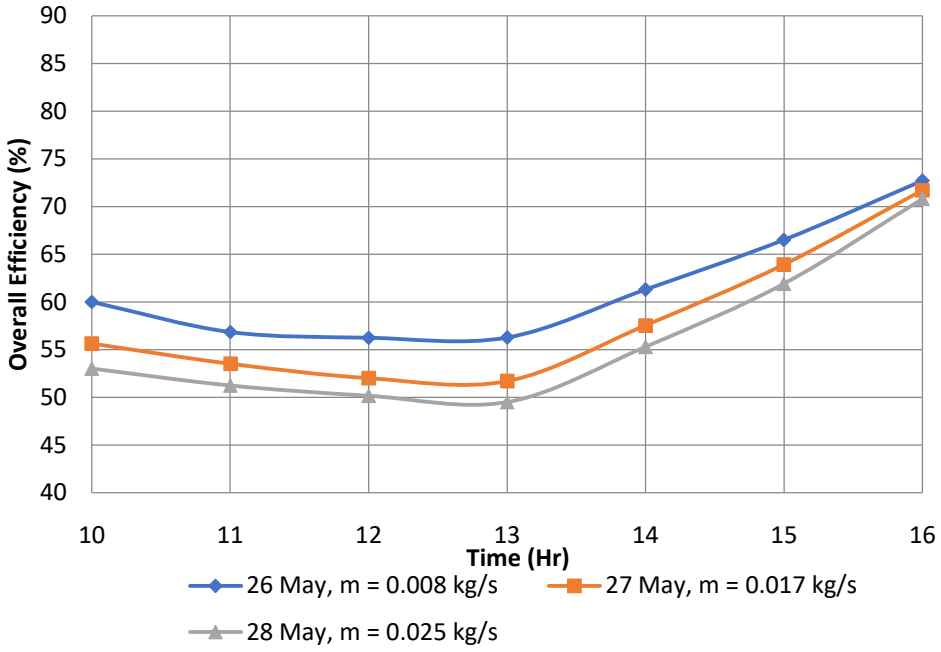


**Fig. 6.6 Overall efficiency of HCPVT during the test days (26-28 May, 2017)**

### 6.1.2 Results obtained by keeping the inner tube flow rate at 0.091 kg/s

During the third set of experimental run, the inner tube flow rate was maintained at 0.091 kg/s and mass flow rate through HCPVT receiver varied from 0.008 kg/s, 0.017 kg/s and 0.025 kg/s to achieve combined flow rate ranging from 0.1 kg/s to 0.116 kg/s. By doing so, Reynolds's Number during the experiments varied in the range of 1000 to 5000. The experiments were carried for daily 6 hour on three consecutive days from 14 - 16 June 2017. The data obtained from the experiment were compared with theoretical results similar to the analysis carried out in Sec. 6.1.1. During the time of experiments, the solar radiation ranged between 558.2 W/m$^2$ to 1050.8 W/m$^2$ while the ambient temperature varied from 36.2 °C to

41.8 °C. The dataset for solar radiation and ambient temperature was also observed within the close range during these days. The variation of global solar radiation and ambient temperature during the test days (14-16 June) are shown in Fig. 6.7.

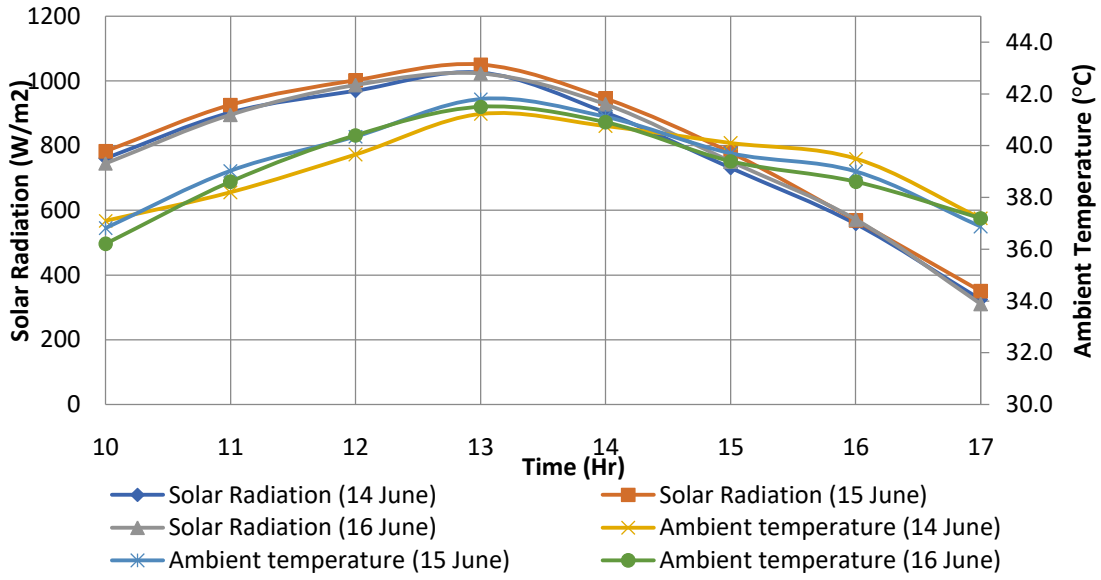


**Fig. 6.7 Variation of solar radiation and ambient temperature during test days (14-16 June, 2017)**

Fig. 6.8 (a), (b) & (c) illustrate the PV panel temperature obtained on an hourly basis during cooling and without cooling condition on test days. From the experiments, it was observed that in no cooling conditions the PV panel temperature ranged from 80.5 °C to 87.8 °C, 81.0 °C to 88.4 °C and 81.7 °C to 89.1 °C during 14, 15 and 16$^{th}$ June 2017 respectively. On the other hand, PV panel temperature dropped with water cooling from 59.6 °C to 65.9 °C, 59.6 °C to 65.6 °C and 59.3 °C to 65.2 °C at constant inner flow rate of 0.091 kg/s with 0.008 kg/s, 0.017 kg/s and 0.025 kg/s and annulus flow rate respectively. It is visible from the graph that with an increase in solar radiation, the panel temperature increases which in turns increases the water temperature. The experimentally observed module temperature was validated with the simulation results and found to be in good agreement with root mean square percent deviation (e) ranging from 6.82% to 8.13%.

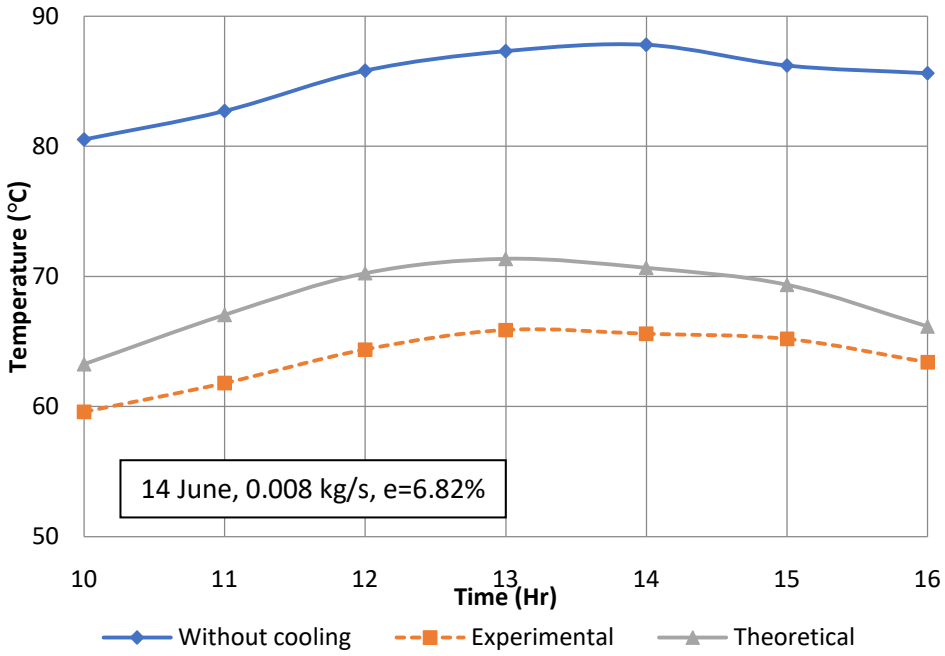
90
80
70
60
50
Temperature (°C)
14 June, 0.008 kg/s, e=6.82%
10
11
12
13
14
15
16
Time (Hr)
Without cooling
Experimental
Theoretical

(a)

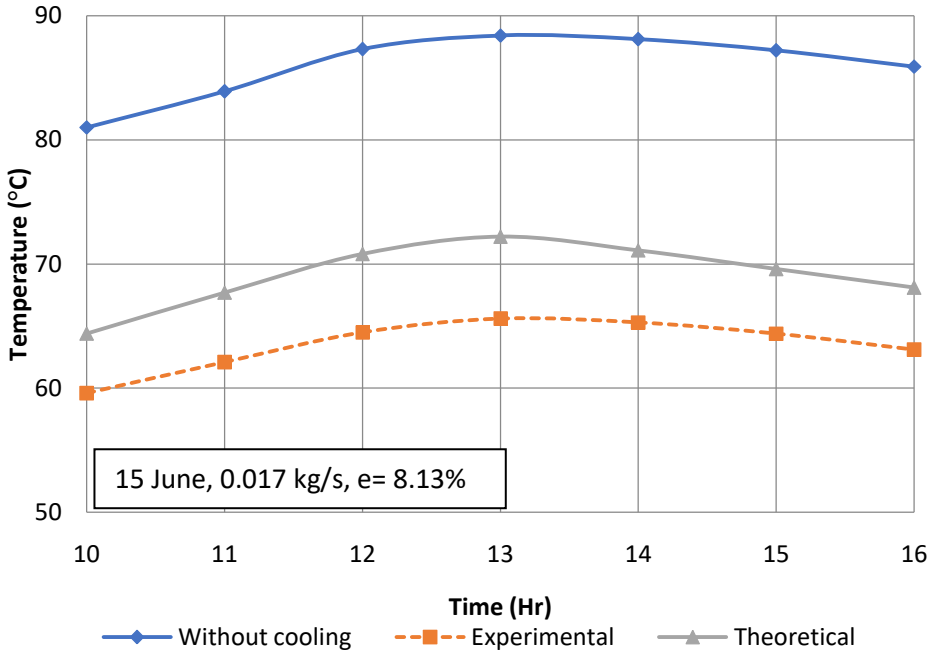
90
80
70
60
50
Temperature (°C)
15 June, 0.017 kg/s, e= 8.13%
10
11
12
13
14
15
16
Time (Hr)
Without cooling
Experimental
Theoretical

(b)

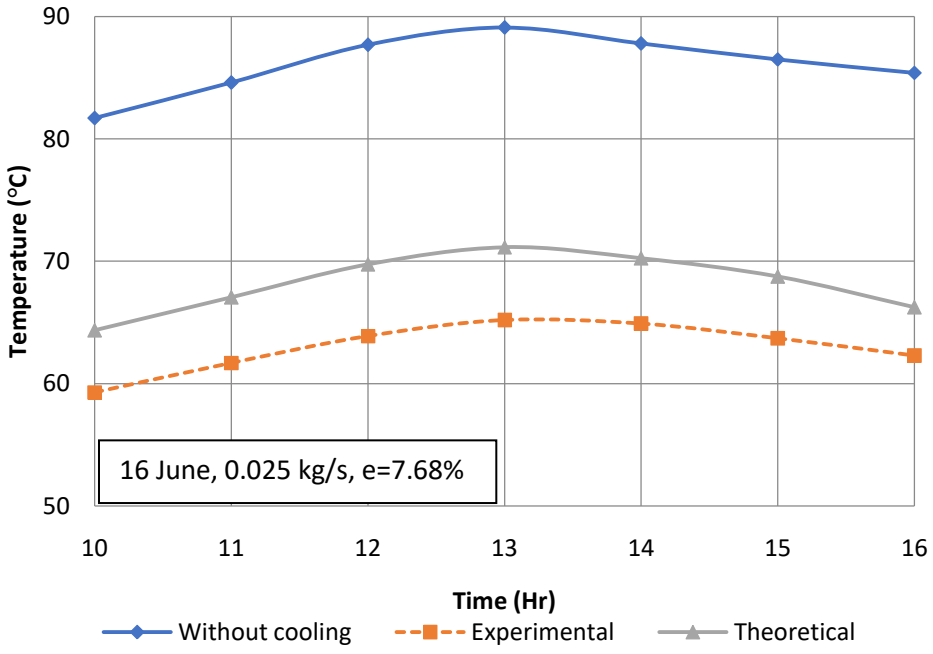


(c)

**Fig. 6.8 (a), (b) & (c) Simulated and experimental values of PV panel temperature in the HCPVT system during the test days (14-16 June, 2017)**

The variation observed during the inlet and outlet temperature of HCPVT during the experimentation is graphically represented in Fig. 6.9 (a), (b) & (c). The experimental results obtained during the testing are validated with the theoretical results obtained using analytical approach. From the analysis, it is found out that the temperatures obtained during the experiment are slightly on the lower level, as compared to the theoretical results due to experimental errors. From Fig. 6.9 it is observed that HCPVT inlet temperature ranged between 35.40 °C to 37.55 °C for all annular flow rates. When the inner tube flow rate was kept constant at 0.091 kg/s, the maximum experimental outlet temperatures obtained was 66.7 °C, 64.1 °C and 60.1 °C for annulus mass flow rate of 0.008 kg/s, 0.017 kg/s and 0.025 kg/s respectively. This implies that at an annulus flow rate of 0.008 kg/s, the maximum temperature difference observed was 29.47 °C. Other external factors like incident solar radiation and CR of the collector, also account for the variation in HCPVT outlet temperature. From the statistical analysis, it was observed that the root mean square percent

deviation (e) varied from 6.54% to 7.59%, which indicates that the experimental and theoretical results are in a good agreement.

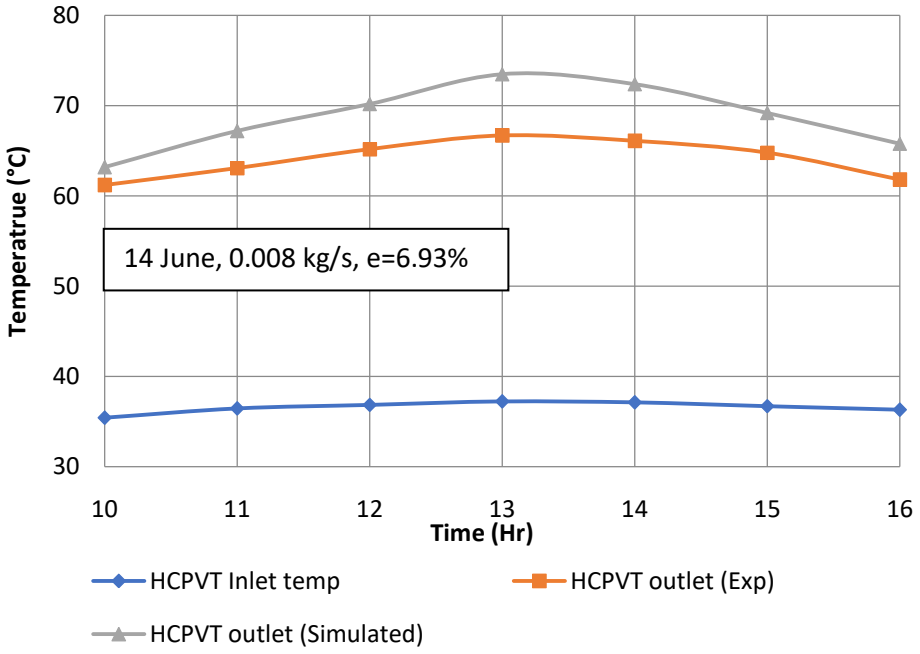


(a)

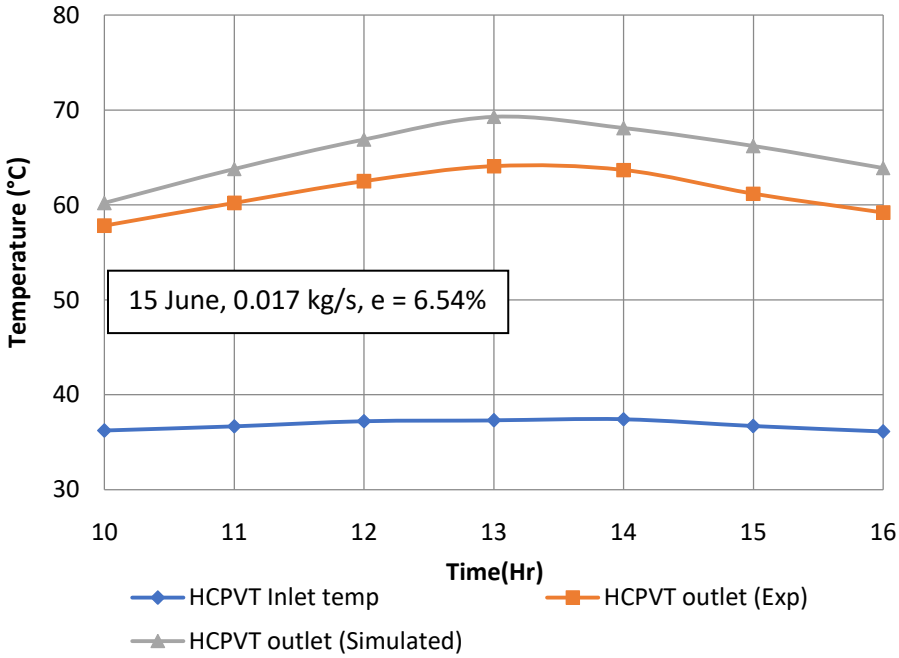


(b)

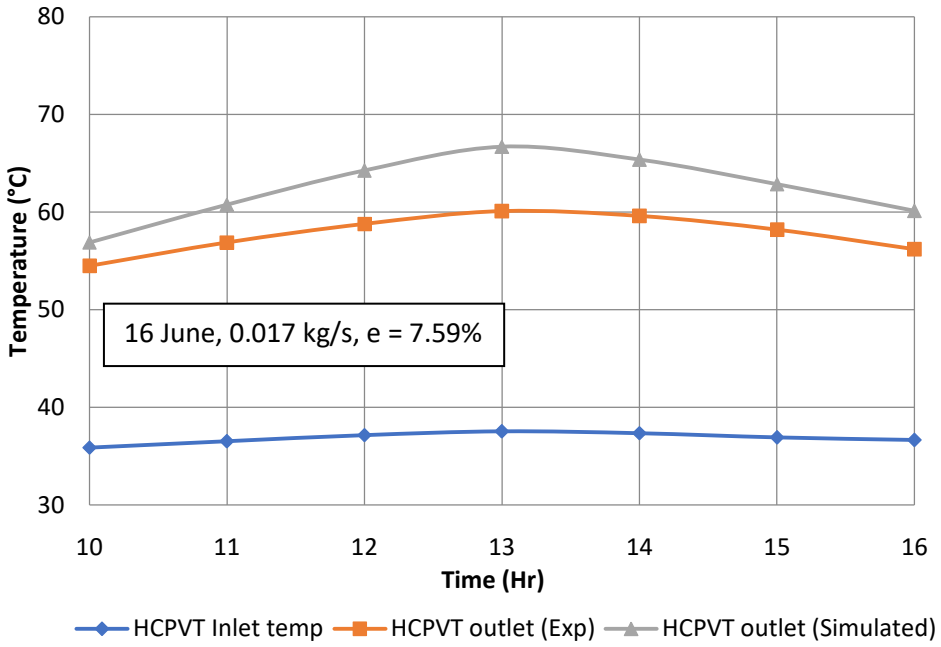


(c)

**Fig. 6.9 (a), (b) & (c) Simulated and experimental values of HCPVT inlet and outlet temperature during the test days (14-16 June, 2017)**

Fig. 6.10 (a), (b) & (c) shows the variation of electrical efficiency of HCPVT without cooling and with cooling, along with PV panel temperature variation for different mass flow rates. In cooling mechanism, when inner tube flow rate was kept constant at 0.091 kg/s and annulus flow rates varied from 0.008 kg/s, 0.017 kg/s and 0.025 kg/s, the maximum experimental electrical efficiency obtained ranged between 11.98% to 12.39%, 12.00% to 12.39% and 12.02% to 12.41% respectively. In the case of no flow condition, the electrical efficiency varied from 10.45% to 11.01%. This variation indicates that with an increase in PV panel temperature and without any cooling mechanism, the efficiency decreases. It was also observed that during peak afternoon, the efficiency was on the lower side as compared to the values obtained during the morning and evening period.

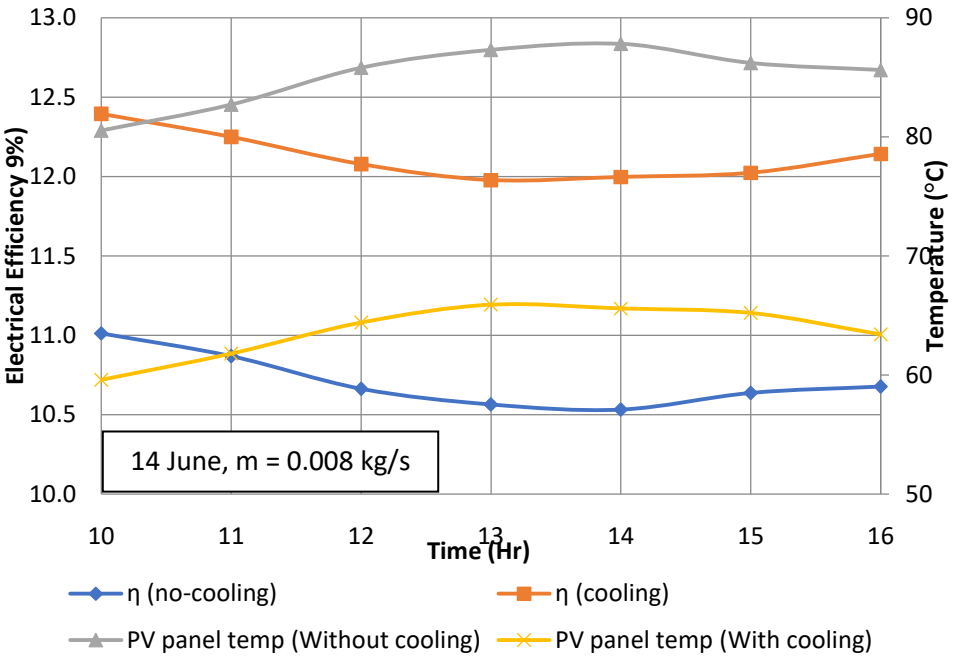
13.0
12.5
12.0
11.5
11.0
10.5
10.0
Electrical Efficiency 9%)
90
80
70
60
50
Temperature (°C)
14 June, m = 0.008 kg/s
10
11
12
13
14
15
16
Time (Hr)
η (no-cooling)
η (cooling)
PV panel temp (Without cooling)
PV panel temp (With cooling)

(a)

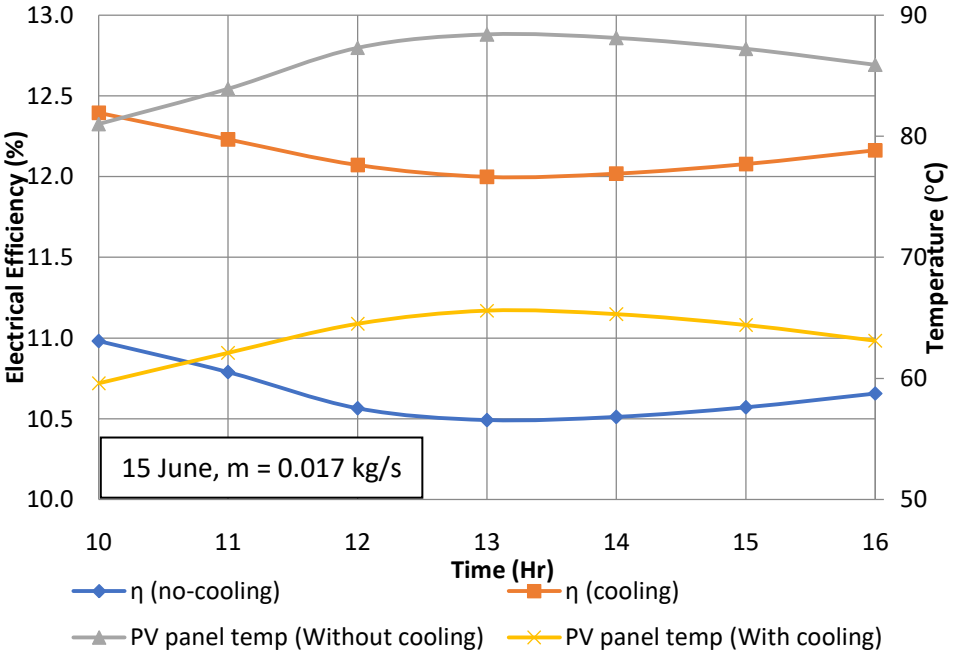
13.0
12.5
12.0
11.5
11.0
10.5
10.0
Electrical Efficiency (%)
90
80
70
60
50
Temperature (°C)
15 June, m = 0.017 kg/s
10
11
12
13
14
15
16
Time (Hr)
η (no-cooling)
η (cooling)
PV panel temp (Without cooling)
PV panel temp (With cooling)

(b)

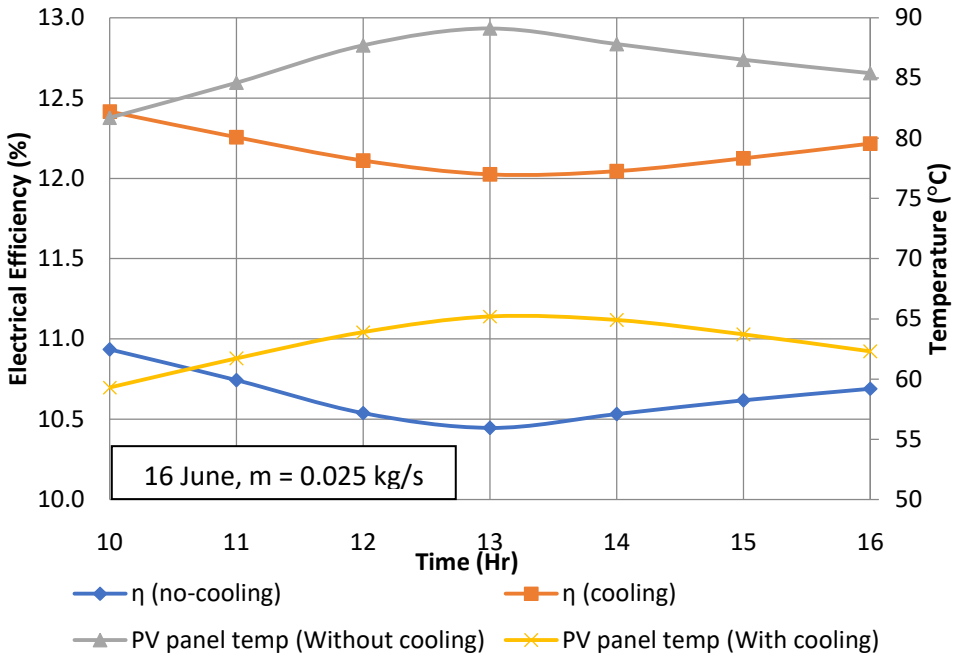


(c)

**Fig. 6.10 (a), (b) & (c) Electrical efficiency and PV panel temperature of HCPVT system with and without cooling during the test days (14-16 June, 2017)**

The hourly variation of thermal efficiency of HCPVT system during the test days (14-16 June) at different mass flow rates is graphically represented in Fig. 6.11 (a), (b) & (c). It was observed that at inner tube flow rate of 0.091 kg/s and experimental thermal efficiency of the system varied from 48.53% to 63.46%, 47.25% to 60.52% and 44.83% to 56.60% for annulus flow rates of 0.008 kg/s, 0.017 kg/s and 0.025 kg/s respectively. It was observed that during peak afternoon, the thermal efficiency was on the minimum side as compared to values observed during morning and evening. This may be because due to peak sunshine, the ambient temperature increases which also increases the thermal losses due to convection. When the data obtained from experiment was compared with the simulation results, it was found out to be in good agreement with root mean square percent deviation varying from 9.61% to 10.57%.

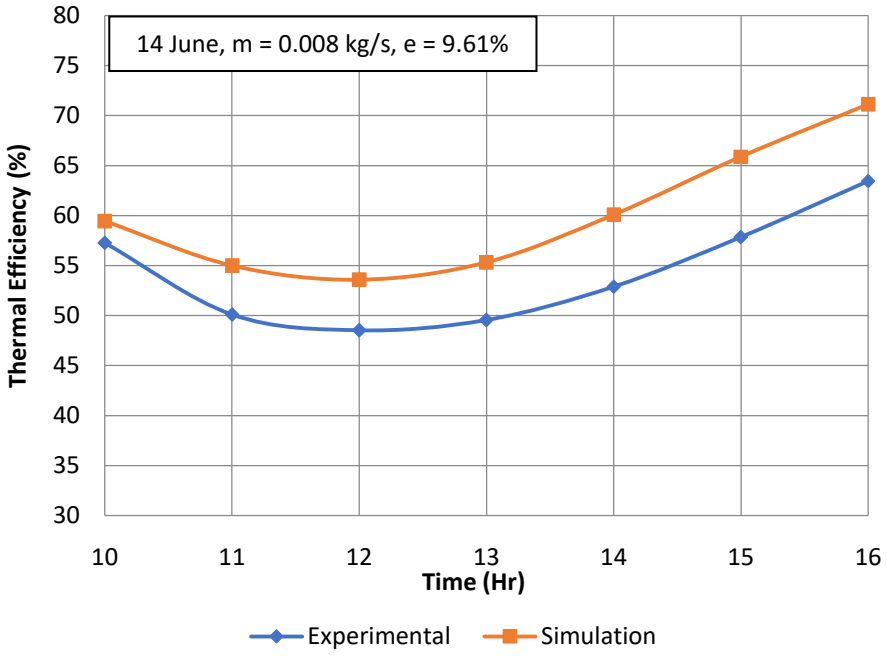
14 June, m = 0.008 kg/s, e = 9.61%
Thermal Efficiency (%)
80
75
70
65
60
55
50
45
40
35
30
10
11
12
13
14
15
16
Time (Hr)
Experimental
Simulation

(a)

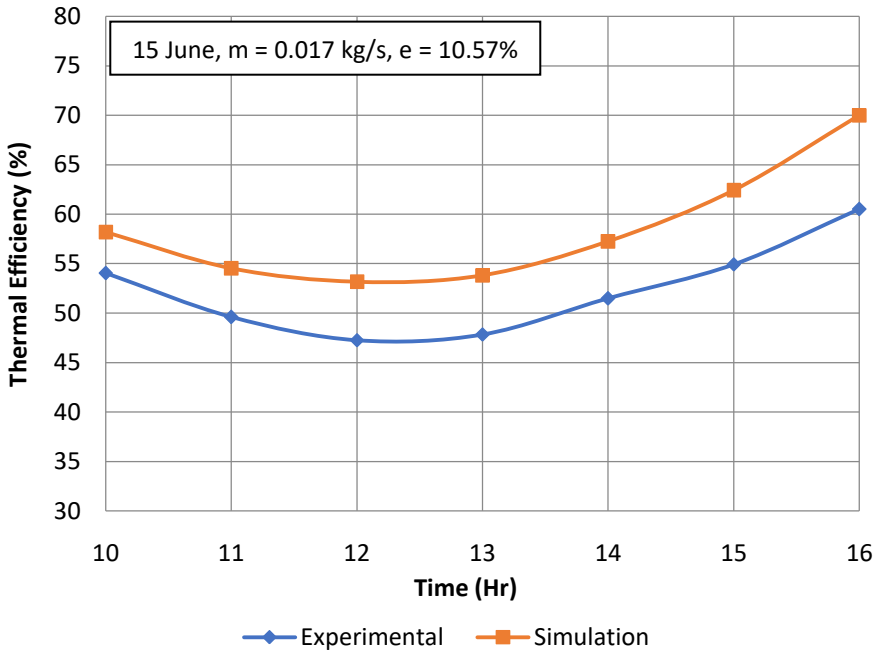
15 June, m = 0.017 kg/s, e = 10.57%
Thermal Efficiency (%)
80
75
70
65
60
55
50
45
40
35
30
10
11
12
13
14
15
16
Time (Hr)
Experimental
Simulation

(b)

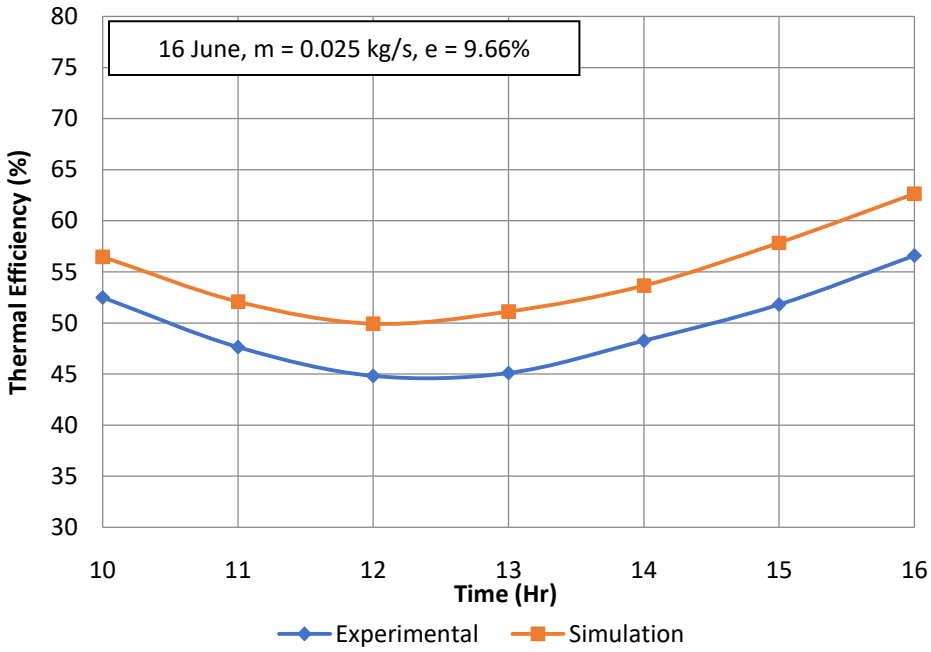


(c)

**Fig. 6.11 (a), (b) & (c) Thermal efficiency of HCPVT system during the test days (14-16 June, 2017)**

Using Eq. (4.49), the overall efficiency of HCPVT system was calculated and is shown in Fig. 6.12. It was found out that during test days, the mean overall efficiency of HCPVT comes out to be 66.36%, 64.37% and 61.71% for annulus mass flow rate of 0.008 kg/s, 0.017 kg/s and 0.025 kg/s respectively. It was observed that the overall efficiency decreases with an increase in annulus flow rate at a constant inner tube flow rate.

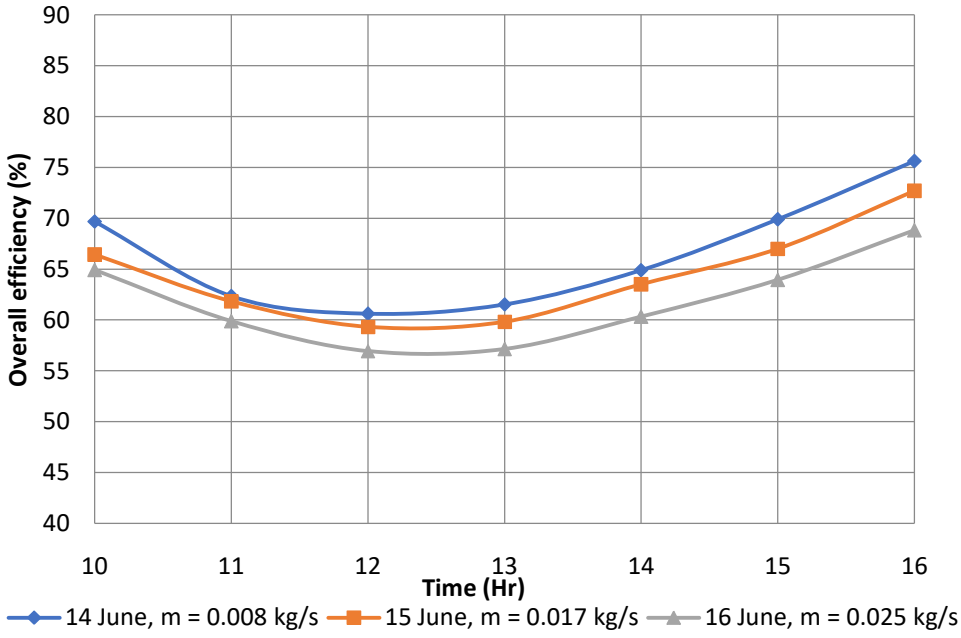


**Fig. 6.12 Overall efficiency of HCPVT system during the test days (14-16 June, 2017)**

## 6.2 Performance analysis of HCPVT system with varying inner tube flow rate

As discussed earlier, the experiments were carried out in sets of three consecutive days (26-28 May, 09-11 June and 14-16 June). In the previous section, the analysis was carried out when inner flow rate was kept constant at 0.075 kg/s and 0.091 kg/s and the annulus flow rate varied from 0.008 kg/s, 0.017 kg/s and 0.025 kg/s. By doing so, Reynolds's Number during the experiments varied in the range of 1000 to 5000. On 26$^{th}$ May, the inner flow rate was maintained at 0.075 kg/s, on 9$^{th}$ June, it was maintained at 0.083 kg/s and on 14$^{th}$ June, the same was maintained at 0.091 kg/s. In the current section, the variation of the inner tube rate is discussed when the annulus flow rate was maintained at 0.008 kg/s. The variation of solar radiation along with the ambient temperature during the test days, i.e. 26 May, 9 June and 14 June, are shown in Fig. 6.13. During the time of experiments (26 May, 9 June and 14 June), the solar radiation varied from 543.2 W/m$^2$ to 1025.4 W/m$^2$, which implied that maximum deviation observed during these days was ±5.76%. Similarly, the ambient temperature varied from 37.1 °C to 43.7 °C, which gave the maximum deviation of ±5.73%. This indicated that the dataset of the test days was within the permissible range.

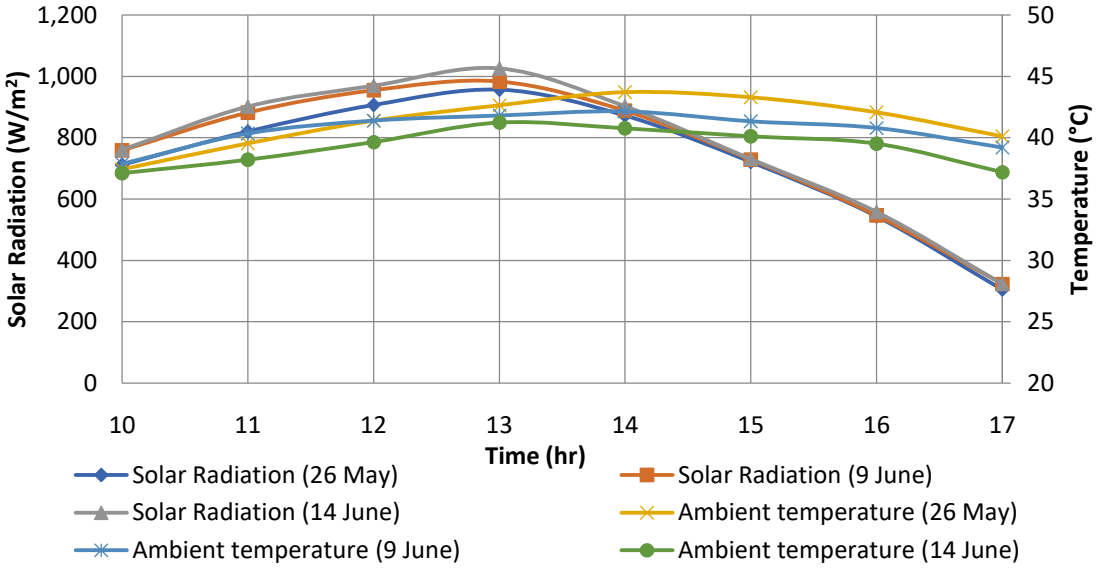


**Fig. 6.13 Variation of solar radiation and ambient temperature during test days (26 May, 9 June and 14 June, 2017)**

Similar to the analysis of inlet and outlet temperature, PV panel temperature, electrical and thermal efficiencies of HCPVT for varying annulus flow rate are discussed here. The hourly variation of inlet and outlet temperature of HCPVT, as observed in Fig. 6.14 (a), (b) & (c), shows that inlet temperature during the test days varied from 35.4 °C to 37.6 °C for all inner tube flow rates when the annulus flow rate was kept constant at 0.008 kg/s. During this period, the outlet temperature varied from 58.4 °C to 65.3 °C, 60.1 °C to 66.5 °C and 61.2 °C to 66.7 °C for the inner tube flow rate of 0.075 kg/s, 0.083 kg/s and 0.091 kg/s respectively. This implied that at the inner flow rate of 0.091 kg/s, the maximum temperature difference between inlet and outlet was 29.5 °C. The root mean square percent deviation (e) ranged from 6.01% to 6.93% indicating the validation of theoretical results with the experimental data.

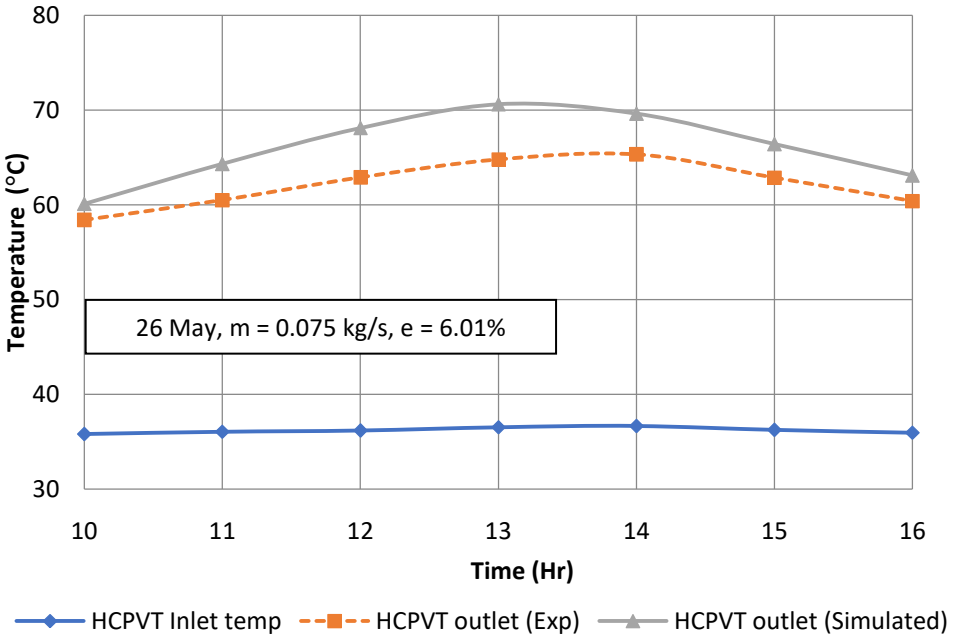


(a)

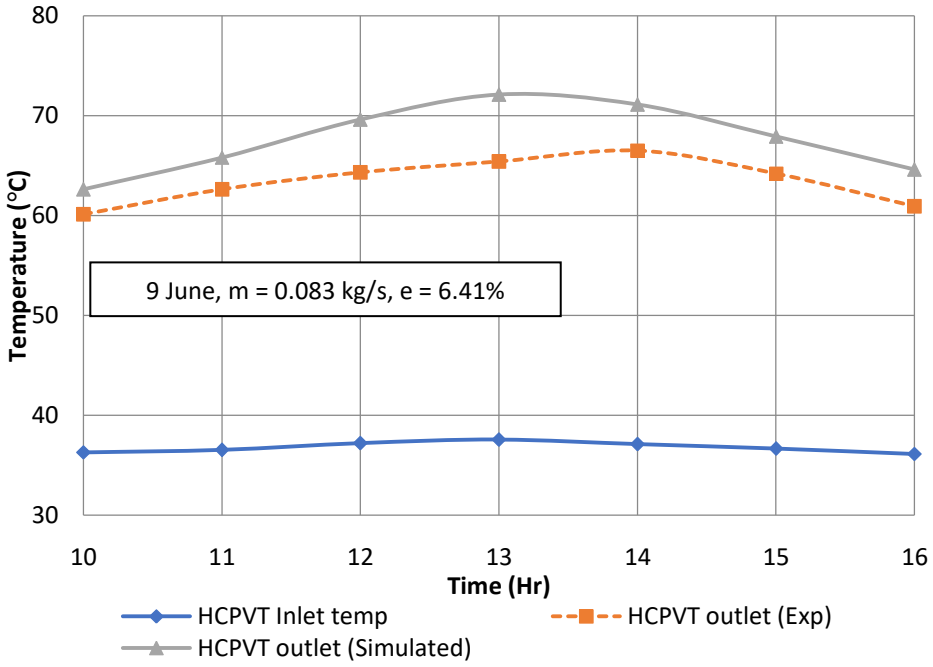


(b)

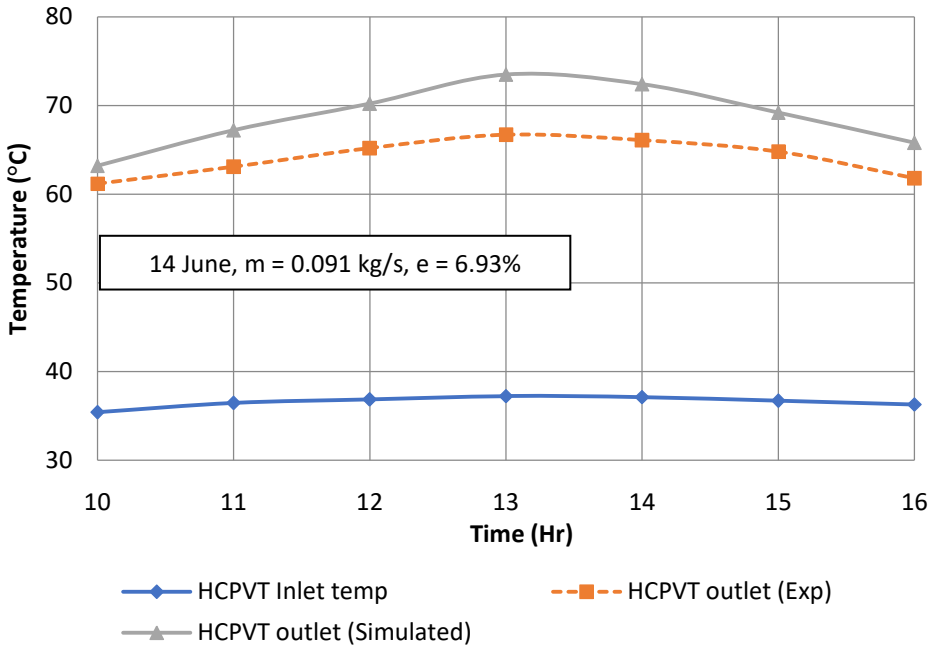


(c)

**Fig. 6.14 (a), (b) & (c) Simulated and experimental values of HCPVT inlet and outlet temperature during the test days (26 May, 9 June and 14 June)**

The effect of varying inner tube flow rate by keeping the annulus flow rate constant was apparent on PV panel temperature, as represented graphically in Fig. 6.15 (a), (b) & (c). In case of no flow condition (without cooling), the PV panel temperature reached the maximum of 88.1 °C, 88.8 °C and 87.8 °C during 26 May, 9 June and 14 June respectively. It is evident from the fact that under high concentration, the PV panel temperature increases and reaches a maximum during peak afternoon. When cooling was provided by varying inner tube flow rate from 0.075 kg/s, 0.083 kg/s and 0.091 kg/s, the PV panel temperature reduced and varied from 62.8 °C to 69.0 °C, 61.4 °C to 67.8 °C and 59.6°C to 65.9 °C respectively at constant annulus flow rate of 0.008 kg/s. The panel temperature observed from the theoretical analysis is also shown in Fig. 6.14 and found out that they were in good agreement with experimental data having root mean square percent deviation (e) ranged from 6.82% to 8.40%.

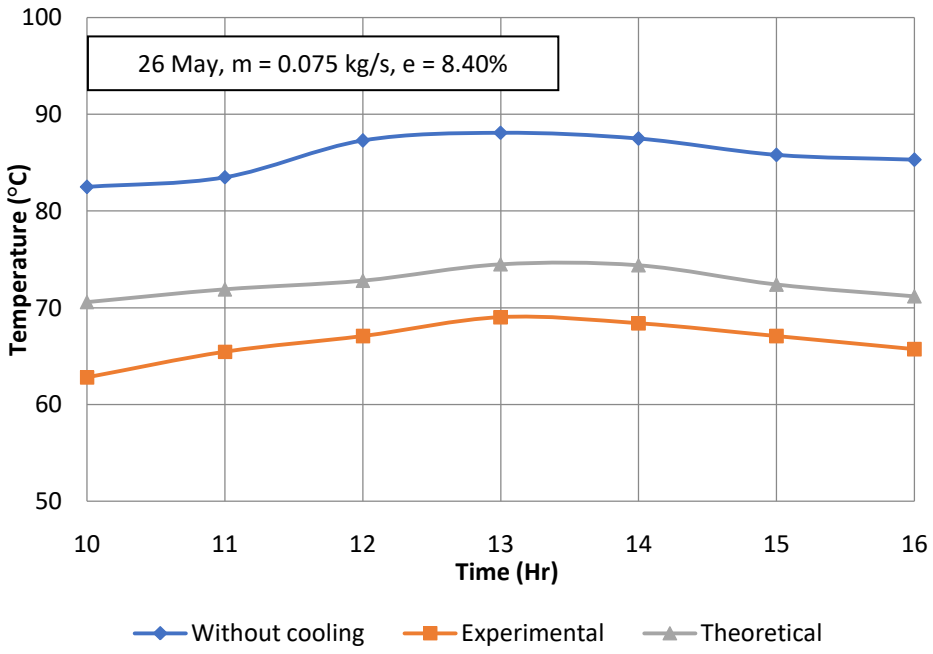


(a)

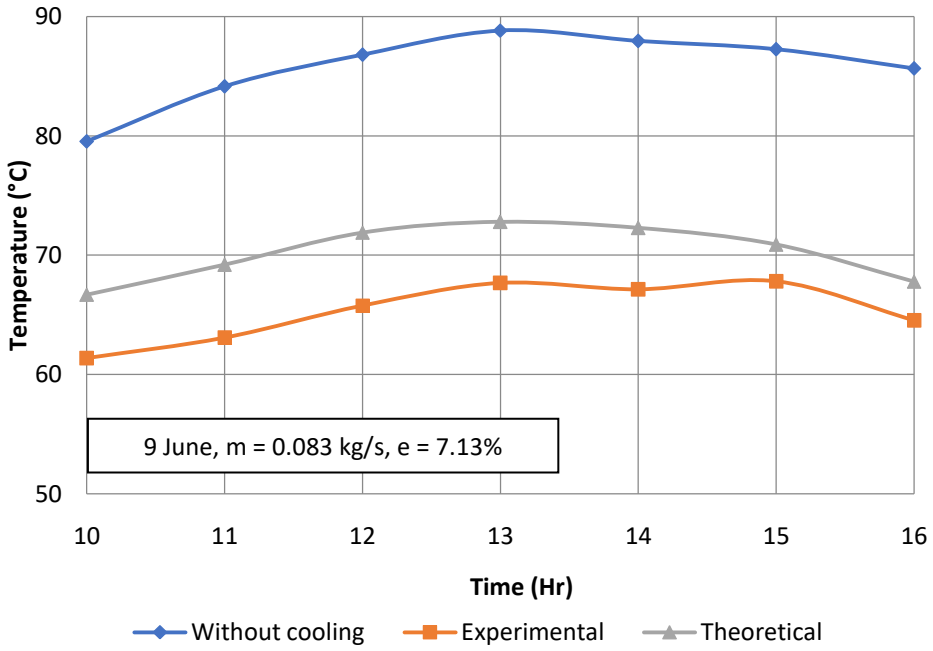


(b)

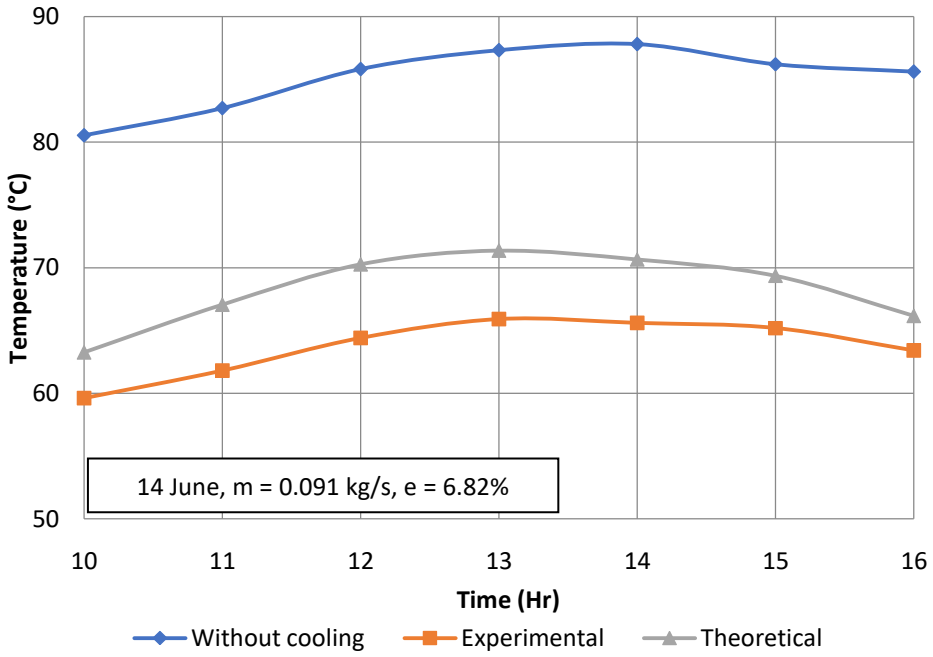


(c)

**Fig. 6.15 (a), (b) & (c) Simulated and experimental values of PV panel temperature in the HCPVT system during the test days (26 May, 9 June and 14 June, 2017)**

With varying mass flow rate the PV panel temperature decreased as compared to no flow condition. This leads to an increase in electrical efficiency of the PV panel. The variation observed in the electrical efficiency with and without flow condition is shown in Fig. 6.16 (a), (b) & (c). When no cooling was provided, the electrical efficiency varied from 10.46% to 11.08%. This changed with cooling of PV panel as electrical efficiency varied from 11.77% to 12.18%, 11.85% to 12.28% and 11.98% to 12.39% for inner tube flow rate of 0.075 kg/s, 0.083 kg/s and 0.091 kg/s respectively. This implies that with cooling the panel efficiency increased by 1.19% to 1.47% during the test days. The efficiency thus observed, was on the higher side during morning and evening as compared to the values obtained during afternoon period. It is because during the morning and evening period, the solar radiation was less which results in less panel temperature and higher PV efficiency.

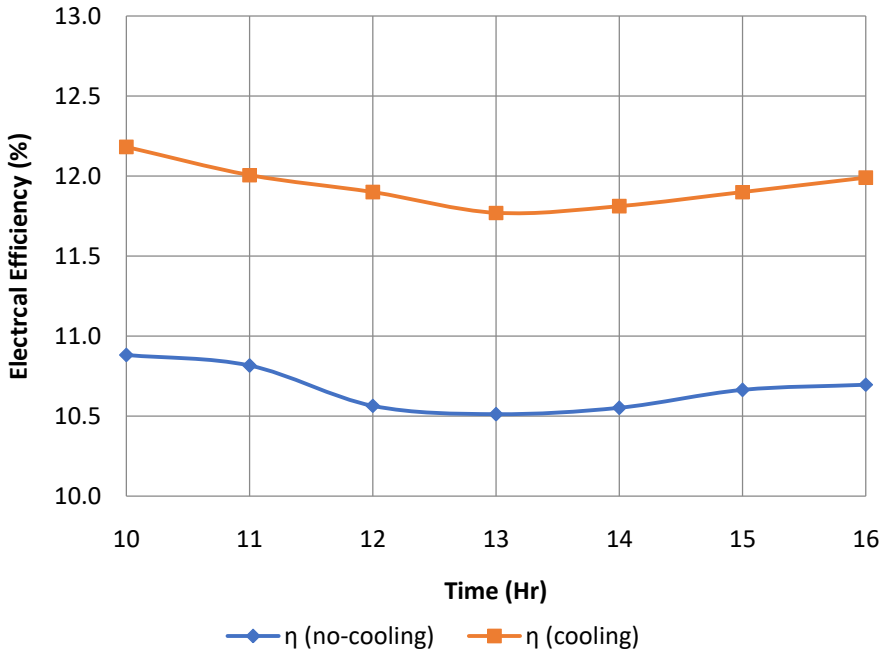


(a)

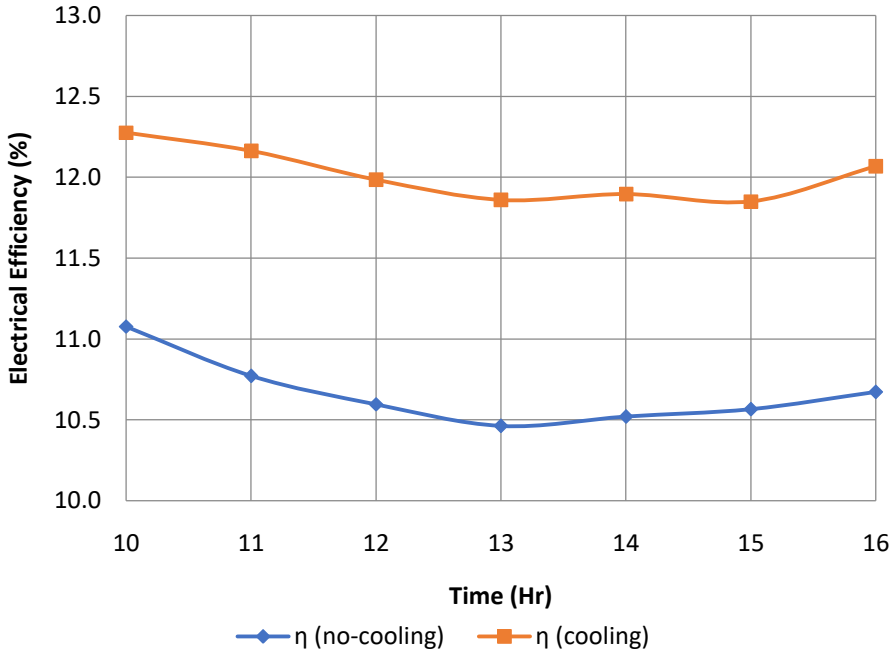


(b)

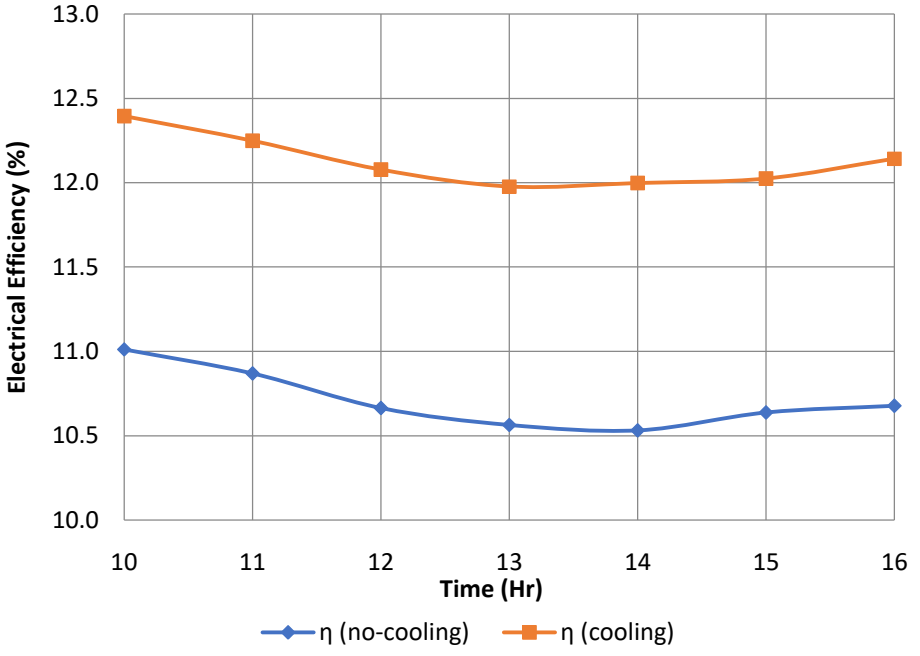


(c)

**Fig. 6.16 (a), (b) & (c) Electrical efficiency of HCPVT system with and without cooling during the test days (26 May, 9 June and 14 June, 2017)**

Fig. 6.17 (a), (b) & (c) shows the hourly variation of thermal efficiency of HCPVT system obtained at different inner tube flow rates while keeping annulus flow rate constant at 0.008 kg/s. It was found out that the thermal efficiency varied from 44.35% to 60.73%,

47.5% to 60.92% and 48.53% to 63.46% for inner tube flow rate of 0.075 kg/s, 0.083 kg/s and 0.091 kg/s respectively. As per the trends of electrical efficiency, the thermal efficiency was also on the higher side during the morning and evening period due to less thermal losses to the ambient. The root mean square percent deviation observed by validating simulation results with experimental data ranged between 7.14% to 10.28%.

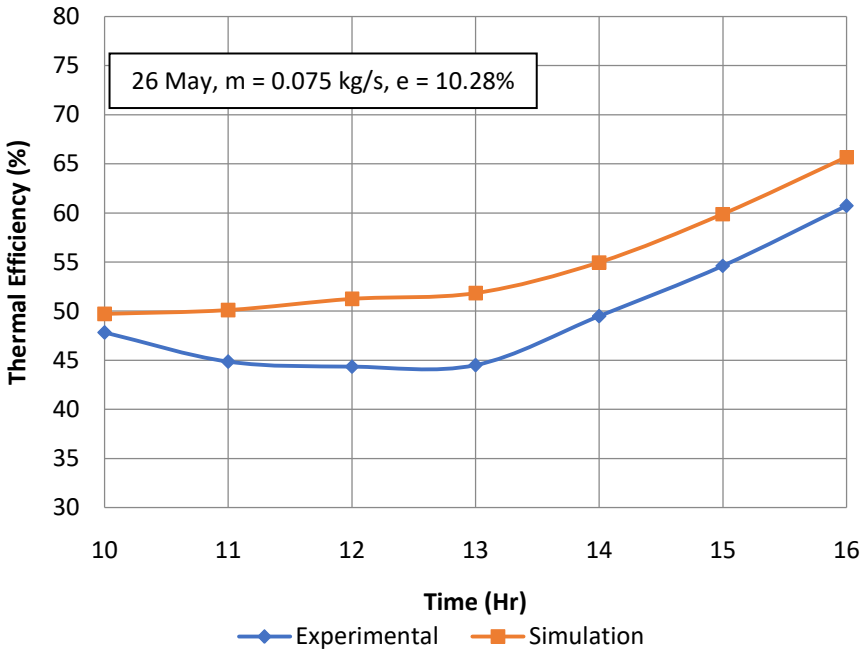


(a)

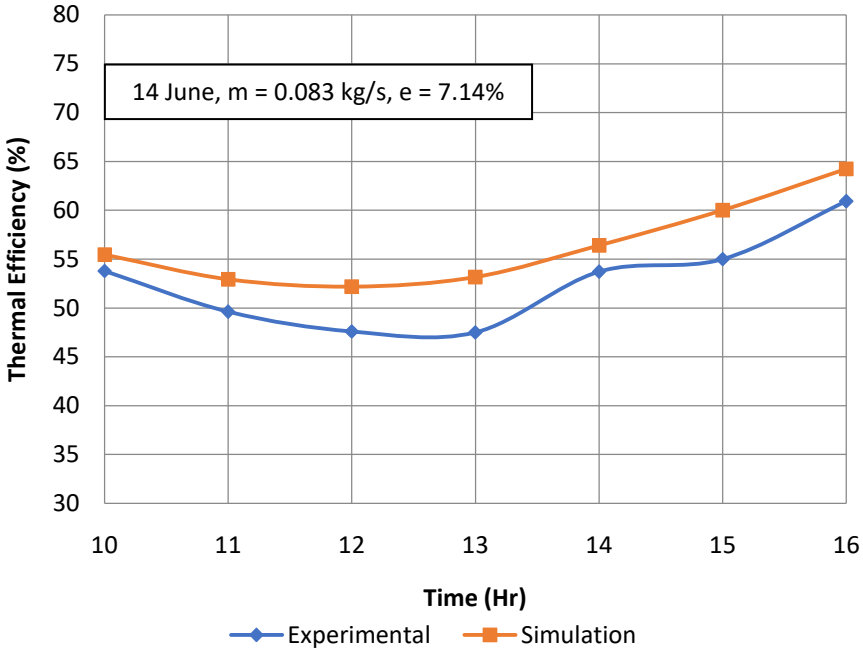


(b)

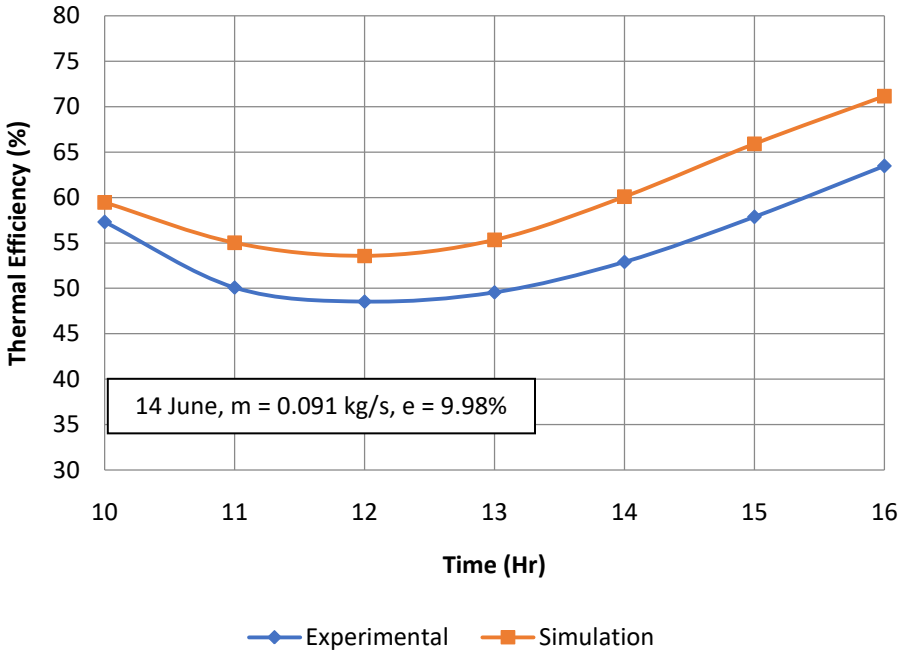


(c)

**Fig. 6.17 (a), (b) & (c) Thermal efficiency of HCPVT system during the test days (26 May, 9 June and 14 June, 2017)**

The overall efficiency of HCPVT system is shown in Fig. 6.18. It was observed that during test days, the mean overall efficiency of HCPVT came out to be 61.42%, 64.61% and 66.36% for inner tube mass flow rate of 0.075 kg/s, 0.083 kg/s and 0.091 kg/s respectively. It was seen that the overall efficiency increased with an increase in inner tube flow rate when the annulus flow rate is kept constant.

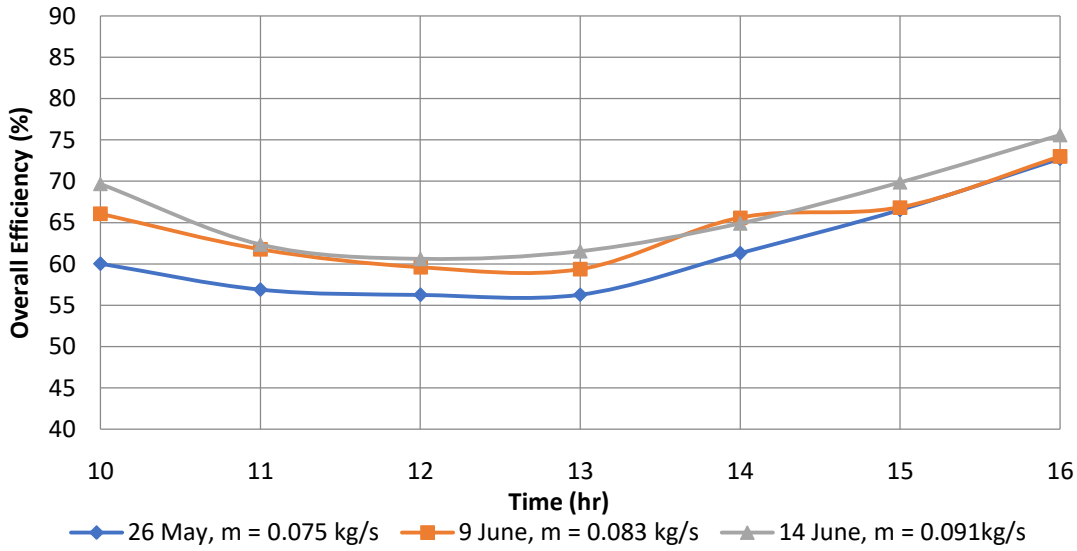


**Fig. 6.18 Overall efficiency of HCPVT system during the test days (26 May, 9 June and 14 June, 2017)**

## 6.3 Exergetic analysis of HCPVT system based on experimental data with varying annulus flow rate

In this section, the exergetic analysis has been carried out for experimental results obtained during 26-28 May 2017. The experimental results during these test days are already discussed in Sec. 6.1.1. The performance of a novel HCPVT system is evaluated by estimating its exergetic efficiency, exergy losses and destruction occurring within the system, using the equations discussed in Sec. 4.5.

### 6.3.1 Results obtained by keeping the inner tube flow rate at 0.075 kg/s

Based on the experimental data of test days, the exergy input and exergy losses were calculated using Eq. (4.60) and Eq. (4.66) respectively. The obtained exergy input rate and exergy losses occurring in the system are shown in Fig. 6.19. From the figure, it is observed that exergy input during the test days ranged from 693.08 W to 1203.93 W, 721.11 W to 1215.46 W and 668.70 W to 1204.21 W for a constant inner flow rate of 0.075 kg/s and varying annulus mass flow rate of 0.008 kg/s, 0.017 kg/s and 0.025 kg/s respectively. The exergy loss during these flow rates varied from 108.30 W to 189.56 W, 111.34 W to 187.68 W, and 100.39 W to 180.87 W respectively. It was found out that with an increase in solar radiation, the PV panel temperature increases which lead to increase in exergy losses. The maximum exergy losses were observed during peak sunshine hours.

Similarly, the comparison of exergy input with respect to exergy destruction occurring in the system is represented graphically in Fig. 6.20. It was observed that for annulus mass flow rate of 0.008 kg/s, 0.017 kg/s and 0.025 kg/s, the exergy destruction varied from 399.84 W to 743.10 W, 446.94 W to 832.52 W and 456.36 W to 889.23 W respectively. From the graphical representation, it was also observed that exergy destruction was highest for annulus mass flow rate of 0.025 kg/s when the inner tube flow rate was kept constant at 0.075 kg/s.

This is because with an increase in annulus mass flow rate the pressure drop in the receiver tube increases, which eventually lead to higher exergy destruction in higher flow rates.

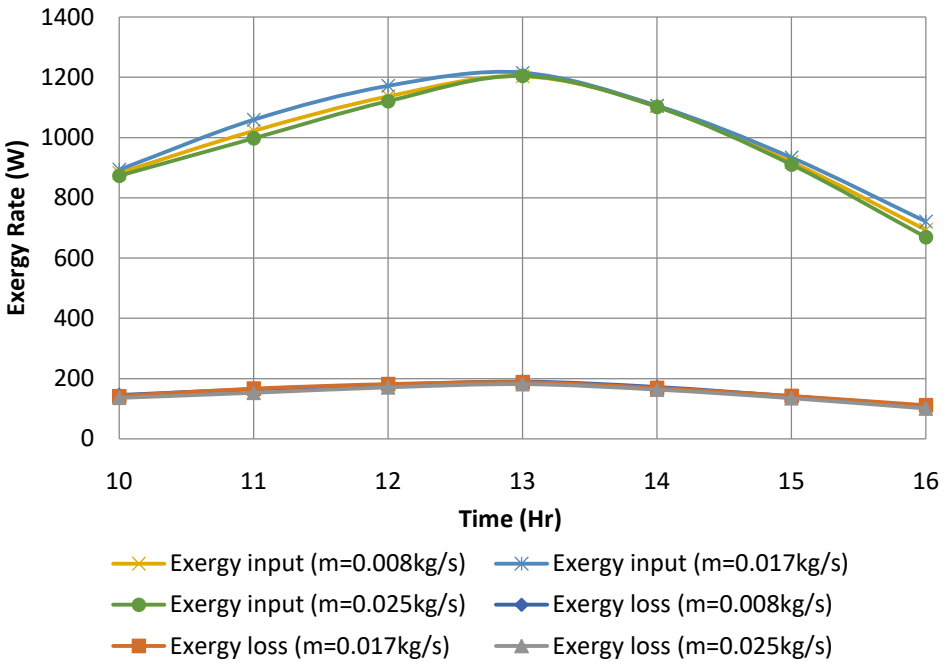


**Fig. 6.19 Exergy input vs exergy losses of HCPVTS during test days (26-28 May, 2017)**

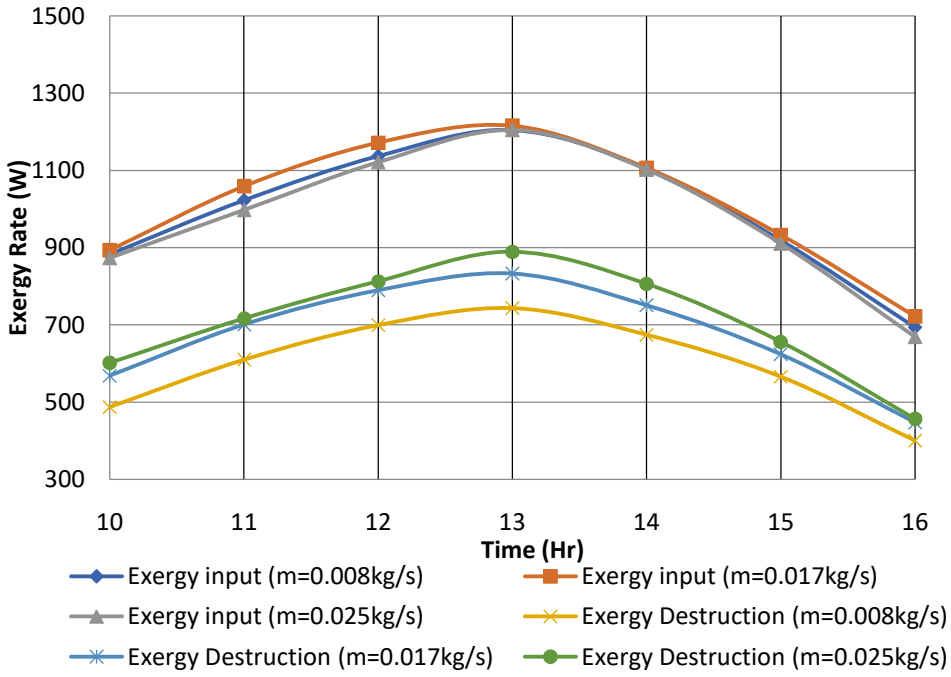


**Fig. 6.20 Exergy input rate vs exergy destruction of HCPVT during test days (26-28 May, 2017)**

Based on the obtained exergy losses and exergy destruction, the exergetic efficiency of the system was calculated on hourly bases using two scenarios, Case I and Case II as per Eq. (4.77) and Eq. (4.78) and is shown in Fig. 6.21. It was found out that the second law efficiency in Case I, varied from 23.72% to 29.36%, 17.28% to 23.77% and 12.36% to 17.98% for annulus mass flow rate of 0.008 kg/s, 0.017 kg/s and 0.025 kg/s respectively. It implies that the exergetic efficiency, for Case I, decreases with an increase in mass flow rate. For Case II, when the exergetic efficiency was represented in terms of exergy losses and exergy destruction, for annulus mass flow rate of 0.008 kg/s, 0.017 kg/s and 0.025 kg/s, it varied from 22.53% to 28.29%, 16.06% to 22.58% and 11.14% to 16.74% respectively. It was also observed that the exergetic efficiency of Case II was slightly less than that obtained through Case I. This may be because Case I does not consider any exergy losses and destruction occurring in the system. In both cases, it was observed that with an increase in annulus mass flow rates, exergetic efficiency decreases.

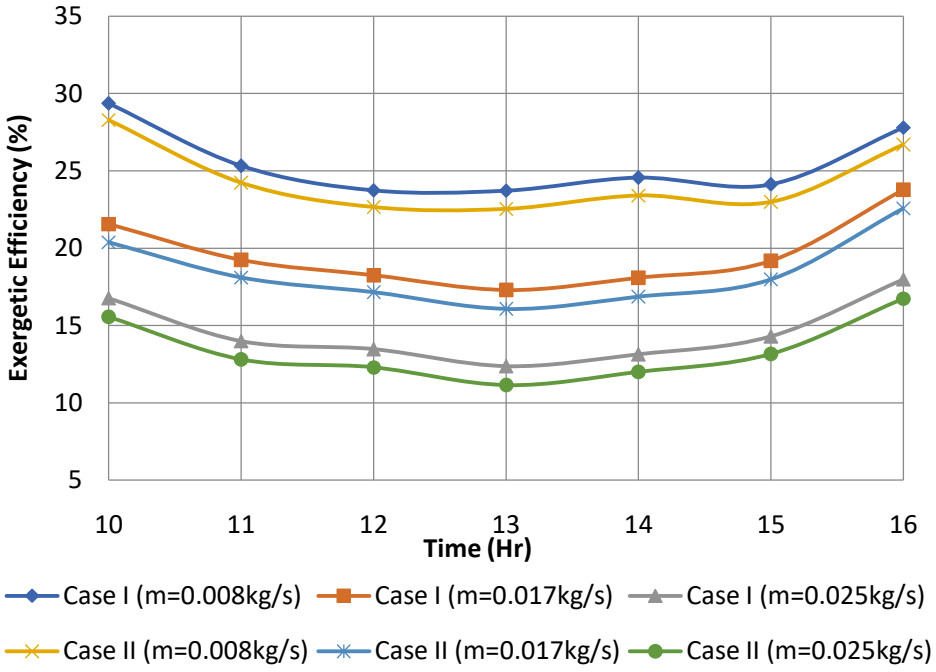


**Fig. 6.21 Exergetic efficiency of HCPVT system in Case (I) and Case (II) at different flow rates (26-28 May, 2017)**

The overall exergy efficiency calculated using Eq. (4.79) is termed as Case III and is represented graphically in Fig. 6.22. As discussed earlier, Case III does not include any optical or thermal losses but considers only exergy destruction. The results showed that exergy efficiency in such case ranged from 38.28% to 44.78%, 31.51% to 38.02% and 26.16% to 31.75% for annulus mass flow rate of 0.008 kg/s, 0.017 kg/s and 0.025 kg/s respectively. It was found out that the exergetic efficiency at a higher flow rate was lowest among the others. It was also observed that maximum exergetic efficiency was achieved during morning and evening time. It is because, with an increase in irradiance, the ambient temperature increases, which supplements the exergy destruction and thus reduces the overall efficiency. It is evident from Fig. 6.21 and Fig. 6.22 that the efficiency of Case III was much higher than that of Case I and Case II. This is because the former considers only exergy destruction term. Although literature uses the equation of efficiency calculations based on Case I and Case II, the standardized equation, as per the definition of exergy, is represented by Case III and should be preferred over the other two.

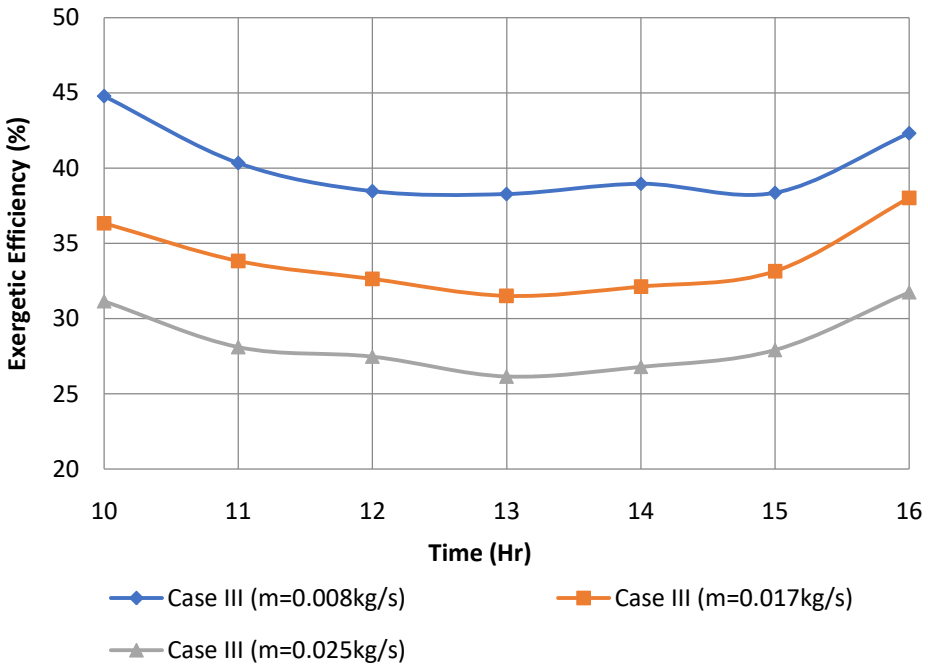


**Fig. 6.22 Exergetic efficiency of HCPVT system for Case (III) (26-28 May, 2017)**

### 6.3.2 Results obtained by keeping the inner tube flow rate at 0.091 kg/s

Similar to Sec. 6.3.1, the exergetic analysis has also been carried out for experimental results obtained during 14-16 June 2017. The experimental results during these test days are already discussed in Sec. 6.1.2. Using the equations discussed in Sec. 4.5, the exergetic efficiency, exergy losses and destruction occurring within the system were determined. Exergy input was calculated using Eq. (4.60) while exergy losses and exergy destruction were calculated using Eq. (4.66) and Eq. (4.69) respectively.

The obtained exergy input rate and exergy losses occurring in the system are shown in Fig. 6.23 which shows that exergy input during the test days ranged from 697.34 W to 1278.13 W, 709.12 W to 1314.15 W and 710.05 W to 1277.30 W for a constant inner flow rate of 0.091 kg/s and varying annulus mass flow rate from 0.008 kg/s, 0.017 kg/s and 0.025 kg/s respectively. The exergy loss during these flow rates varied from 120.24 W to 210.84 W, 120.35 W to 209.74 W, and 117.61 to 199.47 W respectively. It was found out that the exergy loss was maximum during peak sunshine hour due to the fact that at that time the PV panel temperature was also maximum which leads to higher convective losses.

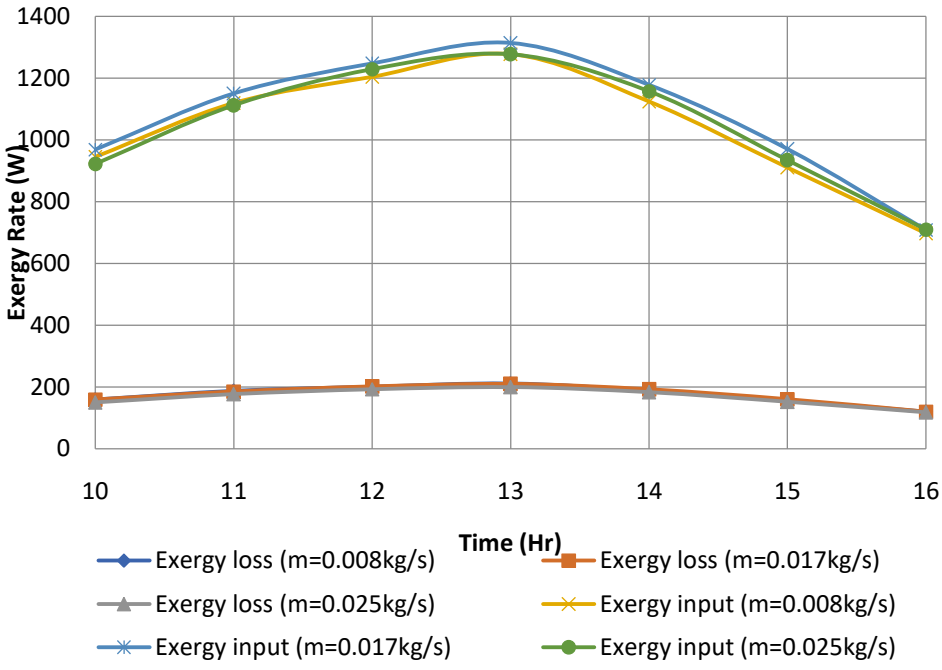


**Fig. 6.23 Exergy input vs exergy losses of HCPVTS during test days (14-16 June, 2017)**

Similarly, the comparison of exergy input with respect to exergy destruction occurring in the system is shown in Fig. 6.24. It was observed that for annulus mass flow rate of 0.008 kg/s, 0.017 kg/s and 0.025 kg/s, the exergy destruction varied from 269.47 W to 657.59 W, 313.08 W to 769.56 W and 368.06 W to 829.05 W respectively. During the test days, it was also observed that among all, the exergy destruction was lowest for annulus mass flow rate of 0.008 kg/s when the inner tube flow rate was maintained at 0.091 kg/s. This may be because at lower mass flow rate, the pressure drop and turbulent effect would be minimum which reduces the exergy destruction occurring within the system. However, during a day, the maximum irreversibility observed during peak afternoon.

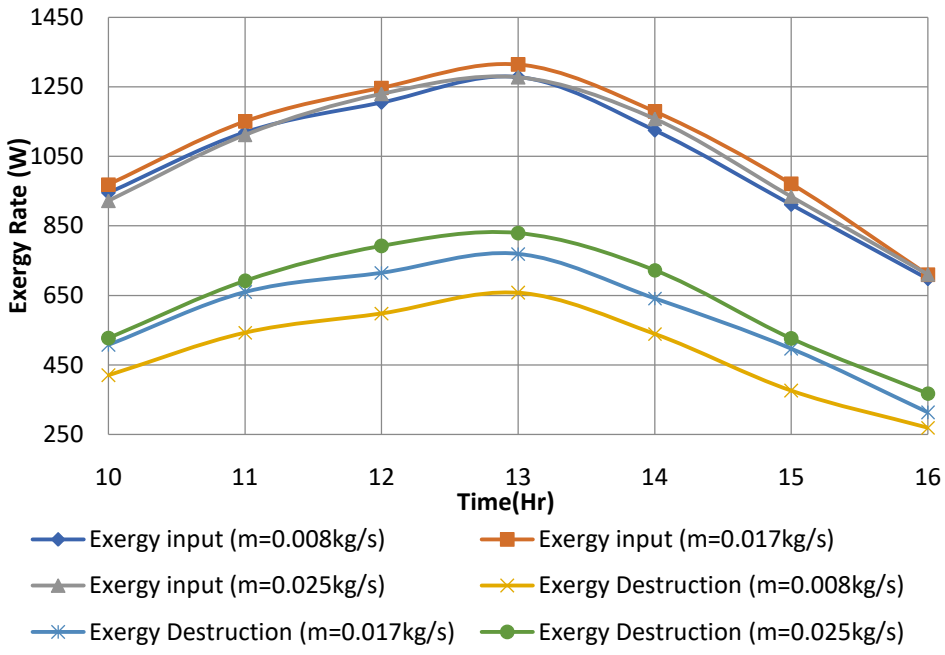


**Fig. 6.24 Exergy input rate vs exergy destruction of HCPVT at constant inner tube flow rate of 0.091kg/s (14-16 June, 2017)**

Similar to the Sec. 6.3.1, the exergetic efficiency of the system was calculated using three scenarios. The values obtained for Case I and Case II as per Eq. (4.77) and Eq. (4.78) are shown in Fig. 6.25. It was observed that the second law efficiency in Case I, varied from 32.88% to 45.12%, 26.50% to 40.09% and 20.70% to 32.99% for annulus mass flow rate of 0.008 kg/s, 0.017 kg/s and 0.025 kg/s respectively. It indicates that the exergetic efficiency, for Case I, increases with decrease in mass flow rate. For Case II, when the exergetic

efficiency was represented in terms of exergy losses and exergy destruction, for annulus mass flow rate of 0.008 kg/s, 0.017 kg/s and 0.025 kg/s, it varied from 32.06% to 44.12%, 25.48% to 38.88% and 19.48% to 31.60% respectively. It was also observed that the exergetic efficiency of Case I was slightly more than that obtained through Case II. This may be because Case II considered any exergy losses and destruction occurring in the system. In both cases it was found out that with an increase in annulus mass flow rates, exergetic efficiency decreases.

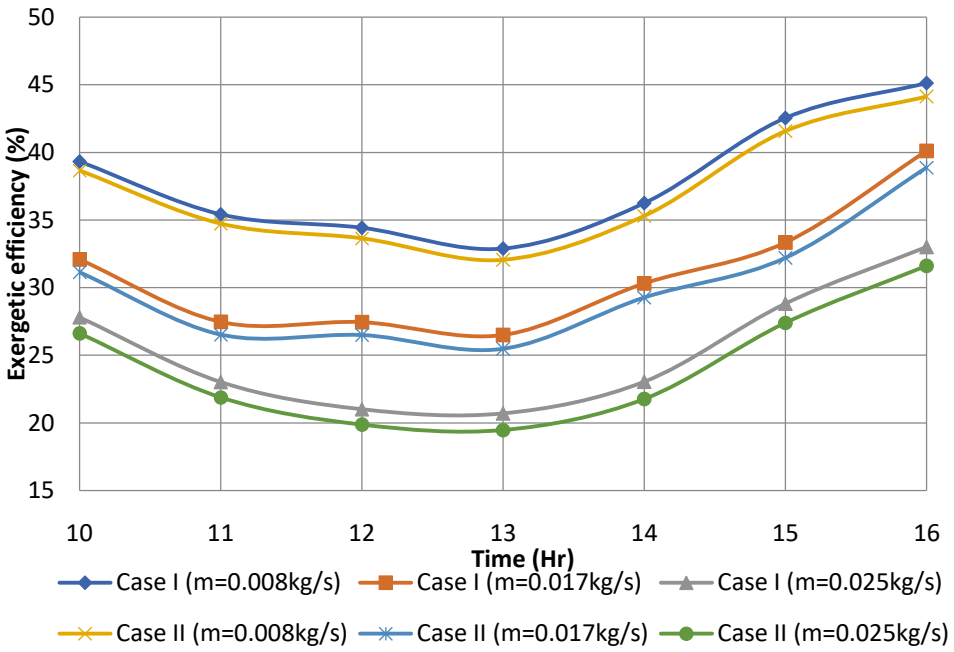


**Fig. 6.25 Exergetic efficiency of HCPVT system in Case (I) and Case (II) at different flow rates during 14-16 June, 2017**

The overall exergy efficiency for Case (III) was calculated using Eq. (4.79) and is shown in Fig. 6.26. As discussed earlier, Case III does not include any losses and considers only exergy destruction as per the standard definition of the exergy. The results showed that exergy efficiency in such case ranged from 48.55% to 61.36%, 41.44% to 55.85% and 35.09% to 48.16% for annulus mass flow rate of 0.008 kg/s, 0.017 kg/s and 0.025 kg/s respectively. It was found out that the exergetic efficiency at a lower flow rate was highest among the others, similar to Case I and Case II. It was also observed that exergetic efficiency was minimum during peak afternoon. It was because, with an increase in irradiance, the

ambient temperature increases, which supplements the exergy destruction and thus reduces the overall efficiency. It was concluded that the efficiency of Case III was much higher than that of Case I and Case II and should be preferred, as it represented calculations based on standardized exergy equation.

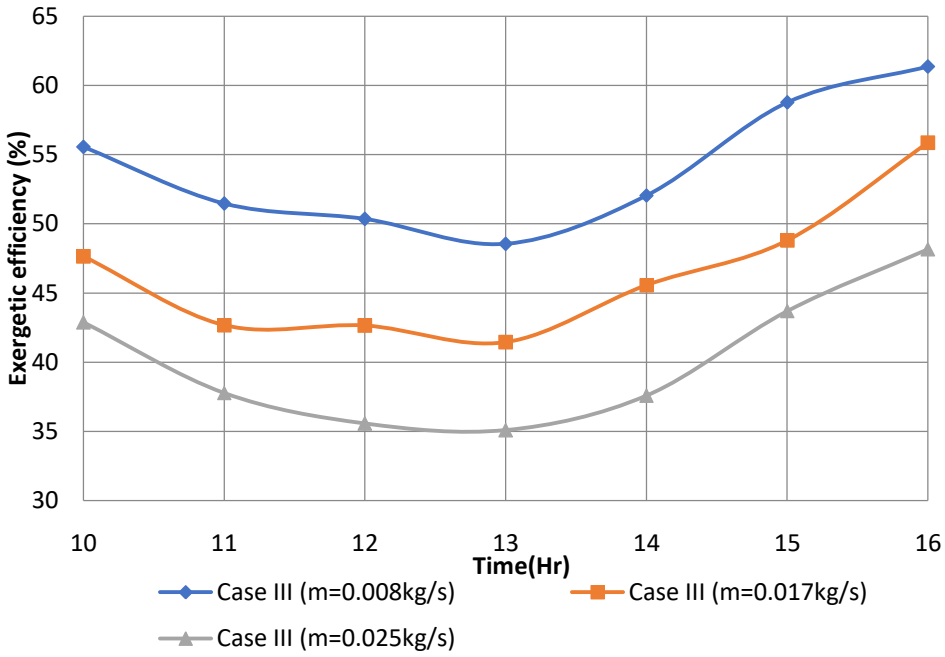


**Fig. 6.26 Exergetic efficiency of HCPVT system for Case (III) at different flow rates during 14-16 June, 2017**

## 6.4 Exergetic analysis of HCPVT System Based on Experimental Data with varying inner tube flow rate

The exergetic analysis by varying annulus mass flow rate was discussed in the previous section. Now, the exergetic analysis is carried out for experimental data obtained by varying inner tube flow rate. The variation of inner tube was achieved during 26 May, 9 June and 14 June as discussed in Sec. 6.2. The performance of the system was evaluated by estimating exergy efficiency, exergy loss and destruction occurring within the system, similar to the analysis carried out in Sec. 6.3.

The graphical representation of exergy input and exergy losses occurring in the HCPVT system during the test days (26 May, 9 June and 14 June) is shown in Fig. 6.27. It was observed that at a fixed annulus flow rate of 0.008 kg/s, the exergy input varied from

693.08 W to 1203.93 W, 691.78 W to 1227.12 W and 697.34 W to 1278.13 W for varying inner tube flow rate of 0.075 kg/s, 0.083 kg/s and 0.091 kg/s respectively. Maximum exergy input was observed during peak afternoon as it was a direct function of incident solar radiation. The exergy losses occurring due to optical and thermal losses varied from 108.30 W to 189.56 W, 112.43 W to 199.88 W and 120.23 W to 210.83 W on 26 May, 9 June and 14 June respectively. The exergy losses also followed the same trend as that of exergy input and were highest during peak afternoon, due to maximum optical and thermal losses at that time.

The comparative illustration of exergy destruction with respect to exergy input is shown in Fig. 6.28. It was observed that the exergy destruction varied from 399.84 W to 743.10 W, 342.74 W to 685.20 W and 269.46 W to 657.58 W when inner tube flow rate varied from 0.075 kg/s, 0.083 kg/s and 0.091 kg/s respectively. It was also seen that the exergy destruction was highest for the inner tube flow rate of 0.075 kg/s when the annulus mass flow rate was 0.008 kg/s. It decreased with an increase in inner tube flow rate. This may be due to the fact that with an increase in inner tube flow rate, more heat was carried away by the fluid which reduces the temperature gradient responsible for exergy destruction.

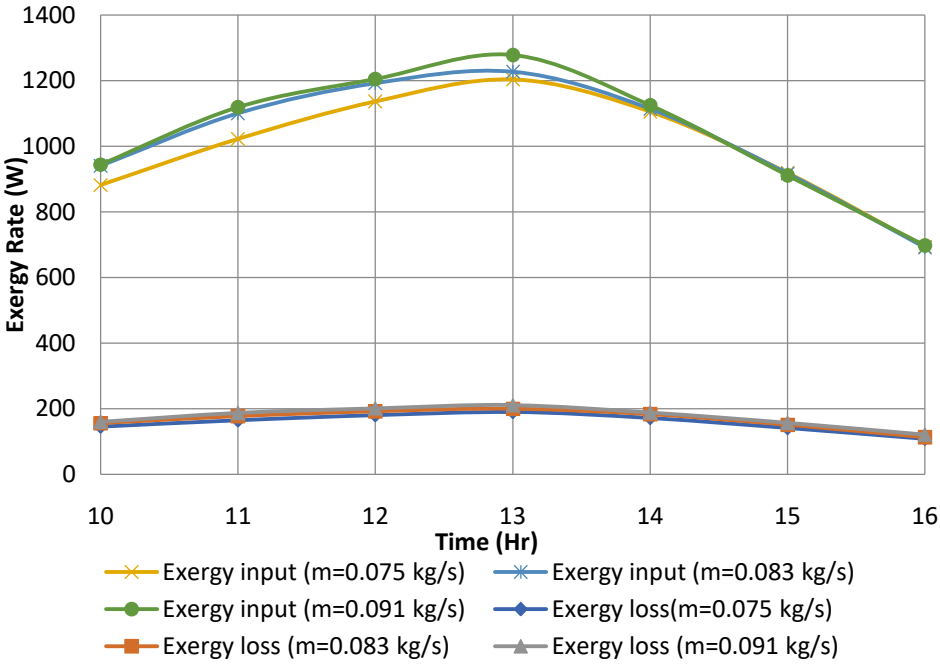


**Fig. 6.27 Exergy input vs exergy losses of HCPVTS during test days (26 May, 9 June and 14 June, 2017)**

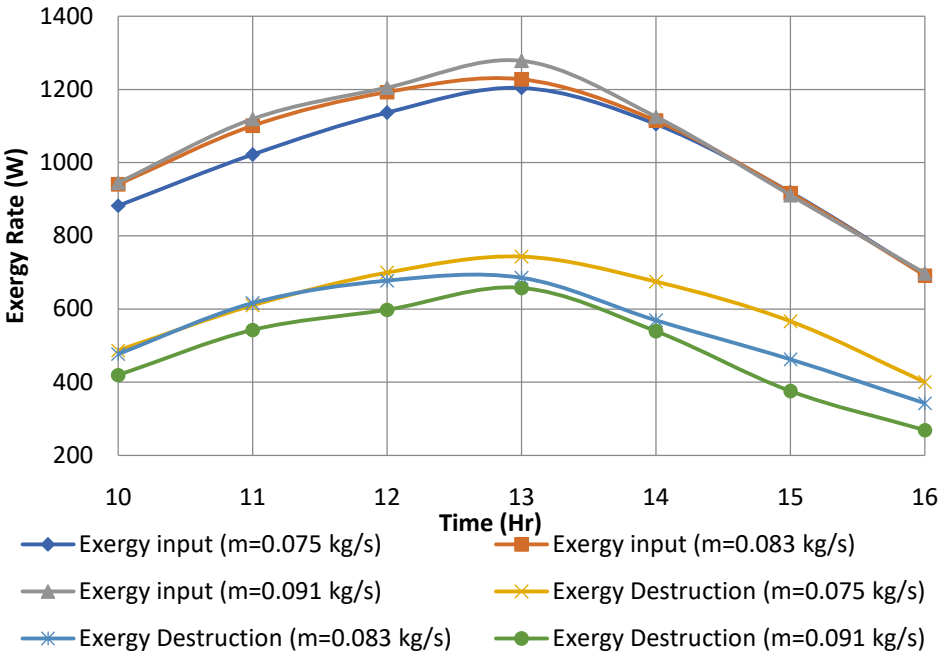


**Fig. 6.28 Exergy input rate vs exergy destruction of HCPVT (26 May, 9 June and 14 June, 2017)**

Similar to the Sec. 6.3, the exergetic efficiency of the system under varying inner tube flow rate condition was calculated by considering three scenarios, i.e. Case I, Case II and Case III. The hourly basis graphical representation of exergetic efficiency obtained during the test days, using Case I and Case II, is shown in Fig. 6.29. It was seen that, for Case I, the exergetic efficiency varied from 23.72% to 29.36%, 27.96% to 35.39% and 32.88% to 45.12% for inner tube mass flow rate of 0.075 kg/s, 0.083 kg/s and 0.091 kg/s respectively. This showed that with an increase in inner tube mass flow rate, the exergetic efficiency increases. For Case II, the exergetic efficiency ranged from 22.53% to 28.29%, 27.04% to 34.20% and 32.06% to 44.12% for inner tube mass flow rate of 0.075 kg/s, 0.083 kg/s and 0.091 kg/s respectively. The minimum exergetic efficiency observed during the peak afternoon due to higher exergy losses and destruction during this time. It was also found out that exergetic efficiency obtained through Case I was slightly more than the efficiency obtained through Case II. This may be because Case I does not consider any losses and

destruction occurring in the system. In both cases, with an increase in inner tube mass flow rates, exergetic efficiency increases.

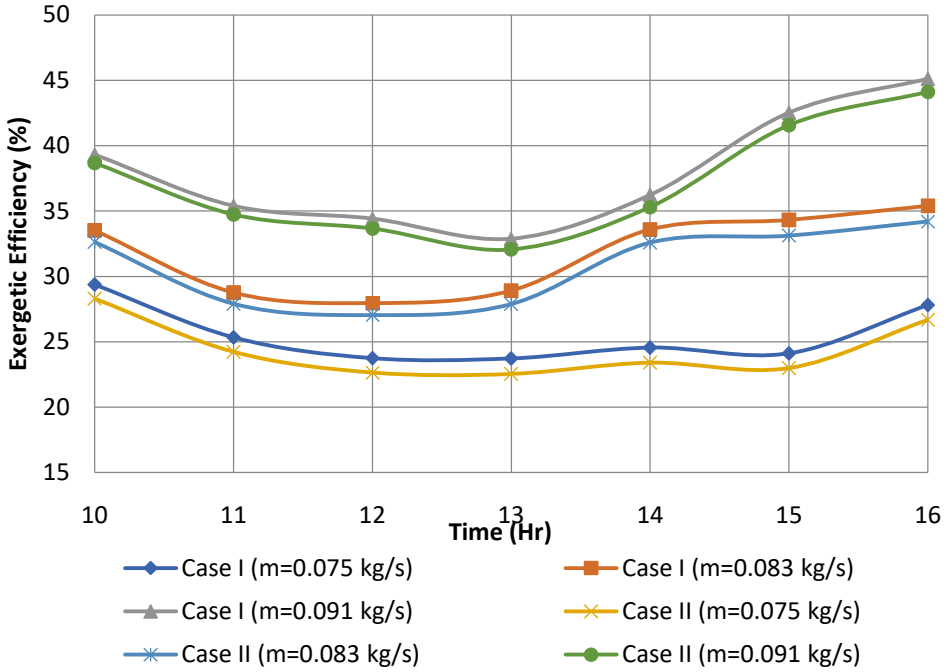


**Fig. 6.29 Exergetic efficiency of HCPVT system in Case (I) and Case (II) (26 May, 9 June and 14 June, 2017)**

The hourly variation of exergetic efficiency calculated by considering only exergy destruction, as Case III, is represented in Fig. 6.30. The results showed that when the annulus mass flow rate was maintained at 0.008 kg/s and inner tube mass flow rate of HCPVT was varied from 0.075 kg/s, 0.083 kg/s and 0.091 kg/s, the exergetic efficiency ranged between 38.28% to 44.78%, 43.17% to 50.46% and 48.55% to 61.36% respectively. It was seen that that exergetic efficiency increases with an increase in inner tube flow rate. Over a day, the exergetic efficiency was lowest during peak sunshine hour because at that time, the ambient temperature was maximum which leads to higher exergy destruction. It is evident from Fig. 6.29 and Fig. 6.30 that the efficiency of Case III was much higher than that of Case I and Case II. This is because the former considers only exergy destruction term rather than overall exergy losses.

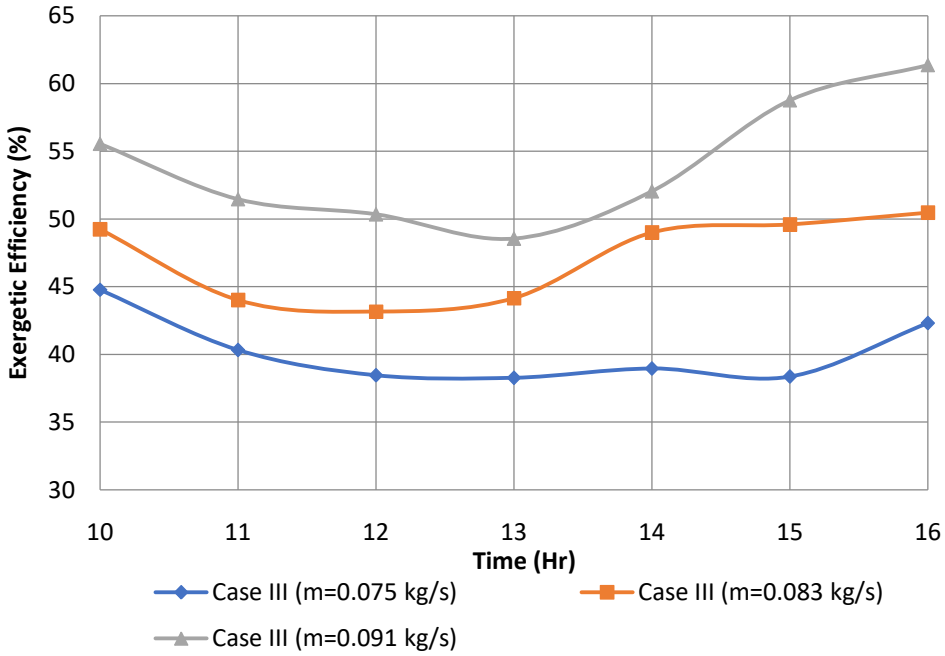


**Fig. 6.30 Exergetic efficiency of HCPVT system for Case (III) (26 May, 9 June and 14 June, 2017)**

## 6.5 Discussion

From the analysis in the previous sections, the performance of novel HCPVT system was evaluated in terms of energetic and exergetic efficiencies. It is evident from the analysis that throughout the day, the overall efficiency first decreases then increase, with respect to change in solar radiation. By varying inner tube and annulus mass flow rate, the efficiencies vary throughout the test days. In order to find out the optimized flow rate to achieve maximum efficiency of the designed novel HCPVT system, the mean overall efficiency observed during all the test days is compared at different flow rate. The graphical representation of the variation observed is shown in Fig. 6.31. From the figure, it is observed that with increase in inner tube flow rate, the overall efficiency increases. However, with an increase in annulus mass flow rate, the overall efficiency decreases. This implies that maximum overall efficiency could be achieved with a high inner tube flow rate and low annulus flow rate.

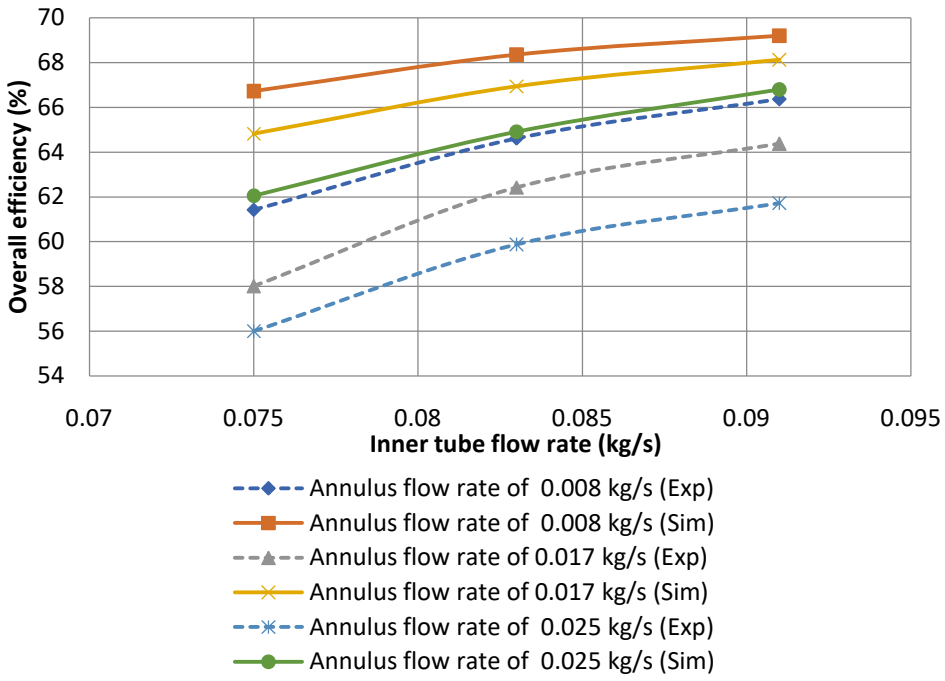


**Fig. 6.31 Mean overall efficiency for different inner and annulus flow rates**

The simulation results show that the optimum efficiency could be achieved at an inner tube flow rate of 0.1 kg/s with annulus flow rate of 0.008 kg/s. Thus at the combined flow rate of 0.108 kg/s, the mean overall efficiency of 69.19% could be achieved. This means that at this flow rate, the novel system would work to give peak efficiency. By considering this flow rate conditions, the output of distillation unit is evaluated which is connected to such HCPVT system. For the same, the model is simulated in Aspen HYSYS using optimum flow rate, similar to Sec. 4.4.1. It is found out that such system would provide a continuous output of 0.2328 kg/hr for each unit intake, under the conditions of Pilani. The simulated model also consumed the power (8.93 W) generated solely from the novel HCPVT system. However, this system being smaller in size provides a limited output. The output could be increased by increasing the receiver length. By doing do, the fluid temperature increases which are desirable for such novel systems. However, after certain length, the effect of cooling of PV panel would diminish as instead of cooling, the high temperature of fluid would increase the PV panel temperature. This would reduce the panel efficiency and may damage the cell integrity. Thus, there is a trade-off required in the length of absorber tube and length of PV

panel. In order to estimate the effect of large length of receiver, the simulation results obtained for PV panel temperature and HCPVT outlet temperature for inner tube flow rate of 0.1 kg/s with annulus flow rate of 0.008 kg/s are shown in Fig. 6.32.

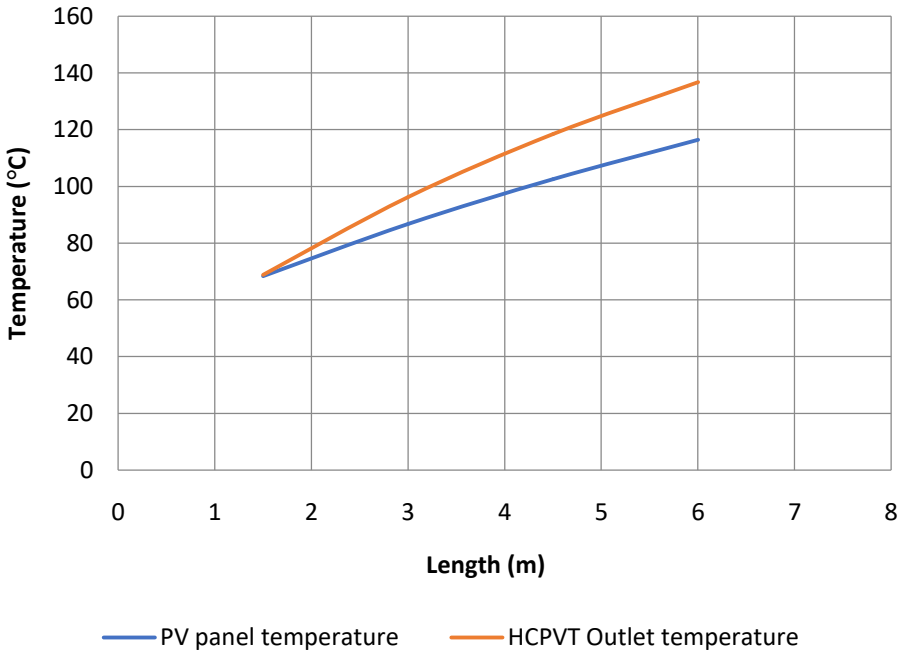


**Fig. 6.32 Effect of increase in length on PV panel temperature and HCPVT outlet temperature**

From the figure, it is observed that with increase in length of absorber, the outlet temperature of HCPVT system and PV panel temperature increases. In order to improve the system performance, the panel temperature needs to maintain less than 80 °C. Thus the length of PV panel may be kept below 2.5 m, while the absorber tube length can be increased as desired to achieve higher thermal energy. The output thus obtained is at threshold panel temperature with sufficient thermal energy to operate a standalone distillation unit. Large scale setup of such distillation units could be utilized for the continuous supply of fresh water in the state of Rajasthan.

## 6.6 Environmental cost analysis

Energy utilization for heat or power would impact environment, especially when resources are used, it leads to carbon emissions. Thus the cost associated with carbon emissions is prominent factor for environmental assessment. The proposed HCPVT system was also evaluated in terms of carbon credit earned on life time basis for the price of $CO_2$ emitted annually. The enviro-economic study would help to estimate yearly carbon mitigation along with its environmental cost. For the estimation, it is taken that coal in power plant would generate average of 980 g $CO_2$/kWh of emissions for electricity production, which eventually utilized for various purposes including heating water. With transmission and distribution losses, taken from the literature, it comes out to be 2.08 kg $CO_2$/kWh [230].

The methodology for the estimation of carbon credit was adopted from Agarwal and Tiwari [231] by estimating total thermal gain of the system over the year and calculating associate cost of energy. The total thermal gain was evaluated using the hourly rate of thermal energy ($Q_{th}$) as evaluated in Eq. (4.48) and summed up to get daily, monthly and hence annual thermal gain. Thus, for total thermal gain the carbon mitigation per annum would be given as [230]

$$CM_{CO_2} = \frac{E_{CO_2} \times \dot{Q}_{th,total}}{10^3} \tag{6.1}$$

Where $CM_{CO_2}$ is carbon mitigation (t $CO_2$/annum), $E_{CO_2}$ is average emission of $CO_2$. It is taken as 2.08 kg $CO_2$/kWh.

In case, the reduction in carbon emission is traded at current rate of €22/t$CO_2$, (equivalent to ₹ 1694, assuming 1 € as ₹ 77), the cost of reduction by the novel HCPVT system per annum would become [232]

$$EC = CP \times CM_{CO_2} \tag{6.2}$$

Where EC is the environmental cost; CP is the carbon price and is taken as ₹ 1694/t$CO_2$. The estimated carbon emissions mitigated and associated cost is calculated for three different scenarios. In Case I, it is taken that the HCPVT would operate at fixed inner tube flow rate and annulus flow rate varies during its operations. For the conditions of Pilani, India, the carbon mitigation and its cost are evaluated for a year. Similarly, in Case II, the annulus flow rate is kept constant and inner tube flow rate varied during its operations. Case III is related to the optimum flow rate which was obtained previously. The results are then compared with a conventional PVT system taken from Agarwal and Tiwari [231] as Case IV and are shown in Table 6.1 and Fig. 6.33.

**Table 6.1 Annual carbon mitigation and environmental cost associated per annum of HCPVT system for the conditions of Pilani, India**

| Scenarios | Carbon Mitigation per annum (tonnes $CO_2$) | Environmental cost (₹/annum) |
|---|---|---|
| Case I | 32.878 | 55694.87 |
| Case II | 35.837 | 60707.57 |
| Case III | 40.230 | 68149.62 |
| Case IV | 10.614 | 17979.50* |

*adjusted to current carbon trading rate of ₹ 1694/annum

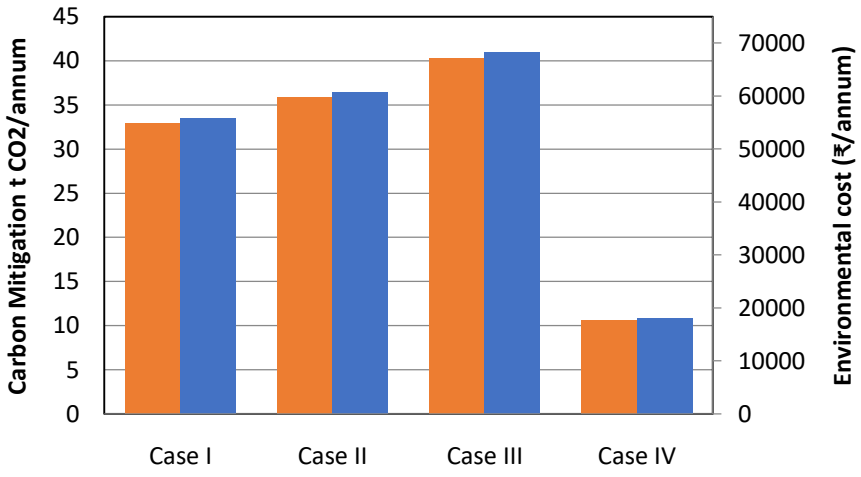


**Fig. 6.33 Carbon mitigation and environmental cost per annum for HCPVT system in different cases**

From the above estimation it is concluded that at optimum flow rate, such novel HCPVT system would help to reduce carbon emission by 40.3 t $CO_2$/yr with associated environmental cost of ₹ 68,149.62 per annum.

# CHAPTER 7

# CONCLUSIONS AND FUTURE SCOPE OF THE WORK

*This chapter discusses the conclusion drawn from the present research work and also incorporates the possibility for the future scope of the work.*

## 7.1 Conclusions

In this research work, an analysis has been carried out to utilize solar energy for water distillation by proposing the design of novel HCPVT system. During the pre-feasibility study, it was found out that the state of Rajasthan has huge potential for solar energy, which can be harnessed for various applications. PV technology is commercially proven technology for power generation. The higher power output and efficiency can be achieved in smaller area with the used of CPV system which works with concentrated solar energy. However, at high concentration the PV panel temperature increases which reduces its life span. This problem can be overcome with the use of CPVT system. Based on the research gaps in literature, a novel design of HCPVT system is proposed for combined heat and power, where the low grade thermal energy can be utilized for distillation purpose. The system was designed and optimized using Aspen HYSYS. The detailed theoretical model of the receiver of HCPVT system was developed in MATLAB using two different configurations i.e. D-shape absorber tube and triangular absorber. The theoretical model of D-shape absorber tube was validated with the data generated from the experimental setup fabricated based on the design. In order to identify the grey areas of improvements, the second law analysis was carried out based on the experimental results. The chapter wise conclusions are given below

### 7.1.1 Potential of solar based water distillation in Rajasthan, India

The pre-feasibility analysis for distillation using solar energy gives the solar power generation potential along with the water availability in the state of Rajasthan (Chapter 2). It is observed that the western part of the state, *viz*, Jaisalmer, Bikaner and Jodhpur, has the highest PV and CSP power generation potential using any of the respective technologies. Further, an attempt has been done to identify the water availability of each district based on available surface water resources, state annual monsoon, domestic wastewater (treated) and groundwater availability. The state has potential for power generation using m-Si, p-Si and TF technology is 1077.44 GW, 811.36 GW and 728.99 GW respectively. The Rajasthan has the power generation potential of 883.31 GW, 569.50 GW and 383.56 GW using LFR, PTC and CTR technology respectively. Jaipur district holds the top position for maximum availability of water supply to have MSF solar plants using any of CSP technology, while Dausa district has the least potential to have RO plant with m-Si technology having capacity more than 6 MLD. Hanumangarh district has minimum wasteland for solar power and thus lacks sufficient power generation potential although it has sufficient water availability for RO plants.

### 7.1.2 Simulation of the novel HCPVT receiver

In Chapter 4, the modeling and simulation of three different designs of absorber tube i.e. circular, D-shape and triangular were carried out using simulation tools. The design of receiver was modeled and simulated using MATLAB following which the HCPVT system coupled with distillation unit was optimized using Aspen HYSYS. It is concluded that the analytical model of MATLAB within the range with a slight variation (error of ±1.7%) with the results obtained in COMSOL. After validation, the theoretical analysis of D-shape and triangular absorber tube was carried out and it was observed that under same set of

parameters, the PV panel temperature and HCPVT outlet temperature in D-shape absorber was 3.3 degrees higher than that of triangular absorber at peak radiation. When the HCPVT system was coupled with distillation unit, the model analysis on Aspen HYSYS showed that for the inlet feed with direct flashing at 110 °C, the maximum distillate output could be achieved at mass flow rate of 0.12 kg/s (7 LPM).

### 7.1.3 Simulation and experimental analysis of HCPVT system

In Chapter 6, theoretical and experimental analysis has been carried out to assess the performance of the proposed HCPVT system in terms of thermal and electrical efficiency. The experimental testing was carried out on D-shape HCPVT receiver, during the month of May and June 2017 in Pilani, Rajasthan for different annulus mass flow rate by keeping the inner flow rate constant and varying inner tube flow rate by keeping annulus flow rate constant. It is concluded that with cooling of PV panel, the temperature drops, which eventually leads to increase in electrical efficiency. The outlet temperature of HCPVT receiver varies with annulus and inner tube flow rate. The maximum mean overall efficiency (thermal and electrical) of the system was observed to be 61.42%, for the annulus mass flow rate of 0.008 kg/s, when inner flow rate was fixed at 0.075 kg/s. It decreases with increase in annulus mass flow rate.

It is also concluded that the theoretical values of HCPVT outlet temperature, PV panel temperature and thermal efficiency obtained from the simulation were in good agreement with the results obtained from the experimental study. In terms of environmental cost analysis, it is concluded that at optimum flow rate, such novel HCPVT system would helps to reduce carbon emission by 40.3 t $CO_2$/yr with associated environmental cost of ₹ 68,149.62 per annum.

### 7.1.4 Exergetic analysis of HCPVT system based on experimental data

In Chapter 6, to identify the grey areas for improvement, second law of thermodynamic analysis was carried out on the proposed D-shape HCPVT system. From the exergy analysis, it is concluded that the maximum exergy input was observed during peak afternoon as it is a direct function of incident solar radiation. The exergy input, exergy losses and exergy destruction varied with inner and annulus flow rate. With an increase in solar radiation, the PV panel temperature increases which lead to increase in exergy losses. The maximum exergy losses were observed during peak sunshine hours. It is also concluded that exergetic efficiency inversely vary with annulus mass flow rate, at given solar radiation. The three cases of exergetic efficiency are discussed but Case III represents the standardized equations of exergy as per its definition, and should be preferred over the two.

## 7.2 Future scope of the work

In the present work, a novel HCPVT system is proposed and was evaluated in terms of its electrical and thermal performance. Following are the future scope of the work:

- For triangular shape receiver, only simulations were done using MATLAB. The experimental investigation may be carried out to investigate it performance.
- The experimental study may be carried out for counterflow water arrangements in the different designs of receiver tube.
- The economic analysis and life cycle analysis can be recommended for further work, which will be required before commercialization of the system.
- The proposed system may be evaluated for different HTF and relevant operating parameters.
- The designed HCPVT system coupled with a distillation unit may be evaluated experimentally.

[1] IEA, “World Energy Outlook 2017 - Excerpt - Water-Energy Nexus,” A report by International Energy Agency. Paris, France, 2017.

[2] BP, “BP Statistical Review of World Energy,” A report by BP p.l.c, Pureprint Group Limited, London, UK, 2018.

[3] IEA, “World energy outlook 2016,” A report by International Energy Agency, Paris, France, 2016.

[4] Central Electricity Authority of India, “Power Sector March-2018,” A report by Ministry of Power, GOI, New Delhi, India, 2018.

[5] IEA, “Key World Energy Statistics,” A report by International Energy Agency, Paris, France, 2017.

[6] International Renewable Energy Agency, “REmap: Renewable Energy Prospects for India,” Abu Dhabi, 2017.

[7] “Ministry of New and Renewable Energy,” 2018. [Online]. Available: http://mnre.gov.in/. [Accessed: 26-Apr-2019].

[8] A. G. Abusharkh, A. Giwa, and S. W. Hasan, “Wind and geothermal energy in desalination: A short review on progress and sustainable commercial processes,” *Ind. Eng. Manag.*, vol. 04, no. 04, p. 175, 2015.

[9] L. García-Rodríguez and A. M. Delgado-Torres, “Solar-powered Rankine cycles for fresh water production,” *Desalination*, vol. 212, no. 1–3, pp. 319–327, Jun. 2007.

[10] W. J. Cosgrove and F. R. Rijsberman, *World Water Vision: Making Water Everybody’s Business*. Paris, France: Routledge, 2014.

[11] S. Verma and S. J. Phansalkar, “India’s Water Future 2050: Potential Deviations from ‘Business-as-Usual,’” *Int. J. Rural Manag.*, vol. 3, no. 1, pp. 149–179, 2007.

[12] C. P. Kumar, “Fresh Water Resources: A Perspective,” National Institute of Hydrology, Roorkee, 2003.

[13] "Groundwater Scenario in India (Pre-Monsoon 2017)," 2017. [Online]. Available: http://cgwb.gov.in/Ground-Water/GW Monitoring Report_PREMONSOON 2017.pdf. [Accessed: 12-Apr-2019].

[14] S. Kalogirou, "Use of parabolic trough solar energy collectors for sea-water desalination," *Appl. Energy*, vol. 60, no. 2, pp. 65–88, 1998.

[15] K. Sampathkumar, T. V. Arjunan, P. Pitchandi, and P. Senthilkumar, "Active solar distillation - A detailed review," *Renew. Sustain. Energy Rev.*, vol. 14, no. 6, pp. 1503–1526, Aug. 2010.

[16] G. N. Tiwari and S. Sinha, "Parametric studies of active regenerative solar still," *Energy Convers. Manag.*, vol. 34, no. 3, pp. 209–218, 1993.

[17] R. Dev and G. N. Tiwari, "Characteristic equation of a hybrid (PV-T) active solar still," *Desalination*, vol. 254, no. 1–3, pp. 126–137, May 2010.

[18] A. Ummadisingu and M. S. Soni, "Concentrating solar power–technology, potential and policy in India," *Renew. Sustain. Energy Rev.*, vol. 15, no. 9, pp. 5169–5175, 2011.

[19] H. Price, "A Parabolic Trough Solar Power Plant Simulation Model," National Renewable Energy Laboratory, Golden, CO, USA, 2003.

[20] M. T. Ali, H. E. S. Fath, and P. R. Armstrong, "A comprehensive techno-economical review of indirect solar desalination," *Renew. Sustain. Energy Rev.*, vol. 15, no. 8, pp. 4187–4199, Oct. 2011.

[21] H. E. S. Fath and A. Ghazy, "Solar desalination using humidification-dehumidification technology," *Desalination*, vol. 142, pp. 119–133, 2002.

[22] S. Jakhar, R. Misra, V. Bansal, and M. S. Soni, "Thermal performance investigation of earth air tunnel heat exchanger coupled with a solar air heating duct for northwestern India," *Energy Build.*, vol. 87, pp. 360–369, 2015.

[23] S. Pandey, "Success in Scaling-up Solar Energy in Rajasthan, India." [Online]. Available: http://re.indiaenvironmentportal.org.in/files/file/Success in Scaling-up Solar Energy in Rajasthan, India.pdf.

[24] S. Jakhar, M. S. Soni, and N. Gakkhar, “Performance Analysis of Photovoltaic Panels with Earth Water Heat Exchanger Cooling,” *MATEC Web Conf.*, vol. 55, no. 02006, pp. 0–5, 2016.

[25] “Rajasthan Map,” *Government of Rajasthan*. [Online]. Available: http://plan.rajasthan.gov.in/content/industries/rajasthan-foundation/about-rajasthan/rajasthan-maps.html.

[26] S. M. Hooda, “Water Assessment - Potential for Private Intervention,” International Finance Corporation, Delhi, India, 2013.

[27] V. Ramakrishna and B. Babu, “Fresh water depletion-a crisis: Causes & remedies,” *Environ. People*, vol. 6, no. 1, pp. 33–39, 1999.

[28] Department of Water Resources, “Study of Planning of Water Resources of Rajasthan State.” [Online]. Available: http://waterresources.rajasthan.gov.in/SPWRR/SPWRR.htm.

[29] State Water Resources Planning Department, “Monsoon Report 2014,” Government of Rajasthan, Jaipur, 2014.

[30] Department of Water Resources, “Monsoon 2014.” [Online]. Available: http://water.rajasthan.gov.in/content/water/en/imtikota/Dataroom/rainfall/monsoonrainfall.html. [Accessed: 12-Dec-2016].

[31] Government of Rajasthan, “Comprehensive full scale integrated Water Resources plan for the State as a whole.” [Online]. Available: http://waterresources.rajasthan.gov.in/SPWRR/chapter/chapters.htm. [Accessed: 20-Oct-2017].

[32] “Study on planning of water resources of rajasthan: Water Supply and Demand by Districts Part C – Water Supply and Demand Balance 2014,” 2014. [Online]. Available: http://water.rajasthan.gov.in/content/dam/water/state-water-resources-planning-department/tahaldata/Report 4.3 Final _Ia.pdf. [Accessed: 28-Oct-2016].

[33] Ministry of Water Resources, “Report of the Ground Water Resource Estimation Committee: Ground Water Resource Estimation Methodology,” p. 113, 2009.

[34] DoWR, “Study on planning of water resources of Rajasthan - Water supply and

demand by districts," A report by Department of Water Resources, GoR, Jaipur, India, 2014.

[35] "Ground Water Year Book - India 2011-12," *Central Ground Water Board, Ministry of Water Resources*, 2012. [Online]. Available: http://cgwb.gov.in/documents/Ground Water Year Book - 2011-12.pdf. [Accessed: 06-Sep-2016].

[36] A. Jain and S. K. Singh, "Prevalence of fluoride in ground water in Rajasthan state: Extent, contamination levels and mitigation," *Open J. Water Piollution Treat.*, vol. 1, no. 2, pp. 50–57, 2014.

[37] S. Suthar, V. K. Garg, S. Jangir, S. Kaur, N. Goswami, and S. Singh, "Fluoride contamination in drinking water in rural habitations of northern Rajasthan, India.," *Environ. Monit. Assess.*, vol. 145, no. 1–3, pp. 1–6, Oct. 2008.

[38] B. S. Yadav, A. Garg, P. K. Santra, S. Santra, and D. K. Jangid, "Study on Fluoride Content in Groundwater of Newai Tehsil in Tonk District Located in Rajasthan and Its Impact on Human," *World J. Appl. Environ. Chem.*, vol. 4, no. 1, pp. 1–6, 2017.

[39] A. Sharma, B. Goswamee, R. Kumar, and A. Agarwal, "Remuneration of Rain Water Harvesting in Shekahwati Region, Rajasthan," *Int. J. Eng. Res. Technol.*, vol. 1, no. 7, pp. 1–5, 2012.

[40] S. Mitharwal, R. D. Yadav, and R. C. Angasaria, "Water Quality Analysis in Pilani of Jhunjhunu Distict (Rajasthan) - The Place of Birla's Origin," *Rasayan J. Chem.*, vol. 2, no. 4, pp. 920–923, 2009.

[41] P. J. Sajil Kumar, P. Davis Delson, J. G. Vernon, and E. J. James, "A linear regression model (LRM) for groundwater chemistry in and around the Vaniyambadi industrial area, Tamil Nadu, India," *Chinese J. Geochemistry*, vol. 32, no. 1, pp. 19–26, 2012.

[42] N. Gakkhar, M. S. Soni, and S. Jakhar, "Influence of Environmental Parameters on Groundwater Contamination in Rajasthan, India," in *7th International Conference on Biology, Environment and Chemistry*, 2016, vol. 98, no. 10, pp. 66–73.

[43] I. Purohit and P. Purohit, "Techno-economic evaluation of concentrating solar power generation in India," *Energy Policy*, vol. 38, no. 6, pp. 3015–3029, Jun. 2010.

[44] L. Dawson and P. Schlyter, "Less is more: Strategic scale site suitability for

concentrated solar thermal power in Western Australia," *Energy Policy*, vol. 47, pp. 91–101, 2012.

[45] Department of Land Resources, "Wasteland Atlas." [Online]. Available: http://www.dolr.nic.in/WastelandsAtlas2011/Wastelands_Atlas_2011.pdf. [Accessed: 22-Aug-2017].

[46] The National Aeronautics and Space Administration, "NASA Surface meteorology and Solar Energy." [Online]. Available: https://www.nasa.gov/. [Accessed: 25-Feb-2018].

[47] I. Purohit, P. Purohit, and S. Shekhar, "Evaluating the potential of concentrating solar power generation in Northwestern India," *Energy Policy*, vol. 62, pp. 157–175, 2013.

[48] C. Sharma, A. K. Sharma, S. C. Mullick, and T. C. Kandpal, "Assessment of solar thermal power generation potential in India," *Renew. Sustain. Energy Rev.*, vol. 42, pp. 902–912, 2015.

[49] M. M. Hoogwijk, "On the global and regional potential of renewable energy sources," PhD Thesis, Universiteit Utrecht, Netherlands, 2004.

[50] R. Mahtta, P. K. Joshi, and A. K. Jindal, "Solar power potential mapping in India using remote sensing inputs and environmental parameters," *Renew. Energy*, vol. 71, pp. 255–262, 2014.

[51] M. S. Soni and N. Gakkhar, "Techno-economic parametric assessment of solar power in India: A survey," *Renew. Sustain. Energy Rev.*, vol. 40, pp. 326–334, 2014.

[52] F. Trieb, C. Schillings, M. O. Sullivan, T. Pregger, and C. Hoyer-klick, "Global Potential of Concentrating Solar Power," in *Solar Power and Chemical Energy Systems (SolarPACES)*, 2009.

[53] S. Gupta, "Demystifying'Tradition': The Politics of Rainwater Harvesting in Rural Rajasthan, India.," *Water Altern.*, vol. 4, no. 3, pp. 347–364, 2011.

[54] C. J. Glendenning and R. W. Vervoort, "Hydrological impacts of rainwater harvesting (RWH) in a case study catchment: The Arvari River, Rajasthan, India: Part 2. Catchment-scale impacts," *Agric. Water Manag.*, vol. 98, no. 4, pp. 715–730, 2011.

[55] A. Alanis-Noyola, A. Prasanna, T. Rannou, and L. Rojas-solórzano, "Pre-Feasibility

Analysis of a Desalination Plant Powered by Renewable Energy in Thira, Greece," *Int. Conf. Renew. Energies power Qual.*, 2012.

[56] G. Fiorenza, V. K. Sharma, and G. Braccio, "Techno-economic evaluation of a solar powered water desalination plant," *Energy Convers. Manag.*, vol. 44, no. 14, pp. 2217–2240, Aug. 2003.

[57] A. Husain, *Integrated power and desalination plants*. Encyclopedia of Life Support Systems (EOLSS) Publisher, Oxford, UK, 2003.

[58] K. S. Spiegler, *Principles of desalination*. Academic Press, NY, USA, 2012.

[59] W. B. Stine and R. W. Harrigan, *Solar energy fundamentals and design*. John Wiley and Sons, Inc., New York, NY, 1985.

[60] R. Winston, "Principles of solar concentrators of a novel design," *Sol. Energy*, vol. 16, no. 2, pp. 89–95, Sep. 1974.

[61] J. A. Duffie and W. A. Beckman, "Solar energy thermal processes," University of Wisconsin-Madison, Solar Energy Laboratory, Madison, WI, Sep. 1974.

[62] G. F. Drew, "Parabolic solar concentrator employing flat plate collector," US Patent 4,038,964, 1977.

[63] A. B. Meinel and M. P. Meinel, *Applied solar energy. An introduction*. Addison-Wesley Series in Physics, USA, 1976.

[64] S. M. A. Moustafa, G. H. Brusewitz, and D. M. Farmer, "Direct use of solar energy for water desalination," *Sol. Energy*, vol. 22, no. 2, pp. 141–148, Sep. 1979.

[65] W. S. Kennedy, "Parabolic trough solar energy collector assembly," US Patent 4,135,493, 1979.

[66] S. J. Wagner and E. S. Rubin, "Economic implications of thermal energy storage for concentrated solar thermal power," *Renew. Energy*, vol. 61, pp. 81–95, Jan. 2014.

[67] R. Forristall, "Heat Transfer Analysis and Modeling of a Parabolic Trough Solar Receiver Implemented in Engineering Equation Solver," Golden, CO, 2003.

[68] R. V. Padilla, G. Demirkaya, D. Y. Goswami, E. Stefanakos, and M. M. Rahman,

"Heat transfer analysis of parabolic trough solar receiver," *Appl. Energy*, vol. 88, no. 12, pp. 5097–5110, Dec. 2011.

[69] Z. D. Cheng, Y. L. He, J. Xiao, Y. B. Tao, and R. J. Xu, "Three-dimensional numerical study of heat transfer characteristics in the receiver tube of parabolic trough solar collector," *Int. Commun. Heat Mass Transf.*, vol. 37, no. 7, pp. 782–787, Aug. 2010.

[70] X. Xiao, P. Zhang, D. D. Shao, and M. Li, "Experimental and numerical heat transfer analysis of a V-cavity absorber for linear parabolic trough solar collector," *Energy Convers. Manag.*, vol. 86, pp. 49–59, Oct. 2014.

[71] G. Coccia, G. Di Nicola, and M. Sotte, "Design, manufacture, and test of a prototype for a parabolic trough collector for industrial process heat," *Renew. energy*, vol. 74, pp. 727–736, 2015.

[72] K. Al-Zahrani, "The Application of Parabolic Trough Technology under Yanbu Climate in Saudi Arabia," *World Appl. Sci. J.*, 2013.

[73] O. Badran and M. Eck, "The application of parabolic trough technology under Jordanian climate," *Renew. Energy*, vol. 31, no. 6, pp. 791–802, May 2006.

[74] A. Scrivani, T. El Asmar, and U. Bardi, "Solar trough concentration for fresh water production and waste water treatment," *Desalination*, vol. 206, no. 1–3, pp. 485–493, Feb. 2007.

[75] B. Prasad and G. N. Tiwari, "Analysis of double effect active solar distillation," *Energy Convers. Manag.*, vol. 37, no. 11, pp. 1647–1656, 1996.

[76] R. Tripathi and G. N. Tiwari, "Effect of water depth on internal heat and mass transfer for active solar distillation," *Desalination*, vol. 173, no. 2, pp. 187–200, 2005.

[77] G. N. Tiwari, V. Dimri, U. Singh, A. Chel, and B. Sarkar, "Comparative thermal performance evaluation of an active solar distillation system," *Int. J. Energy Res.*, vol. 31, no. 15, pp. 1465–1482, 2007.

[78] K. Vinoth Kumar and R. Kasturi Bai, "Performance study on solar still with enhanced condensation," *Desalination*, vol. 230, no. 1, pp. 51–61, 2008.

[79] T. V Arjunan, H. S. Aybar, N. Nedunchezhian, and M. Sakthivel, "Effect of blue metal

stones on the performance of a conventional solar still," *J. Converg. Eng. Technol. Sci.*, vol. 1, no. 1, pp. 17–22, 2009.

[80] A. K. Tiwari and G. N. Tiwari, "Thermal modeling based on solar fraction and experimental study of the annual and seasonal performance of a single slope passive solar still: the effect of water depths," *Desalination*, vol. 207, no. 1, pp. 184–204, 2007.

[81] V. K. Dwivedi and G. N. Tiwari, "Annual Energy and Exergy Analysis of Single and Double Slope Passive Solar Stills.," *Trends Appl. Sci. Res.*, vol. 3, no. 3, 2008.

[82] G. N. Tiwari, J. M. Thomas, and E. Khan, "Optimisation of glass cover inclination for maximum yield in a solar still," *Heat Recover. Syst. CHP*, vol. 14, no. 4, pp. 447–455, 1994.

[83] B. W. Tleimat and E. D. Howe, "Nocturnal production of solar distillers," *Sol. Energy*, vol. 10, no. 2, pp. 61–66, 1966.

[84] S. Sinha, S. Kumar, and G. N. Tiwari, "Active solar distillation system - An investment alternative to a solar hot water system," *Energy Convers. Manag.*, vol. 35, no. 7, pp. 583–588, 1994.

[85] F. F. Tabrizi, M. Dashtban, and H. Moghaddam, "Experimental investigation of a weir-type cascade solar still with built-in latent heat thermal energy storage system," *Desalination*, vol. 260, no. 1–3, pp. 248–253, Sep. 2010.

[86] A. A. El-Sebaii, A. A. Al-Ghamdi, F. S. Al-Hazmi, and A. S. Faidah, "Thermal performance of a single basin solar still with PCM as a storage medium," *Appl. Energy*, vol. 86, no. 7–8, pp. 1187–1195, Jul. 2009.

[87] M. Dashtban and F. F. Tabrizi, "Thermal analysis of a weir-type cascade solar still integrated with PCM storage," *Desalination*, vol. 279, no. 1–3, pp. 415–422, Sep. 2011.

[88] K. Mahkamov and J. S. Akhatov, "Experimental study of the performance of multieffect solar thermal water desalination system," *Appl. Sol. Energy*, vol. 44, no. 1, pp. 31–34, Jun. 2008.

[89] S. Singh, V. Bhatnagar, and G. Tiwari, "Design parameters for concentrator assisted

solar distillation system," *Energy Convers. Manag.*, vol. 37, no. 2, pp. 247--252, 1996.

[90] Z. S. Abdel-Rehim and A. Lasheen, "Experimental and theoretical study of a solar desalination system located in Cairo, Egypt," *Desalination*, vol. 217, no. 1–3, pp. 52–64, Nov. 2007.

[91] A. M. Radhwan, "Transient performance of a stepped solar still with built-in latent heat thermal energy storage," *Desalination*, vol. 171, pp. 61–76, 2004.

[92] K. Voropoulos, E. Mathioulakis, and V. Belessiotis, "Experimental investigation of the behavior of a solar still coupled with hot water storage tank," *Desalination*, vol. 156, no. 1–3, pp. 315–322, Aug. 2003.

[93] M. Al-harahsheh, M. Abu-Arabi, H. Mousa, and Z. Alzghoul, "Solar desalination using solar still enhanced by external solar collector and PCM," *Appl. Therm. Eng.*, vol. 128, pp. 1030–1040, 2018.

[94] A. C. Gangadharan, T. V Narayanan, R. W. Bryes, and E. W. Sommer, "Design optimization of a small scale solar desalination plant," *Colloq. Int. du Cent. Natl. la Rech. Sci.*, vol. 360, p. 205, 1980.

[95] I. S. Al-Mutaz and M. I. Al-Ahmed, "Evaluation of solar powered desalination processes," *Desalination*, vol. 73, pp. 181–190, Sep. 1989.

[96] S. Kalogirou, "Parabolic Trough Collector System for Low Temperature Steam Generation : Design and Performance Characteristics," *Appl. Energy*, vol. 55, no. I, pp. 1–19, Sep. 1996.

[97] S. A. Kalogirou, S. Lloyd, J. Ward, and P. Eleftheriou, "Design and performance characteristics of a parabolic-trough solar-collector system," *Appl. Energy*, vol. 47, no. 4, pp. 341–354, 1994.

[98] G. N. Tiwari and H. P. Garg, "Effect of water flow over the glass cover of a single basin solar still with an intermittent flow of waste hot water in the basin," *Energy Convers. Manag.*, vol. 25, no. 3, pp. 315–322, 1985.

[99] S. Kumar and S. Sinha, "Transient model and comparative study of concentrator coupled regenerative solar still in forced circulation mode," *Energy Convers. Manag.*, vol. 37, no. 5, pp. 629–636, 1996.

[100] S. Kumar and G. N. Tiwari, “Performance evaluation of an active solar distillation system,” *Energy*, vol. 21, no. 9, pp. 805–808, 1996.

[101] S. Kumar and G. N. Tiwari, “Estimation of internal heat transfer coefficients of a hybrid (PV/T) active solar still,” *Sol. Energy*, vol. 83, no. 9, pp. 1656–1667, 2009.

[102] V. Velmurugan, S. Pandiarajan, P. Guruparan, L. H. Subramanian, C. D. Prabaharan, and K. Srithar, “Integrated performance of stepped and single basin solar stills with mini solar pond,” *Desalination*, vol. 249, no. 3, pp. 902–909, 2009.

[103] L. García-Rodríguez and L. Garcia-rodriguez, “Seawater desalination driven by renewable energies : a review,” *Desalination*, vol. 143, no. 2, pp. 103–113, May 2002.

[104] L. García-Rodríguez and C. Gómez-Camacho, “Design parameter selection for a distillation system coupled to a solar parabolic trough collector,” *Desalination*, vol. 122, no. 2, pp. 195–204, 1999.

[105] S. Kalogirou, “Seawater desalination using renewable energy sources,” *Prog. Energy Combust. Sci.*, vol. 31, no. 3, pp. 242–281, 2005.

[106] B. Chaouchi, A. Zrelli, and S. Gabsi, “Desalination of brackish water by means of a parabolic solar concentrator,” *Desalination*, vol. 217, no. 1–3, pp. 118–126, Nov. 2007.

[107] S. Touati, A. Belkaid, R. Benabid, K. Halbaoui, and M. Chelali, “Pre-Feasibility Design and Simulation of Hybrid PV/Fuel Cell Energy System for Application to Desalination Plants Loads,” *Procedia Eng.*, vol. 33, pp. 366–376, 2012.

[108] F. Trieb and H. Müller-Steinhagen, “Concentrating solar power for seawater desalination in the Middle East and North Africa,” *Desalination*, vol. 220, no. 1–3, pp. 165–183, Mar. 2008.

[109] F. Trieb and H. El Noraschy, “Concentrating Solar Power for Seawater Desalination,” in *Twelfth International Water Technology Conference*, 2008.

[110] A. Fernández-García, E. Zarza, L. Valenzuela, and M. Pérez, “Parabolic-trough solar collectors and their applications,” *Renew. Sustain. Energy Rev.*, vol. 14, no. 7, pp. 1695–1721, Sep. 2010.

[111] U. Sahoo, R. Kumar, P. C. Pant, and R. Chaudhury, “Scope and sustainability of hybrid solar–biomass power plant with cooling, desalination in polygeneration process in India,” *Renew. Sustain. Energy Rev.*, vol. 51, pp. 304–316, 2015.

[112] A. D. Khawaji, I. K. Kutubkhanah, and J.-M. Wie, “Advances in seawater desalination technologies,” *Desalination*, vol. 221, no. 1–3, pp. 47–69, Mar. 2008.

[113] L. F. Greenlee, D. F. Lawler, B. D. Freeman, B. Marrot, and P. Moulin, “Reverse osmosis desalination: water sources, technology, and today’s challenges.,” *Water Res.*, vol. 43, no. 9, pp. 2317–48, May 2009.

[114] Z. Amjad, *Reverse Osmosis: Membrane Technology, Water Chemistry, and Industrial Applications*. New York: Chapman & Hall, International Thomson Publishing, 1993.

[115] G. Nebbia and G. N. Menozzi, *A short history of water desalination*. Milan, Italy: Azienda Grafica Italiana, 1966.

[116] S. Sinha and G. N. Tiwari, “Thermal evaluation of concentrator-assisted solar distillation system,” *Heat Recover. Syst.*, vol. 12, no. 6, pp. 481–488, 1992.

[117] B. Van der Bruggen and C. Vandecasteele, “Distillation vs. membrane filtration: overview of process evolutions in seawater desalination,” *Desalination*, vol. 143, no. 3, pp. 207–218, Jun. 2002.

[118] J. Leblanc, A. Akbarzadeh, and J. Andrews, “Modelling Solar-Thermal Desalination Systems,” in *Australian and New Zealand Solar Energy Society (ANZSES) - Solar Conference*, 2005, pp. 28–30.

[119] A. S. Nafey, M. A. Mohamad, S. O. El-Helaby, and M. A. Sharaf, “Theoretical and experimental study of a small unit for solar desalination using flashing process,” *Energy Convers. Manag.*, vol. 48, no. 2, pp. 528–538, Feb. 2007.

[120] J. Blanco, P. Palenzuela, D. Alarcón-Padilla, G. Zaragoza, and M. Ibarra, “Preliminary thermoeconomic analysis of combined parabolic trough solar power and desalination plant in port Safaga (Egypt),” *Desalin. Water Treat.*, vol. 51, pp. 1887–1899, 2013.

[121] K. Zhani, “Solar desalination based on multiple effect humidification process: Thermal performance and experimental validation,” *Renew. Sustain. Energy Rev.*, vol. 24, pp. 406–417, Aug. 2013.

[122] C. Li, Y. Goswami, and E. Stefanakos, “Solar assisted sea water desalination - A review,” *Renew. Sustain. Energy Rev.*, vol. 19, pp. 136–163, 2013.

[123] S. Riffat and A. Mayere, “Performance evaluation of v-trough solar concentrator for water desalination applications,” *Appl. Therm. Eng.*, 2013.

[124] C.-Y. Hsui, “The optimal allocating pumping rate of a multi-well system for a brackish water desalination plant,” *Desalination*, vol. 221, no. 1–3, pp. 215–224, Mar. 2008.

[125] C. Renno and F. Petito, “Energy Analysis of a Concentrating Photovoltaic Thermal (CPV/T) System,” vol. 6, no. 2, pp. 53–63, 2013.

[126] G. Mittelman, A. Kribus, and A. Dayan, “Solar cooling with concentrating photovoltaic/thermal (CPVT) systems,” *Energy Convers. Manag.*, vol. 48, no. 9, pp. 2481–2490, Sep. 2007.

[127] M. Muller, C. Deline, B. Marion, S. Kurtz, and N. Bosco, “Determining Outdoor CPV Cell Temperature,” in *AIP Conference Proceedings*, 2011, vol. 1407, no. 1, pp. 331–335.

[128] L. A. A. Bunthof *et al.*, “Influence of laterally split spectral illumination on multi-junction CPV solar cell performance,” *Sol. Energy*, vol. 170, pp. 86–94, 2018.

[129] L. A. A. Bunthof, J. Bos-Coenraad, W. H. M. Corbeek, E. Vlieg, and J. J. Schermer, “The illumination angle dependency of CPV solar cell electrical performance,” *Sol. Energy*, vol. 144, pp. 166–174, 2017.

[130] F. Reis *et al.*, “Modeling the effects of inhomogeneous irradiation and temperature profile on CPV solar cell behavior,” *IEEE J. Photovoltaics*, vol. 5, no. 1, pp. 112–122, 2015.

[131] A. Royne, C. J. Dey, and D. R. Mills, “Cooling of photovoltaic cells under concentrated illumination: a critical review,” *Sol. energy Mater. Sol. cells*, vol. 86, no. 4, pp. 451–483, 2005.

[132] A. Makki, S. Omer, and H. Sabir, “Advancements in hybrid photovoltaic systems for enhanced solar cells performance,” *Renew. Sustain. Energy Rev.*, vol. 41, pp. 658–684, 2015.

[133] L. Zhu, R. F. Boehm, Y. Wang, C. Halford, and Y. Sun, “Water immersion cooling of PV cells in a high concentration system,” *Sol. Energy Mater. Sol. Cells*, vol. 95, no. 2, pp. 538–545, 2011.

[134] L. Zhu, Y. Wang, Z. Fang, Y. Sun, and Q. Huang, “An effective heat dissipation method for densely packed solar cells under high concentrations,” *Sol. Energy Mater. Sol. Cells*, vol. 94, no. 2, pp. 133–140, 2010.

[135] X. Han, Y. Wang, and L. Zhu, “The performance and long-term stability of silicon concentrator solar cells immersed in dielectric liquids,” *Energy Convers. Manag.*, vol. 66, pp. 189–198, 2013.

[136] H. Xiang, Y. Wang, L. Zhu, X. Han, Y. Sun, and Z. Zhao, “3D numerical simulation on heat transfer performance of a cylindrical liquid immersion solar receiver,” *Energy Convers. Manag.*, vol. 64, pp. 97–105, 2012.

[137] S. Jakhar, M. S. Soni, and N. Gakkhar, “Historical and recent development of concentrating photovoltaic cooling technologies,” *Renew. Sustain. Energy Rev.*, vol. 60, pp. 41–59, 2016.

[138] J. S. Coventry, “Performance of a concentrating photovoltaic/thermal solar collector,” *Sol. Energy*, vol. 78, no. 2, pp. 211–222, 2005.

[139] M. Chaabane, W. Charfi, H. Mhiri, and P. Bournot, “Performance evaluation of concentrating solar photovoltaic and photovoltaic/thermal systems,” *Sol. Energy*, vol. 98, no. PC, pp. 315–321, 2013.

[140] A. Darwish and R. F. Boehm, “Optical and Thermal Analysis for Immersed Cooling of Photovoltaic Cells in a Highly Concentrated Beam,” in *ASME 2011 5th International Conference on Energy Sustainability*, 2011, pp. 557–565.

[141] N. Gakkhar, M. S. Soni, and S. Jakhar, “Second law thermodynamic study of solar assisted distillation system: A review,” *Renew. Sustain. Energy Rev.*, vol. 56, pp. 519–535, 2016.

[142] A. Hepbasli, “A key review on exergetic analysis and assessment of renewable energy resources for a sustainable future,” *Renew. Sustain. Energy Rev.*, vol. 12, no. 3, pp. 593–661, Apr. 2008.

[143] R. Saidur, G. BoroumandJazi, S. Mekhlif, and M. Jameel, “Exergy analysis of solar energy applications,” *Renew. Sustain. Energy Rev.*, vol. 16, no. 1, pp. 350–356, Jan. 2012.

[144] K. Manjunath and S. C. Kaushik, “Second law thermodynamic study of heat exchangers: A review,” *Renew. Sustain. Energy Rev.*, vol. 40, pp. 348–374, Dec. 2014.

[145] H. Sharon and K. S. Reddy, “A review of solar energy driven desalination technologies,” *Renew. Sustain. Energy Rev.*, vol. 41, pp. 1080–1118, 2015.

[146] S. Hou, D. Zeng, S. Ye, and H. Zhang, “Exergy analysis of the solar multi-effect humidification–dehumidification desalination process,” *Desalination*, vol. 203, no. 1, pp. 403–409, 2007.

[147] A. Bejan, D. W. Kearney, and F. Kreith, “Second Law Analysis and Synthesis of Solar Collector Systems,” *J. Sol. Energy Eng.*, vol. 103, pp. 23–28, 1981.

[148] R. V. Padilla, A. Fontalvo, G. Demirkaya, A. Martinez, and A. G. Quiroga, “Exergy analysis of parabolic trough solar receiver,” *Appl. Therm. Eng.*, vol. 67, no. 1–2, pp. 579–586, Jun. 2014.

[149] M. J. Moran, H. N. Shapiro, D. D. Boettner, and M. Bailey, *Fundamentals of engineering thermodynamics*. John Wiley & Sons, 2010.

[150] H. Zhai, Y. J. Dai, J. Y. Wu, and R. Z. Wang, “Energy and exergy analyses on a novel hybrid solar heating, cooling and power generation system for remote areas,” *Appl. Energy*, vol. 86, no. 9, pp. 1395–1404, Sep. 2009.

[151] C. J. Winter, R. L. Sizmann, and L. L. Vant-Hull, *Solar power plants - fundamentals, technology, systems, economics*. Springer-Verlag New York, 1991.

[152] M. Hernández-Román, A. Manzano-Ramírez, J. Pineda-Piñón, and J. Ortega-Moody, “Exergetic and Thermoeconomic Analyses of Solar Air Heating Processes Using a Parabolic Trough Collector,” *Entropy*, vol. 16, no. 8, pp. 4612–4625, Aug. 2014.

[153] J. A. Duffie and W. A. Beckman, *Solar engineering of thermal processes*. John Wiley & Sons, 2013.

[154] N. Singh, S. C. Kaushik, and R. D. Misra, “Exergetic analysis of a solar thermal power

system," *Renew. Energy*, vol. 19, no. 1–2, pp. 135–143, Jan. 2000.

[155] M. J. Montes, A. Abánades, and J. M. Martínez-Val, "Thermofluidynamic Model and Comparative Analysis of Parabolic Trough Collectors Using Oil, Water/Steam, or Molten Salt as Heat Transfer Fluids," *J. Sol. Energy Eng.*, vol. 132, no. 2, pp. 021001:1–7, 2010.

[156] M. K. Gupta and S. C. Kaushik, "Exergy analysis and investigation for various feed water heaters of direct steam generation solar–thermal power plant," *Renew. Energy*, vol. 35, no. 6, pp. 1228–1235, Jun. 2010.

[157] A. Baghernejad and M. Yaghoubi, "Energy , exergy and second law performance of parabolic Trough collector integration into combined cycle system ( ISCCS )," in *Fourth International Conference on Thermal Engineering: Theory and Applications*, 2009, pp. 1–6.

[158] A. Bejan, "Advanced engineering thermodynamics, 1996," *Interscience, New York*, 1996.

[159] A. Baghernejad and M. Yaghoubi, "Exergy analysis of an integrated solar combined cycle system," *Renew. Energy*, vol. 35, no. 10, pp. 2157–2164, Oct. 2010.

[160] A. Baghernejad and M. Yaghoubi, "Exergoeconomic analysis and optimization of an Integrated Solar Combined Cycle System (ISCCS) using genetic algorithm," *Energy Convers. Manag.*, vol. 52, no. 5, pp. 2193–2203, May 2011.

[161] J. L. Silveira and C. E. Tuna, "Thermoeconomic analysis method for optimization of combined heat and power systems. Part I," *Prog. energy Combust. Sci.*, vol. 29, no. 6, pp. 479–485, 2003.

[162] M. A. A. Sharaf, A. S. S. Nafey, and L. García-Rodríguez, "Exergy and thermo-economic analyses of a combined solar organic cycle with multi effect distillation (MED) desalination process," *Desalination*, vol. 272, no. 1–3, pp. 135–147, May 2011.

[163] J. Blanco *et al.*, "Technical comparison of different solar-assisted heat supply systems for a multi-effect seawater distillation unit," in *International Solar Energy Society: Solar World Congress*, 2003, pp. 14–19.

[164] F. Banat and N. Jwaied, "Exergy analysis of desalination by solar-powered membrane

distillation units," *Desalination*, vol. 230, no. 1–3, pp. 27–40, Sep. 2008.

[165] M. K. Gupta, S. C. Kaushik, K. R. Ranjan, N. L. Panwar, V. S. Reddy, and S. K. Tyagi, "Thermodynamic performance evaluation of solar and other thermal power generation systems: A review," *Renew. Sustain. Energy Rev.*, vol. 50, pp. 567–582, 2015.

[166] A. M. Elsafi, "Exergy and exergoeconomic analysis of sustainable direct steam generation solar power plants," *Energy Convers. Manag.*, vol. 103, pp. 338–347, 2015.

[167] H. T. El-Dessouky and H. M. Ettouney, *Fundamentals of Salt Water Desalination*. 2002.

[168] F. A. Al-Sulaiman and B. Ismail, "Exergy analysis of major recirculating multi-stage flash desalting plants in Saudi Arabia," *Desalination*, vol. 103, pp. 265–270, 1995.

[169] S. C. Kaushik, R. D. Misra, and N. Singh, "Second Law Analysis of a Solar Thermal Power System," *Int. J. Sol. Energy*, vol. 20, no. 4, pp. 239–253, Sep. 2000.

[170] V. S. Reddy, S. C. Kaushik, and S. K. Tyagi, "Exergetic analysis and performance evaluation of parabolic trough concentrating solar thermal power plant (PTCSTPP)," *Energy*, vol. 39, no. 1, pp. 258–273, Mar. 2012.

[171] M. Khayet, "Solar desalination by membrane distillation: Dispersion in energy consumption analysis and water production costs (a review)," *Desalination*, vol. 308, pp. 89–101, Jan. 2013.

[172] K. S. Spiegler and Y. M. El-sayed, "The energetics of desalination processes," *Desalination*, vol. 134, pp. 109–128, 2001.

[173] R. Gomri, "Energy and exergy analyses of seawater desalination system integrated in a solar heat transformer," *Desalination*, vol. 249, no. 1, pp. 188–196, Nov. 2009.

[174] F. Nematollahi, A. Rahimi, and T. T. Gheinani, "Experimental and theoretical energy and exergy analysis for a solar desalination system," *Desalination*, vol. 317, pp. 23–31, May 2013.

[175] K. Wark, *Advanced thermodynamics for engineers*. McGraw-Hill New York, 1995.

[176] J. Uche, L. Serra, and A. Valero, "Exergy Costs and Inefficiency Diagnosis of a Dual-

Purpose Power and Desalination Plant," *J. Energy Resour. Technol.*, vol. 128, no. 3, p. 186, 2006.

[177] O. A. Hamed, M. A. K. Al-sofi, G. M. Mustafa, M. Imam, K. Ba-Mardouf, and H. Al-Washmi, "Modeling and Simulation of Multistage Flash Distillation Process," in *4th SWCC Acquired Experience Conference, Riyad*, 2004.

[178] Y. M. El-Sayed, "Design and simulation software," Fremont, CA, USA, 1998.

[179] L. García-Rodríguez and C. Gómez-Camacho, "Thermoeconomic analysis of a solar parabolic trough collector distillation plant," *Desalination*, vol. 122, no. 2, pp. 215–224, 1999.

[180] L. García-Rodríguez and C. Gómez-Camacho, "Exergy analysis of the SOL-14 plant (Plataforma Solar de Almeria, Spain)," *Desalination*, vol. 137, no. 1, pp. 251–258, 2001.

[181] N. Kahraman and Y. A. Cengel, "Exergy analysis of a MSF distillation plant," *Energy Convers. Manag.*, vol. 46, no. 15, pp. 2625–2636, 2005.

[182] A. S. Nafey, H. E. S. Fath, and A. A. Mabrouk, "Exergy and thermoeconomic evaluation of MSF process using a new visual package," *Desalination*, vol. 201, no. 1–3, pp. 224–240, Nov. 2006.

[183] A. S. Nafey, M. A. Sharaf, and L. García-Rodríguez, "A new visual library for design and simulation of solar desalination systems (SDS)," *Desalination*, vol. 259, no. 1–3, pp. 197–207, Sep. 2010.

[184] C. Li, "Innovative Desalination Systems Using Low-grade Heat," PhD Thesis, University of South Florida, USA, 2012.

[185] S. Al-Kharabsheh, "Theoretical and experimental analysis of water desalination system using low grade solar heat," PhD Thesis, University of Florida, USA, 2003.

[186] A. S. Nafey, H. E. S. Fath, and A. A. Mabrouk, "Thermoeconomic design of a multi-effect evaporation mechanical vapor compression (MEE–MVC) desalination process," *Desalination*, vol. 230, no. 1–3, pp. 1–15, Sep. 2008.

[187] Y. Wang and N. Lior, "Performance analysis of combined humidified gas turbine

power generation and multi-effect thermal vapor compression desalination systems," *Desalination*, vol. 207, no. 1–3, pp. 243–256, Mar. 2007.

[188] A. S. Nafey and M. A. Sharaf, "Combined solar organic Rankine cycle with reverse osmosis desalination process: Energy, exergy, and cost evaluations," *Renew. Energy*, vol. 35, no. 11, pp. 2571–2580, 2010.

[189] N. Kahraman, Y. A. Cengel, B. Wood, and Y. Cerci, "Exergy analysis of a combined RO, NF, andEDR desalination plant," *Desalination*, vol. 171, no. 3, pp. 217–232, 2005.

[190] C. S. Rajoria, S. Agrawal, and G. N. Tiwari, "Overall thermal energy and exergy analysis of hybrid photovoltaic thermal array," *Sol. Energy*, vol. 86, no. 5, pp. 1531–1538, 2012.

[191] M. Qu, J. Chen, L. Nie, F. Li, Q. Yu, and T. Wang, "Experimental study on the operating characteristics of a novel photovoltaic/thermal integrated dual-source heat pump water heating system," *Appl. Therm. Eng.*, vol. 94, pp. 819–826, 2016.

[192] G. Evola and L. Marletta, "Exergy and thermoeconomic optimization of a water-cooled glazed hybrid photovoltaic/thermal (PVT) collector," *Sol. Energy*, vol. 107, pp. 12–25, 2014.

[193] R. Tripathi and G. N. Tiwari, "Energetic and exergetic analysis of N partially covered photovoltaic thermal-compound parabolic concentrator (PVT-CPC) collectors connected in series," *Sol. Energy*, vol. 137, pp. 441–451, 2016.

[194] S. A. Kalogirou, S. Karellas, V. Badescu, and K. Braimakis, "Exergy analysis on solar thermal systems: a better understanding of their sustainability," *Renew. Energy*, vol. 85, pp. 1328–1333, 2016.

[195] F. Calise, A. Palombo, and L. Vanoli, "A finite-volume model of a parabolic trough photovoltaic/thermal collector: Energetic and exergetic analyses," *Energy*, vol. 46, no. 1, pp. 283–294, 2012.

[196] M. Chaabane, H. Mhiri, and P. Bournot, "Performance Optimization of Water-Cooled Concentrated Photovoltaic System," *Heat Transf. Eng.*, vol. 37, no. 1, pp. 76–81, 2016.

[197] M. Abdelhamid *et al.*, "Novel double-stage high-concentrated solar hybrid photovoltaic/thermal (PV/T) collector with nonimaging optics and GaAs solar cells reflector," *Appl. Energy*, vol. 182, pp. 68–79, 2016.

[198] B. K. Widyolar *et al.*, "Design, simulation and experimental characterization of a novel parabolic trough hybrid solar photovoltaic/thermal (PV/T) collector," *Renew. Energy*, vol. 101, pp. 1379–1389, 2017.

[199] C. Kandilli, "Performance analysis of a novel concentrating photovoltaic combined system," *Energy Convers. Manag.*, vol. 67, pp. 186–196, 2013.

[200] A. E. Gürel, "Exergetic assessment of a concentrated photovoltaic thermal (CPV/T) system," *Int. J. Exergy*, vol. 21, no. 2, pp. 127–135, 2016.

[201] V. E. Dudley, L. R. Evans, and C. W. Matthews, "Test results, Industrial Solar Technology parabolic trough solar collector," Sandia National Labs, Albuquerque, USA, 1995.

[202] R. V. Padilla, G. Demirkaya, D. Y. Goswami, E. Stefanakos, and M. M. Rahman, "Heat transfer analysis of parabolic trough solar receiver," *Appl. Energy*, vol. 88, no. 12, pp. 5097–5110, Dec. 2011.

[203] N. Gakkhar, M. S. Soni, and S. Jakhar, "Analysis of water cooling of CPV cells mounted on absorber tube of a Parabolic Trough Collector," *Energy Procedia*, vol. 90, pp. 78–88, 2016.

[204] T. L. Bergman, F. P. Incropera, D. P. DeWitt, and A. S. Lavine, *Fundamentals of heat and mass transfer*. New York, USA: John Wiley & Sons, 2011.

[205] S. W. Churchill and H. H. S. Chu, "Correlating equations for laminar and turbulent free convection from a horizontal cylinder," *Int. J. Heat Mass Transf.*, vol. 18, no. 9, pp. 1049–1053, 1975.

[206] V. Gnielinski, "Heat transfer coefficients for turbulent flow in concentric annular ducts," *Heat Transf. Eng.*, vol. 30, no. 6, pp. 431–436, 2009.

[207] M. F. Modest, *Radiative heat transfer*. San Diego, USA: Academic press, 2013.

[208] H. Y. Zhang and M. A. Ebadian, "Heat transfer in the entrance region of semicircular

ducts with internal fins," *J. Thermophys. heat Transf.*, vol. 6, no. 2, pp. 296–301, 1992.

[209] R. M. Manglik and A. E. Bergles, "Laminar flow heat transfer in a semi-circular with uniform waII temperature," *Int. J. heat mass tranfer*, vol. 31, no. 3, pp. 625–636, 1988.

[210] S. Jakhar, M. S. Soni, and N. Gakkhar, "An integrated photovoltaic thermal solar (IPVTS) system with earth water heat exchanger cooling: Energy and exergy analysis," *Sol. Energy*, vol. 157, pp. 81–93, 2017.

[211] S. Dubey and G. N. Tiwari, "Thermal modeling of a combined system of photovoltaic thermal (PV/T) solar water heater," *Sol. Energy*, vol. 82, no. 7, pp. 602–612, 2008.

[212] D. L. Evans, "Simplified method for predicting photovoltaic array output," *Sol. energy*, vol. 27, no. 6, pp. 555–560, 1981.

[213] T. Schott, "Operation temperatures of pv modules: a theoretical and experimental approach," in *EC Photovoltaic solar energy conference. 6*, 1985, pp. 392–396.

[214] I. K. Karathanassis, E. Papanicolaou, V. Belessiotis, and G. C. Bergeles, "Design and experimental evaluation of a parabolic-trough concentrating photovoltaic/thermal (CPVT) system with high-efficiency cooling," *Renew. Energy*, vol. 101, pp. 467–483, 2017.

[215] S. Jakhar and M. S. Soni, "Experimental and theoretical analysis of glazed tube-and-sheet photovoltaic/thermal system with earth water heat exchanger cooling," *Energy Convers. Manag.*, vol. 153, no. September, pp. 576–588, 2017.

[216] Y. A. Cengel and M. A. Boles, *Thermodynamics: an engineering approach*. McGraw Hill Education, USA, 2007.

[217] R. V. Padilla, G. Demirkaya, D. Y. Goswami, E. Stefanakos, and M. M. Rahman, "Analysis of power and cooling cogeneration using ammonia-water mixture," *Energy*, vol. 35, no. 12, pp. 4649–4657, 2010.

[218] C. Borgnakke and R. E. Sonntag, *Fundamentals of thermodynamics*. Wiley New York, 2009.

[219] I. Dincer and M. A. Rosen, *Exergy: energy, environment and sustainable development*. Newnes, 2012.

[220] A. Tiwari, S. Dubey, G. S. Sandhu, M. S. Sodha, and S. I. Anwar, “Exergy analysis of integrated photovoltaic thermal solar water heater under constant flow rate and constant collection temperature modes,” *Appl. Energy*, vol. 86, no. 12, pp. 2592–2597, 2009.

[221] R. Petela, “Exergy of undiluted thermal radiation,” *Sol. Energy*, vol. 74, no. 6, pp. 469–488, 2003.

[222] S. Jakhar, M. S. Soni, and N. Gakkhar, “Exergy analysis of a photovoltaic thermal system with earth water heat exchanger cooling system based on experimental data,” *Int. J. Exergy*, vol. 23, no. 4, pp. 367–387, 2017.

[223] J. Yazdanpanahi, F. Sarhaddi, and M. M. Adeli, “Experimental investigation of exergy efficiency of a solar photovoltaic thermal (PVT) water collector based on exergy losses,” *Sol. Energy*, vol. 118, pp. 197–208, 2015.

[224] A. S. Joshi, I. Dincer, and B. V Reddy, “Analysis of energy and exergy efficiencies for hybrid PV/T systems,” *Int. J. Low-Carbon Technol.*, vol. 6, no. 1, pp. 64–69, 2010.

[225] A. S. Joshi, A. Tiwari, G. N. Tiwari, I. Dincer, and B. V Reddy, “Performance evaluation of a hybrid photovoltaic thermal (PV/T)(glass-to-glass) system,” *Int. J. Therm. Sci.*, vol. 48, no. 1, pp. 154–164, 2009.

[226] A. S. Joshi, I. Dincer, and B. V Reddy, “Thermodynamic assessment of photovoltaic systems,” *Sol. Energy*, vol. 83, no. 8, pp. 1139–1149, 2009.

[227] NASA, “POWER Data Access Viewer.” [Online]. Available: https://power.larc.nasa.gov/data-access-viewer/.

[228] N. Gakkhar, M. S. Soni, and S. Jakhar, “A Liquid-Cooled Hybrid Solar Energy Collector,” Indian Patent Application Number: 201711010510, 2018.

[229] J. P. Holman and W. J. Gajda, *Experimental methods for engineers*, vol. 2. McGraw-Hill New York, 1994.

[230] R. Tripathi, G. N. Tiwari, and V. K. Dwivedi, “Overall energy, exergy and carbon credit analysis of N partially covered Photovoltaic Thermal (PVT) concentrating collector connected in series,” *Sol. Energy*, vol. 136, pp. 260–267, 2016.

[231] S. Agrawal and G. N. Tiwari, “Overall energy, exergy and carbon credit analysis by different type of hybrid photovoltaic thermal air collectors,” *Energy Convers. Manag.*, vol. 65, pp. 628–636, 2013.

[232] H. Caliskan, I. Dincer, and A. Hepbasli, “Exergoeconomic, enviroeconomic and sustainability analyses of a novel air cooler,” *Energy Build.*, vol. 55, pp. 747–756, 2012.

# List of Publications and Awards

**Patent**

- A liquid-cooled hybrid solar energy collector. Application no: 201711010510. Publication date 29/09/2018 (Published)

**Book Chapter**

- **Nikhil Gakkhar**, M.S. Soni, Sanjeev Jakhar, 'Solar Energy Technologies and Water Potential for distillation - A Pre Feasibility Investigation for Rajasthan, India', Book Chapter in 'Progress in Solar Energy Technologies and Applications'. Wiley-Scrivener Publication (accepted; under publication).

**International Journals (Published)**

1. **Nikhil Gakkhar**, M.S. Soni**,** Sanjeev Jakhar, Analysis of Water Cooling of CPV Cells Mounted on Absorber Tube of a Parabolic Trough Collector, Energy Procedia, Volume 90, December 2016, Pages 78-88, ISSN 1876-6102, http://dx.doi.org/10.1016/j.egypro.2016.11.172 (**Scopus Indexed**).
2. **Nikhil Gakkhar,** M.S. Soni, Sanjeev Jakhar, Second Law Thermodynamic Study of Solar Assisted Distillation System: A review, Renewable and Sustainable Energy Reviews, Volume 56, April 2016, Pages 519-535, ISSN 1364-0321, http://dx.doi.org/10.1016/j.rser.2015.11.076 **(Impact factor: 9.184, SCI-E, Scopus**)
3. **Nikhil Gakkhar,** M.S. Soni, Sanjeev Jakhar, "Influence of environmental parameters on groundwater contamination in Rajasthan, India", International Proceedings of Chemical, Biological and Environmental Engineering, Volume 98, 2016, pages 66-73, **ISSN: 2010-4618,** DOI: 10.7763/IPCBEE.2016.V98.10

**Papers (Communicated/Accepted)**

1. **Nikhil Gakkhar**, M.S. Soni, Sanjeev Jakhar, Exergy Analysis and Experimental Study of a Novel Integrated Concentrated Photovoltaic Thermal System. Communicated in 25th SolarPACES Conference 2019 (accepted)

2. **Nikhil Gakkhar**, M.S. Soni, Sanjeev Jakhar, 'Performance investigation of hybrid concentrated photovoltaic/thermal system using parabolic trough collector' communicated in Solar Energy (Impact factor: 4.9, SCI-E, Scopus) (under review)
3. **Nikhil Gakkhar**, M.S. Soni, Sanjeev Jakhar, 'A novel concentrated photovoltaic thermal system for combine heat and power: An exergy analysis.' Communicated in International Journal of Exergy (Inderscience) (Impact factor: 1.377, SCI), (under review)
4. **Nikhil Gakkhar**, M.S. Soni, Sanjeev Jakhar, 'Exergetic Experimental Investigation of a Hybrid Concentrated Photovoltaic Thermal System'. Communicated in Solar World Congress 2019 (accepted)

**International Conferences**

1. **Nikhil Gakkhar**, Manoj S. Soni, Sanjeev Jakhar, "Applicability of concentrated solar thermal based distillation unit for semi arid region", Joint Indo-German Conference on Sustainable Engineering" (theme - Skilling India for Digital and Sustainable Future) September 15−16, 2017 at BITS Pilani, Pilani Campus.
2. Suman Shekhar, **Soni M.S.** and **Gakkhar Nikhil**, Solar Distillation Technologies in India: Past, Present and Future. International Congress on Renewable Energy (ICORE)–2014, "Powering National Growth Through Solar", Manekshaw Centre, Parade Road, Delhi Cantonment, New Delhi, December 8 - 9, 2014 pp: 80-88

**Awards**

Awarded a travel grant from the Centre for International Co-operation in Science (CICS), Chennai, for the presenting a research paper in the International Conference on Biology, Environment and Chemistry (ICBEC 2016), San Francisco, USA (26-28 October 2016)

## About the candidate (Nikhil Gakkhar)

Nikhil Gakkhar, Scientist 'B' in Ministry of New and Renewable Energy, Government of India, is currently working in Sardar Swaran Singh National Institute of Bio-Energy, Kapurthala, Punjab. He graduated with B.E. (Hons) in Mechanical Engineering from BITS Pilani, Goa Campus, in 2009 and post-graduated in M.E. in Mechanical Engineering from BITS Pilani, Pilani Campus in 2013. He also worked as PhD research scholar in BITS Pilani, Pilani campus, till 2016, before joining the Ministry. During his doctoral research he has published a patent, various research papers in internationals journals of repute and many technical papers in international conferences. His research area includes solar thermal technologies, solar water distillation, PV and CPV and solar hybrid systems. During his PhD, he received UGC-BSR fellowship (2013-2015) and a travel grant from CICS for presenting paper at international conference.

## About the Supervisor (Dr. Manoj Kumar Soni)

Dr. Manoj Kumar Soni, is an Associate professor in Mechanical Engineering department at BITS Pilani. He is B.E. in Mechanical Engineering, M.E. in Thermal Power Engineering, Ph.D. in the area of Energy Efficiency. He has total 23+ yrs of teaching and research experience. He rendered his services as a faculty in VNIT Nagpur (NIT, Nagpur) for seven years (1995-2002). He joined BITS Pilani in 2002. He is also the coordinator of Centre for Renewable Energy and Environment Development (CREED) at BITS, Pilani.

His research interest includes solar thermal, thermal engineering, renewable energy and energy efficiency. He has 40 plus publications in high impact factor international journals and international conferences and one patent in his name. He has delivered key note

addresses at various national conferences and workshops. He has conducted faculty development workshops also.

As a research team member, he has visited PT Indo Bharat Rayon, Indonesia an Aditya Birla Group unit in 2011 and in 2015 he was awarded Summer Scholarship under university immersion scheme of BITS Pilani and he visited University of South Florida, Tampa and Columbia University, New York.

He has special interest in spirituality and he has mixed the philosophies of spirituality and thermodynamics. Based on it he has delivered special lectures on 'Thermodynamics- A philosophy of life' and 'A date with entropy' at various institutes. His coveted lecture on Spiritual thermodynamics is very well appreciated by the students, academicians and industries. He delivered his Spiritual Thermodynamics talk at University of South Florida, Tampa, USA and University of Baleric Island, Spain. Out of his five PhD students in the field of solar and solar thermal has successfully completed. He has guided over 50 M. Tech and first degree thesis. He has experimented with lot of pedagogical innovations, like team based and game based learnings in his various courses.

At BITS he is actively involved in industrial collaborations in Work Integrated Programs Division as a coordinator of various collaborative programs: BS and B.Tech Power Engg (Aditya Birla Group, NTPC, NDPL, THDC, ESSAR Power, Tata Power, , JSW Energy), BS and B.Tech Process Engg (Aditya Birla Group Cement Business UltraTech, Hindalco Industries, Birla Cellulosic, Indogulf Fertilizers, Vedanta Aluminium), BS Engg Design (L&T iES, Vadodara), MS Engineering Management (Mahindra & Mahindra), MS Embedded Systems (L&TiES), MS Pharmaceutical Operations & Management (Wockhardt), MS Manufacturing Management (Vedanta Aluminium), and MS Automotive Engg Programs (Tata Technologies).

He is Fellow of Institute of Engineers, and Life member of International Solar Energy Society (Gold Member), and Energy and Fuels Users Association of India (ENFUSE). He is associate member, Solar Cookers International, USA and Senior Member, Universal Association of Mechanical and Aeronautical Engineers i.e UAMAE.

His web page is http://universe.bits-pilani.ac.in/pilani/mssoni/profile